Cross-sections and Electron Distributions Relating to Hot Electron Impact Excitation Efficiencies

A thesis presented by

Stephen Gerard Ayling B.Sc.

to the University of St.Andrews in application

for the degree of Doctor of Philosophy

DECLARATION

I hereby certify that this thesis has been composed by me and is a record of work done by me and has not previously been presented for a higher degree.

The research was carried out in the Wolfson Institute of Luminescence within the School of Physical Sciences in the University of St.Andrews under the supervision of Professor J.W.Allen.

Stephen G. Ayling

CERTIFICATE

I certify that Stephen Gerard Ayling has spent nine terms at research work in the Wolfson Institute of Luminescence within the School of Physical Sciences in the University of St.Andrews under my direction, that he has fulfilled the conditions of the Resolution of the University Court, 1967 , No. 1, and that he is qualified to submit the accompanying thesis in application for the Degree of Doctor of Philosophy.

Research Supervisor.

CAREER

I matriculated at University College in the University of Durham in October 1981. In July 1984 I obtained the Degree of Bachelor of Science with an Upper Second Honours in Physics.

In October 1984, following the award of an SERC Scholarship, I enrolled as a research student under the Resolution of the University Court, 1967, No.1, as a candidate for the degree of Doctor of Philosophy.

ACKNOWLEDGEMENTS

Firstly I would like to thank my supervisor, Professor J.W.Allen, for his invaluable insights, suggestions and corrections throughout the last four years.

I would also like thank Bob Mitchell for the hours of fun we had together looking for leaks in the cryostat and Tom McQueen for always seeming to have the right length of string when it was needed.

I would also like to thank Ralph, Tim and Nicole for not laughing at my results.

Financial support for the research was provided by SERC.

DEDICATION

I would like to dedicate this thesis to my mum and dad who may not understand a word of it but they think its marvellous and love me all the same.

I would also like to remember the support and encouragement of Mr. Ralph Hulme who died tragically before seeing this thesis finished. Though a Chemist he forgave me for studying Physics and he and his wife helped change the course of my life.

CONTENTS

Chapter 1

Introduction

		Page
1.1	**Historical**	**1**
1.2	**This Thesis**	**2**
1.3	**References**	**6**

Chapter 2

Auger Quenching in ZnSe:Mn & ZnS:Mn

		Page
2.1	**Introduction**	**8**
2.2	**Theoretical Background to Auger Quenching**	**9**
2.3	**Electrical Measurements**	
2.3.1	Introduction	12
2.3.2 a	ZnSe:Mn	13
2.3.2 b	Results	13
2.3.3 a	ZnS:Mn	17
2.3.3 b	Results	19
2.4	**Optical Measurements**	
2.4.1	Introduction	23
2.4.2	Spectral Measurements	23
2.4.3	Results	26
2.4.4	Summary	31
2.4.5	Intensity Quenching Measurements	34
2.4.6	Quenching Results	34
2.4.7	Summary	42
2.4.8	Lifetime Measurements	42
2.4.9	Results	43
2.4.10	Summary	45

2.5 Calculation of Auger coefficients

2.5.1 Introduction 47

2.5.2 Results 49

2.5.3 Summary 56

2.6 Concluding Remarks 59

2.7 Appendix 61

Design and Construction of a Short Duration Flashlamp for Photoexcitation

2.7 References 68

Chapter 3

Theory of Impact Excitation Cross-sections

Page

3.1 Introduction 70

3.2.1 Theory : Introduction 70

3.2.2 Derivation of Cross-section 70

3.2.3 First Evaluation of Matrix Integral 75

3.2.4 Second Evaluation of Matrix Integral 76

3.2.5 Momentum Integral 77

3.2.6 Evaluation of $|x_{eg}|^2$ 77

3.2.7 Degeneracy 78

3.3 Further Approximations 79

3.4 Physical Interpretation of Cross-section

3.4.1 Parabolic-Band Cross-section 80

3.4.2 Partially-Parabolic-Band Cross-section 81

3.4.3 Non-Parabolic-Band Cross-section 85

3.5 Conclusion 90

3.6 References 91

Chapter 4

Calculation of Impact Excitation Cross-sections for Three Transitions of Er^{3+} in ZnS

		Page
4.1	**Introduction**	**93**
4.2	**Description of Er^{3+} Excitations**	**95**
4.3	**Description and Choice of the Band Structures**	**96**
4.4	**Digitalisation of the Band Structure**	**98**
4.5	**Calculation of the Cross-sections**	**101**
4.6	**Discussion**	
4.6.1	Parabolic Band Cross-Sections	105
4.6.2	Partially-Parabolic-Band Cross-Sections	105
i)	2.36 eV Excitation	107
ii)	2.25 eV Excitation	110
iii)	1.25 eV Excitation	112
iv)	Summary	113
4.7	**Comparison with other Cross-Sections**	**114**
4.8	**Concluding Remarks**	**117**
4.9	**References**	**119**

Chapter 5

Hot Electron Distribution Functions

		Page
5.1	**Introduction**	**121**
5.2	**Background Theory and Calculation of Emission Intensities**	
5.2.1	Introduction	122
5.2.2	The Rate Equation	125
5.2.3	Approximation of the Electron Velocity $\upsilon(E)$	125

5.2.4	Approximation of the Impact Cross-section $\sigma(E)$	125
5.2.5	The Electron Distribution Functions $n(E)$	
a)	Introduction	127
b)	Theoretical Electron Distribution Functions	128
c)	Discussion and Experimental Evidence for Electron Distributions	130
5.3	**Evaluation of the Impact Excitation Rate**	
5.3.1	Introduction	133
5.3.2	Mathematical Evaluation	133
5.3.3	Experimental Evaluation of Impact Rate Equation : Thin Films	137
5.3.4	Experimental Evaluation of Impact Rate Equation : Schottky Diodes	142
5.4	**Critique of Other Work**	
5.4.1	Critique of Mathematical Evaluation of Rate Equation	155
5.4.2	Critique of Experiments on Thin Film Devices	157
5.4.3	Critique of Experiments on Schottky Diodes	158
5.5	**Conclusion**	160
5.6	**References**	163

Chapter 6

Conclusions

		Page
6.1	**Conclusions**	166
6.2	**Future Work**	168
6.3	**References**	170

Chapter 1

Introduction

1.1 Historical

Luminescence is the term given to the emission of light from a body by any process other than thermal excitation. Luminescent materials are often called phosphors and if the emission is the result of electrical excitation this is called electroluminescence. Electroluminescence was first reported in silicon carbide by Round [1.1] in 1907. In 1923 Lossev [1.2] produced electroluminescence from silicon carbide by directly applying an a.c. or d.c. voltage to the carbide. However this was not a practical method of producing light.

Luminescence was first electrically induced in ZnS by Destriau in 1936 [1.3]. He suspended particles of ZnS powder in oil which was then poured between two parallel-plate electrodes. When an a.c. voltage was applied to the plates the ZnS phosphor emitted light. Little attention was given to these observations until the development of the transparent conductive SnO_2 film. If one of the electrodes were replaced by a glass plate covered with a transparent conductive film then the emitted light would escape and a large area display could be made. Until the advent of the light emitting p-n junction in 1952 [1.4] these powder panel devices were the only electronic light sources available. When the p-n junction appeared it was a far more practical device and especially suitable for indicator lights which had previously been of the hot filament type. However p-n junction could not be used for large area displays and so interest still continued in the powder panels.

Development progressed in the 50's with the oil being replaced by a solid insulator and many commercial devices appeared based on this idea. Two reviews of the time outlined the understanding, problems and uses of the devices [1.5, 1.6]. These displays tended to be unreliable, of short working life and of insufficient brightness to give the good contrast required in moderate ambient light. Work using thin films or single crystals of ZnS was hampered by poor technology at the time and so research was concentrated on powder panels until the early 70's. By 1973 the d.c. electroluminescent powder panel seemed to be the best option in the field of large area displays [1.7].

In 1974 Inoguchi et al announced that they had produced a high brightness a.c. electroluminescent thin film of ZnS:Mn which had a long lifetime [1.8]. These devices were not formed from powdered phosphors but from a deposited thin film. Creation of such devices was made possible by the adaptation of new thin film growth techniques developed for micro-chip production. These devices consisted of a glass plate coated in a transparent conducting film. On to this film was deposited a thin insulating layer. A thin phosphor film was then deposited onto the insulating layer and a second insulating layer deposited onto the phosphor layer. An electrical contact was then attached to the last insulating layer. The insulating layers limited the current in the device to that which flowed due to the capacitive nature of the films and hence the need to use an a.c. driving voltage. The whole sandwich structure was then encased to protect against moisture. This design of device was found to have good contrast, high brightness and excellent stability. With this breakthrough some companies were encouraged to return to commercial production, notably Lohja and Sharp. Current development in these thin films has involved using different structures and phosphors as thin film technology has progressed. However there is still only a limited understanding of how the phosphor is excited by the electric current.

1.2 This Thesis

Details of the processes occurring in thin films are still sketchy and have been reviewed from time to time [e.g. 1.9]. Four simple stages can be conceived;

1) Electron production from traps, donors, defects, interfaces etc.

2) Electron acceleration to optical energies by the internal electrical field.

3) Luminescent centre excitation by the energetic electrons.

4) Photon emission by the centre.

Photoluminescence studies have enabled a detailed analysis of the fourth stage and consequently this is well understood. However the first three stages always occur simultaneously though they may be spatially separated as in Schottky diodes.

In this thesis we were mainly concerned with stage three, the excitation of the luminescence centre. The efficiency of the excitation process (and consequently of the whole device) is dependent upon three factors (as outlined in Chapter 5);

a) The velocity / flux of the energetic electrons.

b) The fraction of the electrons of optical energy

c) The cross-section for the interaction between the energetic electrons and the luminescence centre.

The electron velocity can be derived from the dispersion relation. The electron distribution and the cross-section are more difficult to determine because experiments in electroluminescence measure only the combined effect of these two factors.

Photoluminescence can be used to measure Auger quenching, a process which is the time reversal of impact excitation. From the strength of this quenching mechanism the impact excitation cross-section may be estimated. This was previously done by Gordon et al [1.10] for ZnS:Mn and the Mn cross-section estimated to be about 10^{-16} cm^2 . This value agrees with the experimental cross-section of Mach & Müller [1.11]. Mach & Müller calculated their cross-section from the efficiency needed in their devices to produce the light measured from the current that was know to be flowing in the device. They assumed that all the electrons were of optical energy and so their cross-section must be a lower limit to the true cross-section. Their cross-section also assumes that the excitation process is by impact excitation of the Mn and not by energy transfer from other centres in the device.

In Chapter 2 we use improved experimental and analytical techniques to measure the Auger process for the first time in ZnSe:Mn and to re-measure the Auger quenching in ZnS:Mn. The quenching was measured by intensity and lifetime measurements and related to electron concentration by resistivity and Hall effect measurements. We found the Auger coefficients to be similar and of about 5 $x10^{-10}$ cm^3 s^{-1}. For a purely direct transition these values should have been different from one another with the coefficient for ZnSe:Mn being an order of magnitude greater than for ZnS:Mn because of the shorter Mn lifetime in ZnSe. The coefficients were also many orders larger than predicted by the simple theories of Allen and Langer [1.12, 1.13] based on a simple direct type electric dipole interaction. From this we

propose that the interaction is not a pure direct interaction but involves a significant exchange component.

In Chapter 3 we considered a theoretical derivation of the impact cross-section which we compared with previous work by Yu & Shen [1.14, 1.15]. In our theory we included the effect of a real band structure making no assumptions about parabolic energy variation. We then introduced further approximations allowing for the lower part and then the whole of the conduction band to have a parabolic energy dependence. We found that Yu & Shen's cross-section contained an algebraic error of $(2\pi)^3$. We found that the cross-section could be enhanced by an order of magnitude over the previous simple cross-section by Yu & Shen which used a parabolic conduction band.

In Chapter 4 we applied this theory to Er in ZnS for comparison with experimental results from Luo et al [1.16]. The calculated cross-sections were not in keeping with the experimental values. However it was noted that the calculation of the cross-section was difficult because of uncertainty about the true radiative lifetimes of the excited states. To account for the discrepancy with the experimental values it was proposed that the exchange process may have been considerably enhanced in the experiments or that there was significant energy transfer occurring. In either case it was felt that direct comparison of the Er and Mn cross-sections was premature before the excitation process is firmly established.

In Chapter 5 we turned our attention to the electron distribution and considered experimental evidence from Bryant and co-workers [1.17, 1.18, 1.19] that claimed to demonstrate the type of electron distribution present. We considered how the emissions from different excited states should depend upon the electron distribution for a Maxwell-Boltzmann or Druyvesteyn electron distribution and found some mistakes in the derivation of the excitation rate equations. We found that when correctly analysed this data sometimes favoured the Maxwell-Boltzmann distribution, sometimes the Druyvesteyn distribution and sometimes neither. We noted that for the Schottky diodes the excitation process was unlikely to be impact excitation by hot electrons. This was because the electric fields present were insufficient to accelerate the electrons to optical energies within the implantation region of the diodes. The results from thin films were more convincing and we concluded that the electron distribution

may have been exponentially decreasing with energy but that the precise form could not as yet be determined and may be dependent upon the device and conditions of operation. No definite conclusion could be drawn because of the uncertainty about the precise nature of the excitation process occurring in the experiments considered. It had previously been assumed that the excitation was by impact excitation but this has not been shown to definitely be the case and for the diodes impact excitation seems very unlikely.

References

[1.1] H.J.Round *Electrical World* **February 9** (1907) 309

[1.2] O.W.Lossev *Phil. Mag.* **6** (1928) 1024

[1.3] J.Destriau *J.Chim.Physique* **33** (1936) 587

[1.4] J.R.Haynes & H.B.Briggs *Phys. Rev.* **86** (1952) 647

[1.5] D.Curie *Progr. in Semiconductors* **2** (1957) 249

[1.6] W.W.Piper & F.E.Williams *Sol. Stat. Phys.* **6** (1957) 95

[1.7] A.Vecht, N.J.Werring, R.Ellis & P.J.F.Smith *Proc. IEEE* **61** (1973) 902

[1.8] T.Inoguchi, M.Takeda, Y.Kakihara, Y.Nakata & M.Yoshida *S.I.D.Intern. Sym. Dig.* (1974) 86

[1.9] H.-E.Gumlich *J.Lumin.* **23** (1981) 73

[1.10] N.T.Gordon & J.W.Allen *Solid State Comm.* **37** (1981) 441

[1.11] R.Mach & G.O.Müller *Phys.Stat.Sol.(a)* **81** (1984) 609

[1.12] J.W.Allen *J.Phys. C: Solid State Phys* **19** (1986) 6287

[1.13] J.M.Langer *J.Lumin.* **40/41** (1988) 589

[1.14] Jiaqi Yu & Yongrong Shen *J.Lumin.* **40/41** (1988) 769

[1.15] Jiaqi Yu & Yongrong Shen *J.Phys. C:Solid State Phys.* **21** (1988) 3381

[1.16] Baozhu Luo, Jiaqi Yu & Gou-zhu Zhong *J.Lumin.* **40/41** (1988) 786

[1.17] G.Z.Zhong & F.J.Bryant *J.Lumin.* **24/25** (1981) 909

[1.18] A.Krier & F.J.Bryant *Phys. Stat. Sol. (a).* **83** (1984) 315

[1.19] S.Buddhudu, W.E.Hagston, M.J.R.Swift & A.J.Waring *J.Phys. C: Solid State Phys.* **21** (1988) L725

Chapter 2

Auger Quenching in ZnSe:Mn & ZnS:Mn

		Page
2.1	**Introduction**	**8**
2.2	**Theoretical Background to Auger Quenching**	**9**
2.3	**Electrical Measurements**	
2.3.1	Introduction	12
2.3.2 a	ZnSe:Mn	13
2.3.2 b	Results	13
2.3.3 a	ZnS:Mn	17
2.3.3 b	Results	19
2.4	**Optical Measurements**	
2.4.1	Introduction	23
2.4.2	Spectral Measurements	23
2.4.3	Results	26
2.4.4	Summary	31
2.4.5	Intensity Quenching Measurements	34
2.4.6	Quenching Results	34
2.4.7	Summary	42
2.4.8	Lifetime Measurements	42
2.4.9	Results	43
2.4.10	Summary	45
2.5	**Calculation of Auger coefficients**	
2.5.1	Introduction	47
2.5.2	Results	49
2.5.3	Summary	56
2.6	**Concluding Remarks**	59
2.7	**Appendix**	61
	Design and Construction of a Short Duration Flashlamp for Photoexcitation	
2.7	**References**	68

Chapter 2

Auger Quenching in ZnSe:Mn & ZnS:Mn

2.1 Introduction

Auger processes form a large family of effects in the solid state in which energy is transferred between electrons. The particular Auger process that interests us is when an excited electron, bound to a luminescence centre, transfers its energy to a conduction electron. If the conduction electron then loses this energy non-radiatively this process can quench the luminescence normally seen with the relaxation of the centre. Unlike most Auger processes this quenching involves only one conduction electron and so is linearly dependent on the conduction electron concentration.

At present the most successful material used in commercial electroluminescence devices is ZnS:Mn . This material is preferred to ZnSe:Mn because there is less quenching at room temperature. However, thin film devices are difficult to investigate experimentally because the unknown internal field distribution makes analysis of any results difficult. To overcome this problem Allen and co-workers have used Schottky diodes to gain information on the electroluminescence mechanism. These diodes are treated in a Zn/Al melt to improve the conductivity and non-ohmic contacts added. Emission from such diodes is confined to a small region near the cathode. Quenching in these materials has been attributed [2.1] to the Auger process described above. Luminescence is therefore confined to the depletion region adjacent to the cathode. Similar effects have been observed in CdF_2:Mn by Langer et al [2.2, 2.3] and again this Auger process has been cited as the cause. Langer et al have attempted quantitative measurements of this Auger process in CdF_2:Mn [2.2, 2.3] and in CdF_2:Gd & CdF_2;Tb [2.4]. Their results have been found to agree within experimental error with theories developed by Allen [2.5] and Langer [2.6]. When Gordon measured this Auger quenching in ZnS:Mn [2.7, 2.8] he found it to be four orders of magnitude larger than theory predicted. The reason for this discrepancy is as yet unknown. Allen has noted [2.5, 2.8] that the energy separation of the Γ_1 and X_3 valleys in the conduction band is approximately the same as the excited state energy of the Mn. He has suggested that this creates a resonance because the conduction electron is promoted from one region of high density of states to another thus enhancing the probability of

transition. The low group velocity of electrons in a valley should also enhance the exchange component of the electron interaction between the conduction electron and the bound electron. Such a resonance effect does not occur in CdF_2 and so the approximate theories which consider only the direct term of the Auger process are sufficient. Enhancement of a different type of Auger process has been seen by Burt [2.9] in GaAlAsSb and this enhancement has also been closely linked with the band structure.

Since ZnSe has a similar band structure to ZnS one might expect the Auger process in this material to be enhanced as well. Allen et al [2.10] attempted to measure the Mn luminescence in Zn/Al treated samples of ZnSe:Mn. However no Mn emission was seen. Optical absorption and electroluminescence showed that the Mn was still present in the same state and concentration as before treatment. The absence of luminescence was attributed to very efficient Auger quenching. In this chapter we use less conducting samples of ZnSe:Mn in which the Mn photoluminescence returns when the conduction electrons freeze out onto the donors below room temperature. These experiments have been unsuccessful until now because the low carrier concentrations required can not be reliably controlled during the growth and conductivity treatment. Therefore it was necessary to examine many different samples to find some that were suitable for these measurements. Eventually the samples used were of untreated material which, though far more conductive than is normally expected, still had sufficiently low carrier concentrations. Why this particular growth should have had so many carriers is unknown. These quantitative measurements are an extension of the work by Gordon on ZnS:Mn [2.7, 2.8]. For comparison we also report measurements made on ZnS:Mn using improved experimental and analytical techniques. From these experiments we conclude that the electron interaction must include an appreciable exchange component.

2.2 Theoretical Background to Auger Quenching

The Auger process that interests us involves an electron in an excited state, bound to a luminescence centre. This electron normally returns to its ground state by emitting a photon. However it is possible for the electron to transfer its energy to a single conduction electron which then loses the energy via multiple-phonon collisions or by transfer to a non-radiative

centre. This type of Auger process provides a non-radiative relaxation path for the luminescence centre and so has the effect of quenching luminescence. One peculiarity of this Auger process is that it involves only one conduction electron and so is directly proportional to the electron concentration.

We define an Auger coefficient for this process such that the rate of quenching is the product of this coefficient and the free electron concentration. To measure this coefficient we need to be able to relate the measured radiative efficiency to the conduction electron concentration. Consider a material in which the luminescence centres are optically excited and relax by a purely radiative process. The rate at which the excited state population (N^*) changes with time is

$$\frac{dN^*}{d\tau} = A(N - N^*) - \frac{N^*}{\tau_r} \qquad (2.1)$$

where A is related to the excitation photon flux, N is the total number of luminescence centres and τ_r is the radiative lifetime. Provided that the photon flux is small (or the lifetime τ_r is short) the photo-excitation process never saturates and $N >> N^*$. If the excitation is constant and of a few lifetimes duration we reach a steady state situation where $dN^*/d\tau = 0$, and

$$AN - \frac{N^*}{\tau_r} = 0$$

so

$$N^* = AN\tau_r . \qquad (2.2)$$

In reality the decay will not be purely radiative because of a number of non-radiative relaxation processes. In particular two Auger processes can occur involving free conduction electrons in the Γ_1 valley or weakly bound donor electrons. These processes each have different Auger coefficients γ_f and γ_b respectively. Gordon has estimated that γ_f is 1000 times larger than γ_b in ZnS for Mn [2.7]. Extending his calculations to ZnSe for Mn we find γ_f to be 450 times larger than γ_b . Langer et al [2.3] find for Mn in CdF_2 that γ_f is 400 times greater than γ_b . We can write the total Auger rate as

$$R_{Aug} = N^* \left[(n_o - n_e)\gamma_b + n_e \gamma_f \right] . \qquad (2.3)$$

Normally n_o (the concentration of uncompensated donors) is much greater than n_e (the free electron concentration) assuming extrinsic conduction.

We can allow for thermally independent non-radiative relaxation routes by a net decay rate $R_{nr} = N^*/\tau_{nr}$. Evidence for such processes has been found by Chimczak & Allen [2.11]. The total steady state equation then becomes

$$A N = N^* \left(\frac{1}{\tau_r} + \frac{1}{\tau_{nr}} + n_o \gamma_b + n_e \gamma_f \right)$$
$$= N^* \left(\frac{1}{\tau_o} + n_e \gamma_f \right) \qquad (2.4)$$

where τ_o is the lifetime of the excited state as measured at 4K when most of the free electrons will have frozen onto the donors so that n_e is approximately zero.

Rewriting (2.4) in the same way as (2.2) gives the excited centre population as

$$N^* = A N \left(\frac{1}{\tau_o} + n_e \gamma_f \right)^{-1}$$
$$= A N \tau(T) \qquad (2.5)$$

where $\tau(T)$ is the lifetime of the excited state at temperature T. The emission intensity of the centres is given by

$$I = \frac{N^*}{\tau_r} \qquad (2.6)$$

but τ_r can not be measured because even at 4K there are still non-radiative processes occurring. If we consider emission at 4K, we can define this as I_o where

$$I_o = \frac{N_o^*}{\tau_r} \qquad (2.7)$$

and from (2.5) we have

$$I_o = A N \frac{\tau_o}{\tau_r} . \qquad (2.8)$$

Similarly at any temperature T we have

$$I(T) = A N \frac{\tau(T)}{\tau_r} . \qquad (2.9)$$

We do not know τ_r but if we define η as the radiative efficiency relative to the emission at 4K we find

$$\eta = \frac{I(T)}{I_o} = \frac{\tau(T)}{\tau_o} \qquad (2.10)$$

and expanding $\tau(T)$ from (2.5) gives

$$\eta = \frac{1}{1 + n_e \tau_o \gamma_f} \qquad (2.11)$$

Therefore, it is not necessary to know the true radiative lifetime, instead the Auger coefficient can be related to the lifetime and emission intensity measured at 4K. We assume that in (2.11) the only term with a strong temperature dependence is n_e .

For an extrinsic semiconductor with N_d donors and N_a acceptors the electron concentration is approximately given by

$$n_e = n_o \exp\left(- \frac{E_d}{k T} \right)$$
$$= \frac{\left(N_d - N_a \right) N_c}{N_a} \exp\left(- \frac{E_d}{k T} \right) \quad (2.12)$$

where E_d is the energy difference between the donor levels and the bottom of the conduction band. N_c is the effective density of the conduction band states and is given by

$$N_c = 2\left(\frac{m^* k T}{2 \pi \hbar^2} \right)^{\frac{3}{2}} \quad (2.13)$$

where m^* is the effective electron mass in a parabolic conduction band. The total temperature dependence of the electron distribution may be described by

$$n_e = \beta T^{\frac{3}{2}} \exp\left(- \frac{E_d}{k T} \right) \quad (2.14)$$

where $$\beta = 2\left(\frac{N_d - N_a}{N_a} \right)\left(\frac{m^* k}{2 \pi \hbar^2} \right)^{\frac{3}{2}}.$$

Combining (2.11) and (2.14) we have

$$\eta(T) = \frac{I(T)}{I_o} = \frac{\tau(T)}{\tau_o} = \left(1 + \gamma_f \beta \tau_o T^{\frac{3}{2}} \exp\left(\frac{-E_d}{k T} \right) \right)^{-1} \quad (2.15)$$

Using equations like (2.11) and (2.15) one can use experimental results to show the relationship between the measured radiative efficiency and the free electron concentration. By plotting η with n_e or T in an appropriate manner one can check the linear relationship between these factors and if satisfactory derive a value for the Auger coefficient. If a fully insulating piece of material is available with no Auger quenching or other non-radiative processes it may be possible to measure τ_r in (2.4) and derive a value for γ_b .

2.3 Electrical Measurements

2.3.1 Introduction

Optical measurements of lifetime and emission intensity give a value for the radiative efficiency at any temperature. To relate this to the Auger coefficient we need to know the electron concentration at the same temperatures. It is not possible to make electrical measurements over the whole temperature range of the optical measurements, however sufficient measurements can be made to check that a linear relationship does exist.

Two different techniques are used to find the electron concentration. Where ohmic contacts can be formed a Hall effect measurement is used. Where non-ohmic contacts are made a frequency dependent impedance is measured from which the bulk resistance gives the electron concentration. These two techniques are outlined and results given.

2.3.2a ZnSe:Mn

Ohmic contacts were formed on ZnSe:Mn using indium metal. Samples of ZnSe:Mn were first roughly ground to shape using Carborundum then polished with jeweller's rouge to remove surface damage. The sample was then thoroughly cleaned in methanol and propan-2-ol and then etched in sodium hydroxide and hydrochloric acid. This removes any remaining surface damage and oxide coating. The samples were stored under propan-2-ol to prevent oxidation of the cleaned surfaces. Small pieces of cleaned indium wire were pressed onto the surfaces of the sample whilst under the propan-2-ol. For a Hall effect measurement the four contacts were placed on the four sides of the sample when this was possible. The sample was transferred to a heater on which it was raised to 420°C in a hydrogen/nitrogen reducing atmosphere for a few seconds. The indium melted at 170°C but a temperature of 420°C was required to ensure adequate alloying of the indium to the ZnSe:Mn.

Fine indium tinned wires were then added to the contacts and the I/V characteristic measured to check the ohmic quality. If good contacts were formed a room temperature Hall effect measurement was made to find the electron concentration. If this provided suitable results the sample was transferred to a more elaborate experiment where the Hall effect and resistivity were measured to low temperatures. The experimental set up did not however allow these measurements to be made above room temperature. During the low temperature measurements the sample current had to be constantly monitored as the sample resistance normally exceeded the limit of the apparatus below 220K.

2.3.2 b Results

A total of sixteen different samples of ZnSe:Mn were used. A number proved to be so conductive that the electrons were degenerate. Such samples were still Auger quenched at 4K and so unsuitable for any optical work. This was the same situation as reported earlier by Allen et al [2.10]. One of these samples [ZnSe:Mn(1)] is included in this chapter as an example.

It was found that all of the Zn/Al treated samples were too conductive and so a search was made of untreated material whose electron density only produced total quenching at or above room temperature. Two such samples were found [ZnSe:Mn(2),(3)] and are included here for comparison. Other samples of untreated material were so non-conducting that no electrical measurements could be made on them. One such sample [ZnSe:Mn(4)] was used in an attempt to show the effect of neutral donor quenching.

ZnSe:Mn(1)

The average electron concentration from 300K to 4K was found to be $n_e = 4 \pm 1 \times 10^{16}$ cm^{-3}. As the temperature dropped the resistivity began to rise but the Hall voltage remained within 50% of its room temperature value. This change was attributed to temperature drift over the time required to take the voltage readings (see ZnSe:Mn(3)) . At 4K the Hall voltage settled to a value close to that at room temperature. Despite the low concentration the electrons appeared to be degenerate.

The rise in resistivity could be due to contact problems or a change in the electron mobility. From 300 to 220K the resistivity increased by 60% which is small compared to the changes seen in the other samples. Assuming that this is a typical result the resistivity changes in the other samples must be due to changes in the electron concentration since they show resistivity changes in excess of 60%.

ZnSe:Mn(2)

Room temperature Hall effect measurements gave $n_e = 7 \pm 2 \times 10^{13}$. Resistivity only was measured below room temperature (figure 2.1) and assuming that the change in the electron concentration to be the dominant factor this gives an activation energy of 0.19 eV according to equation (2.14).

ZnSe:Mn(3)

Hall effect measurements were carried out for sample currents of 100μA (high temperatures) and 10μA (low temperatures). At room temperature (285K) the Hall effect gave an electron concentration of $n_e = 4 \pm 1 \times 10^{13}$ cm^{-3} . Hall effect (figure 2.2) and resistivity (figure 2.3) measurements were taken down to 220K but due to the long settling time most of the Hall

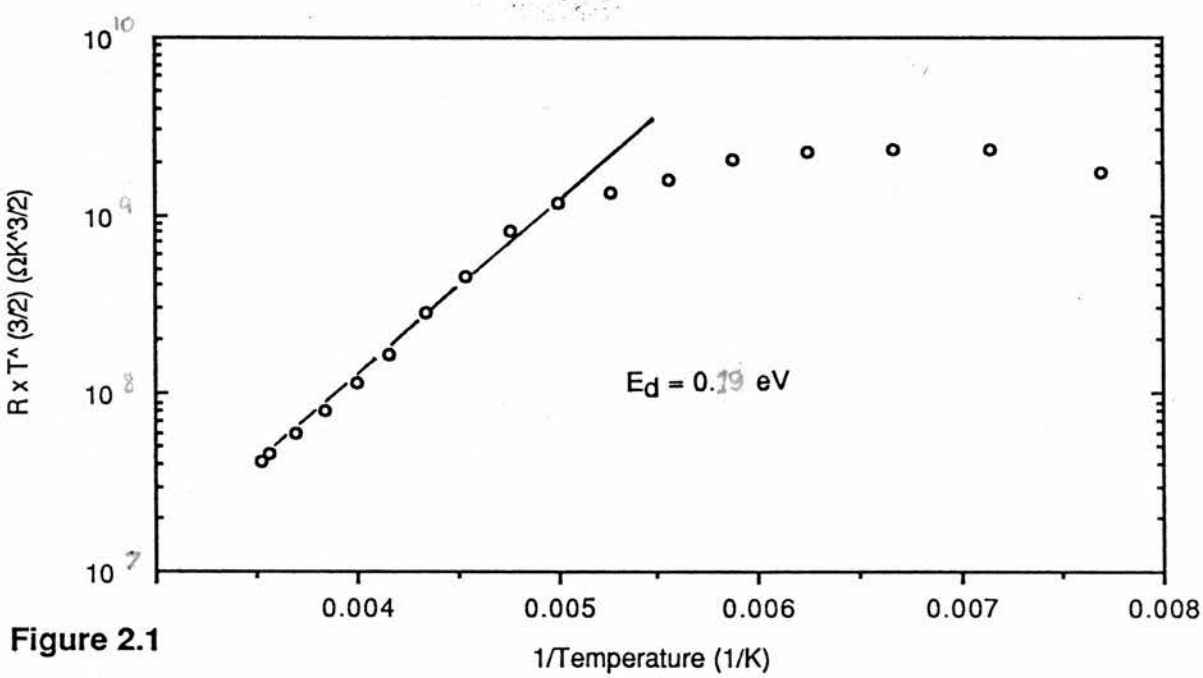

Figure 2.1

[ZnSe:Mn(2)]: Thermal dependence of resistance in accordance with equation (2.14) measured during the Hall effect experiment. Graph levels out when the sample resistance exceeds the experimental limit.

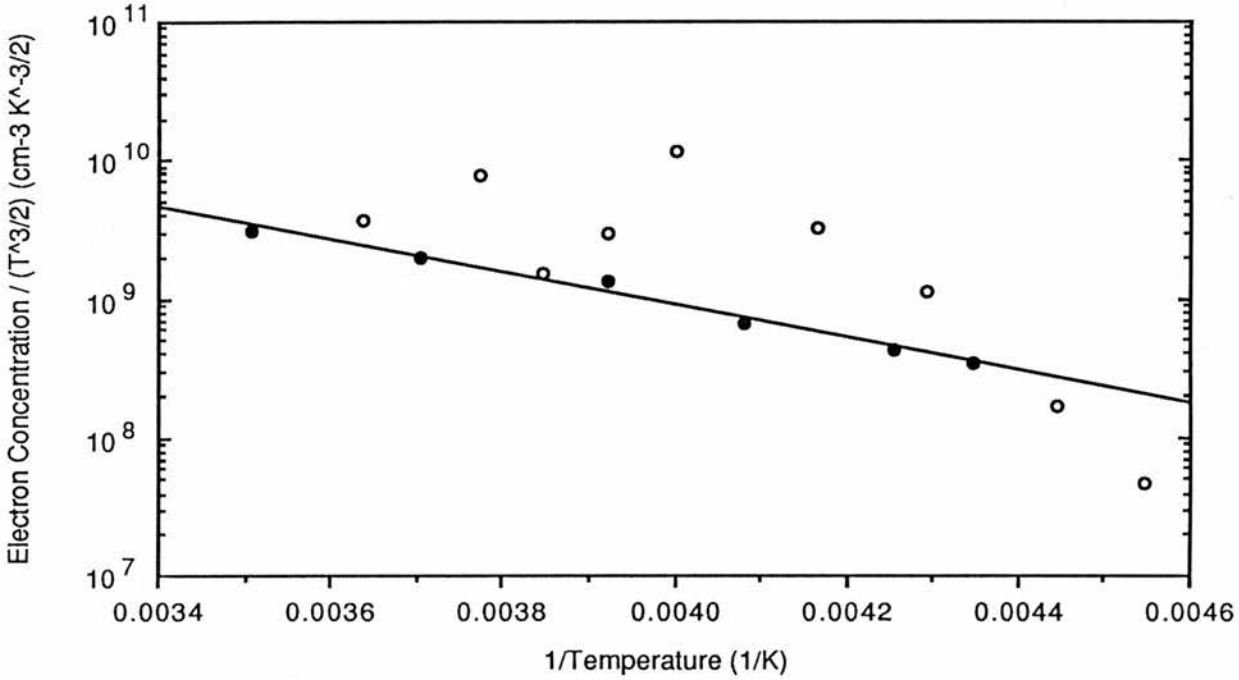

Figure 2.2 [ZnSe:Mn(3)]: Electron concentration as calculated from the Hall voltage (points considered as most reliable are shown as black dots).

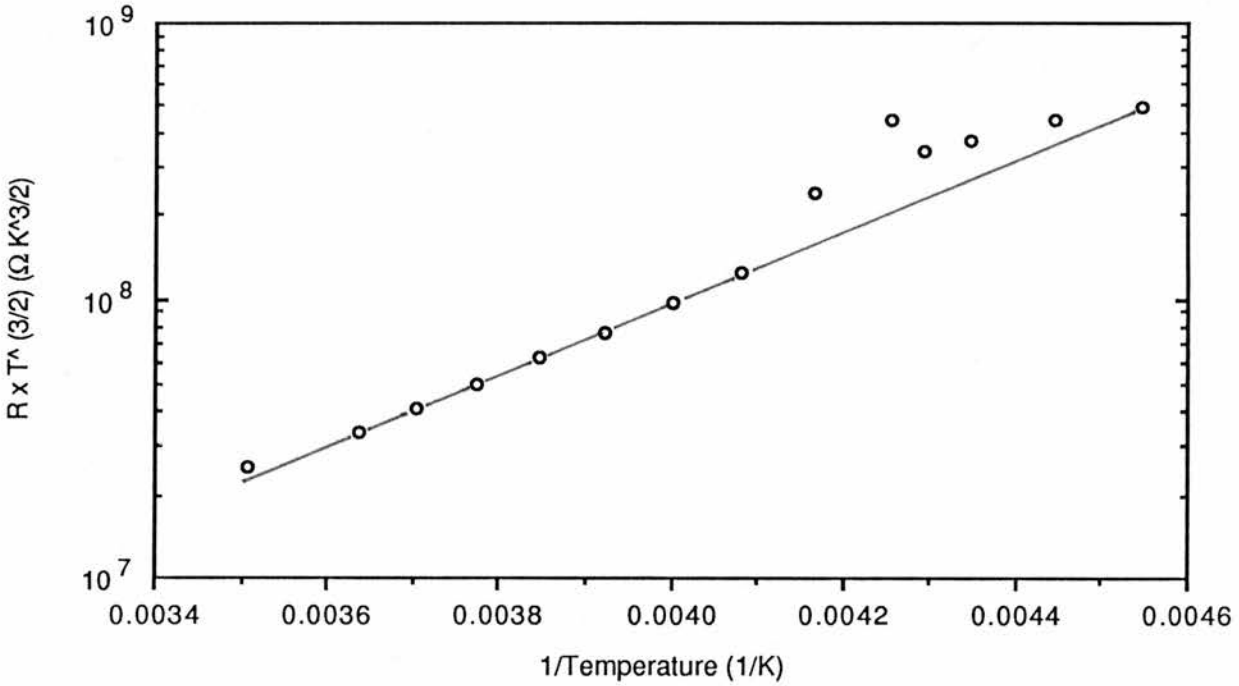

Figure 2.3 [ZnSe:Mn(3)]: Thermal dependence of resistance in accordance with equation (2.14) as measured during the Hall effect experiment.

data was unreliable. The activation energies were 0.23 eV for the Hall effect (using only selected data) and 0.25 eV for the resistivity.

ZnSe:Mn(4)

This sample was of very high resistance and no electrical measurements could be made. It was thought that the sample might contain very few uncompensated donors and hence the low electron concentration. In such a sample there would be little Auger quenching from either free electrons or neutral donors.

2.3.3 a ZnS:Mn

Electrical measurements on ZnS:Mn are more difficult than optical measurements. We needed to ensure that time was not lost making electrical measurements on samples that did not luminesce or which showed no change in quenching. Each sample was first tested under U.V. light for a Mn luminescence. The sample was then cooled in liquid nitrogen and again brought under the U.V. lamp. If the Mn luminescence did not increase or appear for the first time no contacts were added. Altogether eleven different samples were selected in this way.

Contacts were added in a similar way to those on ZnSe except that the sample need only be heated to 340°c to alloy the indium. Two samples out of the first four tried were found to have conducting contacts. The first sample was fairly ohmic but produced erratic Hall voltages. The second though non-ohmic in character gave a more consistent Hall voltage from which we calculated a room temperature electron concentration of $n_e = 6 \pm 4 \times 10^{15}$ cm^{-3}. This is the first sample (ZnS:Mn(1)) on which we attempted decay time measurements.

Since the Hall effect showed spurious results due to the rectifying behaviour of the contacts a new method was sought for finding n_e. Two aluminium contacts were evaporated onto the opposing faces of the sample producing good Schottky contacts. At low frequencies these contacts were highly resistive because of the barrier voltage and the depletion region. At KHz frequencies the contacts began to behave as a capacitor and resistance in parallel. The resistance was dominant and determined the current through the contact. At frequencies of tens of megahertz the capacitive nature of the contacts dominated offering little impedance to the current so that current through the sample now becomes limited by the bulk resistance. The model for the contacts is shown in figure (2.4).

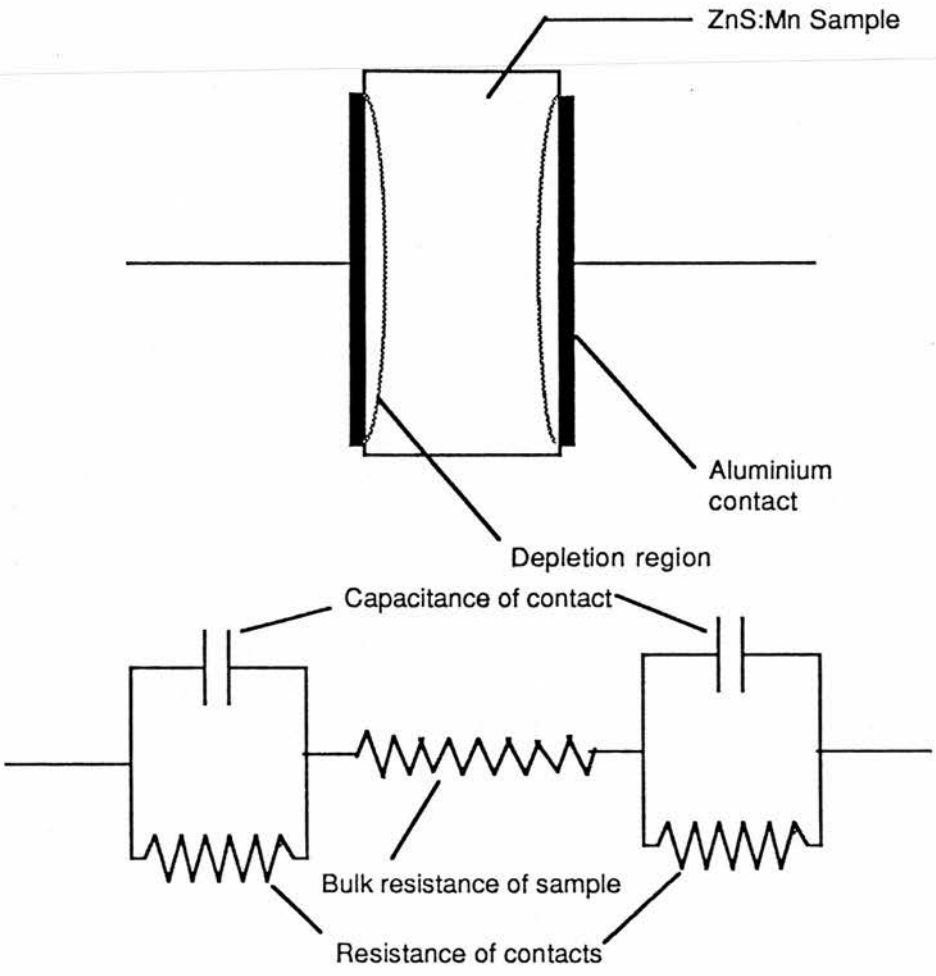

Figure 2.4 Equivalent circuit for a ZnS:Mn sample with two Schottky contacts.

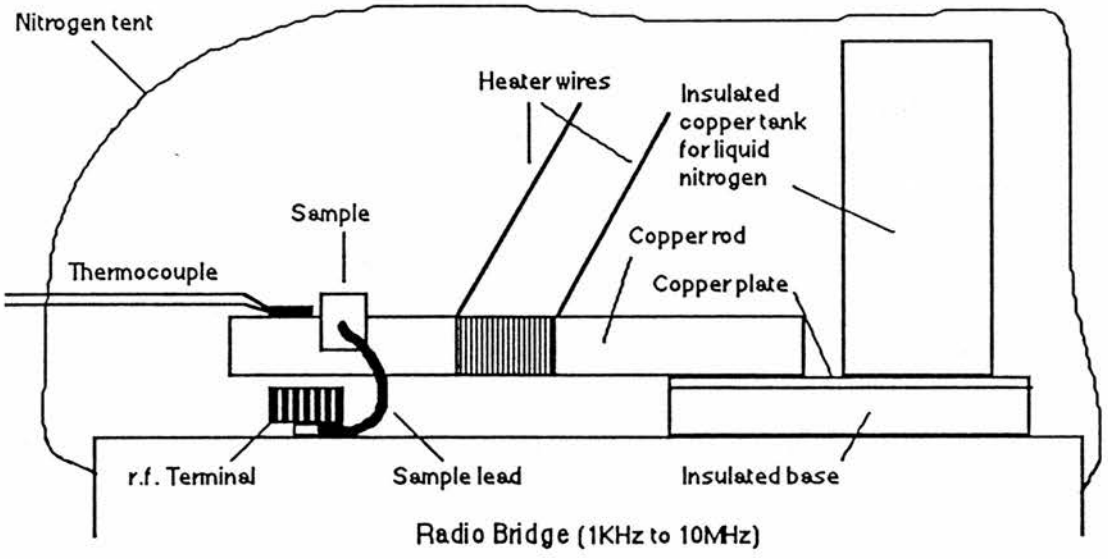

Figure 2.5 Experimental arrangement for measuring sample impedence over a wide temperature range.

The impedance of the sample above 10MHz is of the form

$$Z = \left[\left(\omega L - \frac{1}{\omega C} \right)^2 + R^2 \right]^{\frac{1}{2}} \qquad (2.16)$$

where $\omega = 2\pi$ x frequency , L is the inductance of the sample, C the capacitance and R the bulk resistance. As the frequency is increased Z (the impedance of the sample) tends to R.

When tested few of the samples gave reproducible results as might be expected due to the high frequencies we needed to work at. However two did give acceptable results [ZnS:Mn(2),(3)] and we attempted to measure their bulk resistance over different temperatures.To do this the samples were mounted on a heater as shown in figure 2.5 and secured to the top of a radio bridge. The temperature could be varied from 375K down to 210K. For low temperature work the top of the bridge was enclosed in a nitrogen tent to overcome condensation problems.

2.3.3 b Results

ZnS:Mn(1)

Hall effect measurements at room temperature using 10μA current gave $n_e = 6 \pm 4 \times 10^{15}$ cm^{-3}. No low temperature measurements were made because the high sample resistance meant that the Hall effect apparatus was already at its upper resistance limit.

ZnS:Mn(2)

A bulk resistance was calculated from the impedance (figure 2.6) to be 250 ± 25 Ω. From the physical dimensions of the sample this gave an electron concentration of $n_e = 4 \pm 1 \times 10^{13}$ cm^{-3} (assuming the electron mobility to be 150 cm^2 V^{-1}s^{-1} [2.12]). The bulk resistance was twice measured from 375K to 210K (figure 2.7) and similar activation energies were found; 0.10 eV in the first experiment and 0.12 eV in the second.

ZnS:Mn(3)

As figure (2.8a) shows this sample did not have a clear frequency dependence as expected from equation (2.16). If the capacitance is assumed to be dominant in equation (2.16) the impedance may be approximated as

$$Z = (\omega C)^{-1}. \qquad (2.17)$$

If we now plot the series resistance of the sample against 1/frequency we should see a straight line with an intercept equal to the bulk resistance at 1/frequency = 0. This is shown in

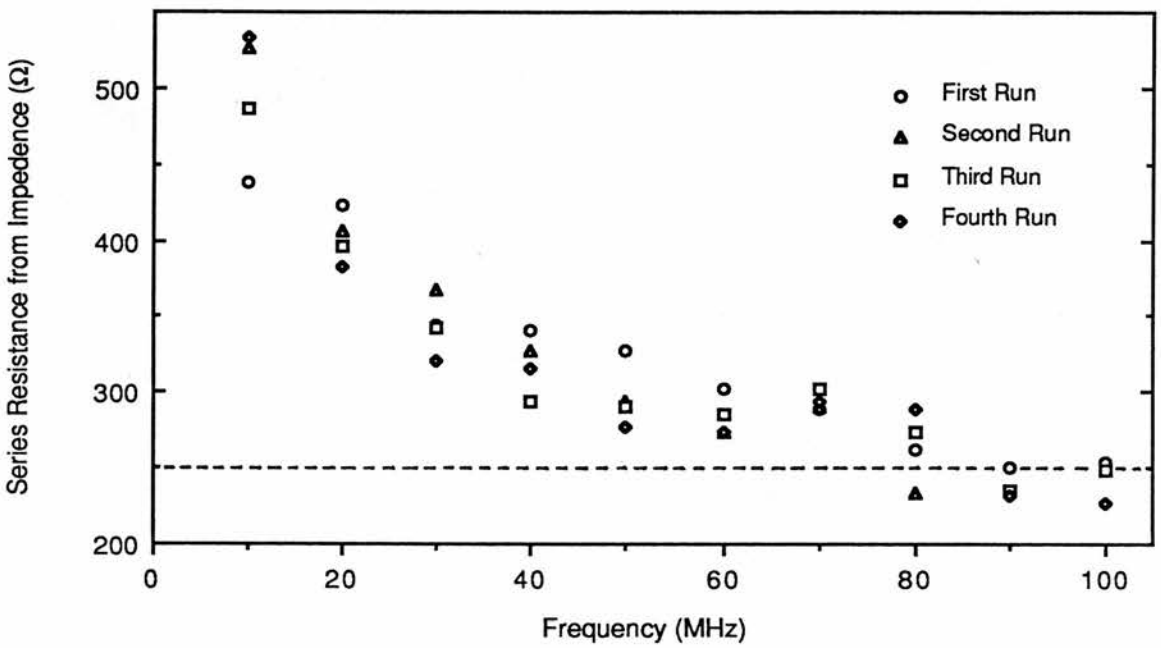

Figure 2.6 [ZnS:Mn(2)]: Four attempts at finding the bulk resistance of the sample from the frequency dependence of the series resistance.

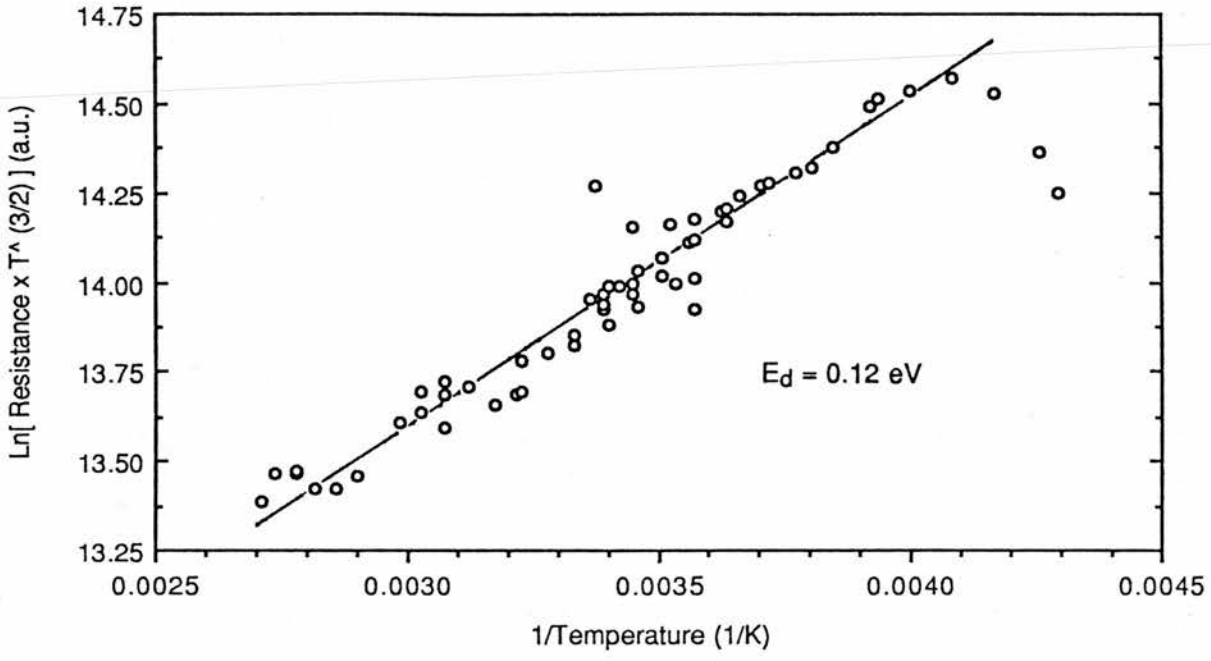

Figure 2.7a [ZnS:Mn(2)]: Thermal dependence of bulk resistance as determined from impedence measurements plotted according to equation (2.14).

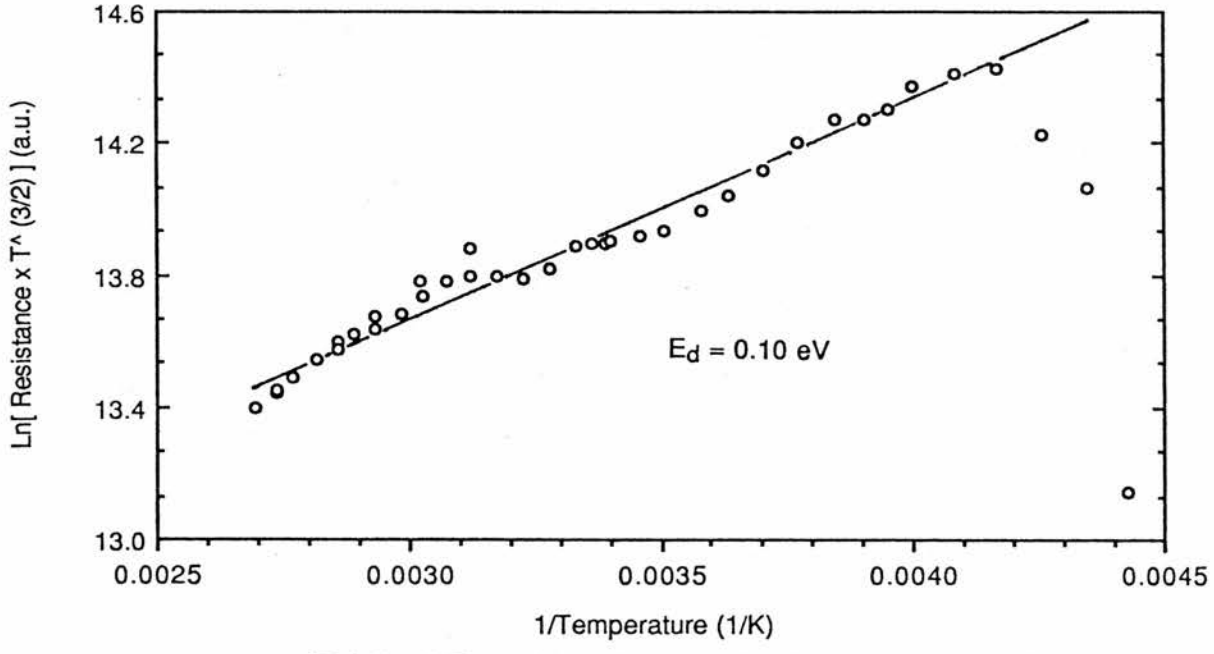

Figure 2.7b [ZnS:Mn(2)]: Thermal dependence of bulk resistance as determined from impedence measurements. Plotted according to equation (2.14).

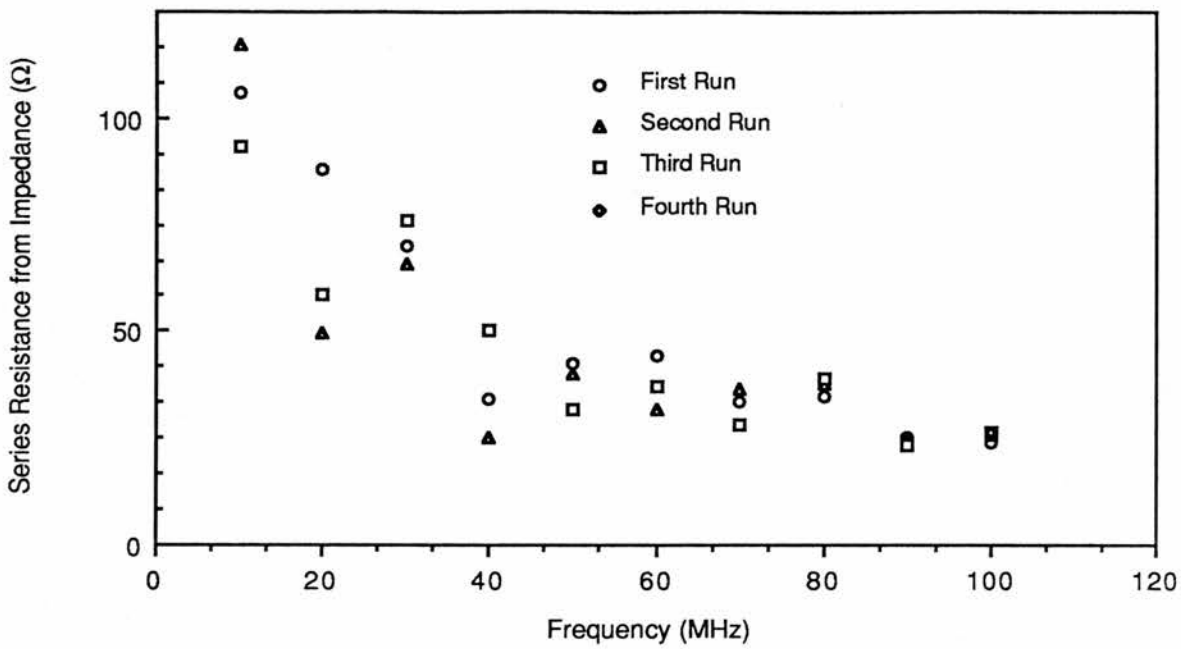

Figure 2.8a [ZnS:Mn(3)]: Four attempts to measure the frequency dependence of the bulk resistance as found from the series resistance of the impedence.

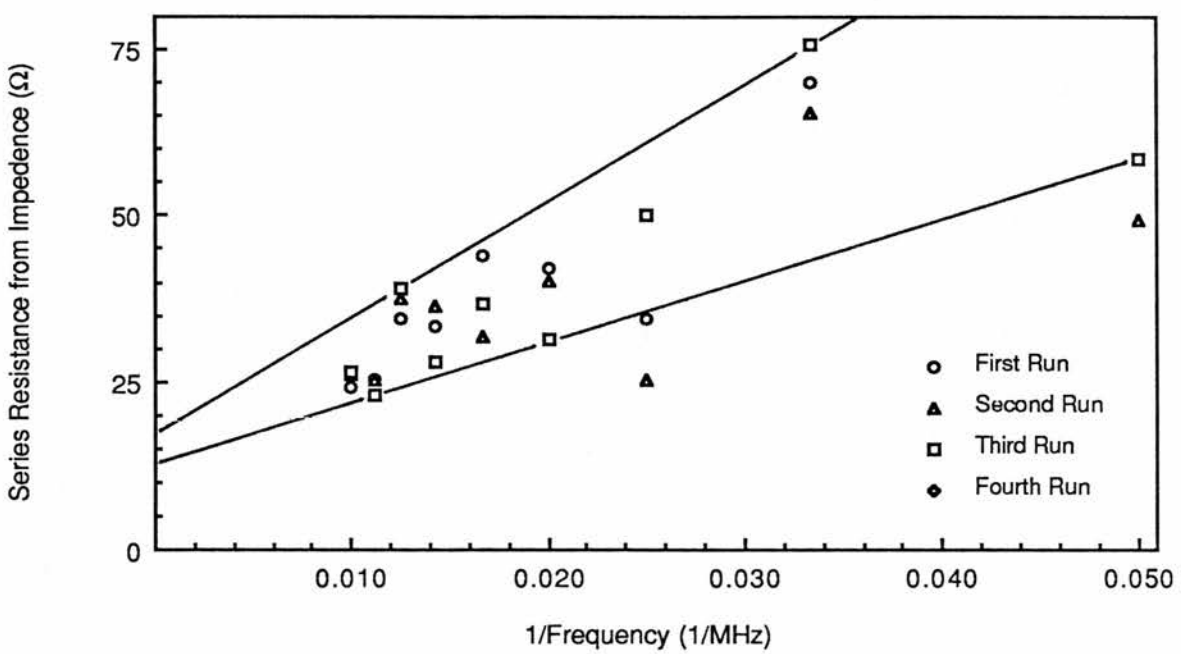

Figure 2.8b [ZnS:Mn(3)]: Plot of series resistance against 1/frequency in an attempt to find the bulk resistance of the sample.

figure 2.8b and from it the resistance is estimated to be 14 ± 1 Ω which from the physical dimensions of the sample gives an electron concentration of ne = 1.1 ± 0.1 x 10^{14} cm^{-3} . When the bulk resistance was measured to find the temperature dependence no consistent or sensible results were found.

2.4 Optical Measurements

2.4.1 Introduction

The motivation behind these optical measurements is two fold. First spectral measurements were used to identify the emissions centres that were present.This was important if we were later to have confidence in measuring the correct quenching process. Secondly intensity quenching or lifetime measurements were used to calculate the radiative efficiency relative to the 4K emission and from this calculate the Auger coefficient.

To perform these measurements we used an Oxford Instruments gas-flow cryostat which had straight-through windows. The sample was mounted directly over a hole through the sample holder as shown in figure (2.9) . The excitation light was directed through the first window onto the sample. The emission was collected from the back of the sample through the second window. This system allowed the maximum efficiency of excitation and collection of the emission. The sample temperature was continuously measured by a thermocouple fixed to the sample holder near the sample.

Various methods were tried for mounting the sample . The most successful was to use a copper sheet fixed rigidly to the holder by screws. A hole was punched through the sheet and the walls of the hole formed a cradle for the sample. The sample was fixed into place by clear nail polish which is optically inert down to 4K but decomposes above 375K giving the upper limit to our experiments.

2.4.2 Spectral Measurements

To identify and separate the emissions two experiments (figure 2.10) were used;

i) Excitation Spectra :Using an interference filter between the emission window and the photomultiplier one region of the emission was selected. The excitation light was passed through a monochromator and chopped before being focused onto the sample. The monochromator showed which excitation energies produce emission at selected frequencies.

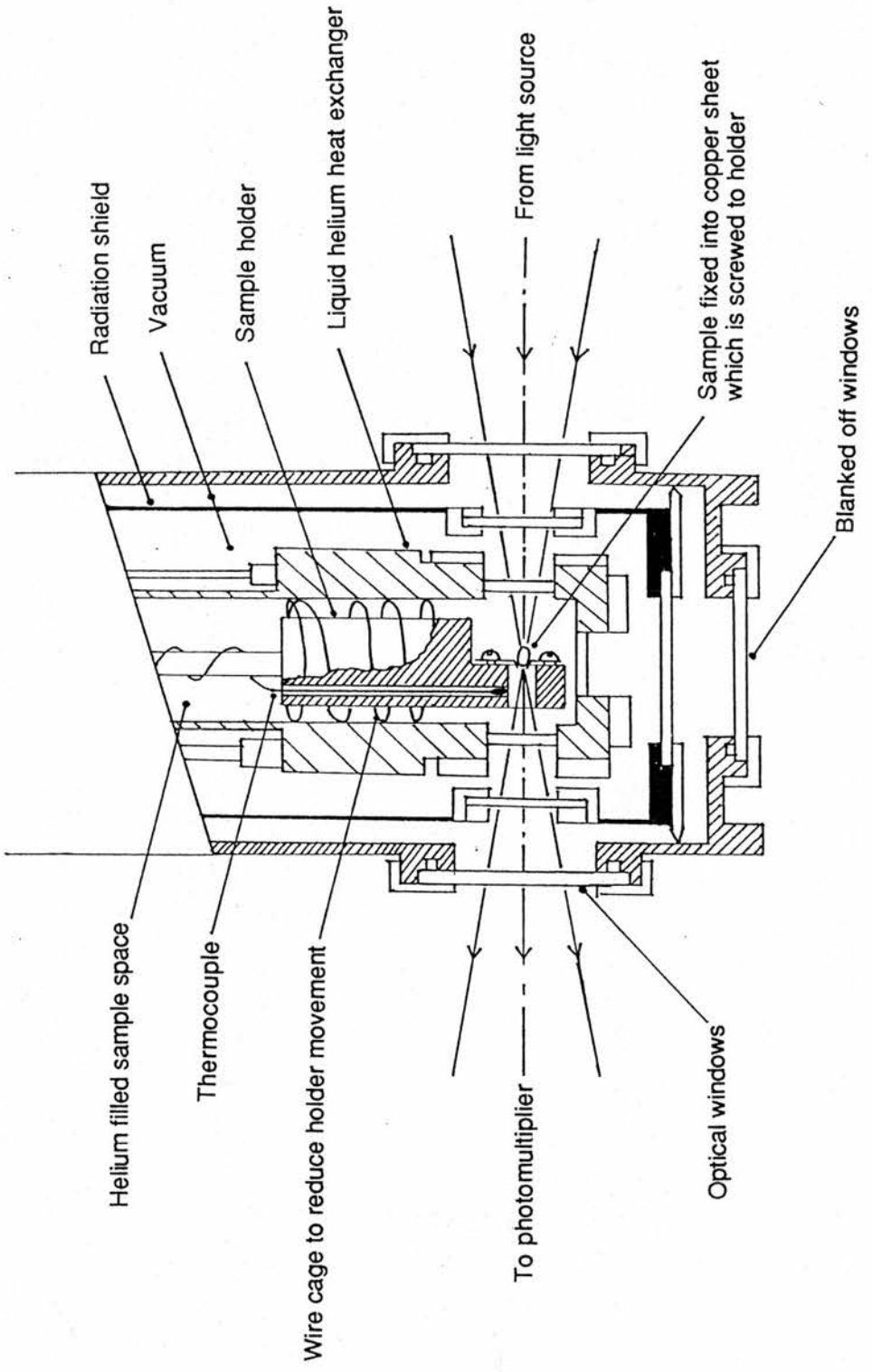

Figure 2.9

Optical arrangements in the cryostat for the excitation of samples and the measurement of emissions.

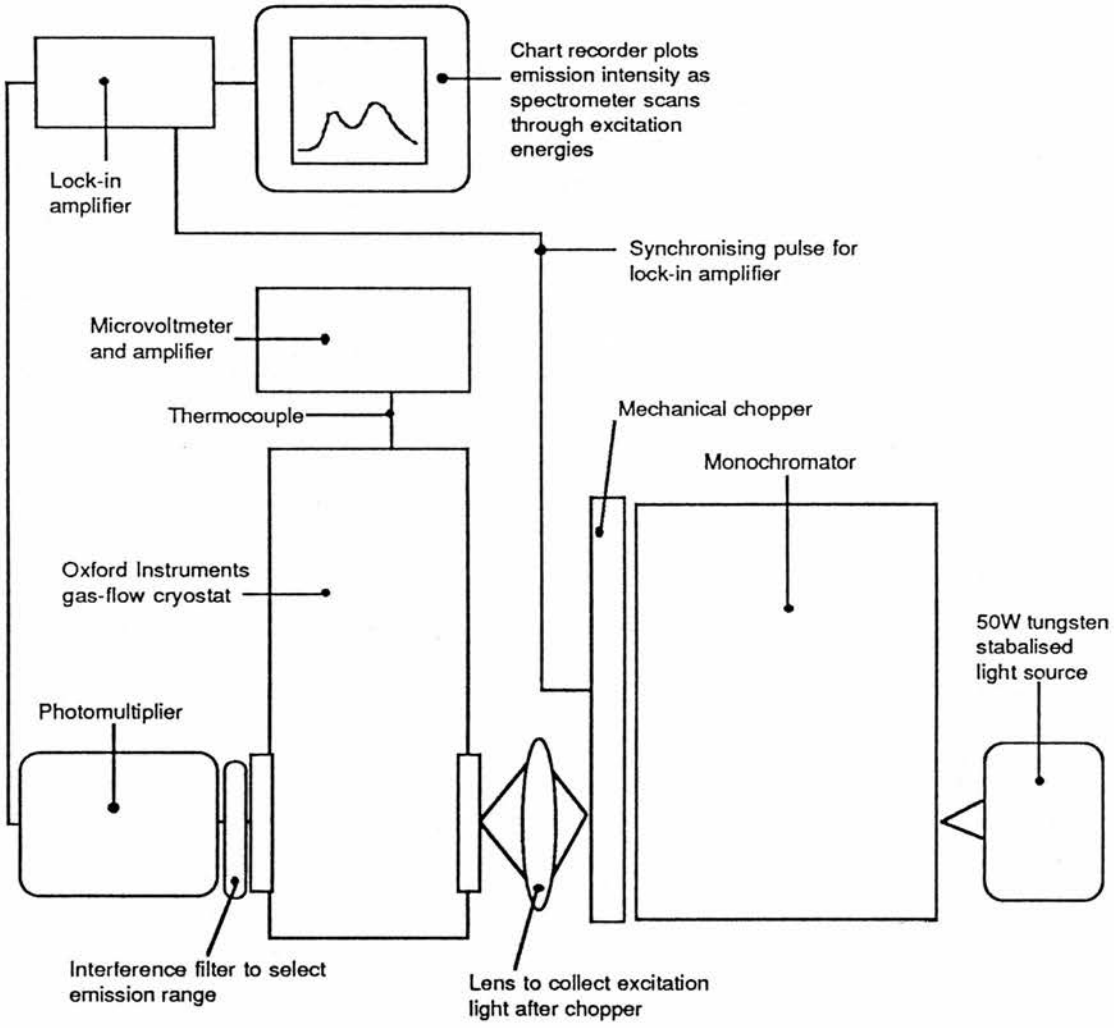

Figure 2.10 Experimental set up used to find the excitation spectra for emissions. A similar set up is also used for emission spectra with the positions of the light source and photomultiplier exchanged.

ii) Emission Spectra : The position of the light source and photomultiplier were exchanged so that now the sample was excited at fixed energies and the different emissions produced could be detected. Normally excitation was as close as possible to the excitation peaks in the first experiment.

None of these spectra were adjusted for the system response.

2.4.3 Results

ZnSe:Mn(1)

This sample showed no Mn emission as might be expected because of its high degenerate electron concentration ($4 \pm 1 \times 10^{16}$ cm^3). It was known that Mn was present because this was shown in an emission spectra for electroluminescence from this sample (figure 2.11). Instead a self-activated (S.A.) luminescence was seen which was either due to unintentional impurities or native defects in the ZnSe. This emission was best excited at 480nm as shown in figure (2.12) and had a broad band emission around 640nm as shown in figure (2.13) . The close proximity to the Mn emission and excitation meant that samples of low Mn concentration and/or strong S.A. emission could show odd effects. A similar emission to this had been found by Miranov [2.13] . They reported a shift in the emission peak from 640nm to 610nm after Zn/Al treatment and a further shift to 570nm with Al doping. We found that excitation at 440nm produced an increase in emission at 610nm (see ZnSe:Mn(2)).

ZnSe:Mn(2)

This sample clearly showed the Mn emission at 580nm which is characteristic of the $^4T_1$ - $^6A_1$ emission. This emission was found to be excited at 540nm ($^4T_2$) and 500nm (^4E, $^4A_1$) (figures 2.14, 2.15). The broad S.A. emission was also found but appeared to be insignificant when the Mn was correctly excited. There was evidence found for a second emission excited at 440nm and emitting from 510nm to greater than 600nm (figure 2.16). It was first thought that this might be a higher Mn excitation similar to that found by Gumlich [2.1] at 450nm in ZnS:Mn. Figure (2.17) shows that at 560 to 640nm the emission is due to an excitation at 455nm and that at greater than 660nm there is an emission excited at 440nm. The 455nm peak we then associate with Mn and the 440nm peak with a second S.A. emission. An electroluminescence spectra showed the same Mn emission as seen in ZnSe:Mn(1) (figure 2.11).

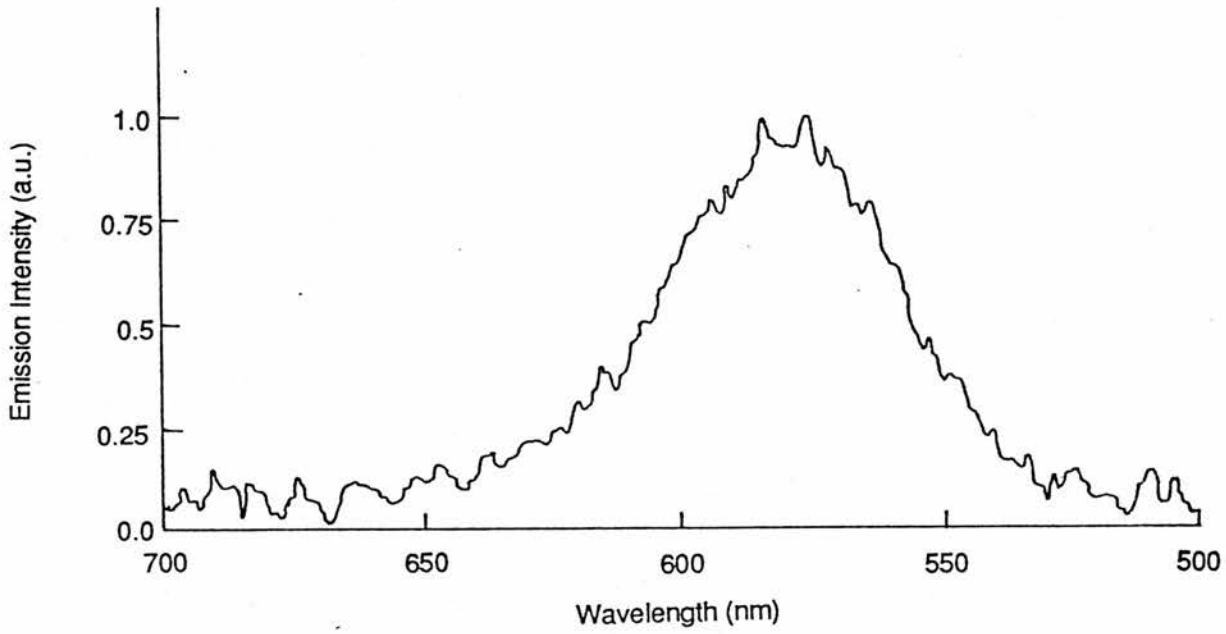

Figure 2.11 [ZnSe:Mn(1)]: Electroluminescence spectra at room temperature for 150μA current in reverse bias.

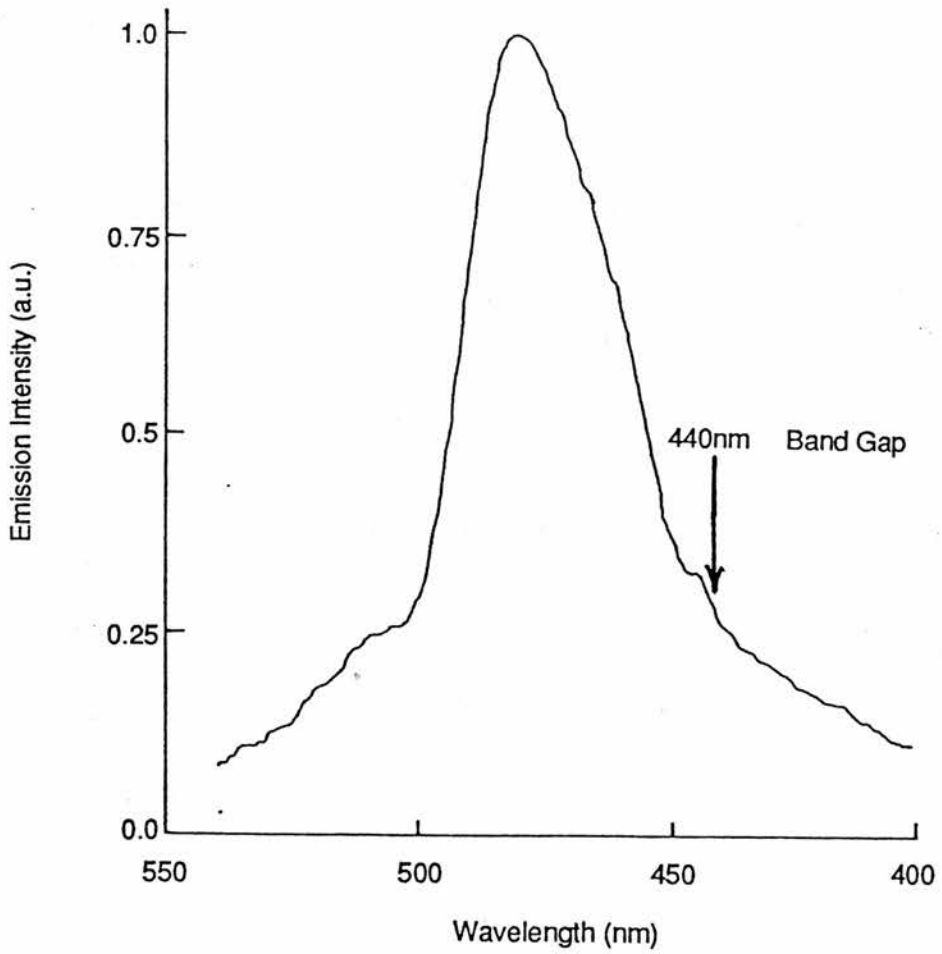

Figure 2.12 [ZnSe:Mn(1)]: Excitation spectra at 4K for S.A. emission at 640nm.

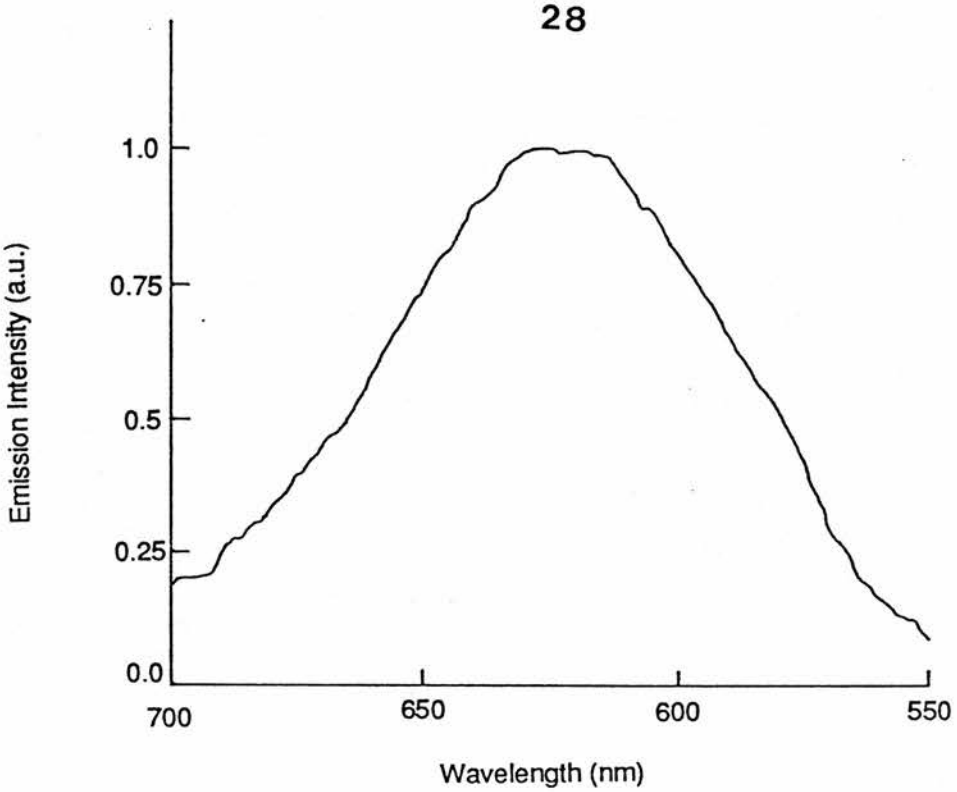

Figure 2.13 [ZnSe:Mn(1)]: Emission spectra at 4K for S.A. emission excited at 480nm

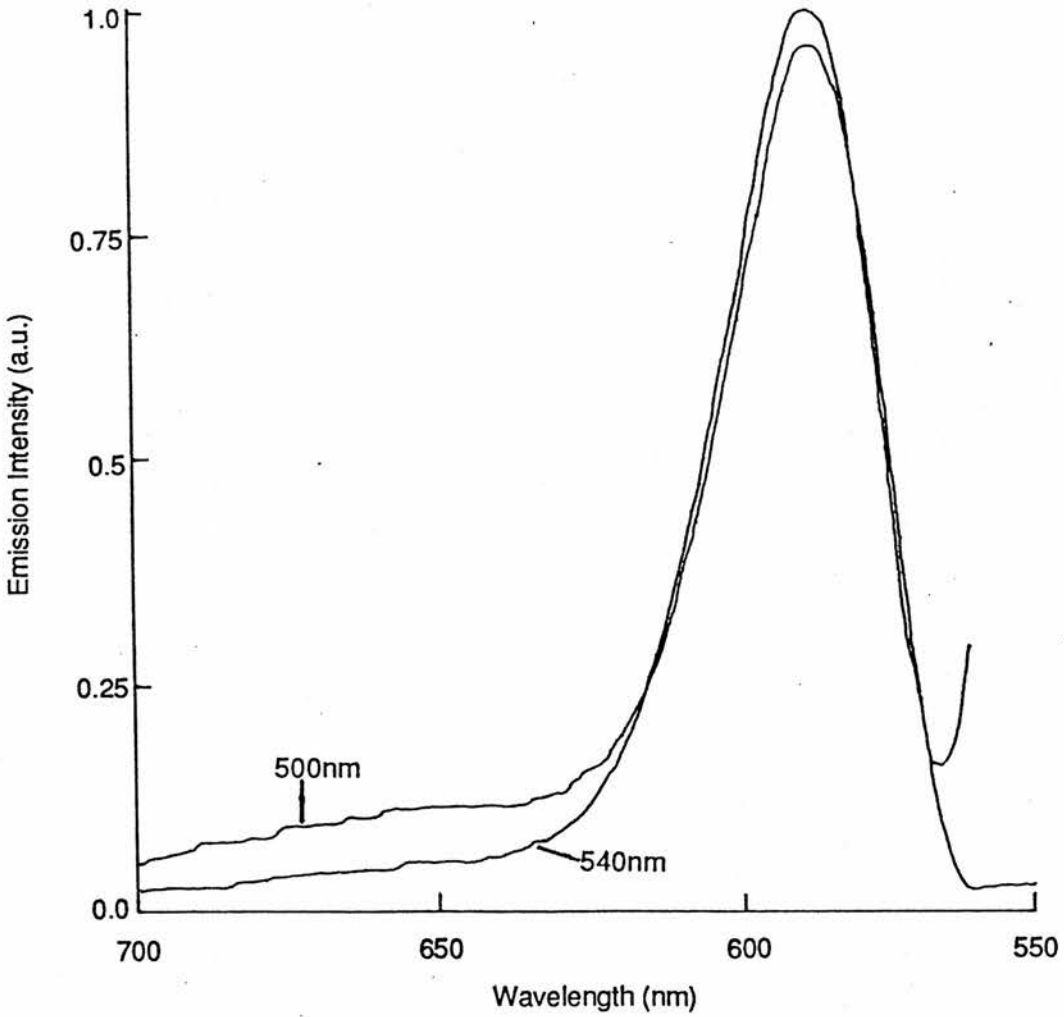

Figure 2.14 [ZnSe:Mn(2)]: Emission spectra at 4K for Mn excited at 500nm and 540nm.

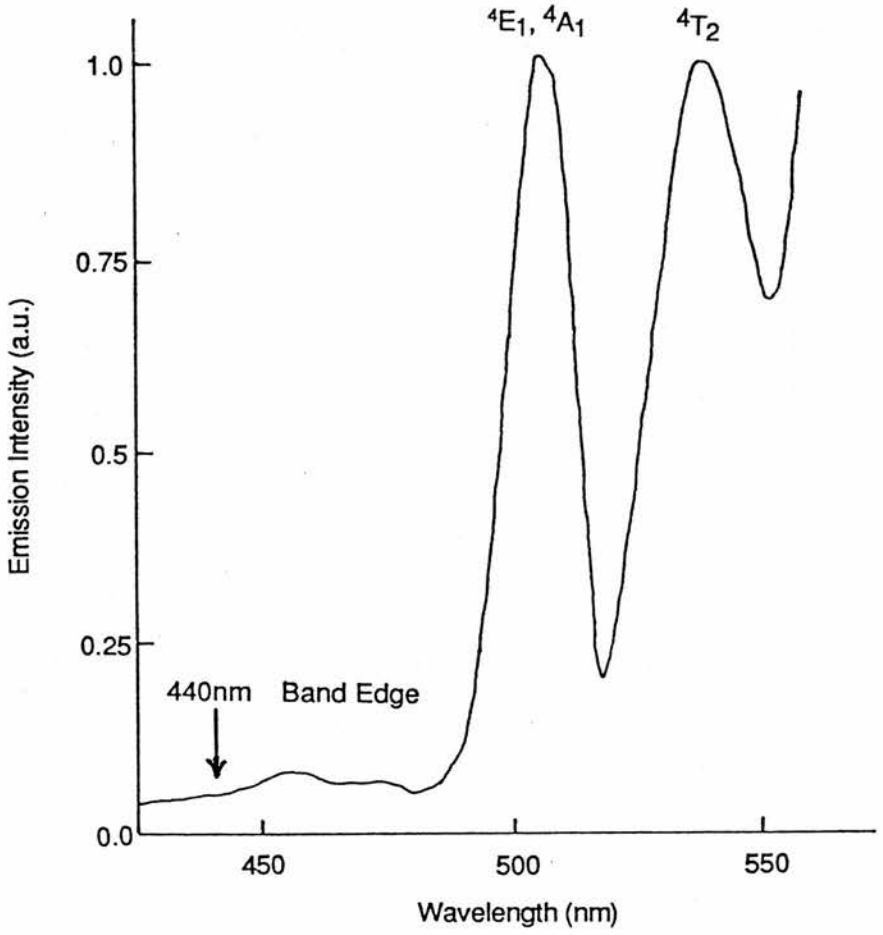

Figure 2.15 [ZnSe:Mn(2)]: Excitation spectra at 4K for 580nm Mn emission showing excited states and position of band edge.

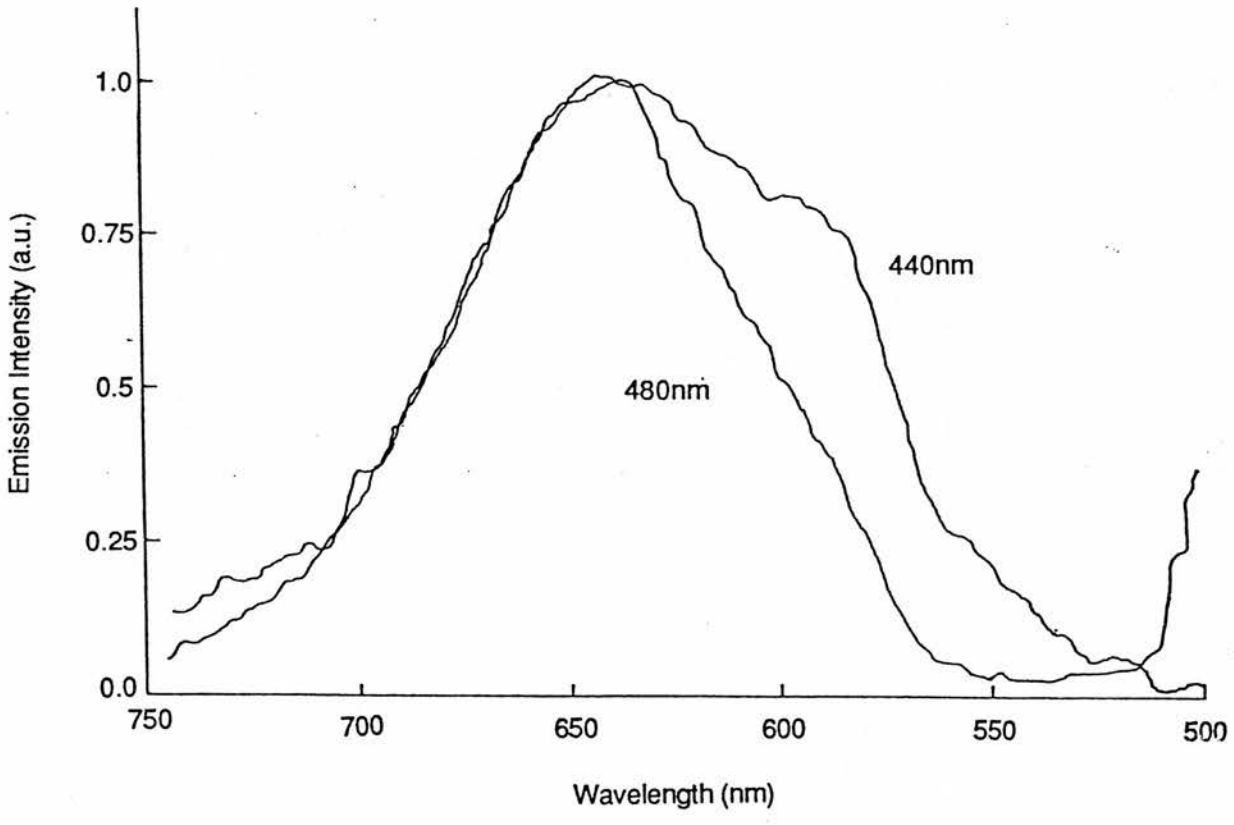

Figure 2.16 [ZnSe:Mn(2)]: Comparison at 4K of S.A. emission excited at 480nm and at 440nm showing presence of at least two different centres.

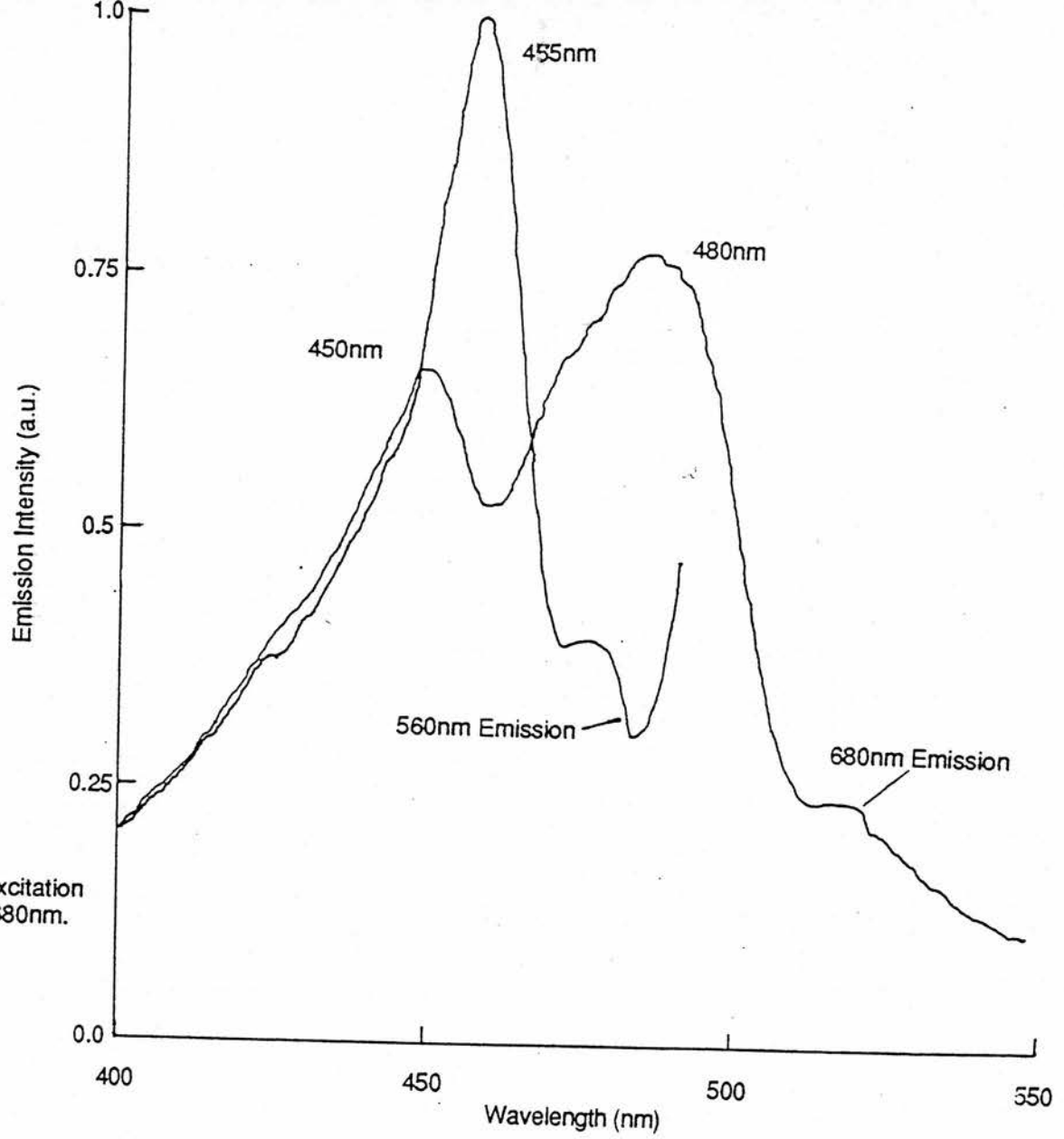

Figure 2.17

[ZnSe:Mn(2)]: Comparison at 4K of excitation spectra for emissions at 560nm and 680nm.

ZnSe:Mn(3)

This sample showed rather similar spectra to that of ZnSe:Mn(2) so no examples are given here.

ZnSe:Mn(4)

Spectra from this sample showed a weak Mn emission but no detectable S.A. emission.

ZnS:Mn(1)

A typical Mn emission similar to that in ZnSe:Mn was seen though rather weaker than we expected. There was no S.A. emission to give any of the problems seen in ZnSe:Mn. No excitation or emission spectra are given here as they are similar to those found for ZnS:Mn(3).

ZnS:Mn(2)

This sample only contained 0.05% Mn so the emission was rather weak and the 540nm excitation could not be used. Two higher Mn excitations are seen at ~465nm and ~420nm in addition to the 500nm excitation. The excitation at 500nm was so weak that emission at 580nm contained nearly an equal amount of excitation light (figure 2.18). This occurs because of cross-over between the filters and could be removed by the addition of broad band filters. No excitation spectra are given as they are similar to those of ZnS:Mn(3) only weaker.

ZnS:Mn(3)

Figure (2.19) shows the four excitations of Mn seen in ZnS. The higher two are normally not seen in ZnSe because of absorption near the band gap energy. The 500nm excitation is very strong compared to that in ZnSe and this may be due to the reduced absorption at 500nm. The higher excitations are not of any practical use. Excitation at 540nm and 465nm produced typical Mn emissions with no S.A. luminescence. Excitation at 500nm and 420nm produced extra emissions (figure 2.20). These were not associated with Mn and did not affect our results.

2.4.4 Summary

In ZnSe:Mn we found that the Mn emission at 580nm may be effectively excited at 540nm and 500nm. Excitation at 455nm may produce a weak Mn emission but it is of no practical use because of the more intense S.A. emission also produced. There are two S.A. emissions ; a broad emission centred at 640nm excited at 480nm and a weaker emission at

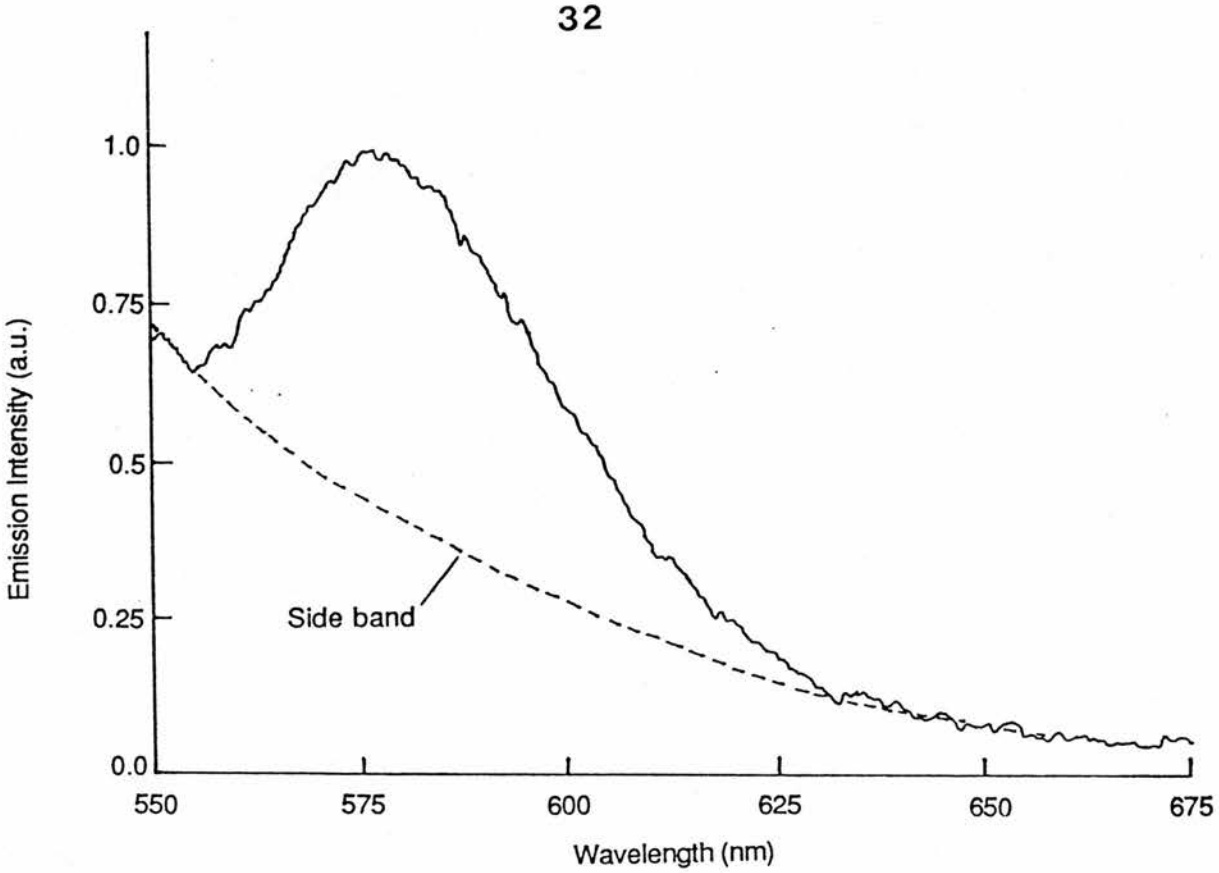

Figure 2.18 [ZnSe:Mn(2)]: Photoluminescence spectra at 4K of 580nm Mn emission for 500nm excitation. Also shown is the estimated background due to cross-over between the interference filters.

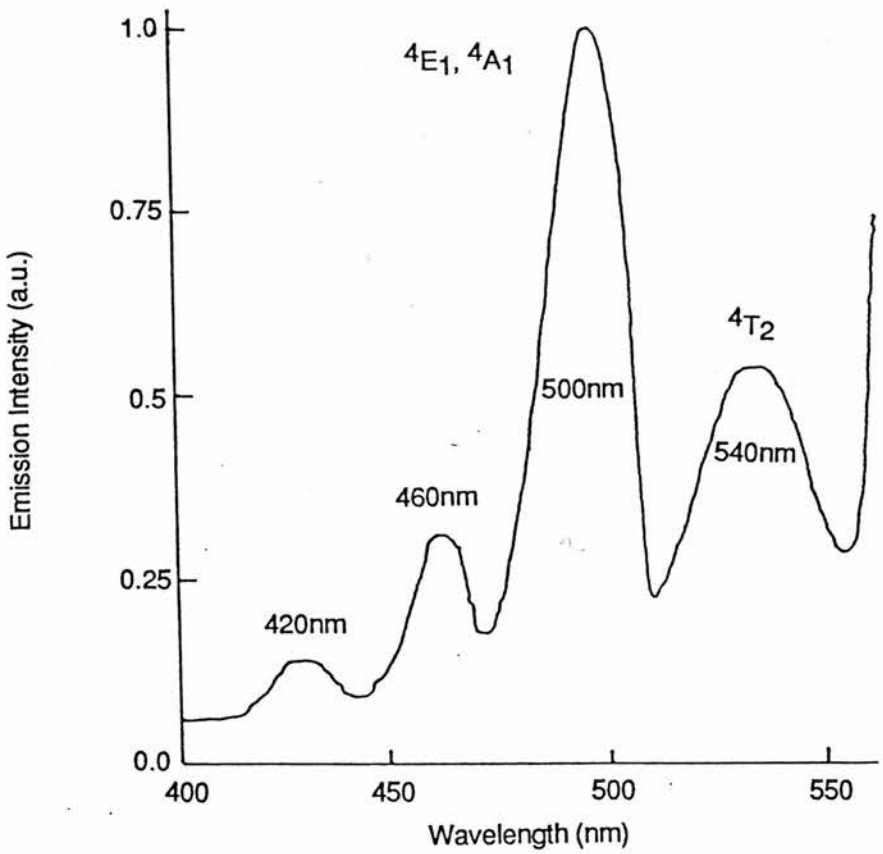

Figure 2.19 [ZnSe:Mn(3)]: Excitation spectra at 4K for 580nm Mn emission ($^4T_1$-$^6A_1$) showing different excited states and corresponding wavelengths.

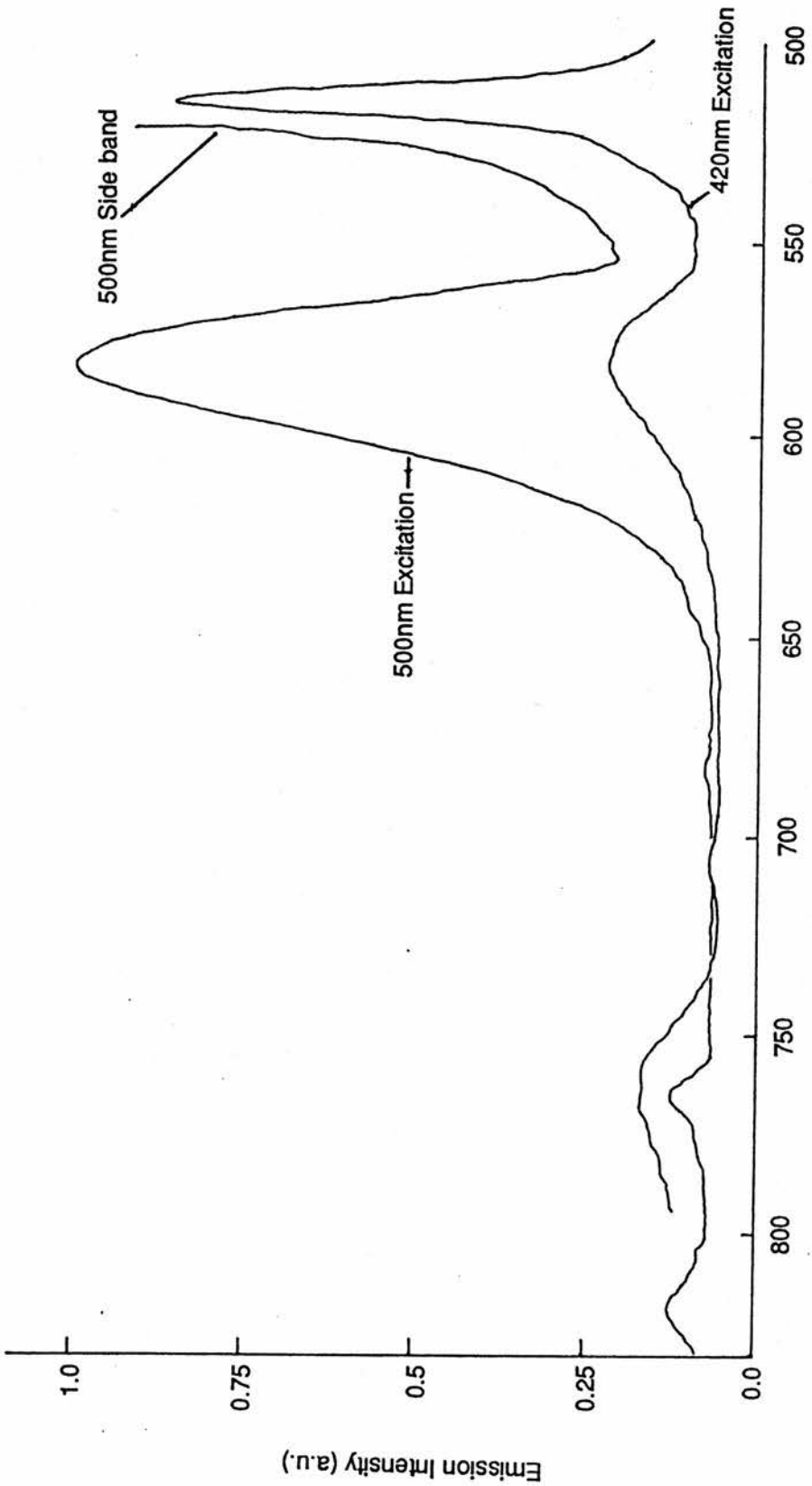

Figure 2.20 [ZnSe:Mn(3)]: Emission spectra at 4K for excitation at 420nm and 500nm.

greater than 640nm excited at 440nm. Figure 2.21 from ZnSe:Mn(3) showed excitation at 480nm produced a good S.A. emission while excitation at 500nm produces a good Mn emission with some S.A. emission (vertical scales are different).

In ZnS:Mn excitation at 500nm is the only feasible way of producing a Mn emission and even so additional broad band filters were necessary to remove the extraneous excitation light in weakly emitting samples. Since there were no S.A. emissions to interfere with the intensity measurements we expected the intensity data to be well behaved. Lifetime measurements should have been feasible on the strongly emitting samples and again there would be no stray lifetimes due to S.A. emissions.

2.4.5 Intensity Quenching Measurements

Using the apparatus shown in figure (2.22) we selectively excited the Mn or the S.A. luminescence and then monitored the emission intensity over a wide temperature range. We also measured the transmission intensity over the same temperature range to see if the absorption was thermally dependent. The signal from the photomultiplier was analysed by a Brockdeal 51A lock-in amplifier triggered by a synchronising pulse from the chopper. Chopping was normally at a low frequency (20Hz) so as to produce a square wave form for the emission intensity. This tended to reduce the drift in the zero point of the lock-in amplifier as the intensity changed. Output from the lock-in amplifier was fed directly to an X-Y recorder. Temperature measurement was by a gold/iron - chromel thermocouple whose e.m.f. was amplified by a micro-voltmeter and fed to the X-Y recorder. In this way a direct and continuous plot was produced of the quenching or transmission.

2.4.6 Quenching Results

Early quenching experiments were marred by condensation problems due to leaks into the sample space of the cryostat. When these were overcome consistent results were produced. One problem that proved to be insoluble was that of contraction of the sample holder arm. On cooling to 4K the sample arm was expected to contract by about 1mm which would be enough to move the sample out of the most intense region of the excitation light. This might be the explanation behind some of the quenching seen at low temperatures where the electrons were

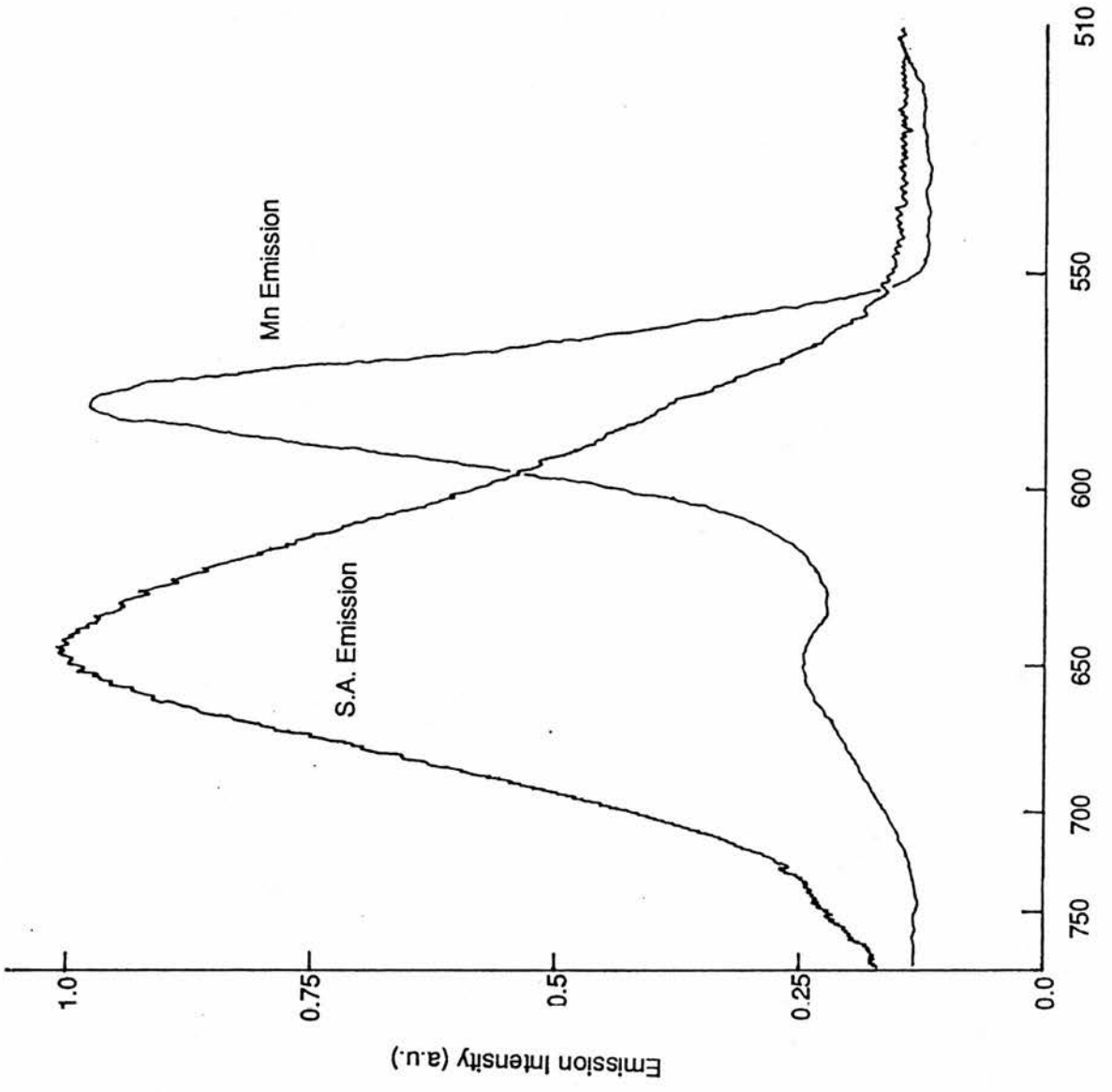

Figure 2.21 [ZnSe:Mn(3)]: Comparison at 4K of spectra for Mn emission (excited at 500nm) and S.A. emission (excited at 480nm). Vertical scales are different.

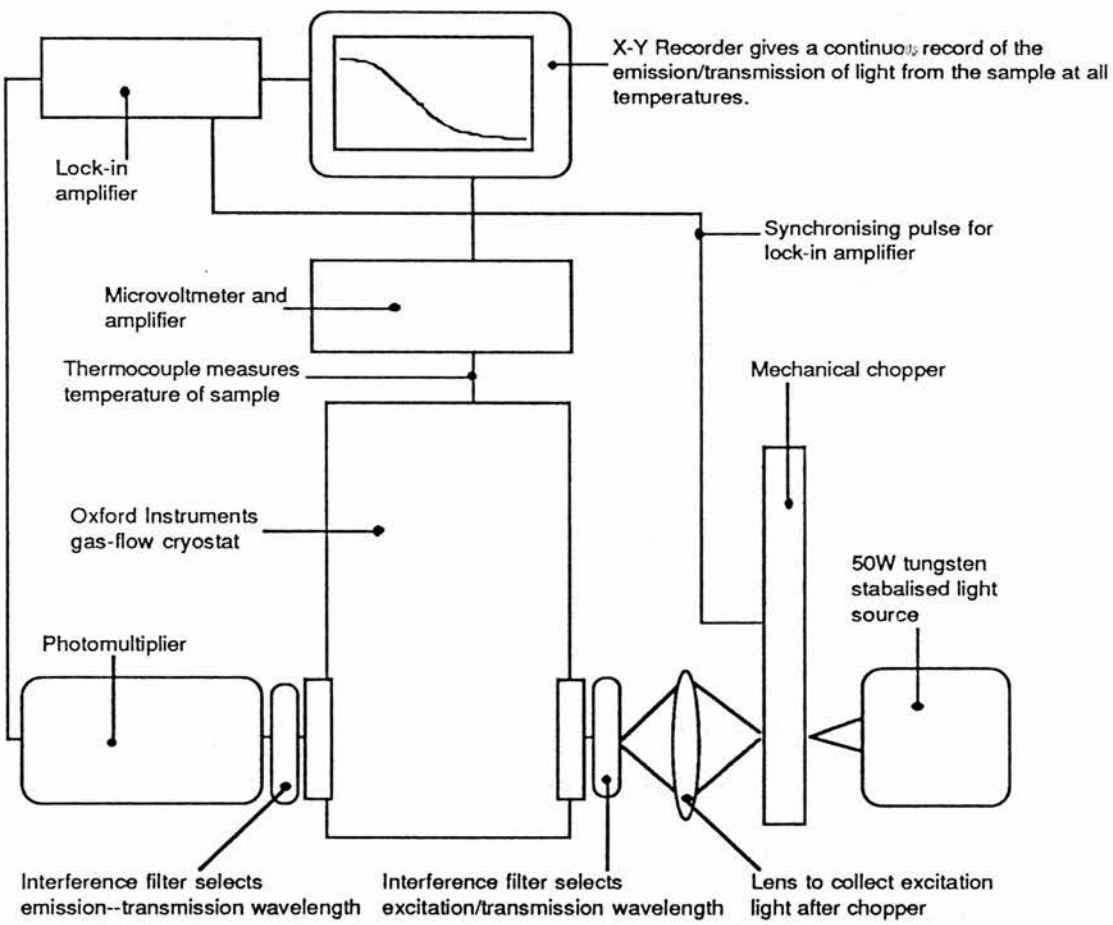

Figure 2.22 Experimental arrangement for measuring emission quenching and light transmission through a sample over a wide temperature range.

supposed to have frozen onto the donors. This problem can only be overcome by redesigning the holder.

There was also a problem with cross-over between the filters. The interference filters used did not totally exclude light outside the specified band widths and two filters together will allow some light to pass through the pair. This was normally very small but if the emission was weak the cross-over became significant at high temperatures where the Mn emission was weakest. This high temperature region normally indicates the final degree of quenching so knowledge of its real value was important. The problem of cross-over could be reduced by the addition of wide band filters; a high pass filter was used in conjunction with the excitation filter and a low pass filter with the emission filter. These filters greatly reduced the cross-over whilst only slightly reducing the luminescence. However such filters were not always practical.

ZnSe:Mn(1)

Only the S.A. emission was present and its quenching was quite similar to that found for the S.A. emission in ZnSe:Mn(2) (figure 2.24). This emission was still present at 300K showing that it was not being quenched by an Auger process.

ZnSe:Mn(2)

The Mn was excited at 500nm and 540nm producing an emission at 580nm. No wide band filters were used so the 540nm excitation (figure 2.23) shows a significant 580nm emission at 385K due the presence of the excitation light. For the 500nm excitation cross-over with the 580nm filter is much less and the high temperature emission approached zero. The kink in the 540nm quenching curve (and less clearly seen in the 500nm excitation) is a genuine feature caused by the additional S.A. luminescence.

Figure 2.24 shows the quenching of the 640nm emission and the transmission of the 480nm excitation through the sample. The close agreement between these curves seems to suggest that the absorption of the excitation light is causing the apparent quenching of the S.A. emission. The S.A. emission could produce a measurable emission at 580nm as shown in figure 2.21. This would seem to be connected with the peculiar bump seen in figure 2.23. The

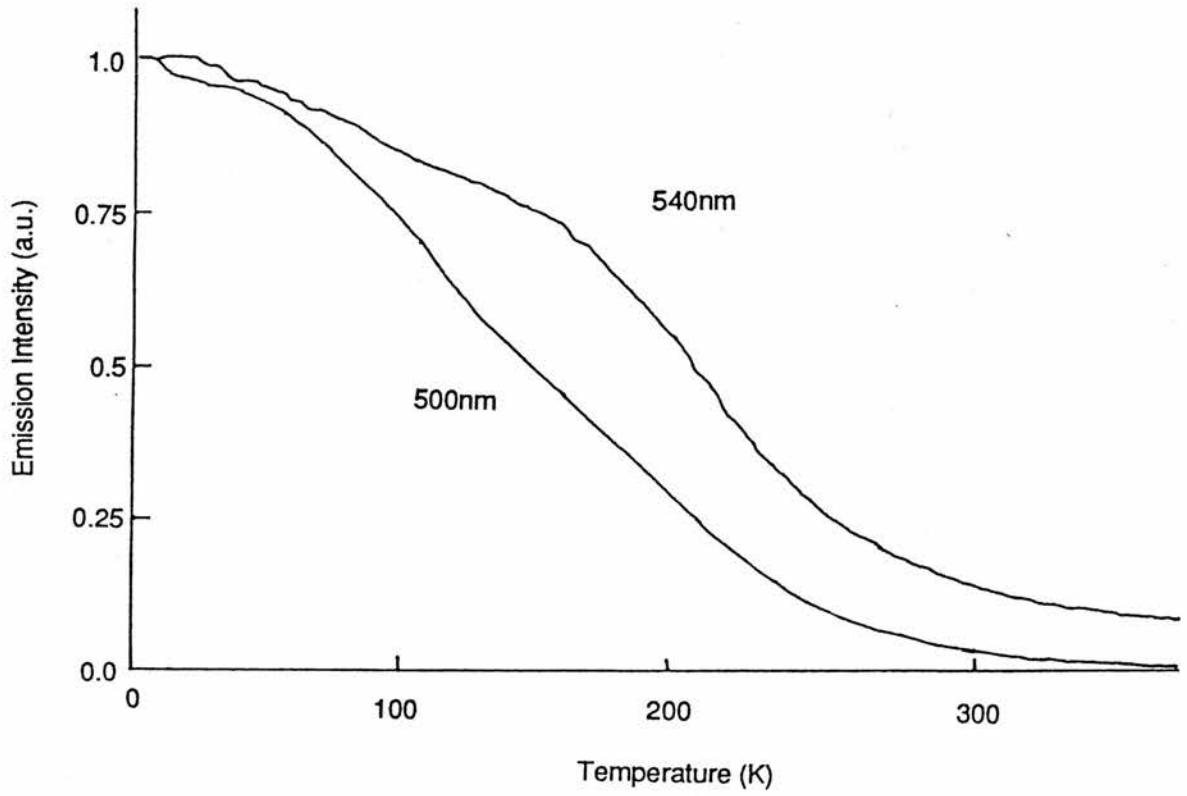

Figure 2.23 [ZnSe:Mn(2)]: Auger quenching of the 580nm Mn luminescence excited at 500nm and 540nm. (Vertical scales are different)

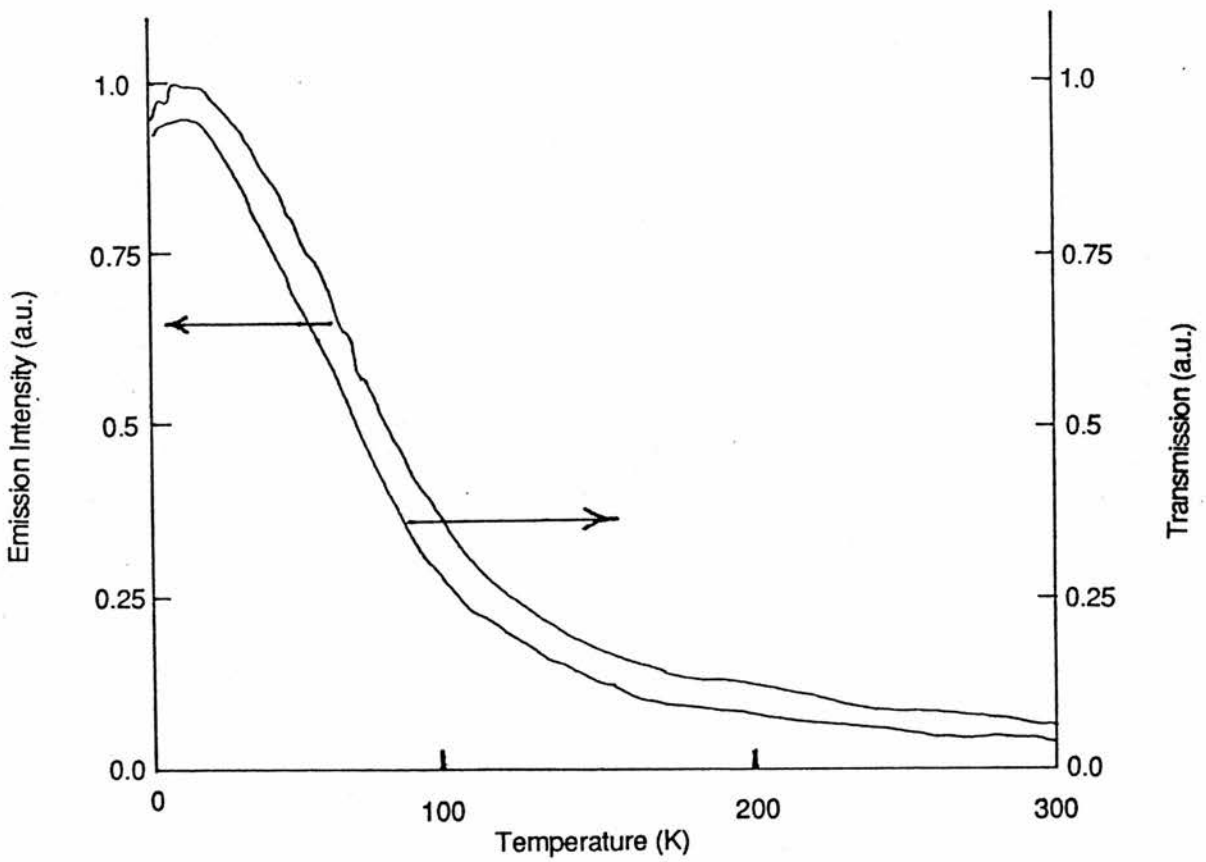

Figure 2.24 [ZnSe:Mn(2)]: Transmission of 480nm excitation light compared with emission intensity of 640nm S.A. emission (excited at 480nm).

bump disappears above 150K which in figure 2.24 is near the point of the minimum in the S.A. emission intensity. This emission was never completely quenched even at 300K.

ZnSe:Mn(3)

These results (figure 2.25) are similar to those of ZnSe:Mn(2) and the same comments apply.

ZnSe:Mn(4)

This sample showed no quenching of the Mn emission on cooling down to 4K and had no S.A. emission.

ZnS:Mn(1)

No intensity measurements were made since it was hoped that it would be possible to derive the Auger coefficient from lifetime measurements instead.

ZnS:Mn(2)

A 500nm interference filter and a no. 44 Kodak Wratten filter were used to produce a pure blue/green excitation light. By combining a 580nm interference filter and a no. 23A Kodak Wratten filter the Mn emission could be isolated from the excitation light. This was necessary because the cross-over between the filters was as large as the Mn emission (figure 2.18). The result was a well behaved quenching curve (figure 2.26) that was later used for calculating the Auger coefficient. No 540nm excitation could be used because of the weakness of the emission. The low temperature emission intensity may have been affected by contraction of the sample holder.

ZnS:Mn(3)

Because of the weakness of the emission, the 540nm excitation could not be used. The 500nm excitation produced a very strange quenching curve (figure 2.27). This sample also produced strange electrical results which might suggest that the donor distribution in the sample was very inhomogeneous as a result of the Zn/Al conductivity treatment. The rapid quenching of the luminescence at low temperatures suggests a high concentration of donors of low activation energy, while the significant emission present at high temperatures suggests a low donor concentration of high activation energy. A visual inspection of the sample did not show any areas that were obviously quenched or unquenched.

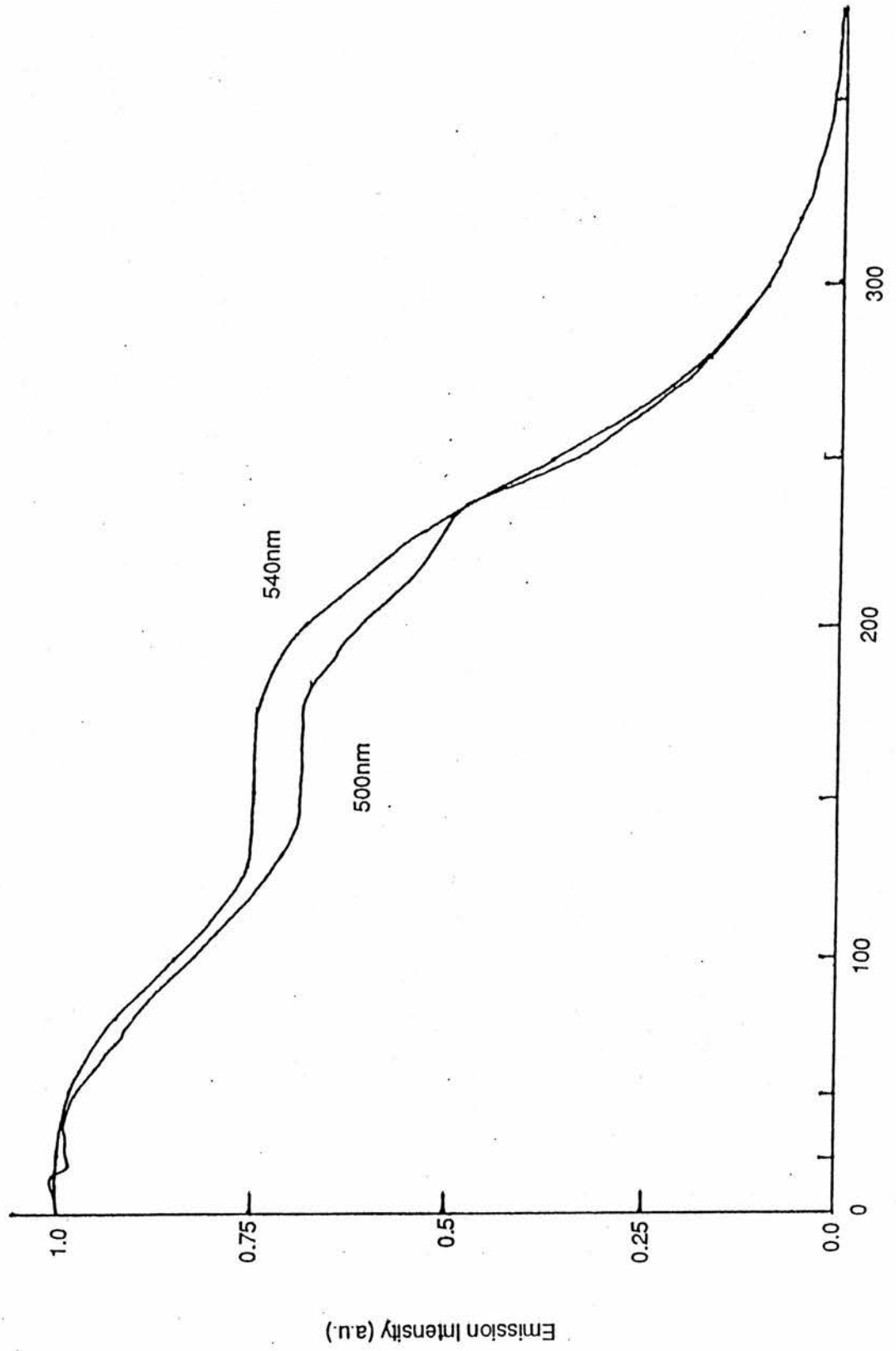

Figure 2.25 [ZnSe:Mn(3)]: Auger quenching of 580nm Mn emission for 500nm and 540nm excitation.

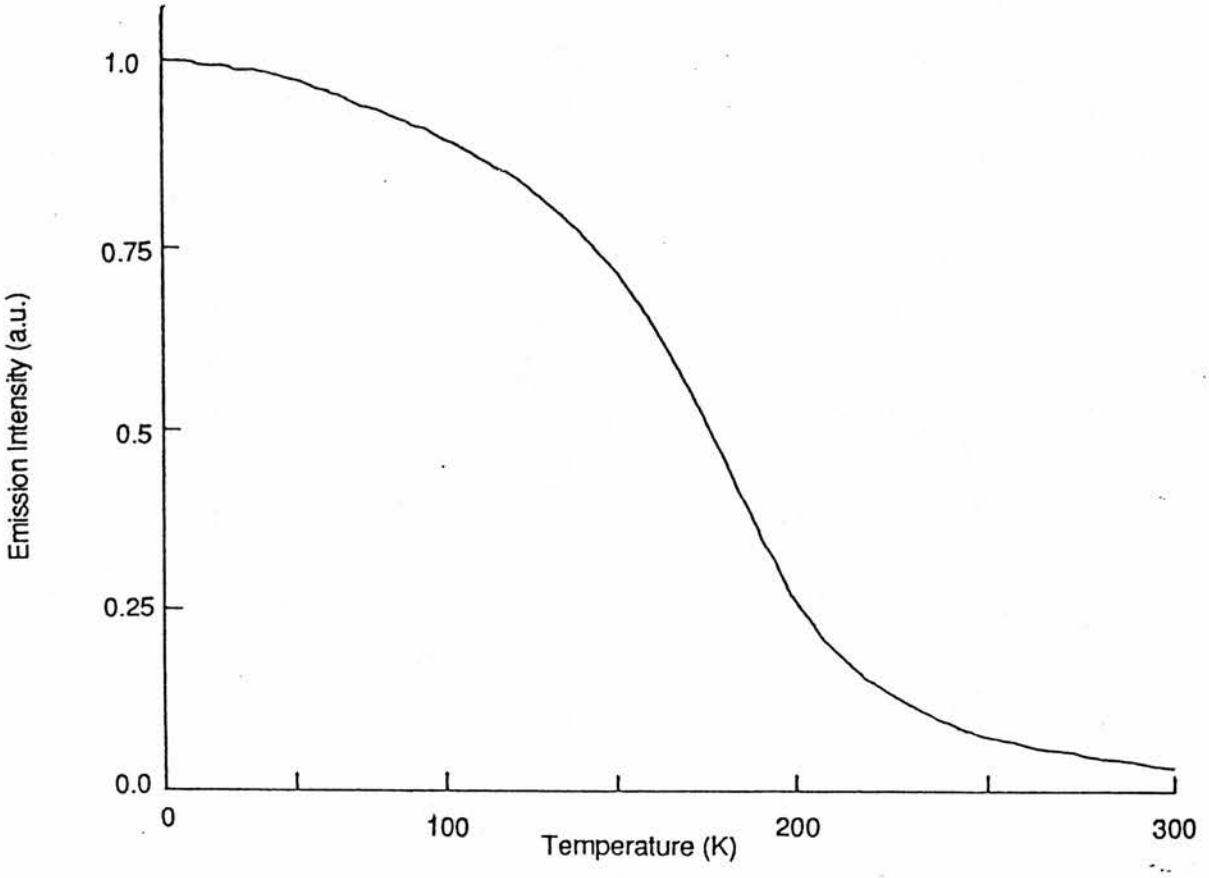

Figure 2.26 [ZnS:Mn(2)]: Auger quenching of the 580nm Mn emission for 500nm excitation using broadband and interference filters to isolate the Mn emission.

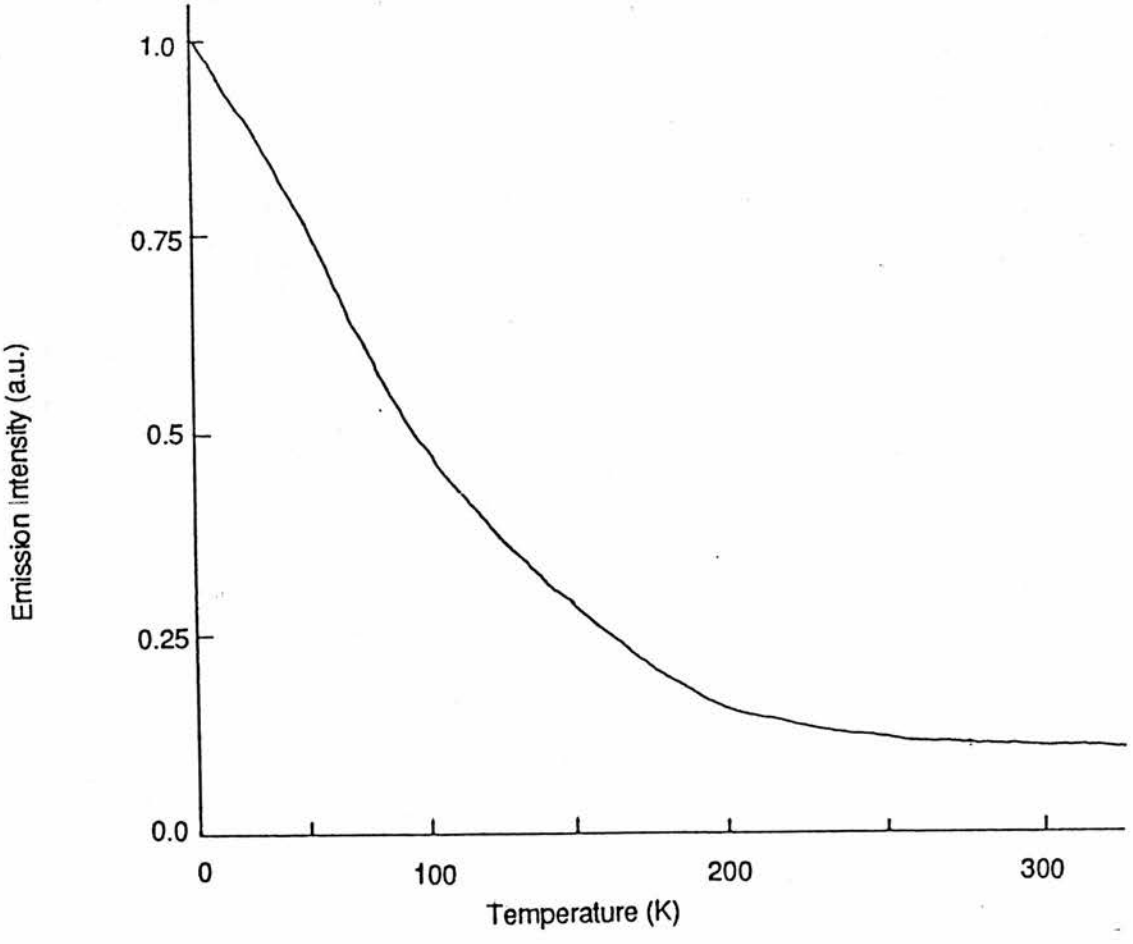

Figure 2.27 [ZnS:Mn(3)]: Quenching of the 580nm Mn emission for 500nm excitation

2.4.7 Summary

Using the information gained from the spectral analysis of the various samples it was on the whole possible to selectively excite the Mn or S.A. luminescence. In ZnSe the Mn emission was complicated by the presence of the S.A. emission making the usefulness of this data questionable. It was possible however to measure the emission over a large temperature range as required. In ZnS the Mn emission was often very weak and in one sample extra filters had to be used to help separate the emission from the excitation. The results appear to be satisfactory. In the last ZnS:Mn sample the emission behaved in a very unexpected manner which might be explained by an inhomogeneous donor distribution.

2.4.8 Lifetime Measurements

Three methods were used to measure the lifetime of the Mn. The first was to use the same equipment as shown in figure (2.22) but with the chopper frequency increased to 100Hz . The output from the photomultiplier was then fed into a box-car triggered by the chopper synchronisation pulse. This method only worked for ZnS:Mn at low temperatures where the lifetime (~1.5msec) was large compared with the cut off time for the chopper (~100μsec).

A second method was to use a strobe of 50μsec pulse duration to replace the chopper and light source. The strobe and Box-car were then both triggered from a signal generator set at 80Hz.

Our final method was the only one capable of measuring the lifetimes of ZnSe:Mn near room temperature. The light source was a 15μsec duration flashlamp with a decay time of 2.5μsec and the emission was detected using a photomultiplier adjusted to have a response time of 2.5μsec. Extra filters were necessary to remove the excitation light because pulsed excitation is inefficient so the Mn emission was weak. The flashlamp was manually triggered in single bursts and the signal from the photomultiplier stored on a digital oscilloscope. The oscilloscope trace was plotted using an X-Y recorder and the traces redrawn on Log-linear paper to give the lifetime.

Lifetime measurements are unaffected by absorption of the excitation light or by additional emissions of significantly different lifetimes. The problems experienced with the intensity quenching measurements are therefore not present here. If we compare the radiative efficiencies from intensity and lifetime measurements they will only agree in an

homogeneous sample where there is no absorption or extra emissions. By measuring the lifetime for 500nm and 540nm excitation we are able to check the validity of these experiments. If both sets of measurements agree this will show that the dominant lifetime is for the 580nm decay and not for transitions from one of the higher excited states.

2.4.9 Results

ZnSe:Mn(1)

Since no Mn emission was present no lifetimes were measured. However we did try to measure the lifetime of the S.A. but this appeared to be at or below the 2.5μsec resolution of the system.

ZnSe:Mn(2)

Because of the weakness of the emission no lifetime measurements were taken.

ZnSe:Mn(3)

The lifetimes were measured for excitation at 500nm and 540nm and were compared to equivalent intensity measurements (figures 2.28 and 2.29). In the region 4K to 150K the lifetimes showed a long and short component which was thought to be due to the S.A. emission. From 150K upwards this emission was quenched (figure 2.24) and no longer affected the decay. If we take the longer lifetimes as being due to the Mn the resulting quenching curve is of the expected form. In figure (2.30) the two lifetime experiments were compared and found to be in fair agreement. Our results give the lifetime at 4K to be ~220μsec which may be compared with a value of 180-200μsec by Xiao-peng et al [2.14] while Allen et al [2.15] obtained a value of 110μsec. The different values are an indication of the variation in the strength of non-radiative processes in these materials. It would appear that the lifetime is the better measure of the radiative efficiency in this sample.

ZnSe:Mn(4)

The lifetime was measured ten times at 4K in this very resistive sample and found to be 235±3μsec. There was no S.A. emission or quenching present to affect the lifetime but the emission was weak hence the need to repeat the measurement to reduce the errors.

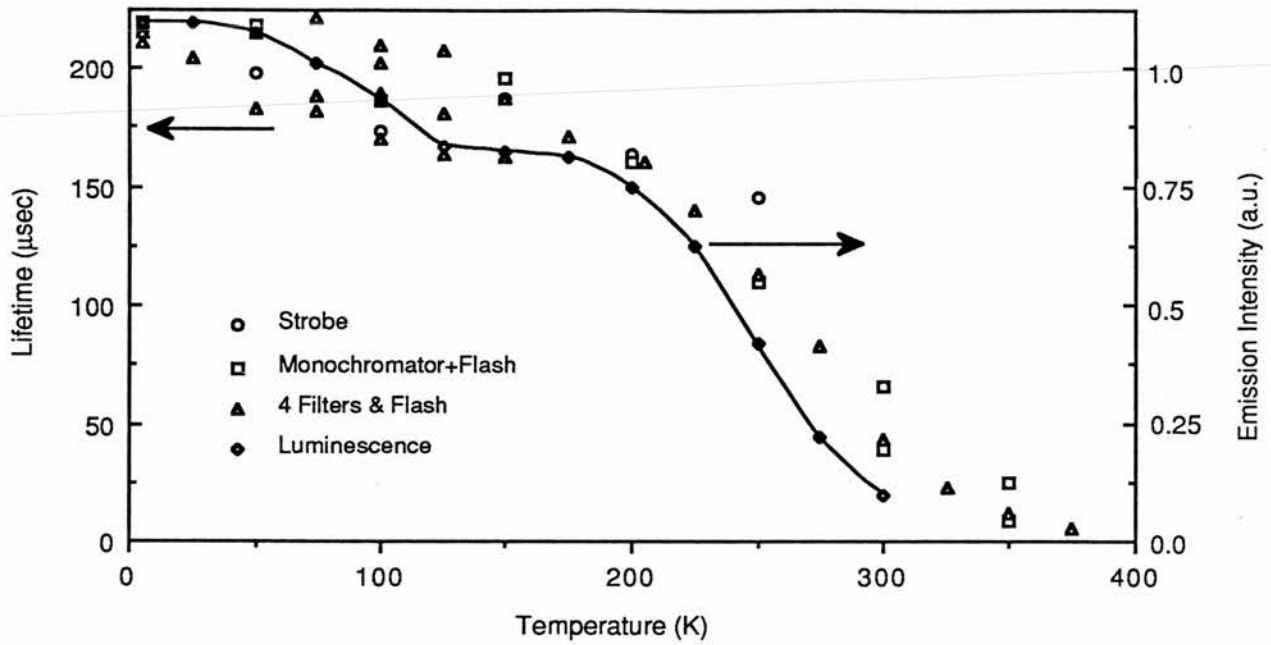

Figure 2.28 [ZnSe:Mn(3)]: Lifetime of the 580nm Mn emission as measured by different methods for the 500nm excitation and compared with the luminescence intensity.

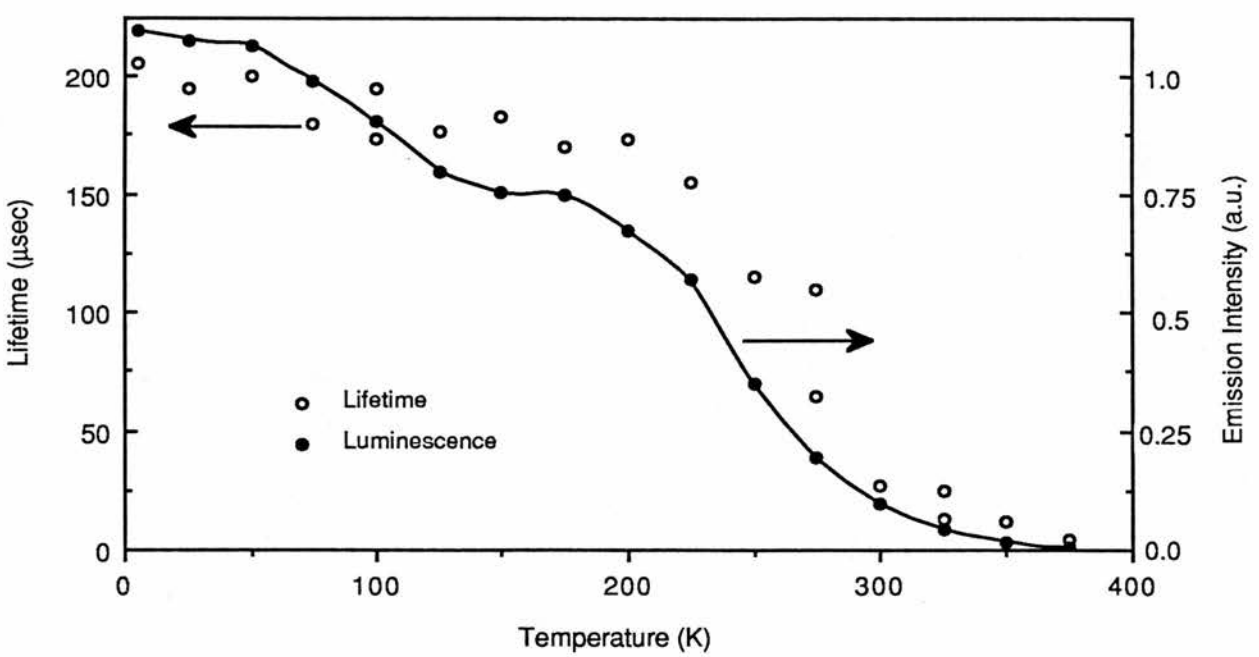

Figure 2.29 [ZnSe:Mn(3)]: Lifetime of 580nm emission for excitation at 540nm and compared with emission intensity.

ZnS:Mn(1)

The lifetime in this sample (figure 2.31) was measured using the chopper method with short and long output averaging on the Brookdeal Box-car. The results show that the lifetime rapidly falls from 1.5msec to 0.8msec by 150K and there onwards remains nearly constant. The sample was however known to be quenched at room temperature so these results showed that this sample was inhomogeneous and unsuitable for quenching measurements.

ZnS:Mn(2)

Because of the weakness of the emission the lifetime for the Mn could not be measured.

ZnS:Mn(3)

Lifetime measurements were made using all three methods. Using a chopper we found the lifetime fell rapidly from 1.4msec to below 1msec as the temperature was raised above 4K (figure 2.32). The results seem to be rather scattered because of the low light levels being used. We attempted to improve the results by using the strobe technique (figure 2.32) and the flashlamp (results not given) but these produced results that were even more scattered. We conclude that the sample was inhomogeneous as suspected from the intensity quenching experiments.

2.4.10 Summary

For ZnSe:Mn the lifetime data for 500nm and 540nm excitation are in good agreement and appear to have overcome problems due to absorption and the S.A. emission. A radiative efficiency calculated from these measurements will be more reliable than using intensity data.

For ZnS:Mn the lifetime measurements were found to be of no use because the Zn/Al treatment had produced an inhomogeneous donor distribution. This problem was also found by Gordon [2.7,2.8] when he attempted similar measurements. Instead intensity measurements were used to find the radiative efficiency.

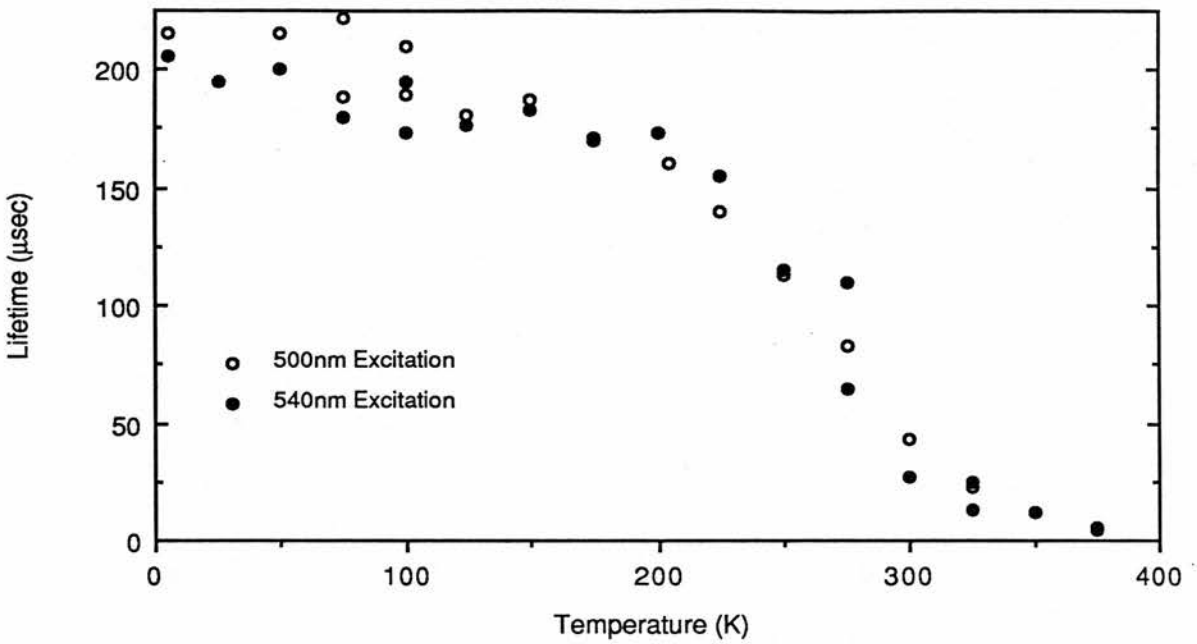

Figure 2.30 [ZnSe:Mn(3)]: Lifetime of the 580nm Mn emission for excitation of 500nm and 540nm. Excitation was by a 15µsec flash lamp using four filters.

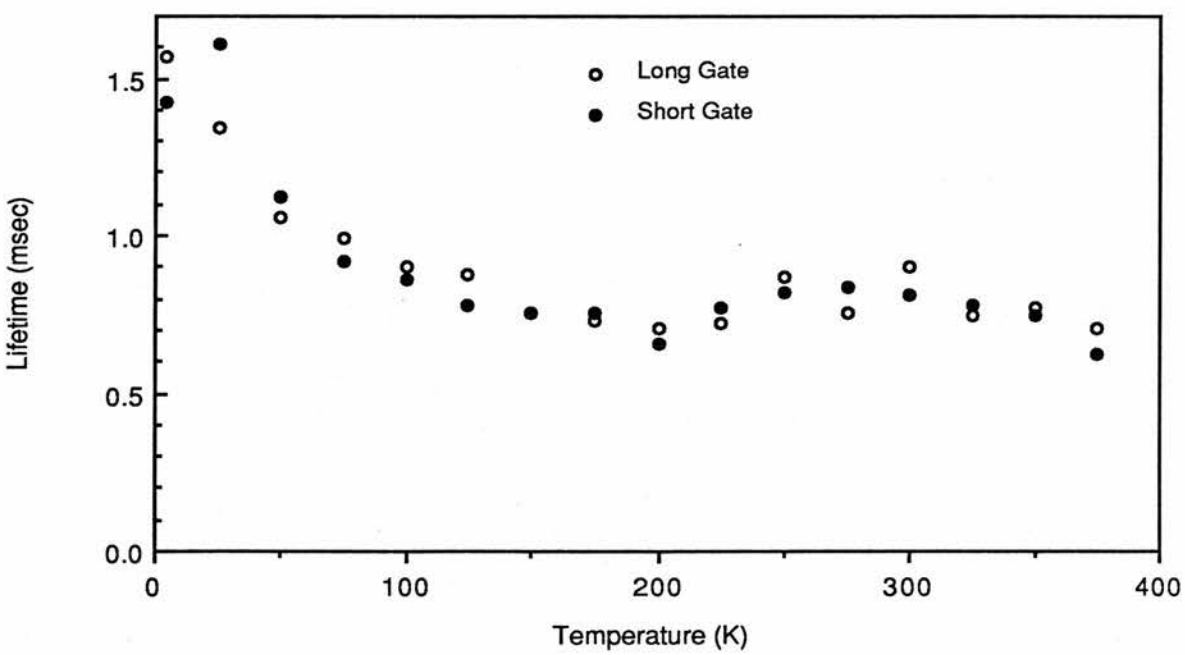

Figure 2.31 [ZnS:Mn(1)]: Lifetime of 580nm Mn emission in ZnS excited at 500nm. Lifetime is measured twice each time with a different gate setting on the Box-car.

2.5 Calculation of Auger coefficients

2.5.1 Introduction

In section 2.2 it was shown how the Auger quenching was related to the electron concentration (equation 2.11) By assuming a thermal dependence for the electron concentration (equation 2.14) one can produce another equation giving the thermal dependence of the Auger quenching (equation 2.15). The strength of the Auger process is given by the Auger coefficient γ_f.

Before starting to analyse the radiative efficiency (η) we need to be sure that the quenching seen is indeed due to an Auger process. The electron concentration (n_e) at various temperatures is already known from the Hall effect and resistivity measurements. Equation (2.15) shows

$$\frac{1}{\eta} = 1 + n_e(T)\,\gamma_f\,\tau_o \qquad (2.15)$$

If the Hall effect data is reliable the electron concentration from this may be used directly by plotting (Radiative Efficiency)$^{-1}$ against n_e as in equation (2.15) and a straight line fit should be found of gradient $\gamma_f \tau_o$ for an Auger process.

The Hall data was either not available or questionable for most of the samples while resistivity often was available. Assuming the electron mobility to be nearly constant the electron concentration $n_e(T)$ at any temperature may be related to the resistance by

$$n_e(T) = \frac{R_{RT}\, ne(RT)}{R(T)} \qquad (2.18)$$

so

$$\frac{1}{\eta} = 1 + \frac{\gamma_f \tau_o R_{RT}\, n_e(RT)}{R(T)} \qquad (2.19)$$

A plot of (2.19) should give a straight line of intercept 1.0 and gradient $\gamma_f \tau_o R_{RT}\, n_e(RT)$. (RT refers to values measured at Room Temperature)

If the fit is not good for either the Hall data or the resistivity then the quenching is not of the Auger type and there is no point in trying a full analysis using equation (2.15). From these quick methods an estimate can be made of the Auger coefficient. If the data did show a

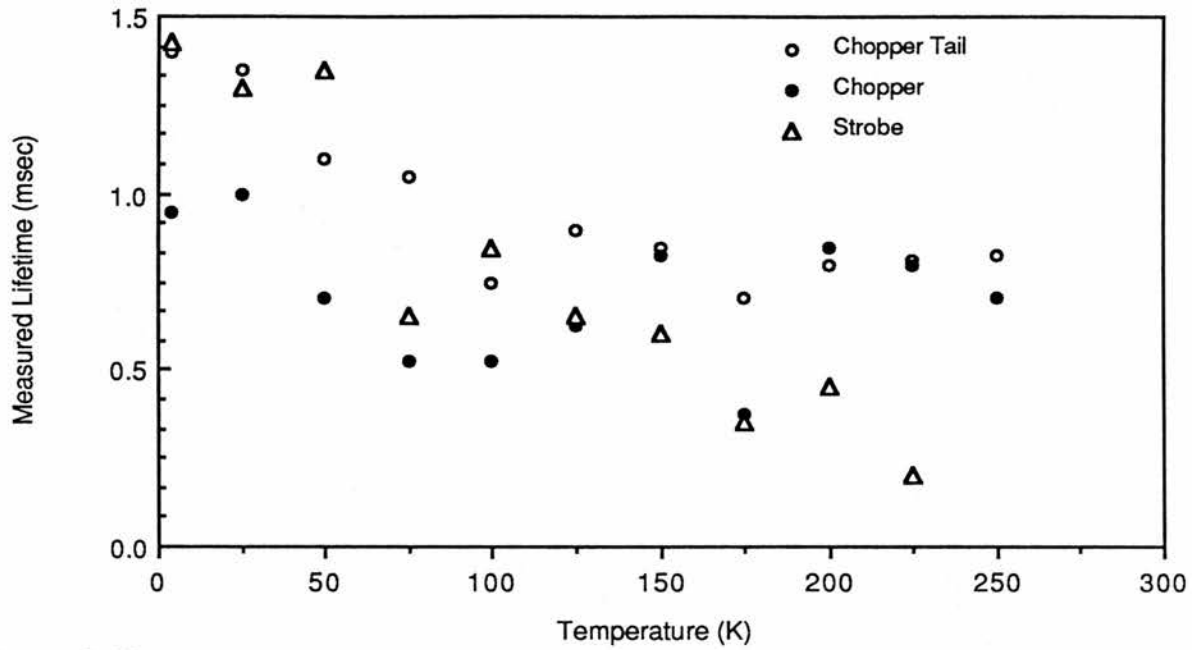

Figure 2.32 [ZnS:Mn(3)]: Plot of lifetime of 580nm Mn emission in ZnS excited at 500nm. The lifetime was measured using a chopped light source or a 50μsec strobe.

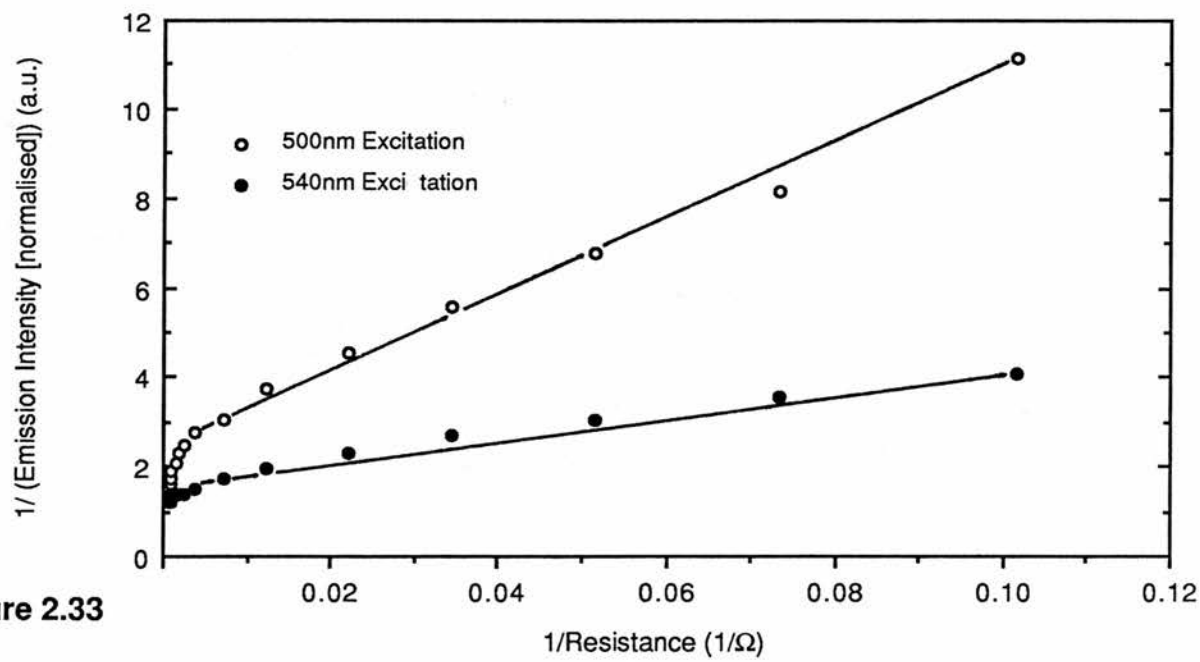

Figure 2.33

[ZnS:Mn(3)]: Comparison of 580nm Mn emission intensity with sample resistance to show dependence of quenching on electron concentration. The gradients may be different because of absorption of the 500nm excitation light by the ZnSe.

dependence on the electron concentration then a full analysis was tried using equation (2.15) and a value found for γ_f.

2.5.2 Results

ZnSe:Mn(1)

There is no quenching data for this sample since the luminescence was always quenched. However an estimate can be made of the lower limit to γ_f . If the quenching is thought to reduce the radiative efficiency by 3 orders of magnitude or more equation (2.15) becomes

$$\eta^{-1} \leq n_e(T)\,\gamma_f\,\tau_o$$

$$\Rightarrow \quad \gamma_f \geq \frac{1}{\eta\, n_e\, \tau_o}$$

$$\geq (10^{-3} \cdot 4 \times 10^{16} \cdot 2.2 \times 10^{-4})^{-1}$$

$$\geq 1.1 \times 10^{-10}\ cm^3\ s^{-1}$$

ZnSe:Mn(2)

Lifetime data was not available for this sample so the radiative efficiency was derived from the emission intensity for excitation at 500nm and 540nm. Room temperature Hall effect and low temperature resistivity data were plotted in figure (2.33) according to equation (2.19). The intercepts were different and not equal to 1.0 due to the S.A. emission present below 150K.The gradients were also slightly different perhaps due to the extra absorption of the 500nm excitation by the ZnSe. The graphs were however straight lines showing that an Auger type process was involved and from the gradients we estimated γ_f to be

$$\gamma_f\ (500nm) = 6 \times 10^{-10}\ cm^3$$

$$\gamma_f\ (540nm) = 2 \times 10^{-10}\ cm^3$$

These first graphs showed that an Auger type process was present and a full analysis using equation (2.15) was tried (figures 2.34 & 2.35) and the following activation energies and Auger coefficients were found;

for the 500nm excitation

$E_d = 0.17\ eV$ $\qquad \gamma_f = 8 \times 10^{-10}\ cm^3\ s^{-1}$

for the 540nm excitation

$E_d = 0.12\ eV$ $\qquad \gamma_f = 2 \times 10^{-10}\ cm^3\ s^{-1}$

These Auger coefficients are similar to the approximate values first derived.

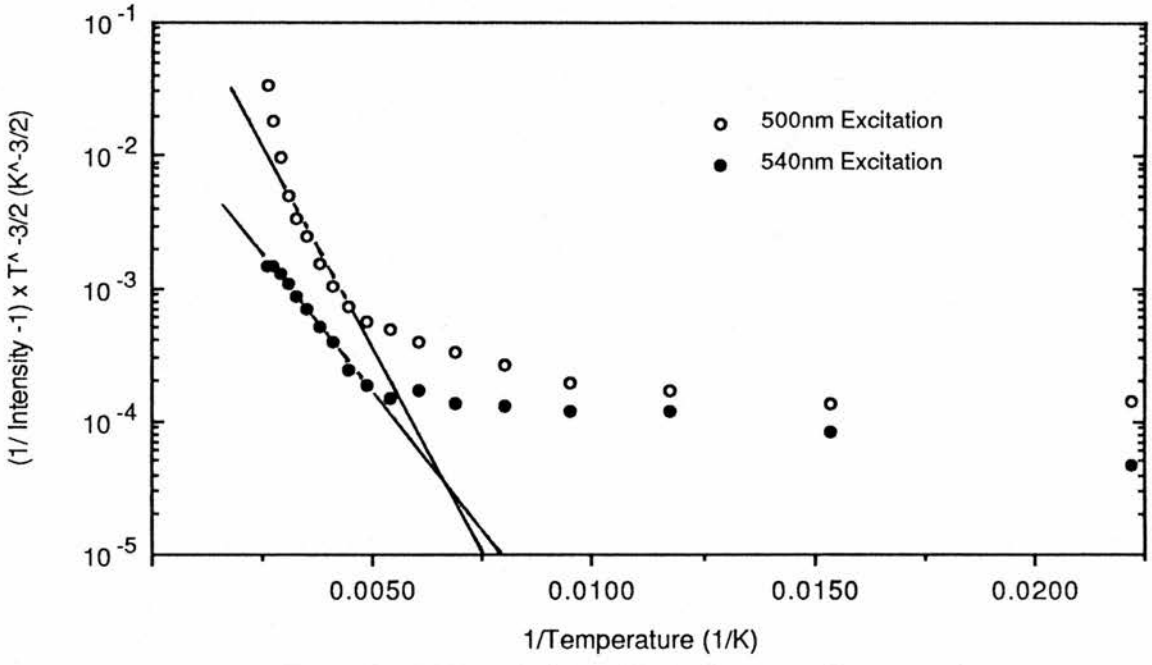

Figure 2.34 [ZnSe:Mn(3)]: Theoretical plot of Mn luminescence (figure 2.23) for 500nm and 540nm excitation in accordance with equation (2.15)

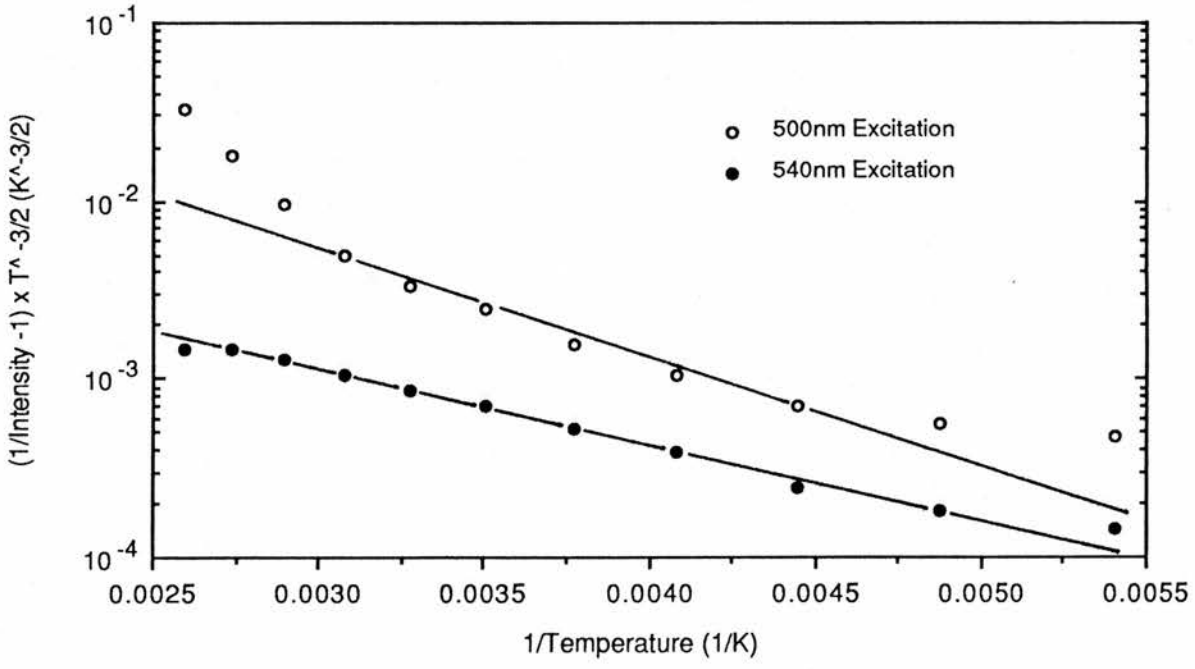

Figure 2.35 [ZnSe:Mn(3)]: Theoretical plot of 580nm Mn luminescence (figure 2.23) for 500nm and 540nm excitation plotted according to equation (2.15) using measurements above 180K.

Chapter 6

Conclusions

6.1 This Thesis

Auger quenching has been measured in ZnS:Mn by Gordon & Allen [6.1] and an Auger coefficient was found of about 10^{-10} cm^3 s^{-1} . If the Auger quenching occurs via a direct electron interaction the Auger coefficient in ZnSe should be about $10^{-9} cm^3$ s^{-1} because of the shorter Mn lifetime in ZnSe. We measured for the first time the Auger coefficient for Mn in ZnSe exciting the Mn emission via two higher excited states. The Auger coefficient was then determined from the temperature and electron concentration dependence of the emission intensity and lifetime. By using two different excitations and two different measures of the quenching we were able to show that one process was responsible for all the quenching behaviour. By relating this quenching directly to electrical measurements of the free electron concentration we were able to show that this was indeed an Auger process. The Auger coefficients from different samples and experiments covered a range of values so a precise value can not be given because of nature of the quenching, but all the values were found in the range 1-11 $x10^{-10}$ cm^3 s^{-1} . This is of the same magnitude as the value of 5 $x10^{-10}$ cm^3 s^{-1} that we found for ZnS:Mn.

The value for ZnS:Mn was determined from one sample using intensity measurements only but was shown to be dependent on the electron concentration. This value for ZnS:Mn is in the range previously given by Gordon & Allen. The coefficients for ZnS:Mn and ZnSe:Mn are about three orders of magnitude greater than the expected value for a direct interaction process. From the Auger coefficients we estimated the impact cross-sections to be about 10^{-16} cm^2 . This value for the impact cross-section is the same order as the lower limit for the cross-section as found by Mach & Müller [6.2].

Using the Born approximation we derived a theoretical cross-section assuming a direct interaction for the impact excitation. We originally derived a cross-section which required no parabolic energy dependence in the conduction bands. We then approximated this cross-section to allow the lower part and then the whole of the conduction band to be parabolic. It was found that for most reasonable situations it was satisfactory to allow the bottom of the conduction band

ZnSe:Mn(3)

Both lifetime and intensity data existed for both excitations of the Mn and there were both Hall effect and resistivity data from 285 to 220K. From this data it was possible to produce eight estimates of the Auger coefficient. Using equation (2.15) (selecting what appear to be the reasonable Hall data values) and equation (2.19) the electrical data was compared with the luminescence data and it was found that both excitations gave similar straight line fits with similar intercepts and gradients from which we estimate the Auger coefficients to be ;

γ_f (Hall effect) = 1.3×10^{-10} cm^3 s^{-1} figure (2.36)

γ_f (Resistivity) = 5.5×10^{-10} cm^3 s^{-1} figure (2.37)

The differences may be due to contact problems affecting the resistivity but the straight line fits are still evidence of an Auger type process. Using equation (2.15) a theoretical fit was found (figure 2.38, 2.39) though there is some difficulty because of a lack of data ;

for 500nm excitation

E_d = 0.15 eV $\gamma_f = 7 \times 10^{-10}$ cm^3 s^{-1} figure (2.39)

for 540nm excitation

E_d = 0.17 eV $\gamma_f = 11 \times 10^{-10}$ cm^3 s^{-1} figure (2.39)

To try and overcome errors introduced by the S.A. emission lifetime data was also used to estimate the radiative efficiency. There were only three lifetimes measured in the range of the electrical measurements so it was not feasible to use Hall data and resistivity data(an approximate linear relationship was found and the Auger coefficients derived are in the range of the previous values). Using equation (2.15) we found the following activation energies and Auger coefficients ;

for 500nm lifetimes

E_d = 0.22 eV $\gamma_f = 1.1 \times 10^{-10}$ cm^3 s^{-1} figure (2.40)

for 540nm lifetimes

E_d = 0.23 eV $\gamma_f = 5.0 \times 10^{-10}$ cm^3 s^{-1} figure (2.41)

The lifetime activation energies are close to the activation energies found from the electrical measurements (0.23 and 0.25 eV). It is not clear why the Auger coefficients should be

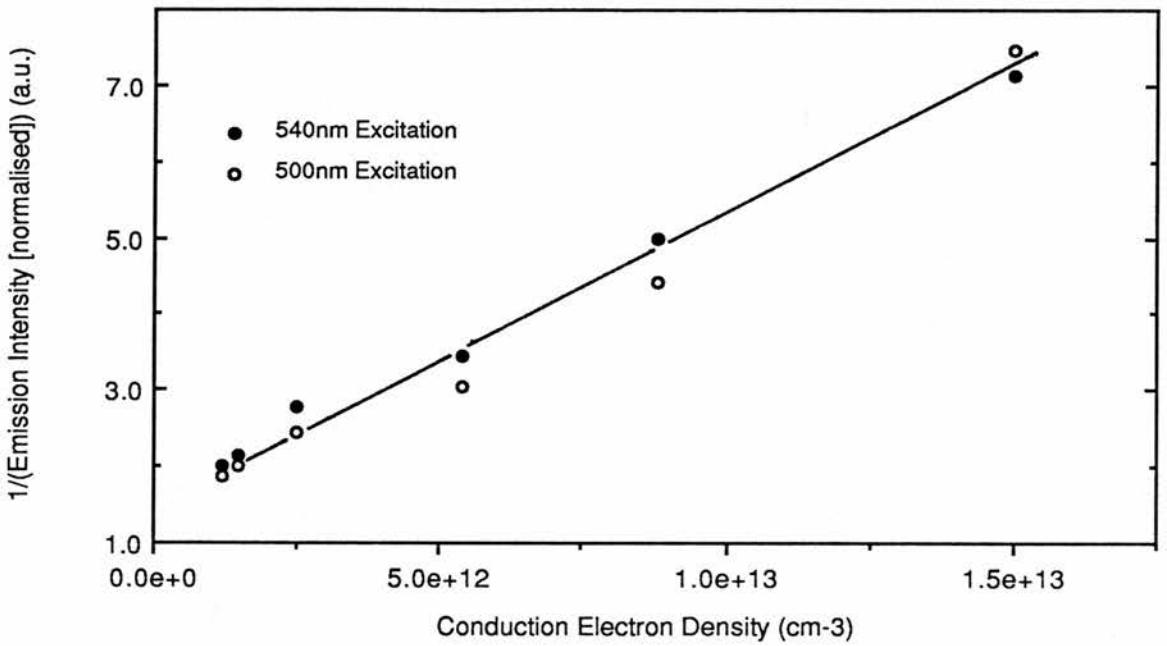

Figure 2.36 [ZnSe:Mn(3)]: Plot of Conduction Electron Density (from Hall effect) and 1/(Emission Intensity) for both excitations of Mn. A linear dependence is an indicator of an Auger process.

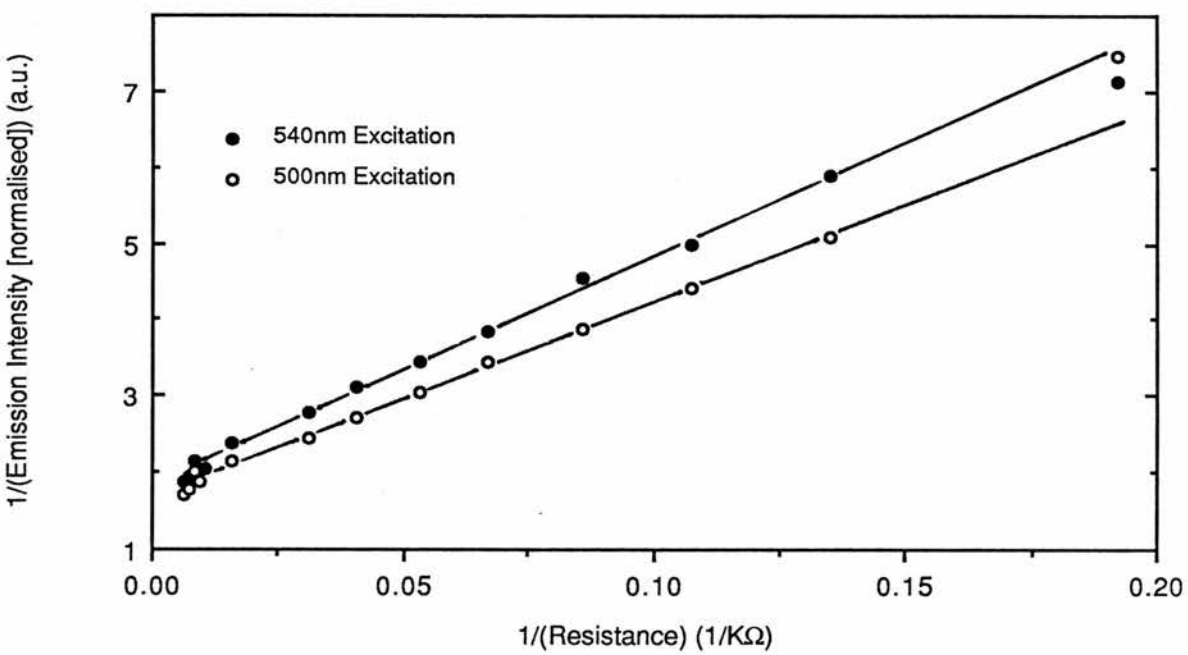

Figure 2.37 [ZnSe:Mn(3)]: Plot of 1/Resistance against 1/(Emission Intensity) for the Mn emission excited at 500nm and 540nm. A linear dependence is an indicator of an Auger process.

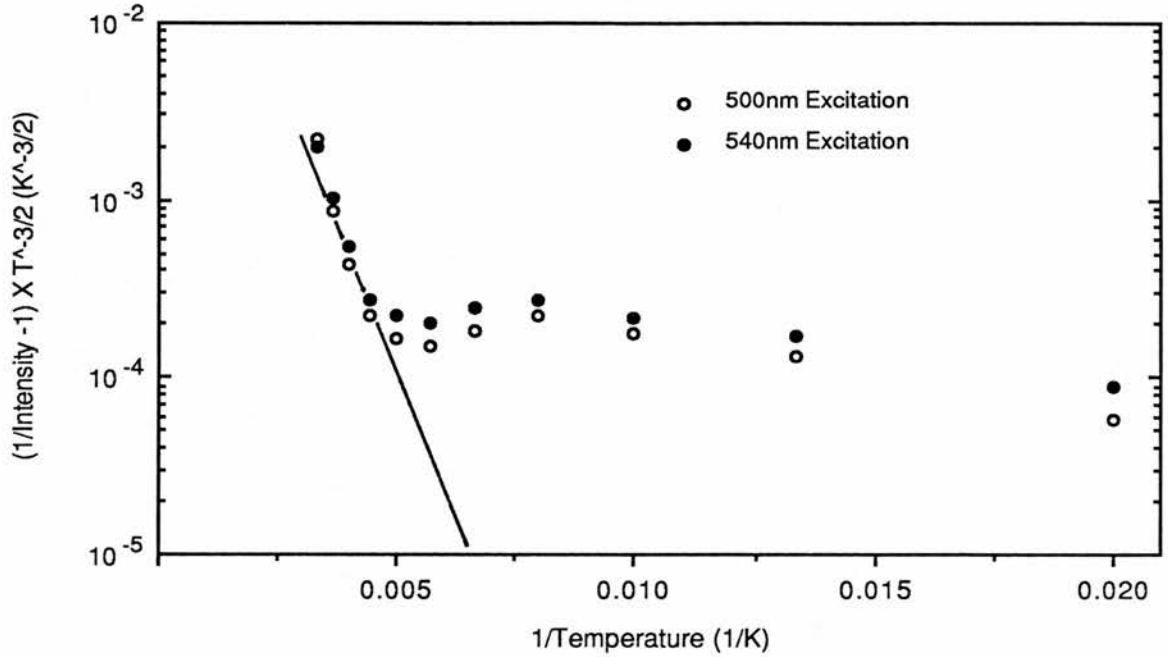

Figure 2.38 [ZnSe:Mn(3)]: Plot of Mn emission intensity according to equation (2.15) for excitation at 500nm and 540nm. Intensity has been normalised to give the effective radiative efficiency.

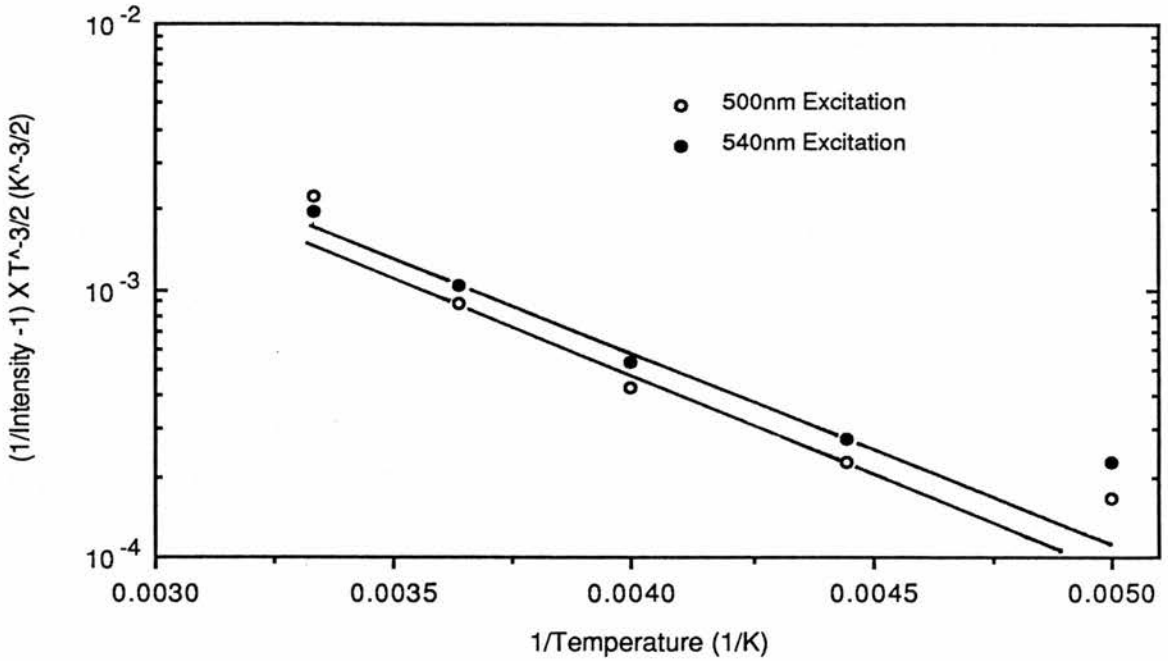

Figure 2.39 [ZnSe:Mn(3)]: Plot of Mn emission intensity according to equation (2.15) for excitation at 500nm and 540nm. Intensity has been normalised to give the effective radiative efficiency.

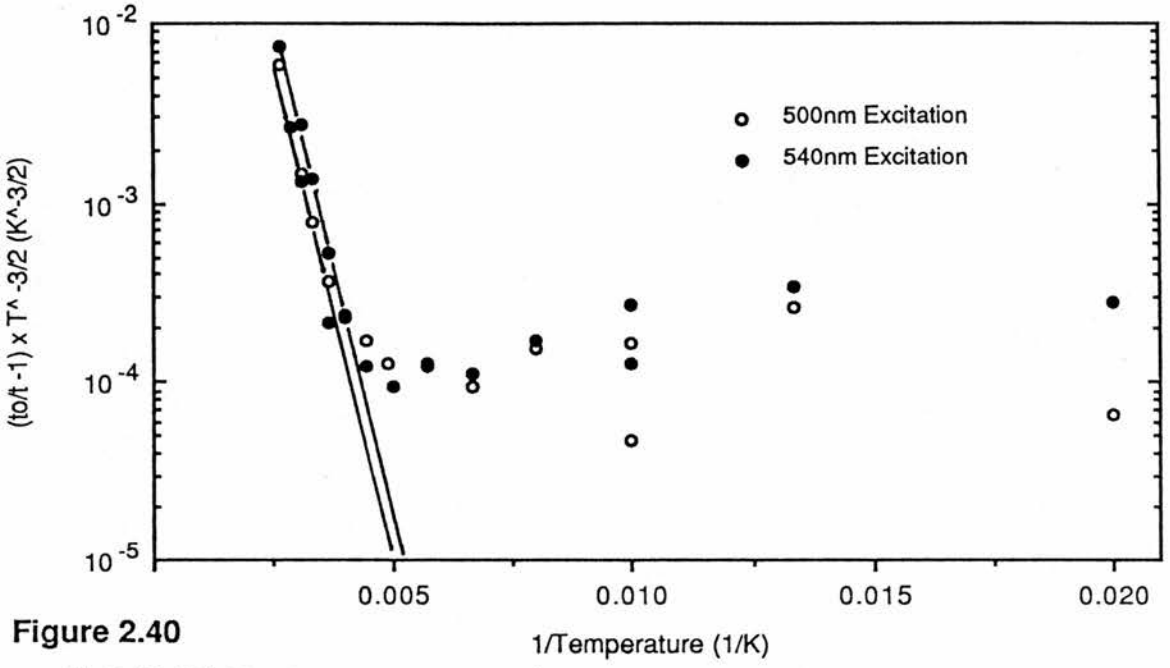

Figure 2.40

[ZnSe:Mn(3)]: Plot of lifetime data for 580nm Mn emission for 500nm and 540nm excitation according to equation (2.15). Lifetime has been divided by 200μsec (τ_o) to give the effective radiative efficiency.

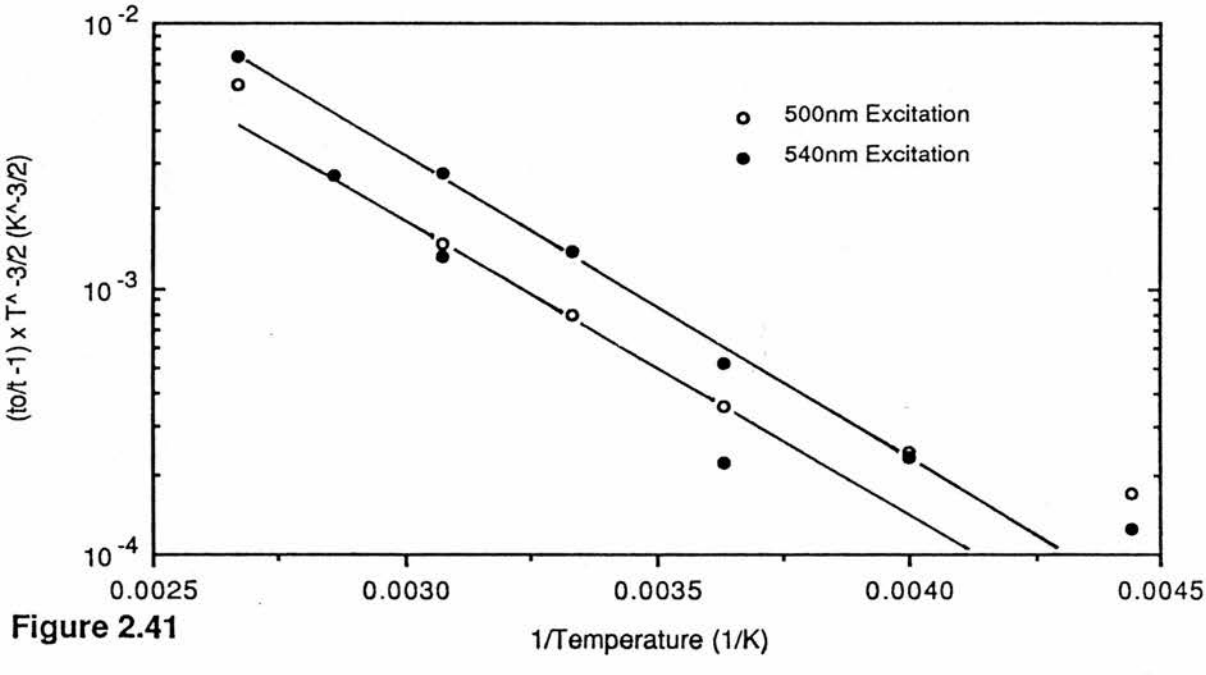

Figure 2.41

[ZnSe:Mn(3)]: Plot of lifetime data for 580nm Mn emission for 500nm and 540nm excitation according to equation (2.15). Lifetime has been divided by 200μsec (τ_o) to give the effective radiative efficiency.

different since the lifetime is supposed to independent of the S.A. emission. This may be an indication of the errors inherent in these experiments.

ZnSe:Mn(4)

No Auger coefficient could be found for this sample since there was no quenching. However it was proposed that an estimate might be made of the Auger coefficient for electrons still bound to the donors (γ_b). The Mn in this sample had a lifetime of 235 ± 2 μsec which it was thought might be close to the true radiative lifetime of the Mn. In ZnSe:Mn(3) the longest lifetime measured was 220 μsec which is reduced from 235 μsec by the neutral donor Auger quenching. From equation (2.4) we have

$$\frac{1}{\tau_o} = \frac{1}{\tau_r} + n_o \gamma_b$$

In ZnSe:Mn(3) n_o (the uncompensated donor density at room temperature) is $6 \pm 2 \times 10^{17}$ cm^{-3} . Using these values we find that $\gamma_b = 5 \pm 1 \times 10^{-16}$ cm^3 s^{-1} which is six orders of magnitude less that γ_f .Gordon has produced a theory [2.7] to estimate the neutral donor Auger coefficient and for ZnSe:Mn it should be only four orders less than the free electron coefficient. The problem may be that we have over estimated n_o or that 235μsec is not the real radiative lifetime because there are still other non-radiative processes present. The estimate for γ_b is based on the assumption that the electron interaction is direct in character so this result may be further evidence for the need to use an exchange interaction.

ZnS:Mn(1)

Lifetime data seemed to indicate that the sample was 50% quenched at room temperature. Using the room temperature Hall effect we have

$$n_e \gamma_f \tau_o \approx 1 \qquad \text{for 50\% quenching}$$

$$\Rightarrow \gamma_f \approx (6 \times 10^{15} . 1.5 \times 10^{-3})^{-1}$$

$$\approx 1.1 \times 10^{-13} \text{ cm}^3 \text{ s}^{-1} .$$

This value of γ_f is three orders of magnitude smaller than that found by Gordon [2.7, 2.8]. The sample was however know to be strongly quenched at room temperature so it was suspected that the sample was very inhomogeneous. It was for this reason that other samples of ZnS:Mn were sought.

ZnS:Mn(2)

The only data available was that for the resistivity and the luminescence intensity. Plotting the luminescence as in equation (2.15) we find the activation energy and Auger coefficient to be ;

E_d = 0.09 eV $\qquad \gamma_f = 4.9 \pm 0.4 \times 10^{-10}$ cm^3 s^{-1} $\qquad$ figure (2.42b)

The energy agrees with that found from the resistivity and γ_f is in the range of values found by Gordon [2.8]. Figure (2.43) shows a numerical fit to the actual luminescence using the values above.

ZnS:Mn(3)

Lifetime data was of no use in this sample because of the inhomogeneity in the conductivity as was found for ZnS:Mn(1). Resistivity data was also useless because it was inconsistent.Trying to fit the intensity data to equation (2.19) gave an Auger coefficient of 1.8 x 10^{-11} cm^3 s^{-1} . However this value is highly questionable since it was not possible to demonstrate that the quenching was indeed an Auger process.

2.5.3 Summary

ZnSe:Mn

Due to a S.A. emission present below 150K it is difficult to determine the Auger coefficient from measurements of the emission intensity. Values determined from this data range from 1 to 11 x 10^{-10} cm^3 s^{-1} . Using lifetime data the range of values becomes 1 to 5 x 10^{-10} cm^3 s^{-1} . For some unknown reason the Auger coefficient determined by exciting the Mn at 540nm is greater than that for excitation at 500nm.

ZnS:Mn

Measurement of the Auger coefficient is difficult because of the uncertainties in the electron concentration and an apparent inhomogeneity in the donor distribution as shown by the different quenching seen for lifetime and intensity measurements. From intensity measurements on the one sample that showed reasonable resistivity we calculate an Auger coefficient of 4.9 x 10^{-10} cm^3 s^{-1} which is in agreement with the previous estimate by Gordon [2.8].

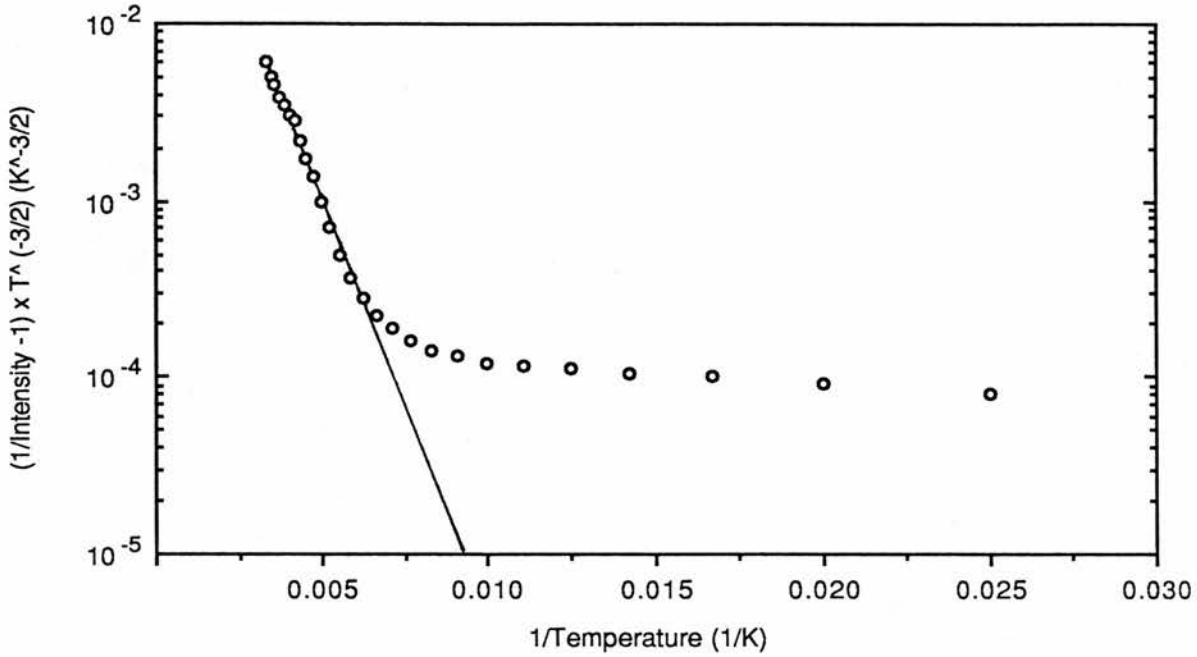

Figure 2.42a [ZnS:Mn(2)]: Plot according to equation (2.15) of normalised luminescence intensity for 580nm Mn emission excited at 500nm.

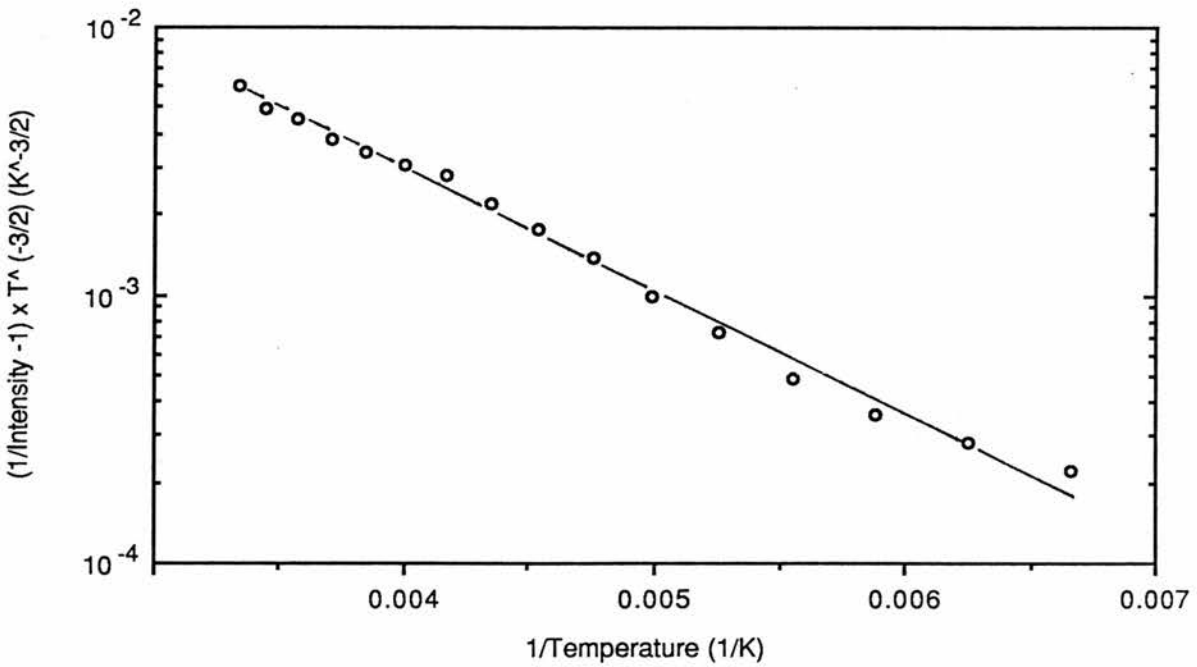

Figure 2.42b [ZnS:Mn(2)]: Plot of the normalised 500nm Mn excitation of the 580nm Mn emission intensity according to equation (2.15).

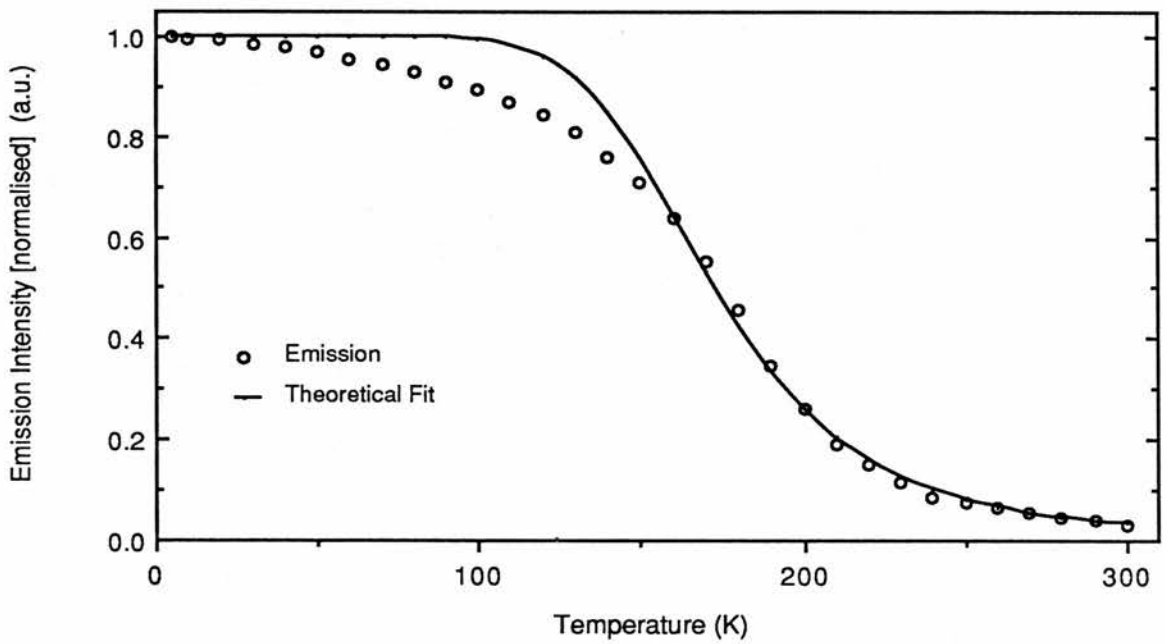

Figure 2.43 [ZnS:Mn(2)]: Comparison of the true luminescence values from figure(2.26) with the luminescence predicted by equation(2.15) using values found from figure(2.42b).

2.6 Concluding Remarks

From the electrical and optical measurements a linear relationship was demonstrated between the quenching of the Mn emission in ZnSe:Mn and ZnS:Mn and the free electron concentration. This was the first time that it has been possible to show that the Mn emission in ZnSe:Mn was quenched by an Auger process. Difficulties in controlling the carrier concentrations in samples has meant that previous samples have always been too quenched for measurements to be made. The linear relation that was found is a characteristic of the Auger process proposed by Allen and others to explain certain luminescence phenomena. Furthermore the different experimental Auger coefficients found for this process are of the same order and yet are in themselves many orders greater than that predicted by current models [2.5, 2.6]. This enhancement of the Auger process must be related to the special combination of Mn in ZnSe and ZnS since Mn in CdF_2 has an Auger coefficient γ_f as predicted and other emissions in ZnSe persist even at free carrier densities of 10^{16} cm^{-3}. Allen has argued that this Auger process occurs via the exchange interaction which is enhanced by the approximate energy matching between the conduction band and the Mn excited state. This idea was proposed when the Auger coefficient had only been measured for ZnS:Mn. Our results show that the same enhancement seems to be occurring in ZnSe:Mn in agreement with Allen's proposal. It is difficult to quantify this enhancement because of uncertainty in the calculation of the conduction band. There is some experimental evidence [2.16] to suggest that the Γ_1 - X_3 valleys in the conduction band are separated by 3.1 eV which would make the matching less important but this is still to be fully demonstrated. Further evidence in favour of an exchange interaction is that from the lifetime one would expect γ_f in ZnSe to be an order larger than γ_f in ZnS for a direct interaction while the experimental evidence shows them to be about equal.

If energy matching is enhancing the Auger process this has some important consequences. From detailed balance the Auger coefficient and the excitation cross-section are directly related. Allen [2.5] has shown that the Mn excitation cross-section and the Auger coefficient are related by

$$\frac{\sigma(E_{eg})\, \upsilon_{eg}}{\gamma} = \frac{\rho(E_l)}{\rho(E_{eg})} . \qquad (2.20)$$

Here $\rho(E_l)$ and $\rho(E_{eg})$ are respectively the density of states at the bottom of the conduction band and at an energy E_{eg} above the bottom of the conduction band, E_{eg} being the excited state energy. γ is the Auger coefficient while υ_{eg} and $\sigma(E_{eg})$ are the electron velocity and impact cross-section at an energy E_{eg} above the bottom of the conduction band. Normaly the electrons involved in Auger quenching are of energy $E_l \sim kT$ above the bottom of the conduction band which at room temperature is about 10^{-2} eV. We can expand (2.20) to give the density of states in terms of energy which gives

$$\sigma(E_{eg}) \sim \frac{\gamma}{\upsilon_{eg}}\left(\frac{m_l^*}{m_{eg}^*}\right)^{3/2}\left(\frac{k\,T}{E_{eg}}\right)^{1/2}. \qquad (2.21)$$

If E_{eg} is near the bottom of the second conduction band υ_{eg} will be small and m_{eg}^* the effective mass will be large and (2.21) will be difficult to evaluate. If we consider the more usual case where E_{eg} is above the bottom of the second conduction band then we may consider the two electron masses to be approximately equal and the electron velocity is typically 10^5 ms^{-1}. The cross-section will then be

$$\sigma(E_{eg}) \sim \frac{10^{-10}}{10^7} \times \left(\frac{1}{1}\right)^{3/2} \times \left(\frac{10^{-2}}{2.12}\right)^{1/2} \sim 10^{-18}\ \text{cm}^2.$$

This does not directly agree with the experimental value for the cross-section found by Mach & Müller [2.17] because this value is for the cross-section just above threshold while the cross-section of Mach & Müller refers to the cross-section averaged over the higher electron energies. In Chapter 3 it can be seen that the initial cross-section is more than an order less than the peak value and so we would expect the averaged cross-section to be 10^{-17} to 10^{-16} cm^2 from the Auger coefficient.

Enhancement of the Auger process should produce a corresponding enhancement of the impact excitation. In the following chapters we show how impact excitation cross-sections can be calculated using a direct interaction model. The values produced for Mn and Er by this method were much less than those found experimentally. Normally the exchange term is not included in such calculations but from the results of Auger quenching it would appear that this may not be justified.

Assuming energy matching is the key to high electroluminescence efficiency it may be possible to admix semiconductors to produce alloys in which the conduction bands match a particular excitation energy level in an emission centre. This might allow the range of

efficient materials to be increased. Limitations will however still exist in increasing the emission intensity. Gordon found [2.18] that as the device voltage was increased the electrons moved out of the X_3 valley which would reduce any energy matching and so decrease the device efficiency. If the current is increased without significant movement of the electrons out of the X_3 valley these electrons can themselves start to Auger quench the emission by transferring to the next highest valley [2.1]. This might seriously inhibit the possibilities of lasing action in such materials as was found by Burt in GaAlAsSb [2.9].

2.7 Appendix

Design and Construction of a Short Duration Flashlamp for Photoexcitation

To make lifetime measurements of Mn in ZnSe:Mn a light source was needed that could be switched on or off in a few micro-seconds. A flashlamp was the only viable solution and as one was not available it was decided to design and build one. The choice of flashlamp and design of the triggering circuitry was made by reference to a technical manual supplied by Nobelight Ltd. Here are stated only the final results of the design decisions.

Before designing a flashlamp it was necessary to show that such a method was practical. Flashlamp excitation is different from that produced by a chopped light source because the number of excited luminescence centres is much less and no equilibrium is established during the excitation.For a chopped light source the final emission intensity after a period of a few lifetimes will be

$$I_{MAX} = A\eta \qquad (2A.1)$$

where A is proportional to the excitation intensity and η is the radiative efficiency. For a flashlamp the radiative efficiency does not affect the final intensity of the emission and at the end of a pulse of duration "t " the emission intensity is

$$I_{FLASH} = A\frac{t}{\tau_r} \qquad (2A.2)$$

when $t << \tau_r$. To be practical we might insist that $I_{FLASH} \geq I_{MAX}$. Allowing for the different energetic and geometrical efficiencies of the tungsten lamp and the flash lamp we estimated that a 50W tungsten lamp was equivalent to a 750W flashlamp. For a 5μsec flash this

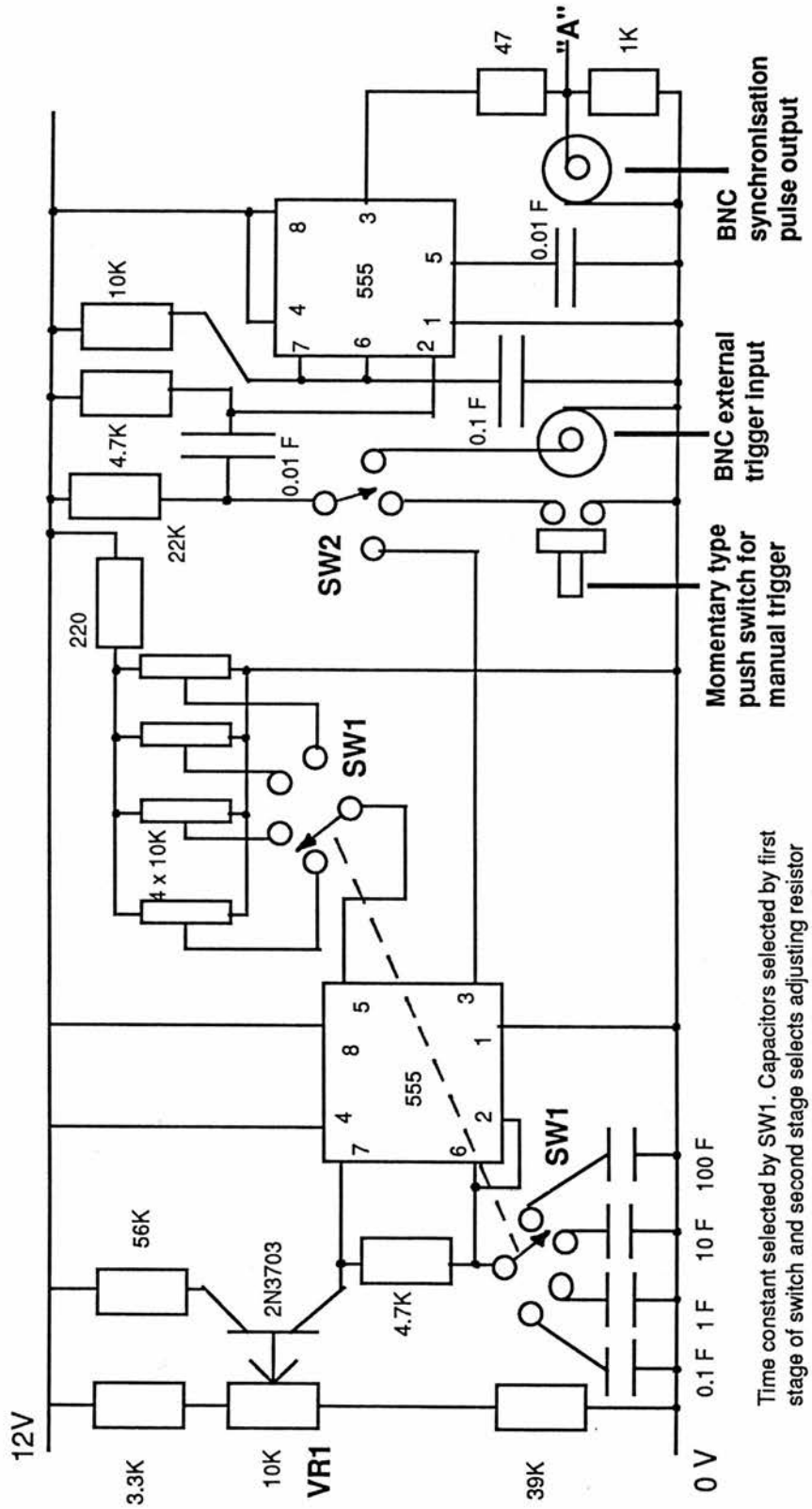

Time constant selected by SW1. Capacitors selected by first stage of switch and second stage selects adjusting resistor preset to give an accurate time base. Using VR1 the time base can be multiplied by a fator of up to 10.

Frequency ranges:
0.1 F 100 to 10 Hz
1 F 10 to 1 Hz
10 F 1 to 10 seconds
100 F 10 to 100 seconds

SW2 selects triggering mode. "A" is trigger signal for triggering thyristor in tigger unit (figure 2A.2)

Figure 2A.1a Design of rate generator allowing for automatic, manual and external triggering of falshlamp with an output facility for a synchronising pulse.

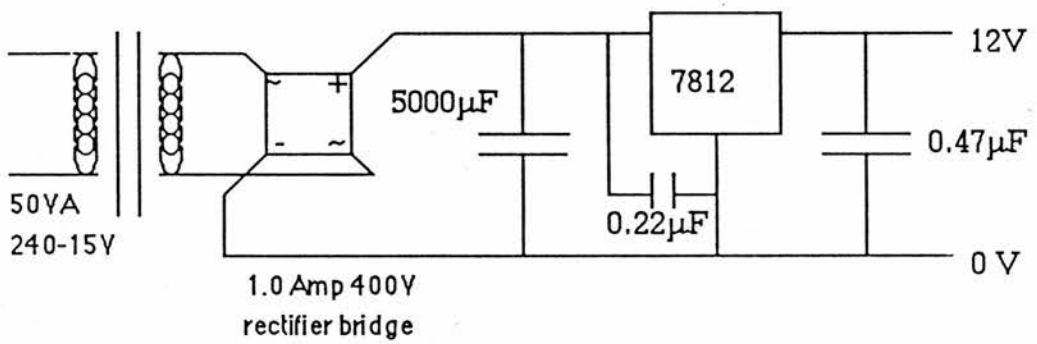

Figure 2A.1b 12Volt stabalised power supply for tigger control unit

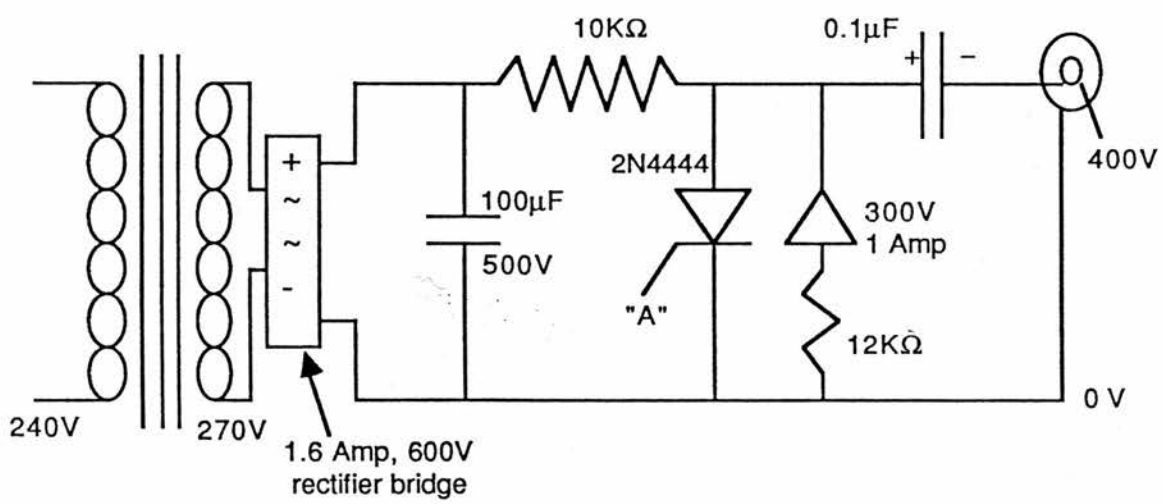

Figure 2A.2 Trigger unit for firing flash lamp

is equal to discharging about 4mJoules. This was considered to be well with in the capabilities of a flashlamp.

It was required that the flashlamp should have a reasonable lifetime (i.e. greater than 1000 flashes), a short pulse duration (about 1 to 5 μsec) and a high energy (a few tenths of a Joule) to provide adequate excitation in the small excitation period. The most suitable lamp with these features should have a short electrode gap (to reduce resistance) and a wide bore (to further reduce resistance and to lower the current density which determines the degradation of the gas fill).A short gap and wide bore will confine the discharge to a small area increasing the intensity of the lamp and making it easier to focus the discharged light onto a sample. The lamp selected was designated 2.15XAM, a miniature Xenon filled air cooled lamp of 2mm bore and 15mm gap.(A better replacement lamp would be a 4.15XAM or a short arc pulsed Xenon lamp of the SAPX100 series e.g. SAPX10015, consult the Nobelight technical manual for details).

From the formulae given by Nobelight it was calculated that for a 1μsec flash the electrical system should have an inductance of 0.3μH which is the order of the native inductance of the coaxial cable used in the circuit, so no extra inductance was needed. The lamp was to be used in single pulses so that it could be operated at its extreme limits . Even so the final current density had to be greater than the maximum recommended by the manufacturer. A capacitor bank was built out of nineteen 0.1μF capacitors rated at up to 1200V (figure 2A.5). In this way it was hoped that the total capacitance could be easily varied by connecting different numbers of capacitors until the lamp was critically damped and so of minimum decay time. The normal operating voltage was 500 to 1000V and all nineteen capacitors were eventually used giving a total energy of up to one Joule. For a 5μsec flash this is equivalent to 190KW continuous power.

A pulse generator (figure 2A.1) based on the suggested circuit in the Nobelight manual was built which allowed automatic and manual triggering of the lamp and produced a synchronising signal for a digital oscilloscope. The tigger pulse from this generator activated a trigger unit (figure 2A.2) producing a 400V pulse needed to drive the trigger transformer in the flashlamp housing (figure 2A.3). The trigger transformer was connected to the outside of

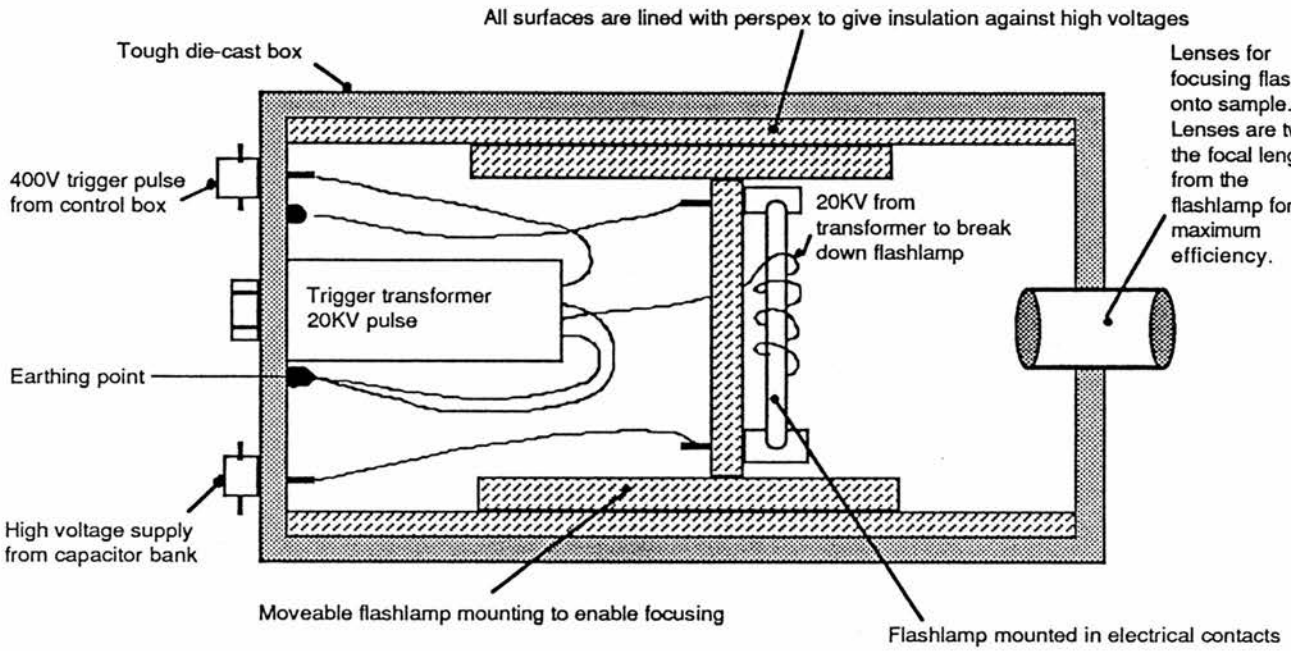

Figure 2A.3 Construction of flash lamp housing containing 20KV trigger transformer and flash lamp.

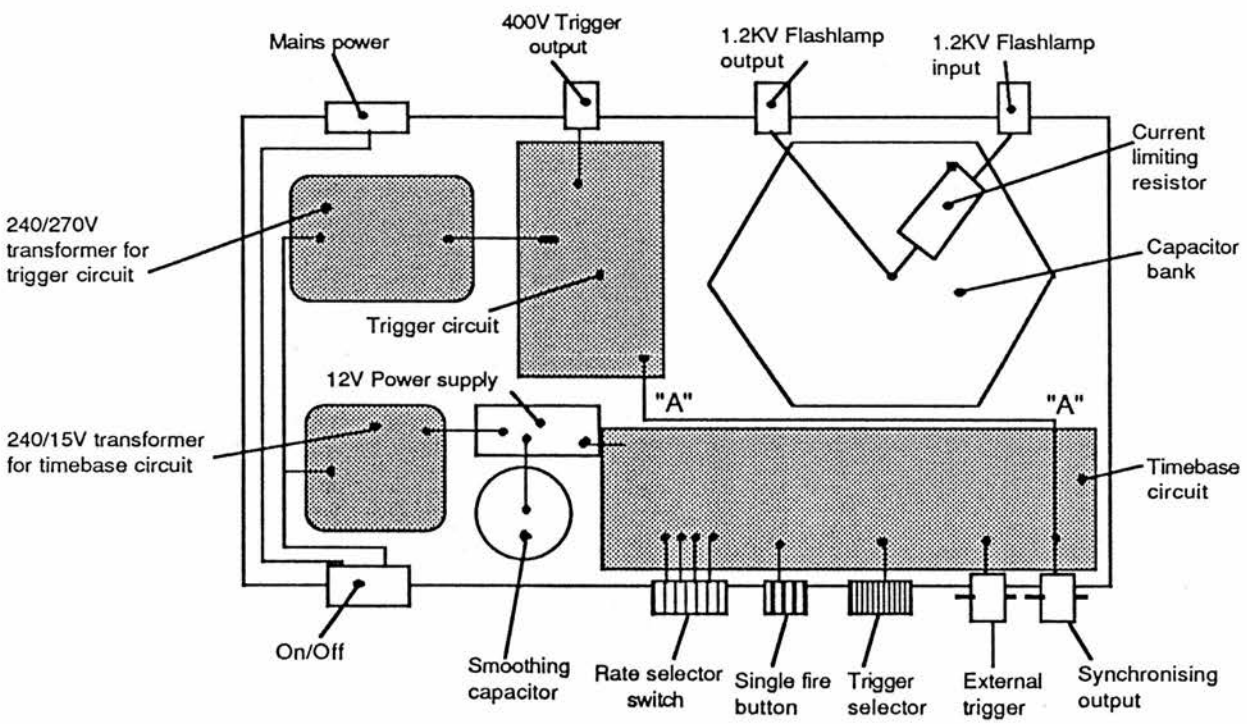

Figure 2A.4 Layout of circuits, power supplies and capacitor bank in control box

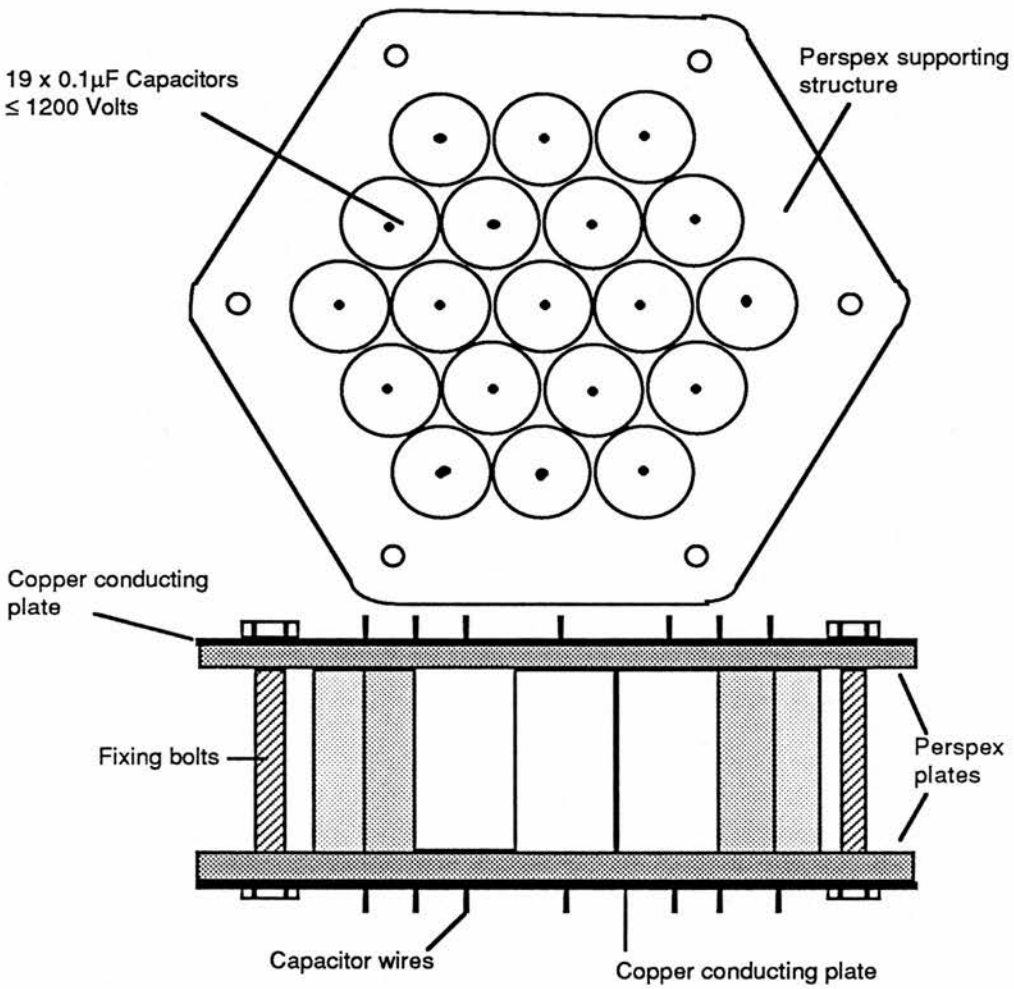

Figure 2A.5

Construction of capacitor block using 19 x 0.1μF capacitors assembled so that there is little induction and low resistance. Mounting must be able to withstand high voltages. Total capacitance can be varied by connecting different numbers of capacitors.

the flashlamp and produced a 20KV pulse that breaks down the gas in the tube. The inside of the flashlamp housing was covered in 5mm thick perspex to provide insulation and the mounting for the lamp is built from the same material. By moving the lamp mounting it is possible to change the position of the lamp image produced by the double lens system in the housing.

One practical aspect of the flashlamp that we had not realised was that the ratio of the excitation intensity to the luminescence intensity is much greater than for our tungsten lamp. If we let the excitation efficiency be α then for an excitation intensity L we have

$$A = \alpha L \qquad (2A.3)$$

and

$$\frac{I_{MAX}}{L} = \alpha\eta \qquad (2A.4)$$

so the ratio varies with η as is already known. For a flashlamp the equivalent equation is

$$\frac{I_{FLASH}}{L} = \frac{t\alpha}{t_r} \qquad (2A.5)$$

For small values of t (2.5μsec compared with 200μsec) the emission is two orders weaker and can only be separated from the excitation by using additional broad band filters. For the excitation a no. 44 Kodak Wratten filter was used with a 500nm interference filter and for the emission a no. 23A Kodak Wratten filter was used with a 580nm interference filter.

Chapter 2

2.7 References

[2.1] H.-E.Gumlich *J.Lumin.* **23** (1981) 73

[2.2] J.M.Langer *J.Lumin.* **23** (1981) 141

[2.3] J.M.Langer, A Lemánska-Bajorek,A.Suchocki, W.Walukiewicz & B.Wiktor *J.Lumin.* **24/25** (1981) 889

[2.4] J.M.Langer & Le Van Hong *J.Phys.C: Solid State Phys.* **17** (1984) L923

[2.5] J.W.Allen *J.Phys.C: Solid State Phys.* **19** (1986) 6287

[2.6] J.M.Langer *J.Lumin.* **40/41** (1988) 589

[2.7] N.T.Gordon *PhD Thesis, St.Andrews University*

[2.8] N.T.Gordon & J.W.Allen *Solid State Comm.* **37** (1981) 441

[2.9] M.G.Burt *J.Phys.C: Solid State Phys.* **14**(1981) 3269

[2.10] J.W.Allen, M.D.Ryall & E.M.Wray *Phys. Stat.Sol.(a)* **17** (1973) K101

[2.11] E.Chimczak & J.W.Allen *J.Phys.D: Solid State Phys..***18** (1985) 951

[2.12] M.Aven & C.A.Mead *Appl. Phys. Letts.* **7** (1965) 8

[2.13] I.A.Miranov, Ya A.Oksman & Yu. S.Ryzhkin *Sov.Phys.Semicond.* **2** (1969) 1155

[2.14] Hu Xiao-peng, Hai Ying, Yu Jia-qu, Li Hong, Lü An-de, Yang Bao-jun, Jiang Xue-yin, Huang Shi-hua & Dong Yu-min *Lumin. Display Devices.* **2** (1983) 11

[2.15] T.C.Leslie & J.W.Allen *Phys. Stat.Sol.(a)* **65** (1981)545

[2.16] N.E.Rigby & J.W.Allen *J.Phys.C: Solid State Phys.* **21** (1988) 3483

[2.17] R.Mach & G.O.Müller *Phys. Stat. Sol. (a)* **81** (1984) 609

[2.18] N.T.Gordon *I.E.E.E. Trans.* **E.D.- 28** (1981) 434

Chapter 3

Theory of Impact Excitation Cross-sections

		Page
3.1	**Introduction**	**70**
3.2.1	**Theory :** Introduction	**70**
3.2.2	Derivation of Cross-section	**70**
3.2.3	First Evaluation of Matrix Integral	**75**
3.2.4	Second Evaluation of Matrix Integral	**76**
3.2.5	Momentum Integral	**77**
3.2.6	Evaluation of $\|x_{eg}\|^2$	**77**
3.2.7	Degeneracy	**78**
3.3	**Further Approximations**	**79**
3.4	**Physical Interpretation of Cross-section**	
3.4.1	Parabolic-Band Cross-section	**80**
3.4.2	Partially-Parabolic-Band Cross-section	**81**
3.4.3	Non-Parabolic-Band Cross-section	**85**
3.5	**Conclusion**	**90**
3.6	**References**	**91**

Chapter 3

Theory of Impact Excitation Cross-sections

3.1 Introduction

Conduction electrons in a host lattice can impact excite deep level impurities e.g. luminescence centres. However, it is not clear how great a role the band structure plays in determining the efficiency of this process. In this chapter we give a derivation for the impact cross-section based on the work by Mott & Massey [3.1] and adapted by Allen [3.2] and others [3.3,3.4] for the solid state. To calculate the cross-section we consider the direct term of the matrix element for the electron interaction. Unlike previous calculations of the cross-section we derive a form that makes no assumption about a parabolic conduction band. By further approximations this is compared to the cross-section of Yu & Shen [3.3] and comments are made on any differences. The aim of this chapter is to describe the physical processes involved in impact excitation and to show how the band structure influences the cross-section.

3.2.1 Theory : Introduction

Consider the effect of a conduction electron passing close to an electron bound to an impurity as shown in figure (3.1). The free and bound electrons interact via their electric fields which mix their wave functions allowing the excitation energy to be transferred between them. The free electron will change its energy (E_u) and momentum (k_u) as shown in figure (3.2a) transferring from the upper to the lower region of the conduction band and changing its direction of motion. Similarly the bound electron is promoted from the ground state to an excited state as in figure (3.2b). The initial (E_u) and final (E_l) energies of the incident electron are related to the excitation energy by $E_u = E_l + E_{eg}$. If the bound electron returns to the ground state by emitting a photon the impurity can form a luminescence centre. Any change in the momentum of the incident electron is taken up by the impurity.

3.2.2 Theory : Derivation of Cross-section

The cross-section for an interaction between two particles can be calculated by solving the appropriate Schrodinger equation by a Green's function method. The physical

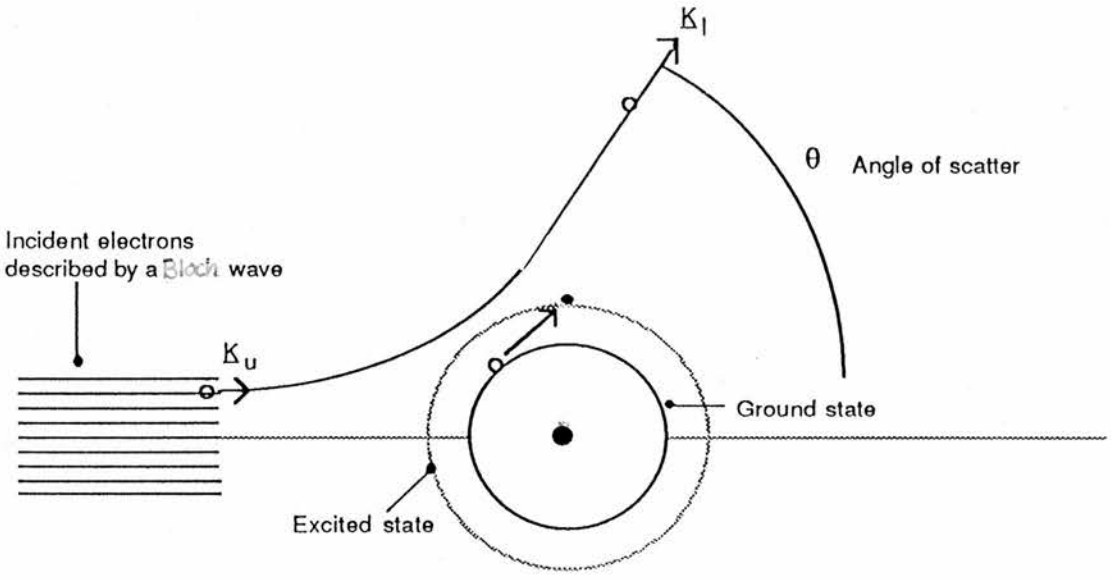

Figure 3.1 A diagram showing how the incident electron is scattered through an angle θ while the bound electron is promoted from the ground to an excited state.

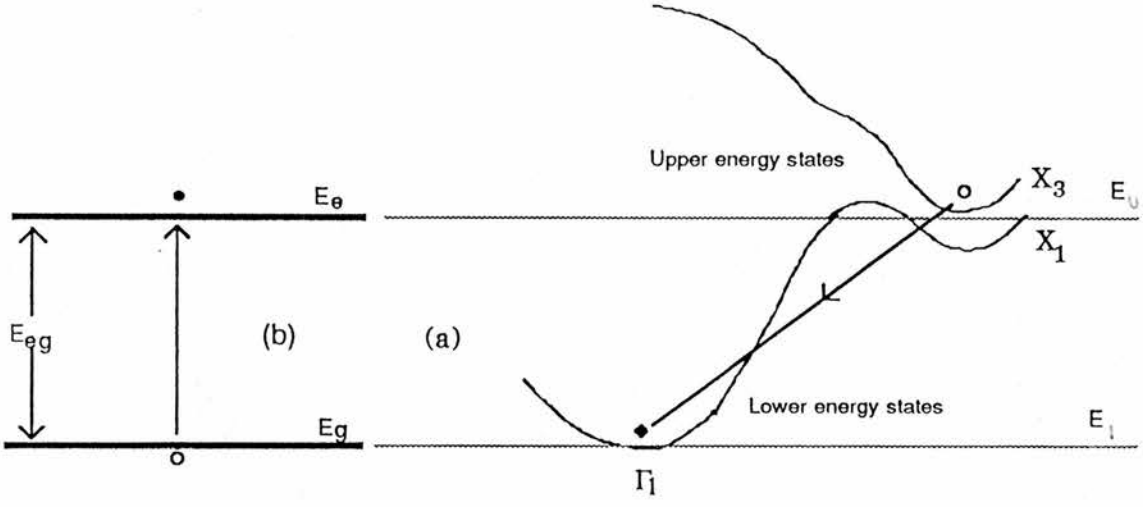

Ground and excited states ofa luminescence centre

Band structure of ZnS showing how an energetic electron transfers from a high energy to a low energy state during impact excitation.

Figure 3.2

interpretation of this method is difficult which makes adaptation to the solid state uncertain. An alternative is to apply Fermi's Golden Rule to the system and evaluate the transition rate by the Born approximation. The Born approximation is normally considered to be suitable only for high energy collisions but has been shown to be a good approximation in the solid state [3.5].

For a single conduction electron in a volume L^3 the normalised wave functions are

a) Initial wave function $\psi_i = L^{-3/2} U_{k_u}(r_1) \exp(i\underline{k}_u \cdot r_1)$

b) Final wave function $\psi_f = L^{-3/2} U_{k_l}(r_1) \exp(i\underline{k}_l \cdot r_1)$ (3.1)

where $\underline{k}_u$ and $\underline{k}_l$ are the electron momentum in the upper and lower regions of the conduction band and $U_{\underline{k}}(r)$ is the cell periodic part of the Bloch function. The bound electron is described by the wave functions $\psi_g(r_2)$ and $\psi_e(r_2)$ of the unperturbed ground and excited states respectively.

For the direct interaction process we need only consider one spin state as spin is conserved. Perturbations due to spin and magnetic interactions are not included as these will be small compared to the perturbation due to the incident electron. It is sufficient then to take the unsymmetrised product of the bound and incident electron wave functions.

The flux density of the incident electron is $L^{-3} V_u$ where V_u is the electron velocity in the upper region of the conduction band. The partial cross-section σ_p for electrons of energy E_u is defined as the ratio of the scattered electron flux in a solid angle $d\Omega$, to the incident flux. Since this scattering induces an electronic transition we use Fermi's Golden Rule to write

$$d\Omega V_u L^{-3} \sigma_p(E_u, \theta, \phi) = \frac{2\pi}{\hbar} \left| \left\langle L^{-3/2} U_{k_u}(r_1) \exp(i\underline{k}_u \cdot r_1) \psi_g(r_2) \right| \mathcal{H}' \right| L^{-3/2} U_{k_l}(r_1) \exp(i\underline{k}_l \cdot r_1) \psi_e(r_2) \right\rangle \Big|^2 \rho \, d\Omega \qquad (3.2)$$

where ρ is the density of states for one spin in the angle $d\Omega$ into which the electron is scattered.

For the scattered electron the density of states is

$$N(E_l) = N(k_l) \frac{dk}{dE} = \frac{4\pi k_l^2}{\left(\frac{2\pi}{L}\right)^3} \frac{1}{\left(\frac{dE}{dk}\right)_l} . \qquad (3.3)$$

Since $\left(\frac{dE}{dk}\right)_l = \hbar V_l$ this becomes

$$\rho\, d\Omega = N(E_l)\frac{d\Omega}{4\pi} = \frac{k_l^2 L^3}{8\pi^3}\frac{1}{\hbar V_l}\, d\Omega . \qquad (3.4)$$

If the potential is long range and slowly varying it is possible to factor out the two cell periodic Bloch functions $\left(U_{\underline{k}}(\underline{r})\right)$ from the integral as a constant S_{lu} and (3.2) now becomes

$$\sigma_p(E_u,\theta,\phi)\, d\Omega = \frac{k_l^2}{4\pi^2\hbar^2}\frac{S_{lu}^2}{V_l V_u}\left|\iint \mathcal{H}'\exp(i(\underline{k}_u - \underline{k}_l).\underline{r}_1)\psi_g(\underline{r}_2)\psi_e^*(\underline{r}_2)\, d\tau_1\, d\tau_2\right|^2 d\Omega . \qquad (3.5)$$

Figure (3.3) shows how the incident electron is scattered through angles θ and ϕ. Because momentum is not a unique function of energy the magnitude of $\underline{k}_l$ will change with θ and ϕ i.e. the energy surface in k-space is not spherical. This makes integration of (3.5) difficult but we must evaluate this integral to give the total cross-section for scattering into any angle. If the incident electron loses most if its energy in the collision the electron will be scattered into the Γ_1 valley which to a good approximation is parabolic and isotropic. The momentum vectors $\underline{k}_l$ will then all touch a sphere of radius k_l and (3.5) has no inherent ϕ dependence as shown in figure (3.3) . Integrating (3.5) with respect to ϕ introduces a factor of $2\pi\sin\theta$

$$d\Omega \rightarrow d\omega = 2\pi\sin\theta\, d\theta . \qquad (3.6)$$

To scatter the incident electron the momentum needs to be changed as in figure (3.4).

where $\underline{K} = \underline{k}_u - \underline{k}_l$

so $K^2 = k_u^2 + k_l^2 - 2k_u k_l \cos\theta$

and $2KdK = 2k_u k_l \sin\theta\, d\theta .$ (3.7)

Using (3.7) $d\omega$ may be written as

$$d\omega = 2\pi\sin\theta\, d\theta = \frac{2\pi K}{k_u k_l} dK . \qquad (3.8)$$

The partial cross-section (3.5) can now be written as

$$\sigma_p(E_u,\theta)\, d\omega = \frac{S_{lu}^2}{2\pi}\frac{k_l}{k_u}\frac{K}{\hbar^2 V_l V_u}\left|\iint \mathcal{H}'\exp(i\underline{K}.\underline{r}_1)\psi_g(\underline{r}_2)\psi_e^*(\underline{r}_2)\, d\tau_1\, d\tau_2\right|^2 dK . \qquad (3.9)$$

The actual value of S_{lu}^2 is unknown and difficult to find but is less than or equal to 1. We take 1 as the value to give an upper limit to the cross-section as have Yu & Shen [3.3].

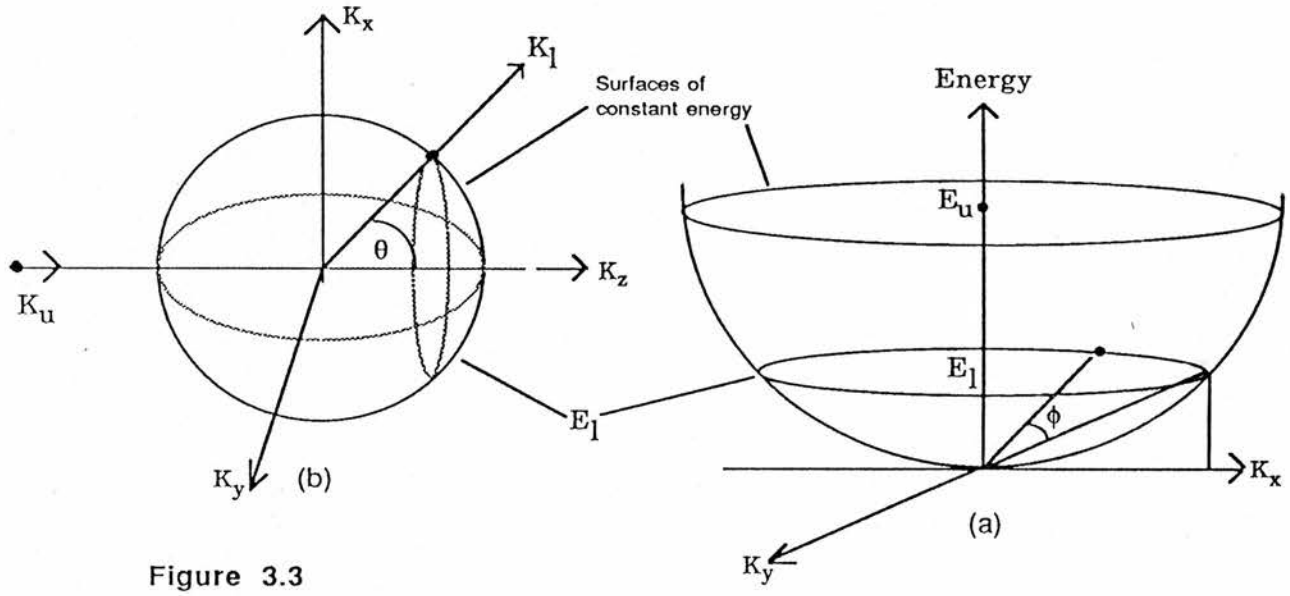

Figure 3.3

A diagram showing how the incident electron is scattered through angles θ and ϕ so that final momentum vector touchs a surface of constant energy (and constant magnitude of momentum for an isotropic conduction band).

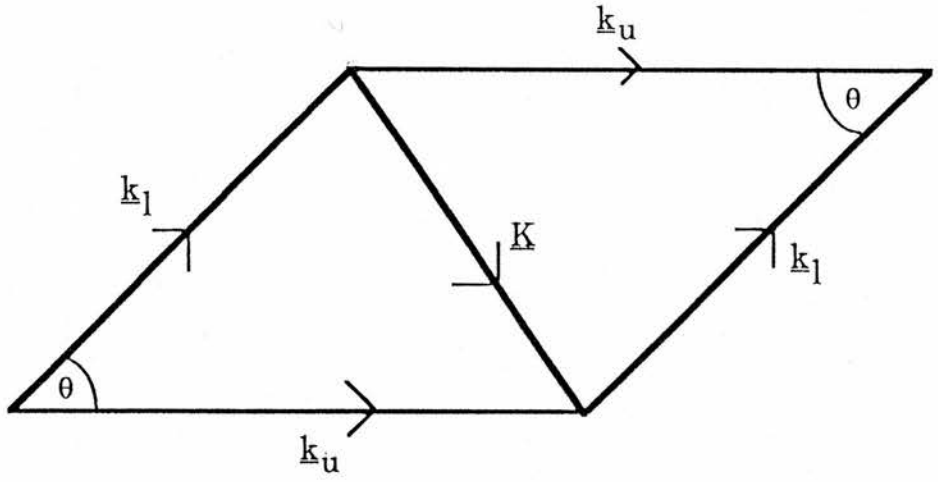

Figure 3.4

This figure shows the relationship between the incident electron momentum $\underline{k}_u$, the scattered electron momentum $\underline{k}_l$ and the momentum change $\underline{K}$ for scatter through an angle θ.

3.2.3 First Evaluation of the Matrix Integral

The matrix Hamiltonian may by described in two physically identical forms; as a simple coulomb repulsion between the electrons, or as a monopole-dipole interaction between the incident and bound electrons.

Considering the simple coulomb form first we have

$$\mathcal{H}' = \frac{e^2}{\varepsilon |\underline{r}_1 - \underline{r}_2|} . \qquad (3.10)$$

The matrix integral is then

$$\iint \frac{e^2}{\varepsilon |\underline{r}_1 - \underline{r}_2|} \exp(i\underline{K}.\underline{r}_1)\psi_g(\underline{r}_2)\psi_e^*(\underline{r}_2)\, d\tau_1 d\tau_2 . \qquad (3.11)$$

The electric fields of the electrons are screened by the surrounding matter and this is included by the factor ε . The precise value of ε is unknown and will vary with the separation of the electrons and the velocity at which the electrons approach one another. At large separations ε will be the d.c. dielectric constant but at such distances the interaction will be negligible. At close quarters the interaction changes rapidly with time so the high frequency a.c. dielectric constant is more appropriate. However at distances of a few Å the rate of change of the field is so rapid that even the a.c. dielectric constant is insufficient to estimate the screening. We use the a.c. value as this gives an upper limit to the screening that occurs. The value of ε is estimated from

$$\varepsilon_\infty = n^2 \qquad (3.12)$$

where n is the refractive index of the host material. Yu & Shen [3.3] use a lower limit for the screening by assuming $\varepsilon = 1.0$ implying that the surrounding material is unable to react to the electric field within the interaction time. The choice of ε has been discussed by Nash [3.6] who concludes that the use of unity overestimates the electron-electron interaction in the solid state.

To integrate with respect to τ_1 we use the Bethe integral [3.7] shown in equation (3.13)

$$\int \frac{1}{|\underline{r}_1 - \underline{r}_2|} \exp(i\underline{K}.\underline{r}_1)\, d\tau_1 = \frac{4\pi}{K^2} \exp(i\underline{K}.\underline{r}_2) . \qquad (3.13)$$

For simplicity we define the X-axis for $\underline{r}_2$ in the direction of $\underline{K}$. We then expand the exponent as a power series of $\underline{K}.\underline{r}_2$ [3.8] for which $\underline{K}.\underline{r}_2$ is small because $\underline{r}_2$ is for a locally bound electron

$$\exp(i\underline{K}.\underline{r}_2) = \exp(iKx_2) = 1 + iKx_2 + \frac{1}{2}(iKx_2)^2 + \ldots \qquad (3.14)$$

Applying (3.13) and (3.14) to (3.11) we have

$$(3.11) = \frac{4\pi e^2}{\varepsilon K^2}\left[\int \psi_g(\underline{r}_2)\psi_e^*(\underline{r}_2)d\tau_2 + iK\int x_2\psi_g(\underline{r}_2)\psi_e^*(\underline{r}_2)d\tau_2\right]$$

$$= \frac{4\pi e^2}{\varepsilon K^2}\left[0 + iK|x_{eg}|\right]$$

$$= \frac{4\pi i e^2}{\varepsilon K}|x_{eg}| \qquad (3.15)$$

where $|x_{eg}|$ is the matrix element of x with respect to the ground and excited states of the impurity.

3.2.4 Second Evaluation of the Matrix Integral

To check the sufficiency of the above evaluation we evaluate the matrix integral using the monopole-dipole Hamiltonian. The Hamiltonian is now

$$\mathcal{H}' = \frac{e^2}{\varepsilon}\frac{\underline{r}_1.\underline{r}_2}{r_1^3} \qquad (3.16)$$

and the matrix element is

$$\iint \frac{e^2}{\varepsilon}\frac{\underline{r}_1.\underline{r}_2}{r_1^3}\exp(i\underline{K}.\underline{r}_1)\psi_g(\underline{r}_2)\psi_e^*(\underline{r}_2)\,d\tau_1 d\tau_2 \ . \qquad (3.17)$$

Again choosing the X-axis for $\underline{r}_1$ to be in the direction of $\underline{K}$ the dot product in the exponential reduces to one component. The integral can now be separated.

$$(3.17) = \frac{e^2}{\varepsilon}\int\frac{\underline{r}_1}{r_1^3}\exp(iKx_1)\,d\tau_1 \ . \int \underline{r}_2\psi_g(\underline{r}_2)\psi_e^*(\underline{r}_2)d\tau_2 \ . \qquad (3.18)$$

The first integral is evaluated like Bethe's integral and the second is the average value of $\underline{r}_2$, the radius of the bound electron orbital. The matrix element is then

$$(3.17) = \frac{e^2}{\varepsilon}\frac{4\pi i}{K}\hat{\underline{x}}.\,|\underline{r}_2| = \frac{4\pi i e^2}{\varepsilon K}|x_{eg}| \qquad (3.19)$$

which is the same as (3.15) showing that the descriptions of the interaction are indeed equivalent.

At this point it is good to look at (3.15) & (3.19) to explain the physical significance of the equations. The interaction is inversely proportional to K the change in the momentum of the incident electron, which is transferred to or from the impurity by the interaction. This equation

tells us that the ability to transfer energy between the electrons is inversely proportional to the magnitude of the change of momentum and is proportional to the electric dipole moment in the direction of the momentum change.

3.2.5 The Momentum Integral

Combining (3.19) and (3.9) we have

$$\sigma(E_u,\theta)2\pi\sin\theta\, d\theta = \frac{8\pi e^4}{\hbar^2 \varepsilon^2}\frac{k_l}{k_u}\frac{1}{V_u V_l}\frac{dK}{K}\,|x_{eg}|^2 \,. \qquad (3.20)$$

Integrating (3.20) gives the total cross-section. The left hand side is integrated for θ from 0 to π and the right hand side is integrated for K from the minimum to the maximum momentum change corresponding to θ varying from 0 to π, i.e.

for $\theta = 0$ $\qquad K_{min} = k_u - k_l$

for $\theta = \pi$ $\qquad K_{max} = k_u + k_l$.

This gives

$$\sigma(E_u)_{Total} = \frac{8\pi e^4}{\hbar^2 \varepsilon^2}\frac{k_l}{k_u}\frac{1}{V_u V_l}\,|x_{eg}|^2\,\mathrm{Ln}\left|\frac{k_u + k_l}{k_u - k_l}\right| \,. \qquad (3.21)$$

3.2.6 Evaluation of $|x_{eg}|^2$

We still need to evaluate $|x_{eg}|^2$ in terms of a readily available parameter. It is impractical to calculate $|x_{eg}|^2$ from the wave functions of the excited state as these are unknown for the impurity. Instead we use the lifetime of the excited state which depends on $|x_{eg}|^2$. Langer [3.9] uses a similar evaluation of the matrix element to calculate the Auger coefficient. He notes that the radiative lifetime may not be for a purely electric dipole transition but may include a magnetic dipole component. In that situation the cross-section will need to be multiplied by the fraction of the electric dipole contribution to the radiative lifetime. From Dexter [3.10] we have

$$|x_{eg}|^2 = \frac{1}{\tau_{eg}}\frac{1}{\left[n\left(\frac{\varepsilon_{eff}}{\varepsilon_o}\right)^2\right]}\frac{\hbar^4 c^3}{4e^2 E_{eg}^3} \qquad (3.22)$$

where n is the refractive index of the light in the host lattice, E_{eg} is the energy of the excited state and $\left(\frac{\varepsilon_{eff}}{\varepsilon_o}\right)$ is the effective field ratio for the electron in the excited state. Dexter discusses the use

of this constant in his paper. For centres where the excited states have diffuse, spread out wave functions the dielectric constant is that of the host medium and the ratio is taken as unity. In a well shielded unfilled inner shell as found in rare-earths and transition metals the ratio is approximately given by

$$\left(\frac{\varepsilon_{eff}}{\varepsilon_o}\right) = 1 + \frac{n^2 - 1}{3} . \qquad (3.23)$$

At this point we note an apparent mistake in the equivalent equation given by Yu & Shen [3.3]. When comparing their cross-section with ours it would appear that in (3.22) they have used h instead of $\hbar$ when relating E_{eg} to the frequency of the emitted photon. This increases their cross-section by a factor of $(2\pi)^3$.

3.2.7 Degeneracy

In the derivation of the cross-section we have written Fermi's Golden rule (3.2) in a form involving only the incident and bound electrons. In reality however the impurity has many electrons in the outer shell each one of which can be excited. At first sight it would seem appropriate then to multiply the cross-section by the number of electrons in the shell. However this simple approach requires that the electrons are independent of one another. If the electrons were truly independent then there would be no mixing of the wave functions and the transitions that we are interested in would not occur since they are spin forbidden. Therefore this simple approach is not valid.

If we instead consider the electron wave functions to be strongly coupled then the electrons are split into many levels and the degeneracy becomes complicated but the transitions that are of interest are now allowed. Fermi's Golden Rule (3.2) could be rewritten for the electron impact using a many electron wave function to describe the impurity and this would include a degeneracy factor. The same wave functions and degeneracy factor would also appear in the lifetime equation (3.22) and so when the matrix element $|x_{eg}|^2$ is calculated the degeneracy factors would cancel in the final cross-section.

Substituting (3.22) and (3.23) into (3.21) we have

$$\sigma(E_u)_{Total} = \frac{18\pi e^2 \hbar^2}{\varepsilon^2 n(n^2+2)^2} \frac{c^3}{E_{eg}{}^3 \tau_{eg}} \frac{k_l}{k_u} \frac{1}{V_l V_u} \mathrm{Ln}\left|\frac{k_u + k_l}{k_u - k_l}\right| \qquad (3.24)$$

This cross-section can be evaluated from knowledge of the band structure and the lifetime of the excited state. We refer to this cross-section as the non-parabolic band cross-section since we make no assumptions about the band structure being parabolic. The total cross-section is a measure of the ease with which a centre may be excited by an electron of a particular energy and is not dependent on the angle of scatter of the incident electron.

3.3 Further Approximations

For the above derivation we have only assumed that the band structure is spherically symmetric. If we add the further assumption that the band is parabolic at low energies we may replace V_l in (3.24) by

$$V_l = \frac{\hbar k_l}{m_l^*} \tag{3.25}$$

where m_l^* is the effective mass of the electrons in the Γ_1 valley of the conduction band. This is equivalent to assuming that the density of final states ρ in (3.4) is proportional to k_l i.e.

$$\rho = k_l \frac{m_l^*}{8\pi^3 \hbar^2} . \tag{3.26}$$

Since the effective mass increases at higher energies this approximation will underestimate the density of final states and reduce the cross-section at high energies.

This approximation gives the total cross-section as

$$\sigma(E_u)_{Total} = \frac{18\pi m_l^* e^2 \hbar}{\varepsilon^2 n(n^2+2)^2} \frac{c^3}{E_{eg}^3 \tau_{eg}} \frac{1}{k_u V_u} \mathrm{Ln}\left|\frac{k_u + k_l}{k_u - k_l}\right| \tag{3.27}$$

which is the form derived by Allen [3.2]. This form we call the partially parabolic-band cross-section. At the same time we should also replace k_l in the log term by $k_l = \sqrt{2m_l^* E_l/\hbar^2}$ but at this stage it is inconvenient to do so and does not introduce any significant error (see section 3.4.2).

A further approximation would be to assume that the conduction band is parabolic for all energies with a constant effective mass. The energy , momentum and electron velocity are then linked by

$$E = \frac{1}{2}\hbar V k = \frac{1}{2m^*}\hbar^2 k^2$$

so

$$k_u \propto \sqrt{E_u}$$

and $$k_l \propto \sqrt{E_l} = \sqrt{E_u - E_{eg}} \ . \qquad (3.28)$$

V_u appears in the cross-section because it gives the incoming electron flux. It can also be thought of as a measure of the interaction time between the incident and bound electrons. Using a parabolic band the electron velocity is over-estimated at high energies reducing the interaction time and the cross-section. We can write the cross-section using just the energy of the incident electron.

$$\sigma(E_u)_{Total} = \frac{9\pi m_l^* e^2 \hbar^2}{\varepsilon^2 n(n^2+2)^2} \frac{c^3}{E_{eg}^3 \tau_{eg}} \frac{1}{E_u} \mathrm{Ln}\left|\frac{\sqrt{E_u} + \sqrt{E_u - E_{eg}}}{\sqrt{E_u} - \sqrt{E_u - E_{eg}}}\right| \qquad (3.29)$$

This cross-section we call the parabolic-band cross-section. To obtain the cross-section given by Yu & Shen [3.3] m_l^* is taken as the free electron mass and the dielectric constant is taken as unity (and a factor of $(2\pi)^3$ must be included).

3.4 Physical Interpretation of Cross-section

In the previous section we derived three forms for the impact excitation cross-section of an impurity. These cross-sections differed in their assumptions as to the form of the conduction band. It is not however immediately clear to what degree these assumptions will affect the cross-sections. To clarify this we calculate for each form the impact cross-section of two hypothetical excitations of different energy (1.0 eV and 2.0 eV) but the same lifetime (100μsec). By comparing the energy dependence of each cross-section we see the effect of the different approximations and from that make a judgement as to which forms are the most practical to use.

The cross-sections are calculated numerically using energy, momentum and velocity values for the electron derived from the band structure of ZnS as given by Cohen and Bergstresser [3.11]. We start with the parabolic-band cross-section as this is the simplest model.

3.4.1 Parabolic-Band Cross-section

In the cross-section given in (3.29) the incident electron energy appears by itself outside the log term. However this energy does not come directly from the derivation of the cross-section but is an amalgamation of various terms which for a free electron are collectively inversely proportional to the electron energy. To understand this better we deconvolute this energy term back into its constituent parts.

$$\sigma(E_u)_{Total} = \frac{2\pi}{\hbar}\left(\frac{k_l^2}{8\pi^3\,\hbar V_l}\right)\left(\frac{1}{V_u}\right)\left(\frac{72\pi^3\,e^2}{\varepsilon^2\,n(n^2+2)^2}\;\frac{\hbar^4\,c^3}{\tau_{eg}E_{eg}^3}\;\frac{1}{k_u k_l}\;Ln\left|\frac{k_u + k_l}{k_u - k_l}\right|\right) \qquad (3.30)$$

(1) (2) (3)

where (1) is the density of final states, (2) is the incident electron flux (or the interaction time for the excitation to take place) and (3) is the transition matrix integrated over momentum space. For a parabolic band we can write the energy dependence of each part as

$$\sigma(E_u)_{Total} \propto \left(\sqrt{E_u - E_{eg}}\right)\left(\frac{1}{\sqrt{E_u}}\right)\left(\frac{1}{\sqrt{E_u}\sqrt{E_u - E_{eg}}}\;Ln\left|\frac{\sqrt{E_u} + \sqrt{E_u - E_{eg}}}{\sqrt{E_u} - \sqrt{E_u - E_{eg}}}\right|\right) \qquad (3.31)$$

(1) (2) (3)

where $E_u - E_{eg} = E_l$.

Near threshold $E_u \cong E_{eg}$ so that the density of states (1) is small because the incident electron is scattered into the bottom of the conduction band. The density of states factor is balanced by a similar energy term in the matrix integral (3). This term in (3) shows that if the final momentum is small the excitation is more likely to occur. Near threshold the log term in (3) will also be small but increases quickly until E_u is significantly greater than E_{eg}, after that the log term increases slowly (figure 3.5). It is this log term which determines the initial rise in the cross-section as the excitation first becomes possible as shown in figure (3.6). Above threshold the cross-section is dominated by the electron flux (2) (or interaction time as it can be considered) and the first part of the momentum integral. As the energy of the incident electron increases so does the electron velocity, and the interaction time decreases. At the same time the momentum change becomes more difficult as the final momentum increases. The over all result is that the cross-section will decrease at higher energies.

3.4.2 Partially-Parabolic-Band Cross-section

Conduction bands are only parabolic for all energies in the free electron model. In reality the electron wave functions are modified by the periodic potential of the lattice and for some energies the bands are deformed. In the partially-parabolic-band cross-section (3.27) we allow for this distortion of the band only at high energies. The cross-section must be calculated using the momentum (k_u) of the incident electron which can be found from a band structure diagram (see Chapter 4 for a detailed discussion of the choice of the band structure and the

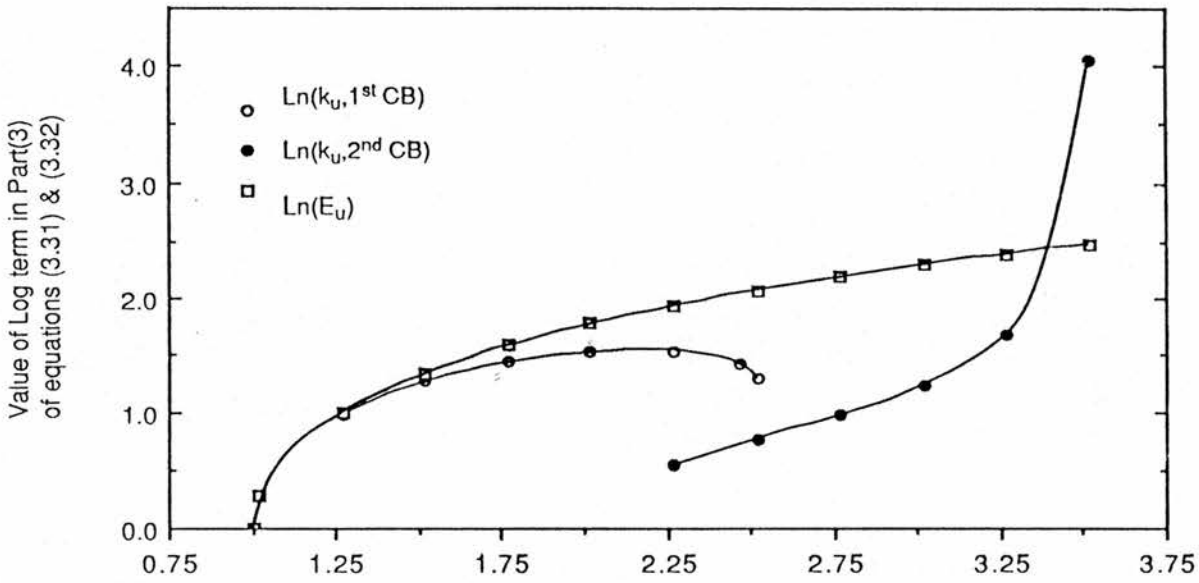

Figure 3.5a

In this graph we compare the Log terms of the matrix integral {part(3) in equations (3.31 & 3.32)} for an excitation of 1.0 eV, calculated using the energy (E_u) or the momentum (k_u) of the incident electron

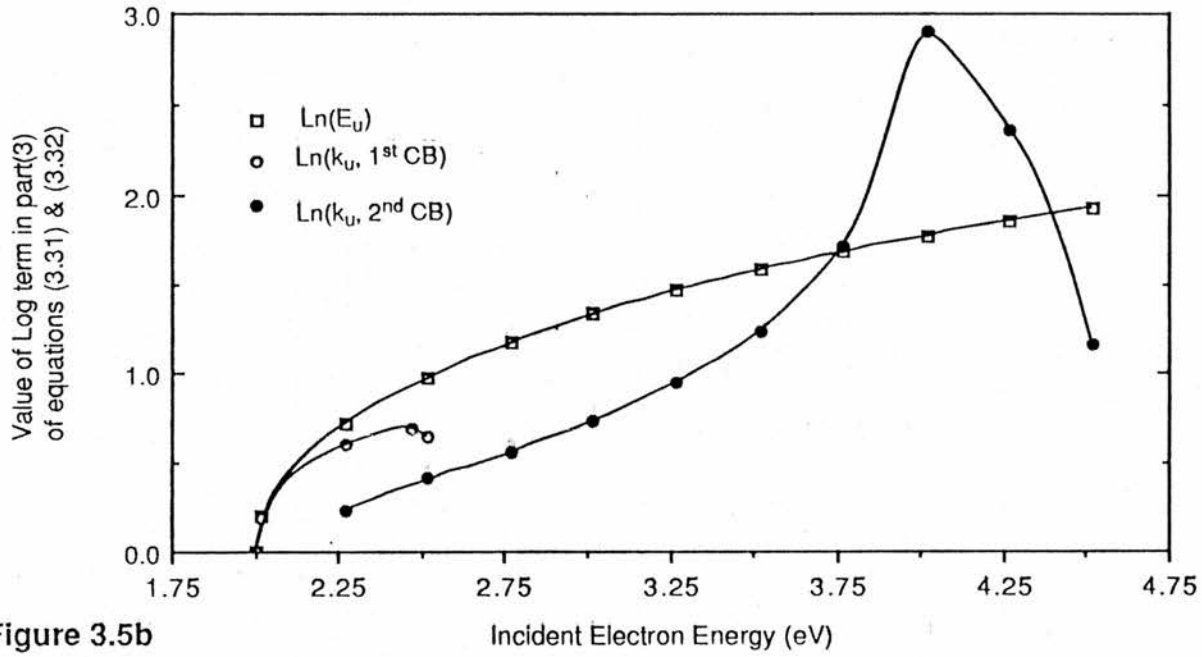

Figure 3.5b

In this graph we compare the Log terms of the matrix integral {part(3) in equations (3.31 & 3.32)} for an excitation of 2.0 eV, calculated using the energy (E_u) or the momentum (k_u) of the incident electron

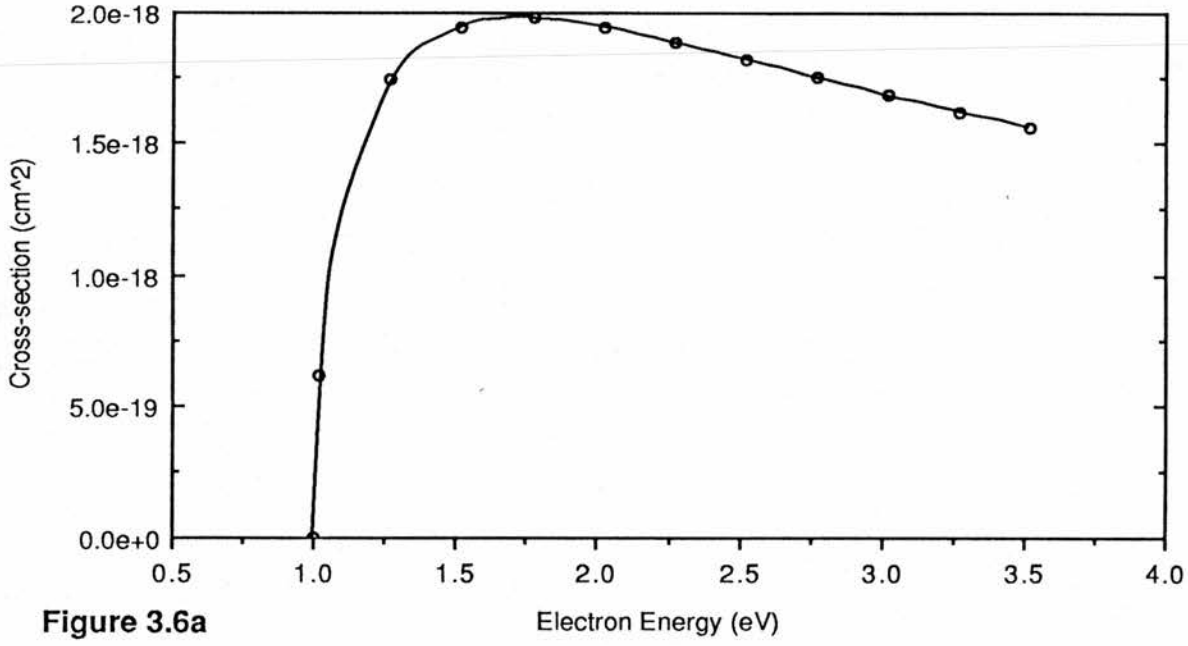

Figure 3.6a

Cross-section for the 1.0 eV excitation as calculated for a parabolic conduction band.

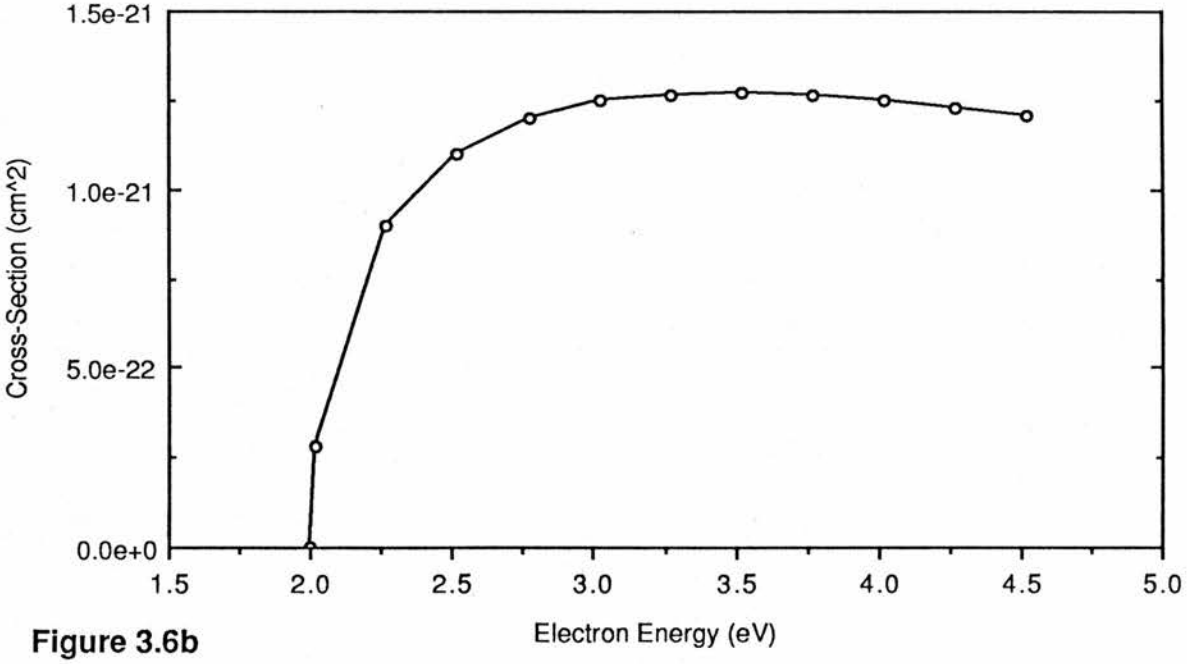

Figure 3.6b

Cross-section for the 2.0 eV excitation as calculated for a parabolic conduction band.

calculation of k and V). To be fully consistent we should continue to derive the crystal momentum (k_l) of the scattered electron from the energy E_l, but instead we chose for convenience to use the momentum from the band structure diagram. The error in doing this will be small since k_l only appears in the log term of the cross-section.

By allowing a non-parabolic dispersion the cross-section is changed in two ways. First the interaction time between the electrons (part (2) in (3.30)) will change and second the log term in the matrix integral will change (part (3) in (3.30)). We can write the momentum dependence of the cross-section as

$$\sigma(E_u)_{Total} \propto (k_l)\left(\frac{1}{V_u}\right)\left(\frac{1}{k_u\, k_l}\,\mathrm{Ln}\left|\frac{k_u + k_l}{k_u - k_l}\right|\right) \qquad (3.32)$$

(1) (2) (3)

We can calculate the log term of part (3) in (3.32) using momentum values from the band structure of ZnS by Cohen & Bergstresser [3.11]. ZnS is used as an example because these cross-sections are calculated again in Chapter 4 for Er in ZnS. We only consider the cross-section for electrons in the Γ_1 valley or those scattered into the Γ_1 valley from the second conduction band.

In figure (3.5) we compare the log terms of the part (3) as calculated using the electron energy (from equation 3.31) and then the crystal momentum (from equation 3.32). For the 1.0 eV excitation there is no appreciable difference in these terms until we change from the Γ_1 valley to X_3 valley of the conduction band. Now we see a new phenomenon not present in the simple parabolic-band model. As the incident electron energy rises we are forced to change conduction band and there follows a sudden increase in the electron momentum. Because greater momentum is involved the magnitude of the log term decreases.

When the energy of the incident electron increases further its momentum starts to decrease and begins to approach that of the scattered electron. This does not happen in the parabolic-band model. When the momentum of the incident and scattered electron states become comparable (i.e. the momentum change is small) the log term passes through a singularity.

For the 1.0 eV excitation the incident and scattered electron momentum never become equal over the range considered but this is possible with the 2.0 eV excitation and figure (3.5)

shows that at this energy the cross-section is enhanced. Apart from the energies at which there is a change of conduction band or a direct transition (i.e. no momentum change) the log terms for each approximation are similar.

In the previous cross-section terms in parts (2) and (3) had been combined to be represented by the energy of the incident electron (3.28). In the partially-parabolic-band cross-section we can have regions of the energy dispersion in which an electron may have a high energy and high crystal momentum but a low velocity. In these regions the interaction time between the electrons will be enhanced by the low velocity. Figure (3.7) compares the term $\frac{1}{2}\hbar k_1 V_1$ for the electron with the energy of the electron. From figure (3.7) it can be seen that at 1.0 eV the energy of the electron gives a fair estimate of the term $1/2\hbar k_1 V_1$. At higher energies the use of energy in the cross-section over-estimates this term and so under-estimates the cross-section.

We can introduce both of the above changes separately to show which is responsible for enhancement at different energies. This is done in figure (3.8) and we see that the change in the momentum integral has the least effect.

Combining both changes we have the partially-parabolic-band cross-section shown in figure (3.9). This cross-section follows the parabolic-band cross-section at low energies but is soon enhanced by the lower electron velocity.At the change over of the conduction bands the two cross-sections agree only because the decrease in the electron velocity matches the decrease in the matrix integral.

3.4.3 Non-Parabolic-Band Cross-section

The partially-parabolic-band cross-section should be an adequate approximation over most of the electron energy range. However at high incident energies the electron will be scattered into a non-parabolic region of the first conduction band. To show how great an effect this will have we use the non-parabolic band cross-section and take the values for the momentum and velocity of the scattered electron from the band structure diagram. This step is equivalent to allowing the effective mass of the electron to vary with energy as shown in figure (3.10). This allows the final density of states to be included more accurately. In the previous cross-sections the density of the final states is under-estimated so reducing the cross-section.

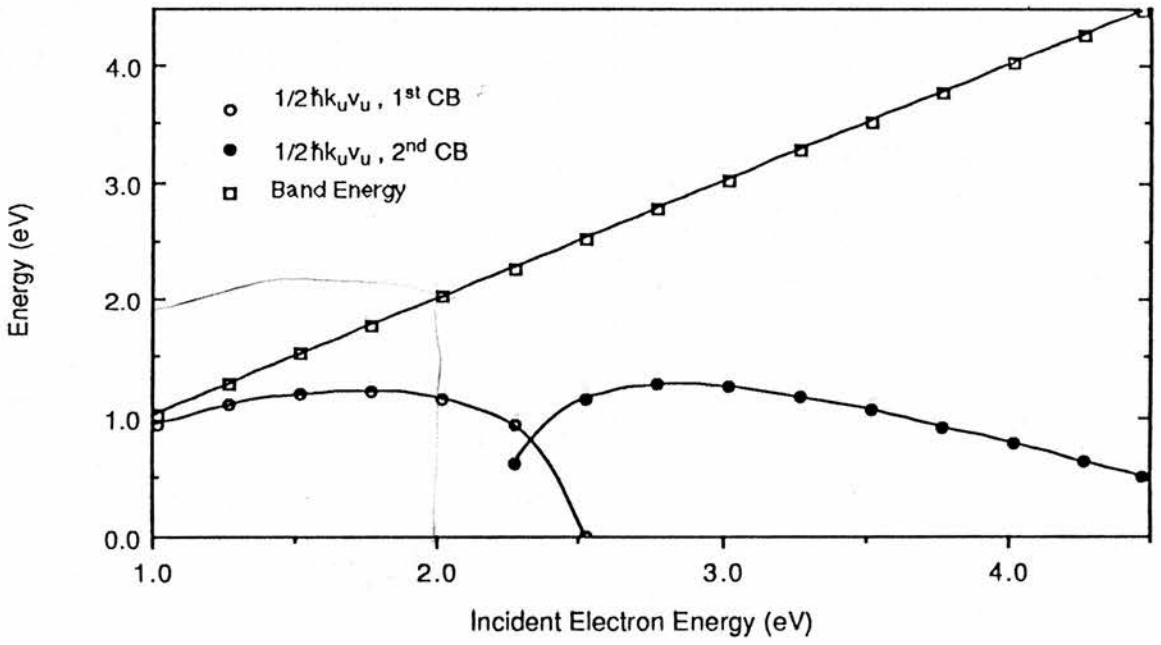

Figure 3.7 Comparison of the factor $(1/2\hbar k_u v_u)$ for the incident electron with the energy of the electron (E_u) showing how the use of energy in the parabolic-band approximation over-estimates this factor.

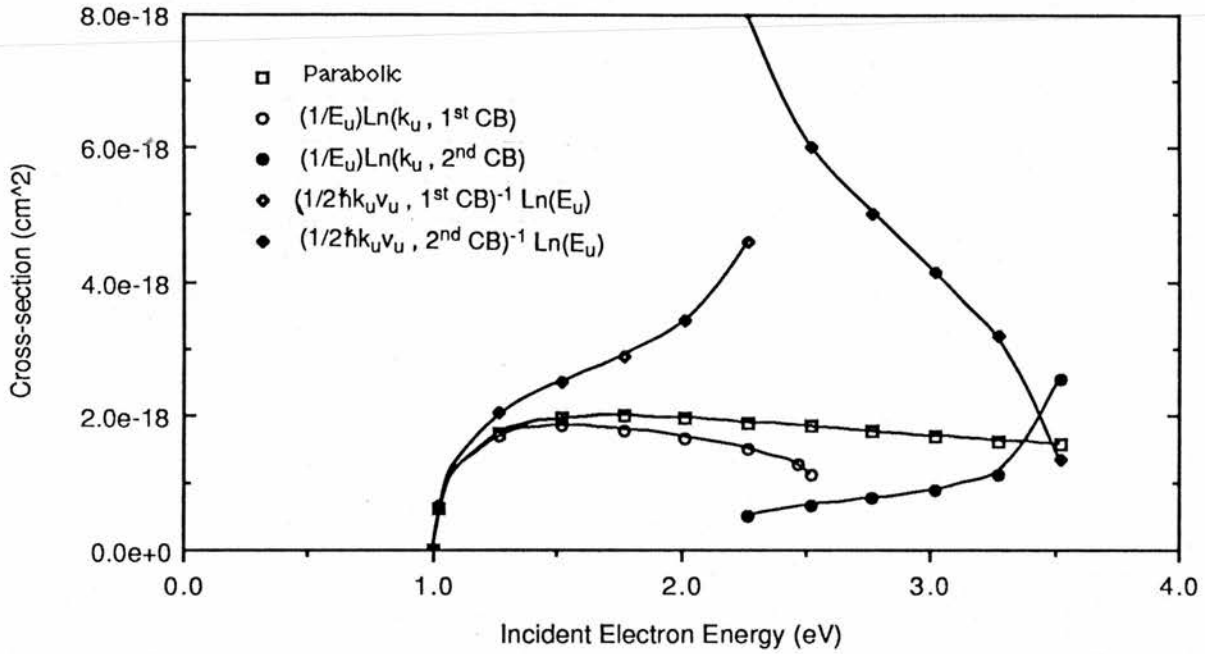

Figure 3.8a Comparison of the effect on the cross-section energy profile of using momentum instead of energy to calculate the cross-section for the 1.0 eV excitation.

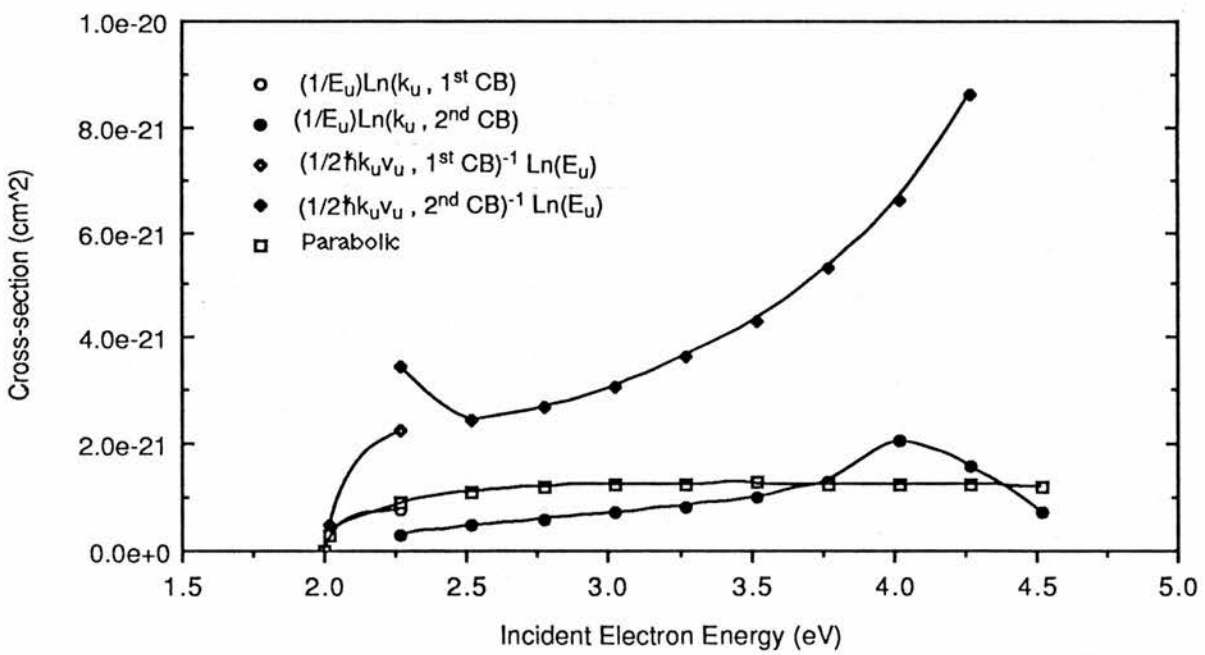

Figure 3.8b Comparison of the effect on the cross-section energy profile of using momentum instead of energy to calculate the cross-section for the 2.0 eV excitation.

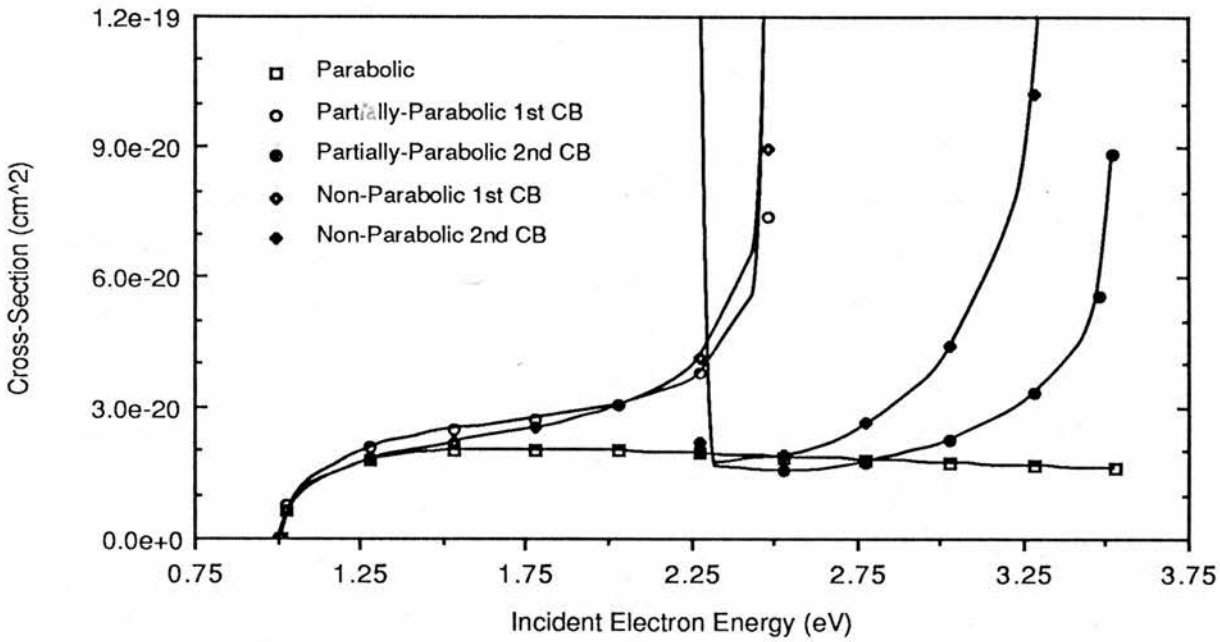

Figure 3.9a Comparison of the cross-sections for the 1.0 eV excitation calculated by the three cross-section approximations (3.24), (3.27) & (3.29).

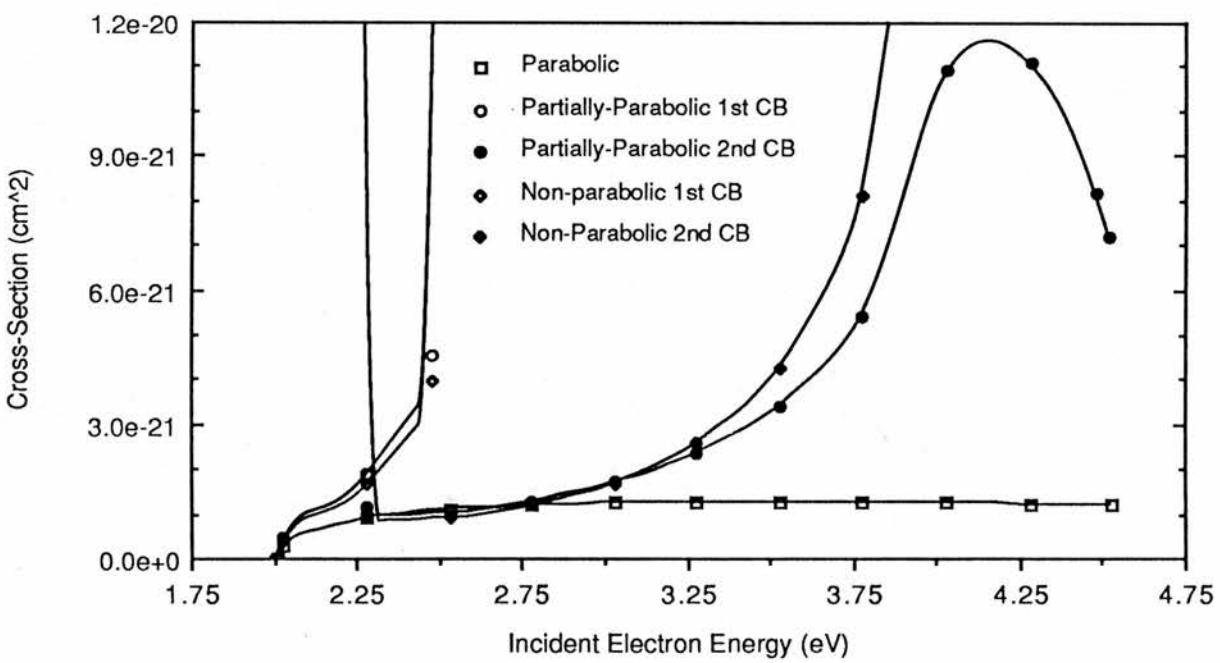

Figure 3.9b Comparison of the cross-sections for the 2.0 eV excitation calculated using the three different cross-section approximations (3.24), (3.27) & (3.29).

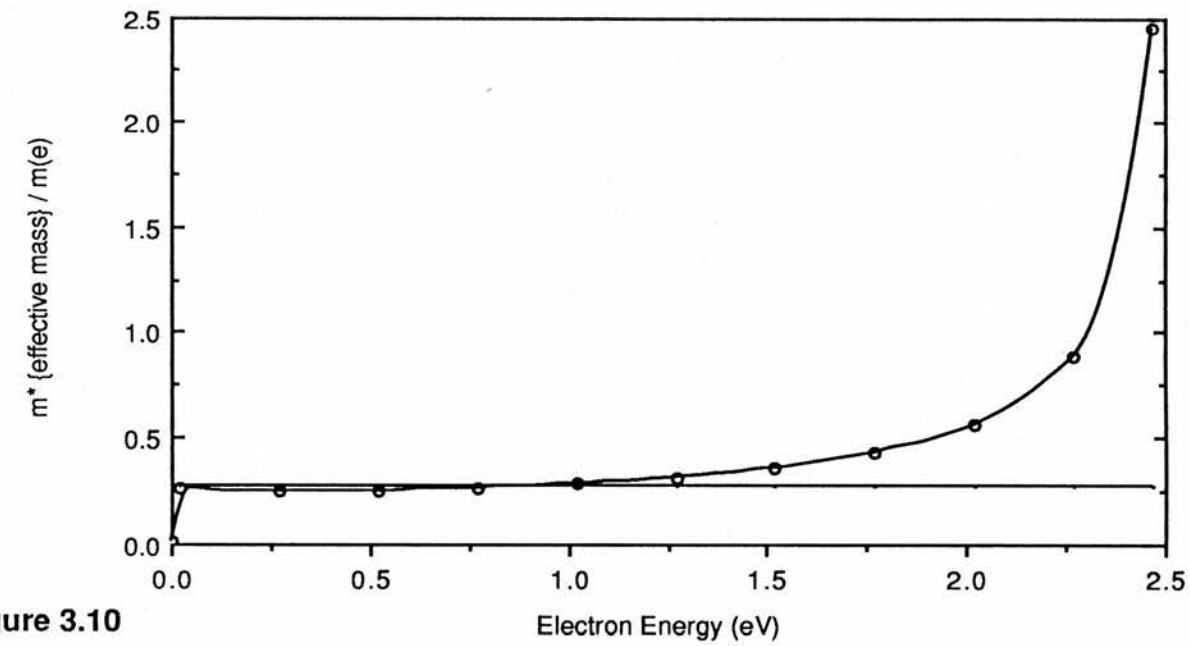

Figure 3.10

Plot showing how the effective mass of an electron in the first conduction band increases as the electron energy increases. For comparison the effective mass of 0.281 is included on the graph.

In figure (3.9) we compare the non-parabolic-band cross-section with the two previous models. The cross-section only differs from the simpler partially-parabolic-band cross-section at high energies where the incident electron has an energy of 1.5 eV above the threshold for excitation.

3.5 Conclusion

From examining the effects of the various approximations and substitutions that gave the three different cross-section models we conclude that the band structure affects the cross-section in three ways;

i) A non-parabolic band structure allows for incident electrons of high energy and momentum that have low velocities and hence longer interaction times with the impurity electron.

ii) A non-parabolic band structure allows for a direct transition of the incident electron to a low energy state with little change of momentum enhancing the probability of such a transition.

iii) A non-parabolic band structure allows for an increase in the number of states into which the incident electron is scattered.

These effects are noticeable at high energies, at a valley in the conduction band or at an energy where a direct transition is possible. We note that the partially-parabolic-band cross-section is a reasonable approximation to the non-parabolic-band approximation over most energies. We also note that the calculation of the cross-section requires a definite knowledge of the electric dipole contribution to the radiative lifetime. If the relaxation involves a magnetic dipole component or energy transfer the experimental lifetime can not be used directly.

In the next chapter we proceed to analyse a real centre (Er in ZnS) and look for the various effects that we have seen in the two hypothetical excitations.

Chapter 3

3.6 References

[3.1] N.F.Mott & H.S.W.Massey "Theory of Atomic Collisions" *1st Edition,Oxford Uni. Press 1933.* Pages 96-98 & 159-177.

[3.2] J.W.Allen *J.Phys.C:Solid State Phys.* **19** (1986) 6287

[3.3] Jiaqi Yu & Yongrong Shen *J.Lumin.* **40/41** (1988) 769

[3.4] A.S.Baltenkov & E.D.Belorusets *Sov.Phys.Semicond.* **12** (1978) 893

[3.5] Landau & Lifschitz "Quantum Mechanics" *Pergamon Press* (1965) 479 p 72

[3.6] K.J.Nash *J.Phys.C: Solid State Phys.* **19** (1986) 181

[3.7] H.Bethe *Ann. der Phys.* **5** (1930) 325

[3.8] N.F.Mott & H.S.W.Massey "Theory of Atomic Collisions", Page 174

[3.9] J.M.Langer *J.Lumin.* **40/41** (1988) 589

[3.10] D.L.Dexter *Solid State Physics* **6** (1958) 353

[3.11] M.L.Cohen & T.K.Bergstresser *Phys. Rev.* **141** (1966) 789

Chapter 4

Calculation of Impact Excitation Cross-sections for Three Transitions of Er^{3+} in ZnS

		Page
4.1	**Introduction**	**93**
4.2	**Description of Er^{3+} Excitations**	**95**
4.3	**Description and Choice of the Band Structures**	**96**
4.4	**Digitalisation of the Band Structure**	**98**
4.5	**Calculation of the Cross-sections**	**101**
4.6	**Discussion**	
4.6.1	Parabolic Band Cross-Sections	105
4.6.2	Partially-Parabolic-Band Cross-Sections	105
i)	2.36 eV Excitation	107
ii)	2.25 eV Excitation	110
iii)	1.25 eV Excitation	112
iv)	Summary	113
4.7	**Comparison with other Cross-Sections**	**114**
4.8	**Concluding Remarks**	**117**
4.9	**References**	**119**

Chapter 4

Calculation of Impact Excitation Cross-sections for Three Transitions of Er^{3+} in ZnS

4.1 Introduction

It has been known for some time that impurity luminescence can be excited by hot-electron impact excitation [4.1, 4.2]. The efficiency of such a process is determined by the hot electron distribution and the impact excitation cross-section of the impurity. In Chapter 5 the electron distribution is considered in some detail. Cross-section calculations have been available for atomic elements for some time and many text books deal with this subject (e.g. [4.3]) and these calculations have been extended into the solid state for simple atoms [4.4 plus others]. In the previous chapter we derived three approximations for the excitation cross-section.

Various approaches have been tried to measure impact excitation cross-sections for Er and Mn [4.5, 4.6, 4.7, 4.8]. In table 4.1 we list some theoretical and experimental cross-sections already published. The experimental cross-sections represent an average cross-section for the electron distribution while the theoretical cross-sections are normally for some energy above the threshold for excitation. Measurement of the cross-section is difficult without some knowledge of the electron distribution. The theoretical calculations generally assume that the conduction band is parabolic. There is however growing experimental evidence that the real non-parabolic dispersion can considerably alter the electron distribution in preference to the hot electrons [4.2, 4.9, 4.10, 4.11, 4.12 and Chapter 5] thus increasing the efficiency of impact excitation. This might also affect the interpretation of the cross-sections measured experimentally. In this chapter we show that a non-parabolic dispersion can also alter the impact cross-section producing an enhancement by as much as an order of magnitude over the simpler parabolic-band approximation.

Table 4.1

A Comparison of Theoretical and Experimental Cross-sections

Phoshor (and Transition)	Theoretical (cm^{-2})	Experimental (cm^{-2})	Reference
ZnS:Mn ($^4T_1$)	~ 10^{-18}	~ 10^{-16}	[4.5]
ZnS:Mn ($^4T_1$)		4.0×10^{-16}	[4.8]
ZnF_2 :Mn ($^4T_1$)	3×10^{-16}	3×10^{-16}	[4.13]
ZnS:Mn ($^4T_1$)	2×10^{-16}		[4.13]
ZnS:Mn ($^4T_1$)		~ 10^{-16}	[4.14]
ZnS:ErF_3 ($^4S_{3/2}$)		8×10^{-16}	[4.6]
ZnS:Er ($^4S_{3/2}$)		2×10^{-16}	[4.7]
ZnS:Er ($^4S_{3/2}$)	2.0×10^{-17}		[4.15]
ZnS:Er ($^2H_{11/2}$)	1.8×10^{-16}		[4.15]

In the above theoretical calculations there is a variation in the assumptions made. Where the band structure is considered it is taken as being parabolic and the exchange term in the matrix element is not included. Screening of the impurity and the effective mass of the electron are not always fully considered. These cross-sections are generally held to be upper limits to the true cross-section.

In this chapter we apply two of the theoretical models derived in Chapter 3 to Er in ZnS. We calculate the cross-sections over an energy range of about 3 eV (covering most of the first and second conduction bands). We first calculate the cross-section using the parabolic-band approximation similar to that of Yu & Shen [4.15] but with corrections for screening and the effective mass (and the algebraic error noted in Chapter 3). For comparison we calculate the cross-section using the partially-parabolic-band approximation for the same transitions. By comparing the two sets of cross-sections we show that the assumption of a parabolic dispersion is inadequate for these excitations in ZnS.

We conclude by finding that for the $^2H_{11/2}$ (2.36 eV) transition the cross-section at 4.0 eV is 6×10^{-19} cm^2 (c.f. 1.8×10^{-16} cm^2 in [4.15]) and for the $^4S_{3/2}$ (2.25 eV) transition 3×10^{-20} cm^2 (c.f. 2.0×10^{-17} in [4.15]). These cross-sections are three orders below the given experimental values. However it must be noted that by chosing a band structure such that the

X_3 - Γ_1 energy separation is close to 2.36 eV or 2.25 eV these theoretical cross-sections could be enhanced further and this may explain in part why the experimental cross-sections are so large in comparison.

4.2 Description of Er^{3+} Excitations

There are many excitations of Er in ZnS. We selected three which ranged in energy from 1.25 eV to 2.36 eV and had lifetimes from 970 μsec to 5.7 μsec. This allowed us to investigate how the change in excitation energy affected the influence of the band structure. Table 4.2 summaries the characteristics of the three Er excitations that we chose to investigate.

Table 4.2

Ground State	Excited State	Excitation Energy (eV)	Excited State Lifetime (μsec)	Reference
$^4I_{15/2}$	$^2H_{11/2}$	2.36	5.7	[4.7]
$^4I_{15/2}$	$^4S_{3/2}$	2.25	50	[4.7]
$^4I_{15/2}$	$^4H_{11/2}$	1.25	970	[4.16]

The decreasing lifetime with increasing energy showed that the higher energy transitions were less spin forbidden due to increased mixing of the wave functions. We expected then that the higher energy excitations would have larger cross-sections than the lower energy excitations and this we did indeed find. The lifetimes quoted in this table for the $^2H_{11/2}$ and $^4S_{3/2}$ excited states are not definite as a range of values are given in the literature. For the $^2H_{11/2}$ excited state the lifetime has been quoted as high as 25 μsec by Xu et al [4.7] this value being derived from intensity measurements. Xu et al use this method to find the radiative lifetime because there is a strong relaxation path to the $^4S_{3/2}$ state which greatly reduces the overall lifetime of the $^2H_{11/2}$ state. The directly measured lifetime is therefore not the value appropriate for calculating the cross-section. We use 5.7 μsec as this is the lowest lifetime given by Xu et al (and hence the largest cross-section) and is in agreement with the optically measured lifetime by Krier & Bryant [4.17].

For the $^4S_{3/2}$ transition Xu et al found the lifetime to vary from 49 to 228 μsec depending upon the lattice site where the Er was found. The value of 50 μsec is taken as the shortest possible lifetime and hence the largest cross-section. Krier & Bryant give the lifetime as 6.9 μsec

showing the great uncertainty in this lifetime.

For the $^4H_{11/2}$ excited state Razi [4.16] measured a lifetime of 970 μsec and Krier & Bryant [4.7] measured 220 μsec. Without a clear understanding as to why these lifetimes vary so greatly it is uncertain which values should be used. The decay directly to the ground state is the reverse of the transition for impact excitation, so the lifetime for this transition (if known) should be the most appropriate. For the $^4H_{11/2}$ state we use the 970 μsec lifetime as it is the longest and so more likely to apply to the direct transition to the ground state. For the previous excited states we continue to use the shorter lifetimes assuming that the relaxation is still to the ground state but that the change in lifetime is due to the different degrees of wave mixing in the different lattice sites.

All the experimental lifetimes quoted above may still be inappropriate if the radiative decay includes a significant magnetic dipole component. If this is the case then only the electric dipole component should be used in the cross-section.

4.3 Description and Choice of Band Structure

The calculation of the impact cross-section for an incident electron of given energy requires knowledge of the conduction electron velocity and momentum. These quantities were calculated from band structures published by other groups [4.18, 4.19, 4.20, 4.21]. Table 4.3 lists the critical point energies of the four band structure calculations considered. The band structure of Cohen & Bergstresser [4.21] was only used in Chapter 3 but is included here for comparison. From table 4.3 it can be seen that there is quite a variation in the computed values of the critical point energies. This highlights a fundamental problem with ZnS in that there is only one reliable experimental critical point and that is the band gap (Γ_{15L} - Γ_{1C}) of -3.8 eV. Three of the band calculations in table 4.3 are in agreement with the band gap energy only because they have been adjusted to fit this energy.

Table 4.3

Authors	Critical Point Energies (relative to Γ_{1C})				Reference
	Γ_{15L}	Γ_{15C}	X_3	X_1	
Huang & Ching	-3.81	5.42	3.80	1.95	[4.18]
Wang & Klein	-2.26	4.78	2.32	1.35	[4.19]
Walter & Cohen	-3.74	4.05	1.49	0.86	[4.20]
Cohen & Bergstresser	-3.72	5.2	2.3	1.50	[4.21]

Various methods were used to construct these band structures. All start with a Hamiltonian which modifies the coulomb potential of the ions by allowing for the screening effect of the electrons. To describe the electron screening it is necessary to guess at the wave functions for the electrons. Electrons close to the nucleus can be adequately described by atomic wave functions. The valence electrons however must be allowed to overlap with the neighbouring atoms and hence have a molecular type wave function. For ZnS it appears to be difficult to produce satisfactory wave functions for these valence electrons because of the mixed ionic-covalent character of the bonding.

To help guide the process of mixing the electron wave functions the band structure is used to calculate various properties of the semi-conductor, e.g. reflectivity. These help to steer the calculation towards a physically realistic model. However there is some variation in the physical data available and so an inherent uncertainty exists in the properties to which the band structure is to be matched.

One of the modern band structures we considered was that of Huang & Ching [4.18]. They used an orthoganalised linear combination of atomic orbitals to describe the valence electrons and adjusted their calculation to give the correct band gap. To solve the Schrodinger equation a semi-ab initio method was used which though fairly good for the valence bands increased the energy of the conduction bands. Since the conduction bands were the only part of the band calculation that we used this calculation was later abandoned.

Wang & Klein [4.19] used an ab-initio method similar to that of Huang & Ching but adjusted the calculation to fit reflectivity, photoelectron spectroscopy and effective mass data. The result is an even better fit to the valence band critical points but the smallest band gap of the

band structures considered.

A survey of previous band structures found that for ZnS the empirical psuedopotential method was quite successful in reproducing reflectivity data. Cohen & Bergstresser [4.21] used this approach to produce the band structure used in Chapter 3. However this band structure was later updated by Walter & Cohen [4.20] in the light of newer, improved data. These two band structures are quite similar both having approximately the same band gap and differ only by 0.5 eV in the energies of the X_1 and X_3 critical points. Since the form of each is the same it was decided to use the later band structure because of the more reliable experimental data used. These two band structures are shown in figure (4.1a) for comparison. It might be noted that if the band structure of Cohen & Bergstresser had been used the cross-sections for the 2.25 eV and 2.36 eV excitation would have been quite different as the X_3 critical point would have been at 2.3 eV.

4.4 Digitalisation of the Band Structure

The impact cross-section was to be numerically calculated over the expected energy range of the incident electrons using actual values of energy, momentum and velocity for the incident electron. The chosen band structures were photographically enlarged from published papers and the relevant portions digitalised using a Tektronics map digitaliser. We restricted our interest to the 1^{st} and 2^{nd} conduction bands in the Γ - X direction as it was assumed that the electrons would be more likely to be found in this part of the momentum space. Higher conduction bands were not included as these are unlikely to be occupied to any significant degree by conduction electrons. We only considered electrons already in the Γ_1 valley or that were scattered into the Γ_1 valley from the second conduction band.

Once digitalised a smooth 2000 point, order 9 polynomial was fitted to the data to remove random errors introduced by the digitalisation process. This smooth fit was then scaled to give the correct values of momentum and energy needed for the calculations. By differentiating the smooth fit and multiplying by an appropriate factor the electron velocity was derived from this band structure (figure 4.1b).

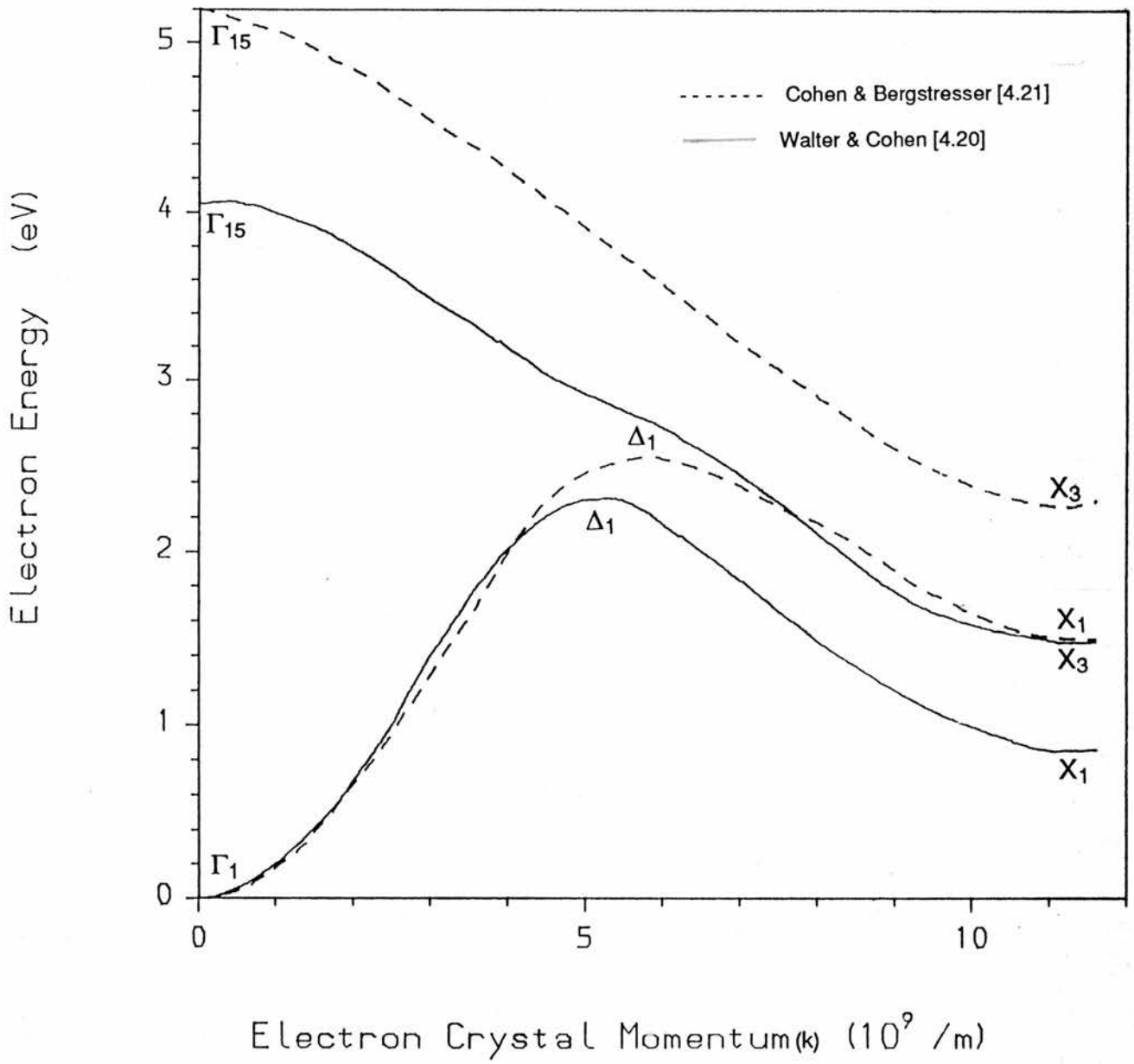

Figure 4.1a

A comparison of the first and second conduction bands in the Γ—X direction for ZnS as calculated by Walter & Cohen [4.20] and by Cohen & Bergstresser [4.21] by the psuedopotential method. Energies are relative to the Γ_1, the bottom of the conduction band.

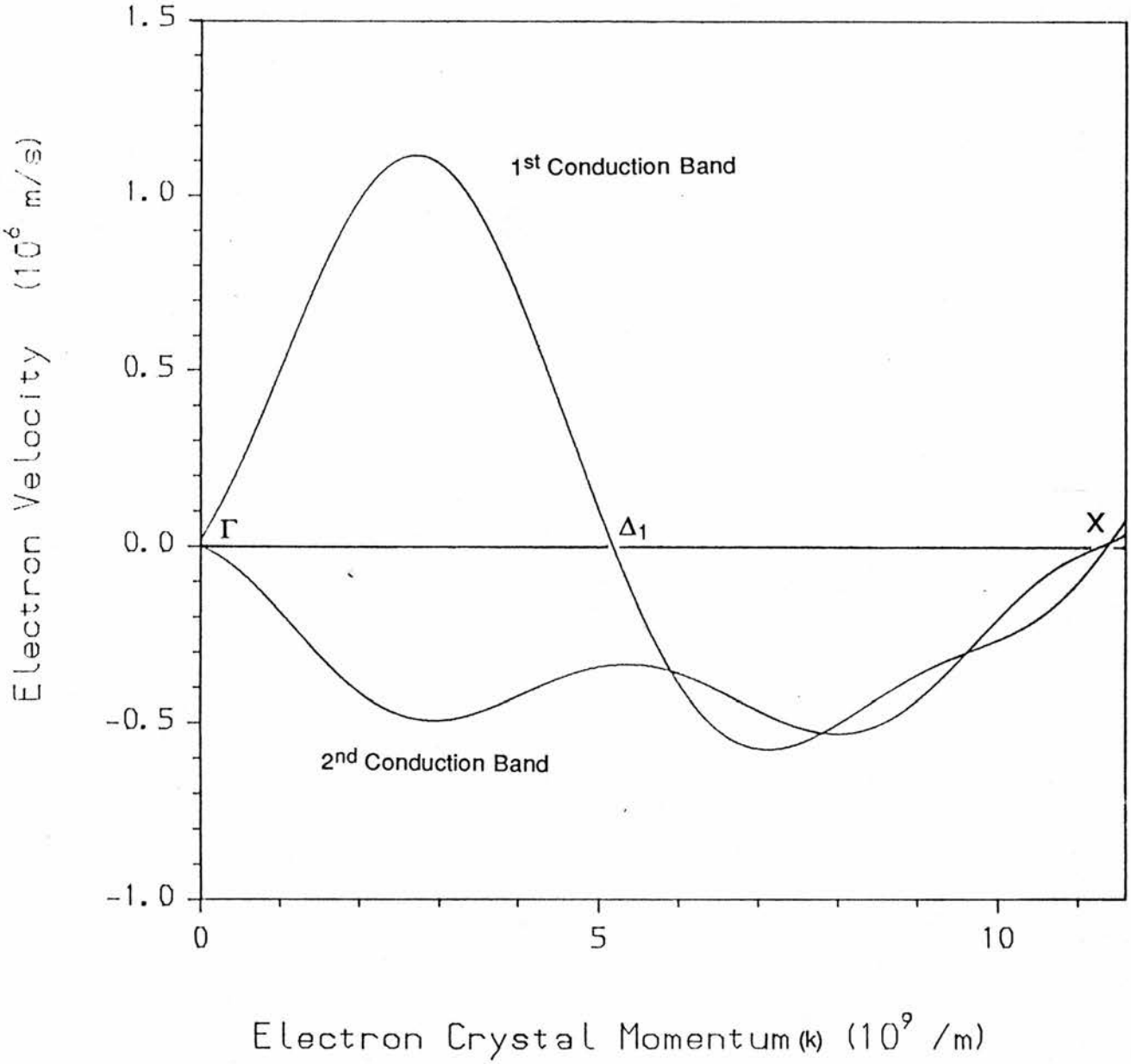

Figure 4.1b

A comparison of the electron velocity in the first and second conduction bands in the Γ—X direction (111) for ZnS as calculated from the band structure diagram of Walter & Cohen [4.20] derived by the psuedopotential method.

4.5 Calculation of the Cross-sections

In Chapter 3 we derived three approximations for the impact cross-section. These approximations differed in the assumptions made as to the form of the conduction band. In this chapter we continue to use the parabolic-band approximation given by

$$\sigma(E_u) = \frac{9\pi m_l^* e^2 \hbar^2 c^3}{\varepsilon^2 n(n^2+2)^2} \frac{1}{E_{eg}^3 \tau_{eg}} \frac{1}{E_u} \mathrm{Ln}\left|\frac{\sqrt{E_u} + \sqrt{E_u - E_{eg}}}{\sqrt{E_u} - \sqrt{E_u - E_{eg}}}\right| . \qquad (4.1)$$

This has been used by other groups (e.g. Yu & Shen [3.3]) and though simple we wish to demonstrate its inadequacy. Two other approximations were developed in Chapter 3 that used a partially-parabolic-band and a non-parabolic-band. These were shown to produce quite similar results except at high energies so for simplicity we used only the simpler partially-parabolic-band approximation given by

$$\sigma(E_u) = \frac{18\pi m_l^* e^2 \hbar c^3}{\varepsilon^2 n(n^2+2)^2} \frac{1}{E_{eg}^3 \tau_{eg}} \frac{1}{k_u V_u} \mathrm{Ln}\left|\frac{k_u + k_l}{k_u - k_l}\right| . \qquad (4.2)$$

For our first attempt at calculating an impact cross-section we chose to use the 2.36 eV excitation of Er. The partially-parabolic-band cross-section was calculated using data from the band structure of Huang & Ching [4.18]. In the Γ -X direction this band calculation has a large energy gap between the first and second conduction bands which results in a corresponding energy gap in the cross-section (figure 4.2). This cross-section is therefore very different from that predicted by the simple parabolic-band approximation. The cross-section is very enhanced at the energy gap because the density of states at these energies is large and the electron velocity small. However the bottom of the energy gap is the Δ_1 peak in the conduction band and electrons are unlikely to be found at this energy. The top of the energy gap is a valley near X_3 but at 3.5 eV above the bottom of the conduction band there are unlikely to be many electrons at this energy.

Because of the large energy gap found when using Huang & Ching's band structure [4.18] it was decided to use Walter & Cohen's band structure instead. The calculations were extended to include the 2.25 eV and 1.25 eV excitations. The individual partially-parabolic-band cross-sections for each excitation are shown in figures (4.3, 4.4 and 4.5) with the corresponding parabolic-band cross-section. The parabolic-band cross-sections are compared in figure (4.6). In figure (4.7) we compare the partially-parabolic-band cross-sections though it

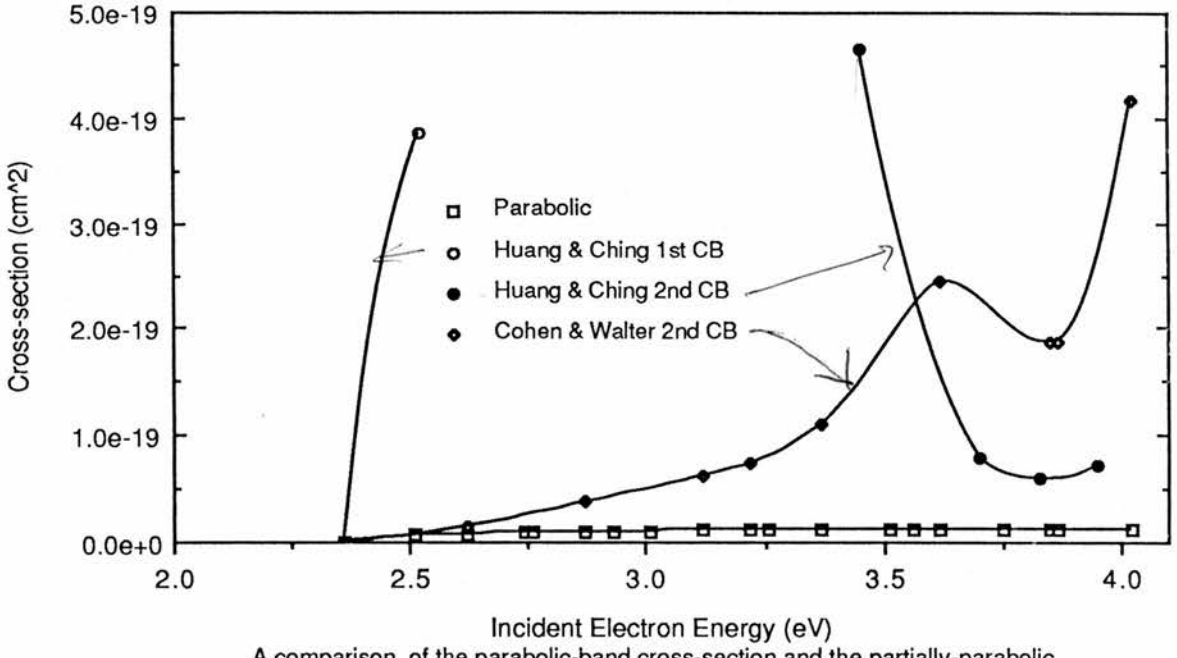

Figure 4.2 A comparison of the parabolic-band cross-section and the partially-parabolic -band cross-sections (calculated using the band structures of Huang & Ching [4.18] and Walter & Cohen [4.20]) for the 2.36 eV excitation of Er in ZnS.

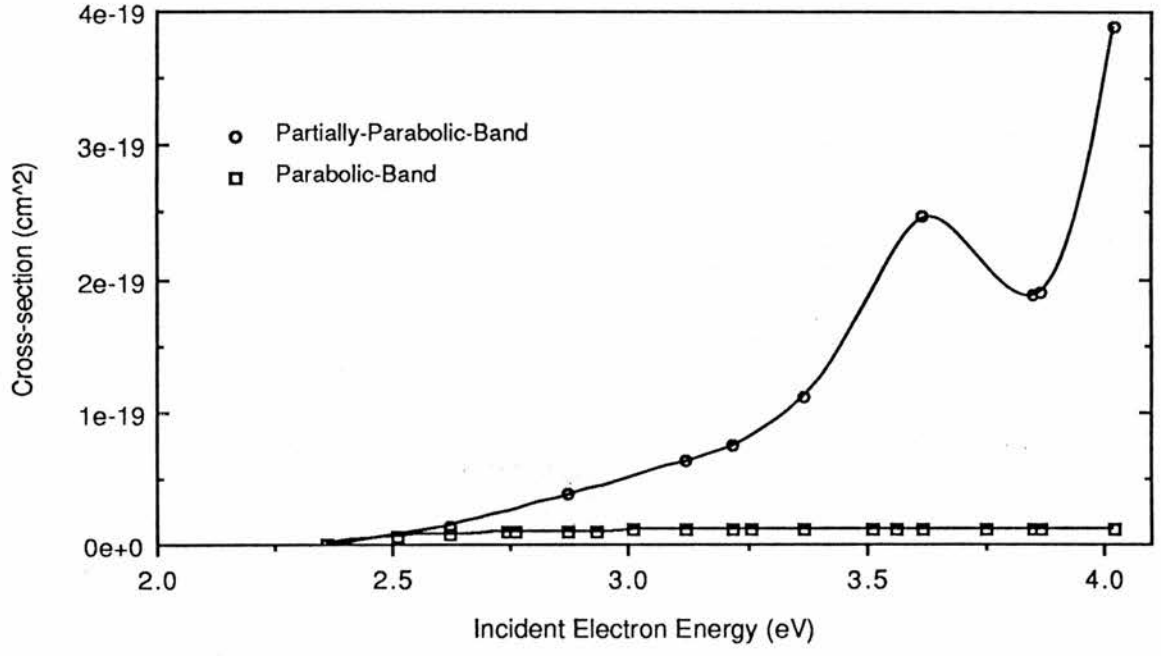

Figure 4.3 Comparison of the cross-section for the 2.36 eV excitation of Er in ZnS as calculated by the parabolic-band and the partially-parabolic-band approximations.

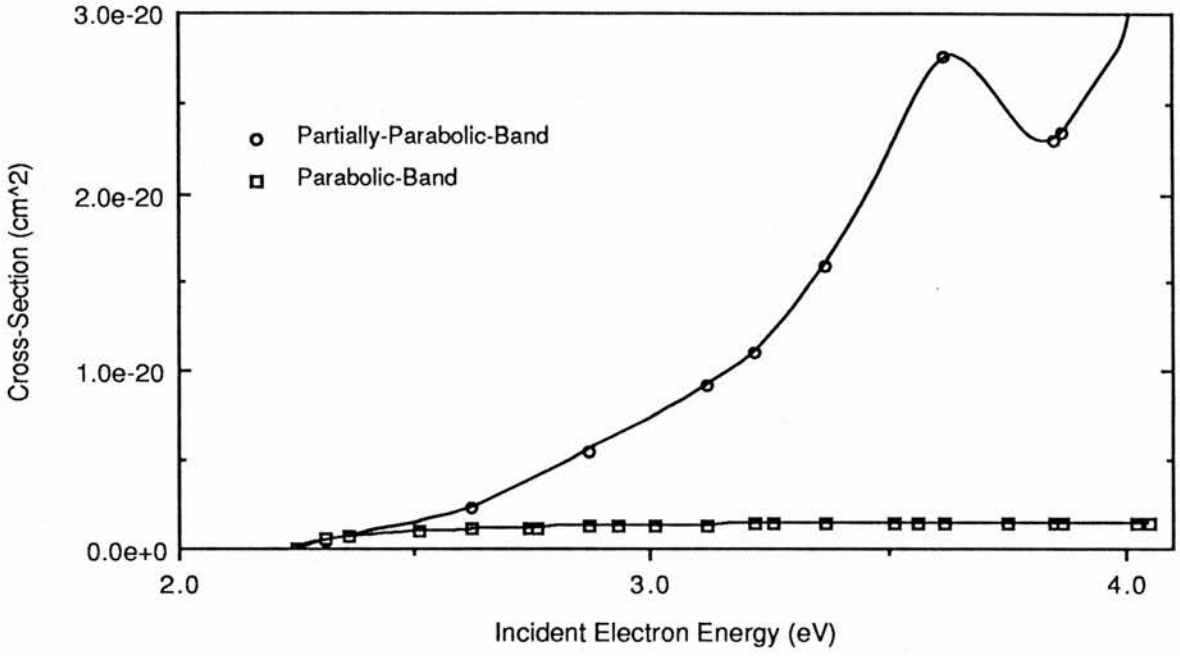

Figure 4.4 A comparison of the cross-section for the 2.25 eV excitation of Er in ZnS as calculated by the parabolic-band and partially-parabolic-band approximations.

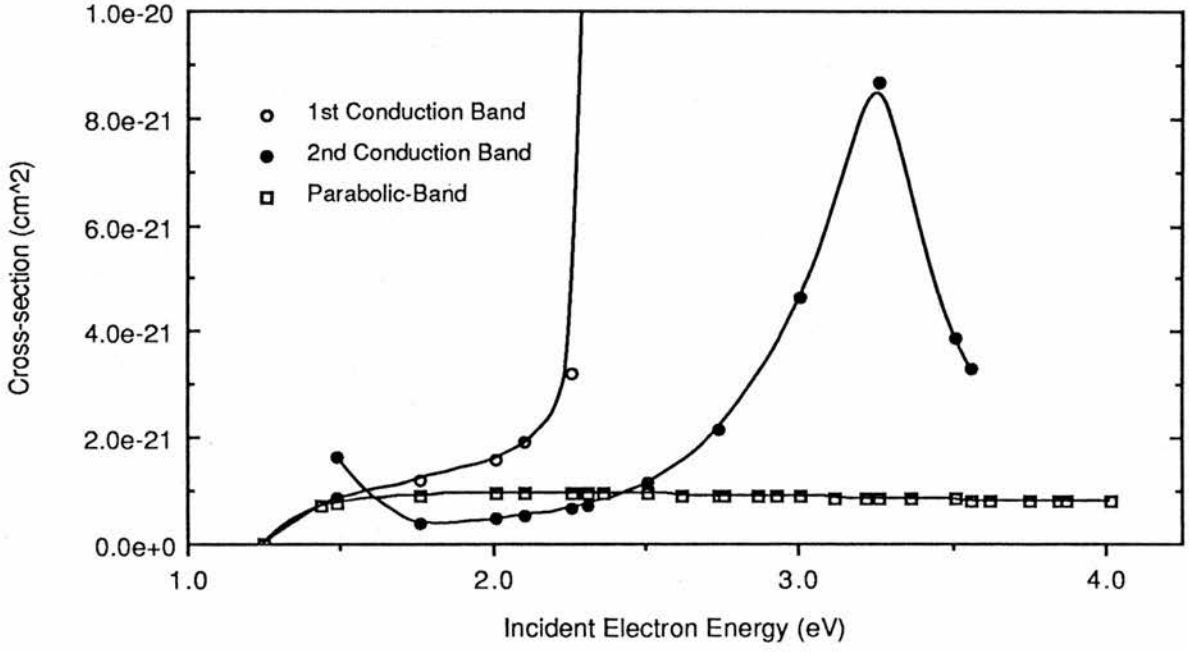

Figure 4.5 Comparison of the cross-sections for the 1.25 eV excitation of Er in ZnS as calculated by the parabolic-band and partially-parabolic-band approximations.

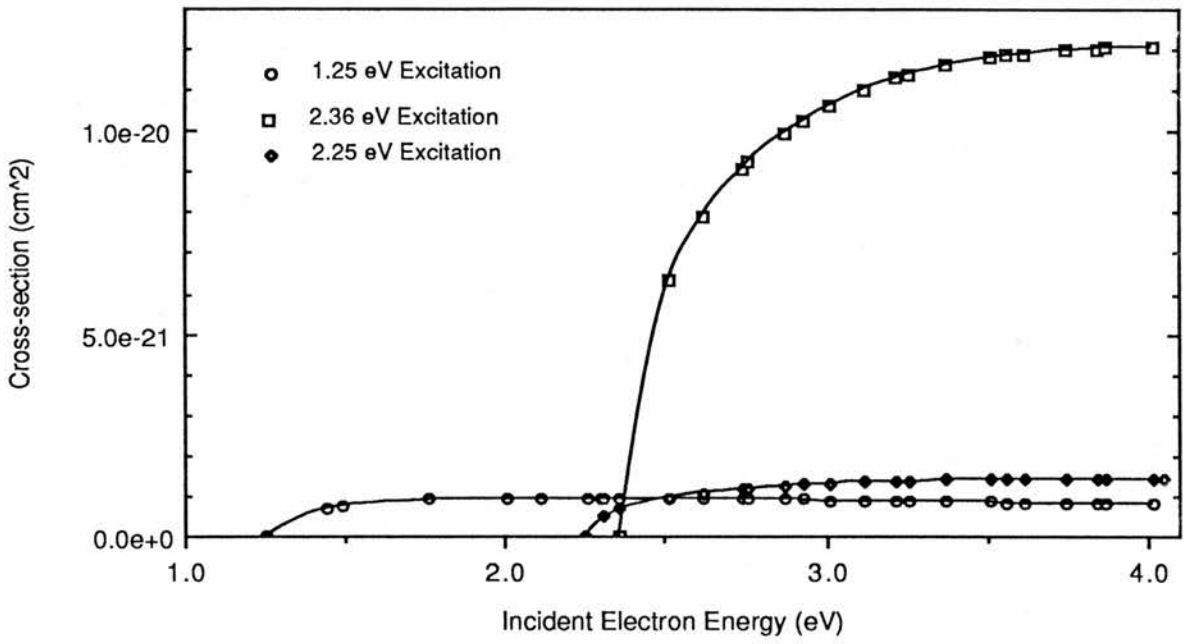

Figure 4.6 Comparison of the excitation cross-sections for different Er excited states as calculated by the parabolic-band approximation.

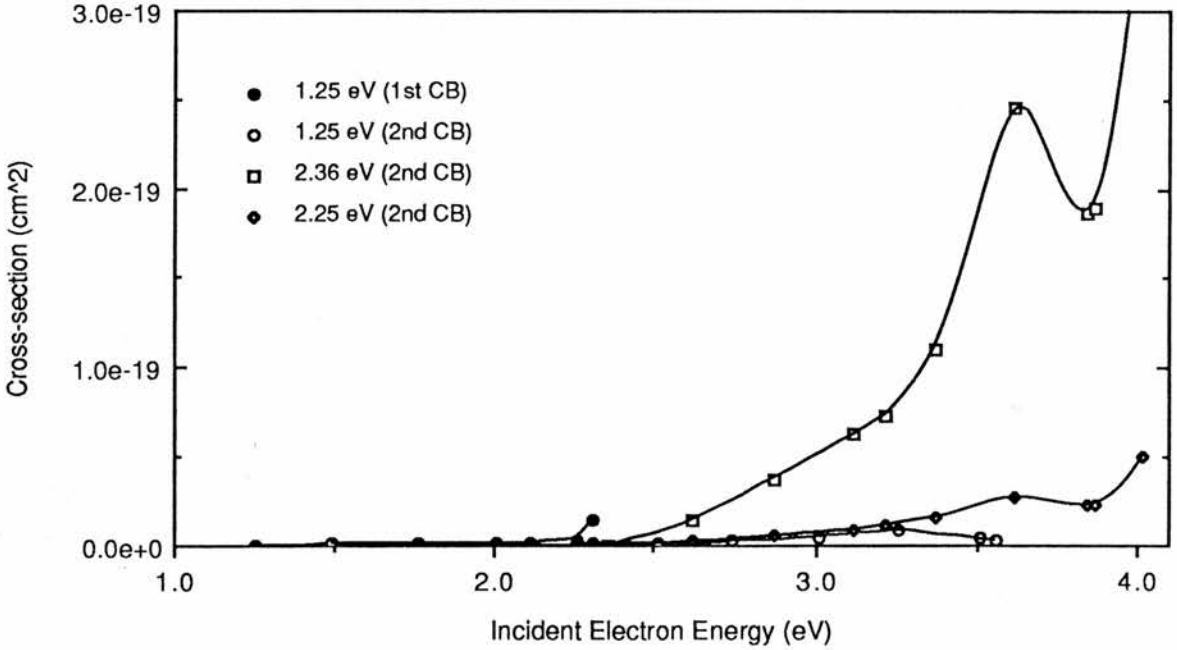

Figure 4.7 A comparison of the cross-sections for the different Er excitations as calculated by the partially-parabolic-band approximation.

is unclear what is happening because of the different orders of each cross-section. To overcome this in figure (4.8) we have replotted these cross-sections, normalizing them by removing the excited state energy and lifetime factors in equation (4.2) which determine the order.

4.6 Discussion

4.6.1 Parabolic-Band Cross-sections

From the discussion in Chapter 3 it was concluded that the order of magnitude of a cross-section is determined by the energy and lifetime of the excited state. That is because the lifetime of the excited state is related to the forbiddeness of the relaxation transition. Shorter lifetimes imply less forbiddeness for a transition and so a large cross-section is to be expected. Balancing this is the factor of the energy of the excitation, higher energy excitations being harder to induce. For the three excitations that we examined in Er the increase in excitation energy is more than compensated for by the decrease in the excited state lifetime so that the overall order of the cross-section increases with excitation energy.

Figure (4.6) shows that the cross-sections all increase rapidly once the threshold energy has been exceeded. As discussed in Chapter 3 (section 3.4) this is because at threshold the excitation of the centre requires that the incident electron loses most of its momentum. This momentum is transferred via the coulomb interaction to the crystal lattice. The transfer of momentum is difficult at the threshold because the momentum change is so large. Above threshold, momentum transfer becomes easier and the cross-section rises rapidly. At about 1 eV above threshold the cross-section begins to slowly decrease. This is because the increasing velocity of the incident electron reduces the interaction time between the incident and bound electrons. This decrease in the interaction time is just greater than the increase in the ease of transferring the excess momentum of the incident electron and so the cross-section decreases. These interpretations are discussed in more detail in Chapter 3.

4.6.2 Partially-Parabolic-Band Cross-section.

As with the parabolic-band cross-section just discussed the order of magnitude of the cross-section is determined by the excitation energy and lifetime of the excited state. As before the order of the cross-section increases as the excitation energy increases because of the

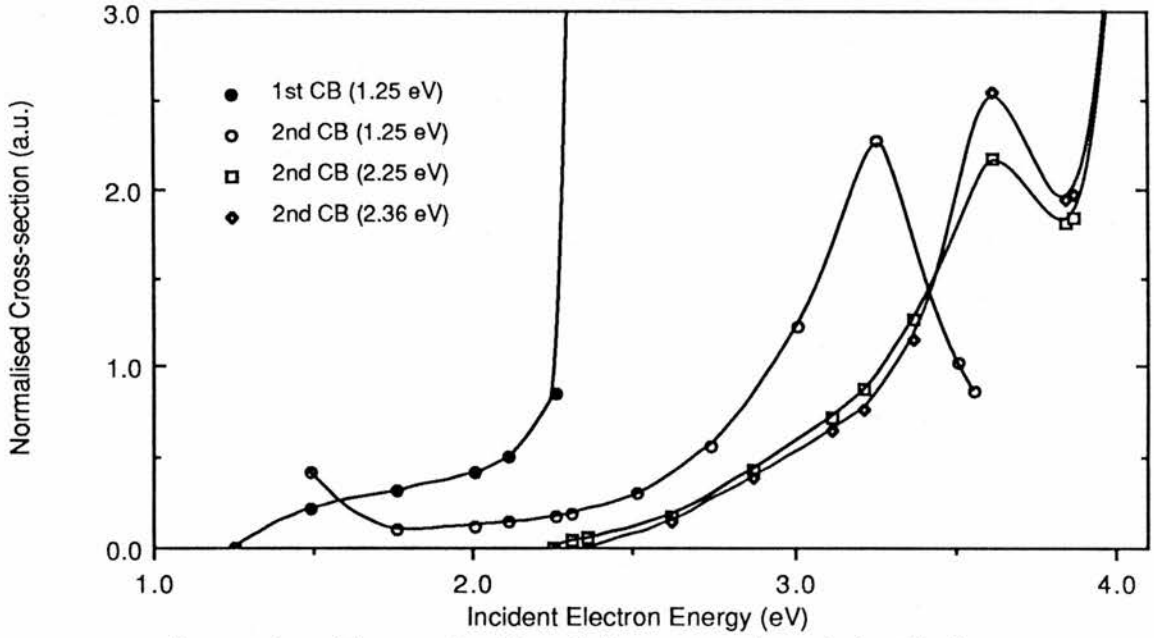

Figure 4.8 A comparison of the normalised Er excitation cross-sections calculated by the partially-parabolic-band approximation using the band structure of Walter & Cohen [4.20]. These cross-sections have had the lifetime and emission energy factors removed.

decreasing forbiddeness. While the order of the cross-section is easy to understand the structure shown in figures (4.3, 4.4 and 4.5) is more complicated. We now discuss each cross-section in turn though there are common factors in each one. In Chapter 3 (section 3.4) there is a more detailed discussion of the interpretation of the features in these cross-sections.

i) 2.36 eV Excitation Figure (4.3)

Initially the cross-section behaves very much like that for the parabolic-band approximation. At threshold the excitation is limited by the need to remove almost the whole momentum of the incident electron. In figure (4.9a) we show how the log terms of the cross-section in equations (4.1) and (4.2) change with energy for the parabolic-band and partially-parabolic-band cross-sections. This log term comes from the momentum change of the incident electron as discussed in Chapter 3. For the first electron-volt the two terms are similar because the initial and final momentum of the incident electron are so different. Above 1 eV the log term increases more quickly for the partially-parabolic-band cross-section because as the energy of the incident electron is increased its momentum decreases and approaches that of the scattered electron state. At 3.6 eV the incident electron is scattered into a final state of about the same momentum. As little momentum is transferred the excitation is greatly enhanced at this energy. This phenomenon is not predicted by the parabolic-band approximation. Above 3.6 eV the scattered electron needs to gain momentum from the lattice so the log term decreases until at 4.0 eV the log term approaches zero. At this energy the incident electron is near the Γ_{15C} peak and has little momentum so the scattered electron must gain most of its momentum from the lattice through the coulomb interaction.

There is only a factor of 2 difference in the log terms for the two approximations. To explain the order of magnitude increase in the cross-section shown in figure (4.3) we need to consider how the incident electron velocity varies with energy. In figure (4.10) the electron velocity expected for a parabolic dispersion is plotted with the electron velocity calculated from the band structure of Walter & Cohen [4.20]. For the 2.36 eV excitation only the velocity in the second conduction band is relevant. The calculated electron velocity is quite different and immediately demonstrates the inadequacy of the parabolic-band approximation to estimate the interaction time between the electrons above 1 eV. This interaction time is underestimated by a

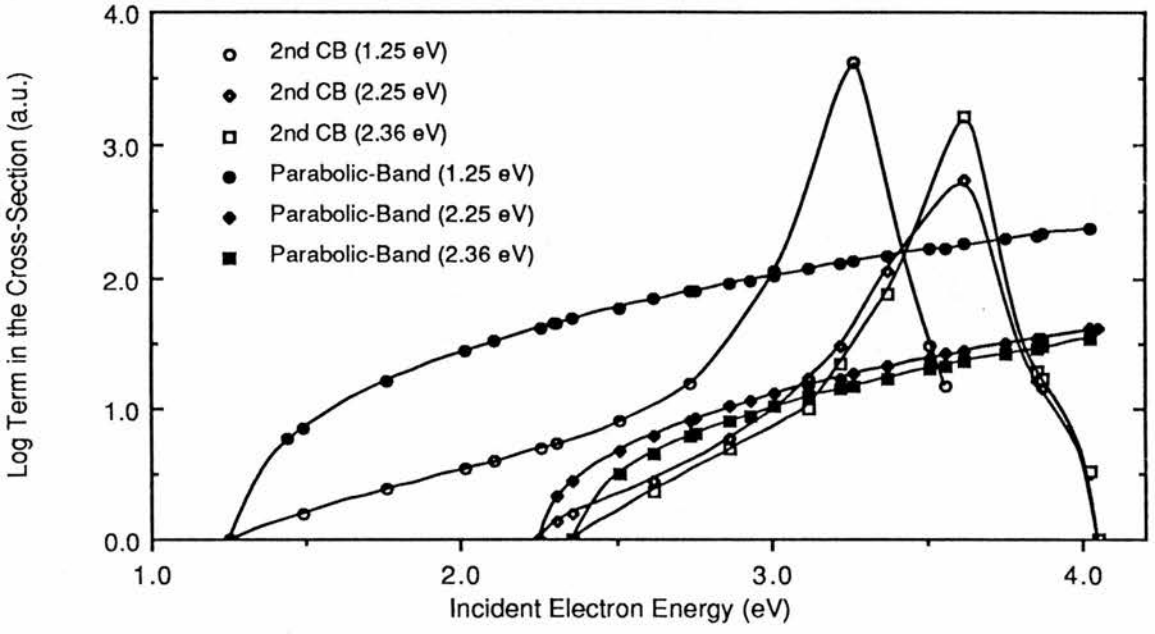

Figure 4.9a

Comparison of the log terms in the cross-section equations (4.1) {parabolic-band approximation} and (4.2) {partially-parabolic-band approximation} for electron energies in the second conduction band.

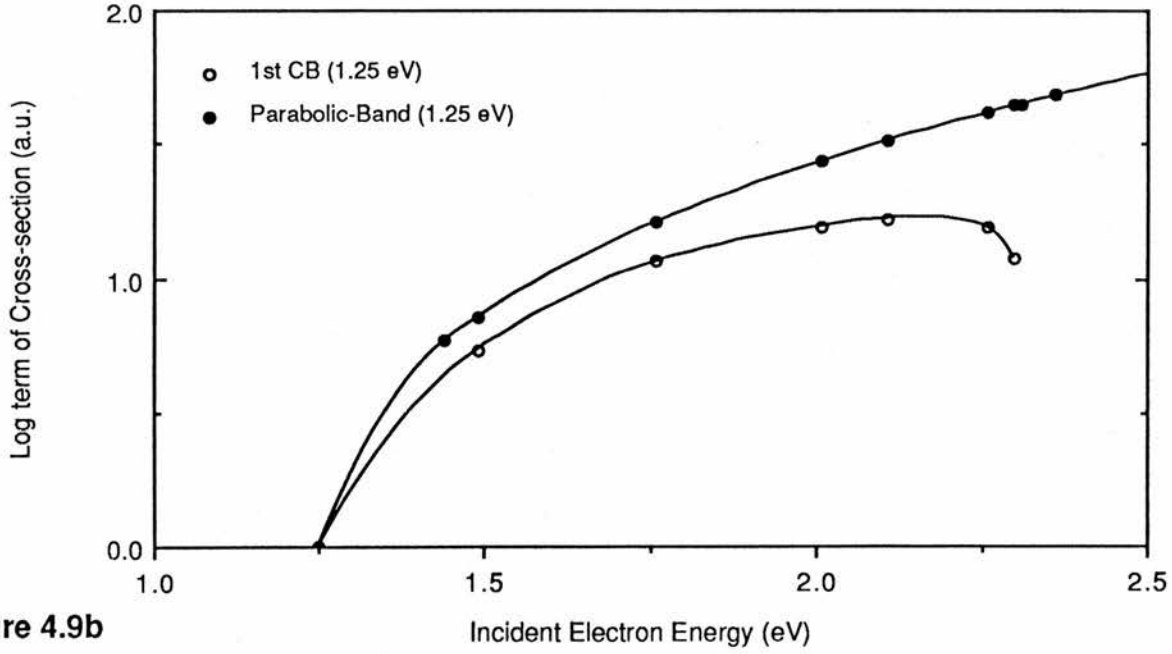

Figure 4.9b

A comparison of the log terms in the cross-sections equation (4.1) {parabolic-band approximation} and (4.2) {partially-parabolic-bandapproximation} which relate to the momentum change of the incident electron.

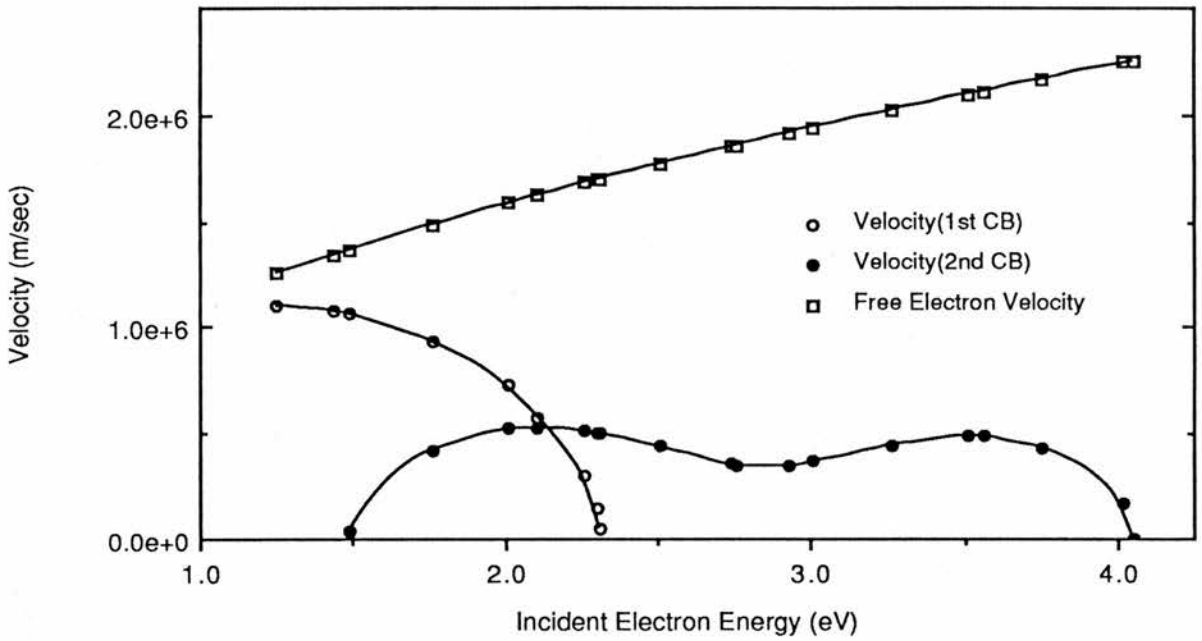

Figure 4.10 A comparison of the free electron velocity with the electron velocity in the first and second conduction bands as calculated from the ZnS band structure of Walter & Cohen [4.20].

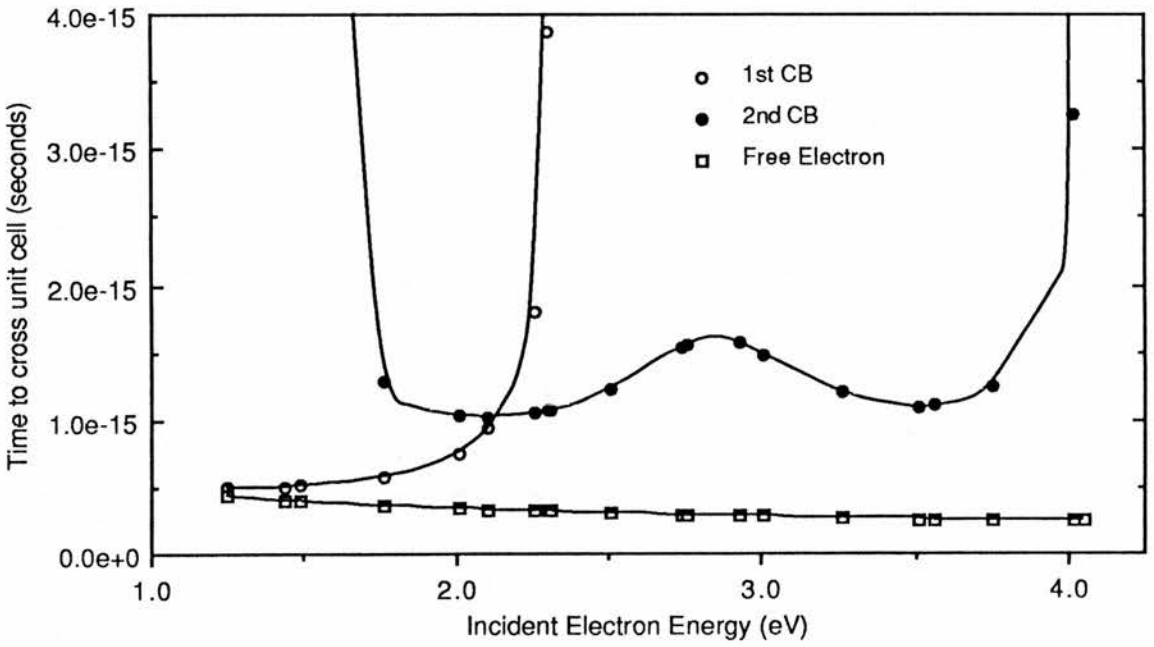

Figure 4.11 A measure of the interaction time between the incident and bound electrons as found from the time required for an electron to cross the unit cell of the lattice.

factor of 3 or more as shown in figure (4.11). This is because in the parabolic-band approximation the term $\frac{1}{2}\hbar k_u V_u$ in equation (4.1) (k_u and V_u being the incident electron momentum and velocity respectively) is substituted by the energy of the electron. However as shown in figure (4.12) this substitution is not very good above 1 eV.

The net effect of these two factors is an enhancement of the cross-section by as much as an order of magnitude and the addition of a peak in the cross-section at 3.6 eV due to a direct transition of the incident electron to its scattered state.

ii) 2.25 eV Excitation Figure (4.4)

It is just possible for electrons at the Δ_1 peak of the first conduction band to impact excite the Er to the 2.25 eV excited state. However there are unlikely to be many electrons found at this point in the band structure because of the electron scattering and the cross-section is rather small anyway. Therefore no cross-section is given here for this impact excitation.

For the excitation due to the electrons in the second conduction band the situation is similar to that for the 2.36 eV excitation. From figure (4.9a) we find that the log term is smaller in equation (4.2) than that found in the parabolic-band approximation, equation (4.1). This is because the shape of the second conduction band means that for a given energy the required momentum change in scattering the incident electron is greater than that predicted for a simple parabolic band up to 3.1 eV. This situation reverses and at 3.6 eV the incident and scattered electron states have approximately the same momentum. As little momentum exchange is needed the excitation cross-section will be enhanced in this region. Above 3.6 eV the scattered electron state has a greater momentum than the incident electron state and so the scattered electron has to gain momentum from the lattice. The amount of momentum required increases with the energy of the incident electron and so the cross-section reduces. This enhancement of the cross-section due to a direct transition of the incident electron is not predicted by the parabolic band approximation.

By considering just the momentum alone we do not expect the partially-parabolic-band cross-section and the parabolic-band cross-section to differ by more than a factor of 2. However as with the 2.36 eV excitation we find that the cross-section is dominated by the interaction time between the bound and incident electrons. Referring again to figure (4.10) we note that the

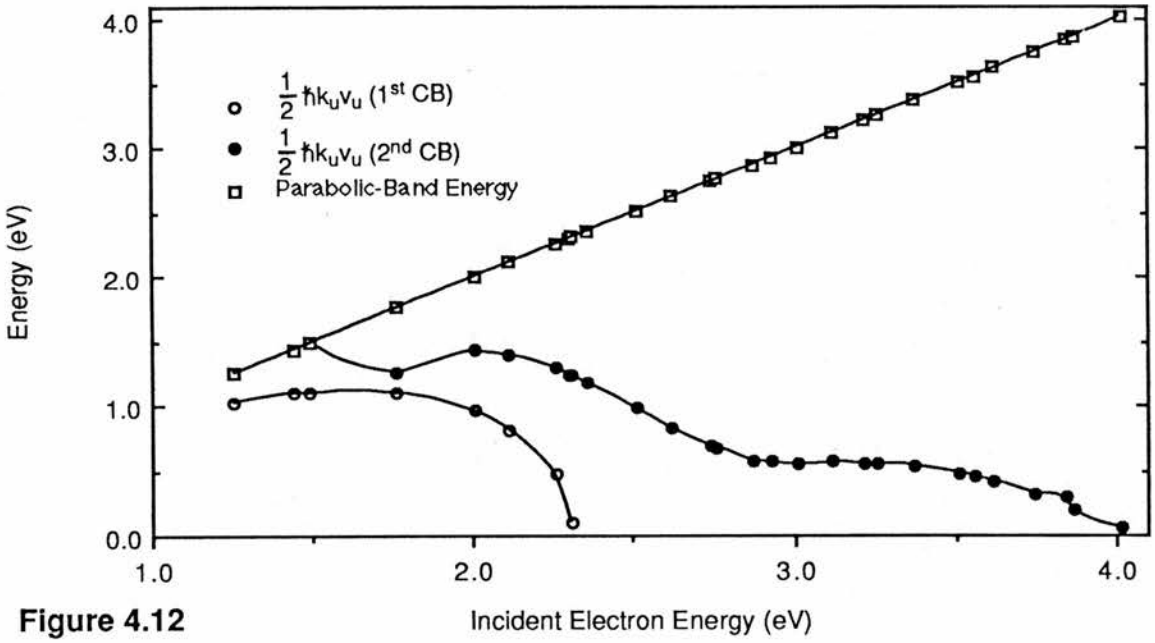

Figure 4.12

A comparison of the term $\frac{1}{2}\hbar k_u v_u$ (as calculated for the first and second conduction bands) with the energy of the incident electron for ZnS, calculated from the band structure of Walter & Cohen [4.20].

parabolic band seriously overestimates the velocity of the incident electron. The slow electron velocity increases the cross-section as shown in figures (4.4) and (4.8) so that it actually exceeds the parabolic-band approximation at all energies.

iii) 1.25 eV Excitation Figure(4.5)

Consider first the cross-section for excitation of the Er by electrons in the first conduction band. The cross-section at threshold is small because of the large momentum change of the incident electron. Figure (4.9b) shows that the momentum integral calculated for a parabolic band for the 1.25 eV excitation is quite similar to that calculated for the first conduction band. We would expect therefore that the cross-sections should be comparable and indeed near the threshold energy they are. However as shown in figure (4.10) at 2 eV the calculated electron velocity for the partially-parabolic band is quite different from that for a parabolic band. The result is that as the electron energy approaches that found at the top of the conduction band the electron velocity drops rapidly and the interaction time between the incident and bound electrons increases. This greatly enhances the cross-section in the partially-parabolic-band cross-section as shown by figure (4.4). This enhancement is not present for the parabolic-band approximation.

For the second conduction band the cross-section is initially large because of the low electron velocity in the X_3 valley. The fast increase in the electron velocity soon reduces this enhancement and the cross-section drops below the parabolic-band cross-section. Within 1 eV however the cross-section rises above the parabolic-band cross-section and remains above it there-after. The cross-section begins to rise again because the incident and scattered electron momentum approach one another allowing a direct transition.

To summarise then we find that initially the parabolic-band approximation agrees with the partially-parabolic-band approximation for the first conduction band until we approach the top of that conduction band where the small electron velocity increases the cross-section. In the second conduction band there is initially an enhancement of the cross-section because of the low electron velocity. This enhancement is soon lost causing a drop in the cross-section. After 1 eV the partially-parabolic-band cross-section is greater again because of the smaller electron velocity and the enhancement due to a direct transition of the incident electron.

iv) Summary

To summarise the results for the two cross-sections approximations we may make the following observations:

i) The order of magnitude of the cross-section is determined mainly by the forbiddeness of the transition. This forbiddeness can be found from the energy and lifetime of the excited state. Higher energy excited states are normally harder to excite (as for the hypothetical excitations in Chapter 3). If however these higher states have short lifetimes this is an indication that the forbiddeness may be decreasing. For the excitations in Er this is indeed the case and so the higher excitations have the larger cross-sections. This fact is demonstrated by both approximations.

ii) While the order of the cross-section is determined by the forbiddeness of the excitation the energy dependence is determined by the momentum change and the velocity of the incident electron. The parabolic-band approximation gives a similar momentum dependence to the partially-parabolic-band approximation. However it fails to predict the direct transition possible in the second conduction band .

iii) The most dominant factor in the shape of the cross-section is the incident electron velocity. The reciprocal of this is related to the interaction time between the bound and free electrons. In the parabolic-band approximation the electron velocity is overestimated and so the cross-section is underestimated. Further-more the parabolic-band approximation fails to predict the enhancement of the cross-section due to low electron velocities at the top of the first conduction band and at the bottom of the second conduction band.

The three partially-parabolic-band cross-sections have similar forms. Increasing the energy of the excitation raises the order of magnitude of the cross-section and shifts the direct transition peak to a higher energy. Other than that the cross-sections for each conduction band are similar (expect of course for the 1.25 eV excitation where the electrons in the first conduction band can attain excitation energies).

4.7 Comparison with other Cross-Sections

We must first consider the Mn impact cross-section because this was used by Xu et al [4.7] to find the cross-section for Er. The Mn cross-section has been theoretically calculated by Bernard et al [4.13] using an argument based on the polarisation of the impurity energy levels by the incident electron. No band structure was considered and though very simplistic an average cross-section of ~10^{-16} cm^2 was estimated for Mn in ZnS and ZnF_2 . This corresponded well with their experimental value of 3 x 10^{-16} cm^2 for Mn in ZnF_2 . However Bernard's theory contains two unjustifiable simplifications. Firstly though he considers the effect of the incident electron on the Mn ion he does not consider what effect the ion has on the incident electron. As the ion is polarised a dipole electric field is produced which repels the incident electron. Only electrons of sufficient energy will approach close enough to the ion to produce the cross-over in the ground and excited state energy levels as required for excitation. This explains why Bernard's cross-section is independent of the energy of the incident electron. The second over simplification is that Bernard considers that the bound electron will immediately transfer to the excited state as soon as polarisation has made the energy levels equal. However this ignores any selection rules which may make such a transition forbidden as in the case of Mn. Even for an allowed transition such a transfer will only have a finite probability of occurring in the time of closest approach of the incident electron. Once in the excited state the ion may just as easily return to its ground state once the incident electron passes and the energy levels return to the previous values leaving the ion in the ground state. Bernard tried to check his theory by estimating the cross-section from an uncertainty argument. This approximation has the wrong energy dependence and does not have a threshold energy. Also this second method does not take into consideration the selection rules.

Hagston [4.14] used the Born approximation to relate the Mn cross-section to the cubic crystal field which he measured by an optical experiment. The average cross-section he derived was also about 10^{-16} cm^2. However in Hagston's model for the excitation he has assumed that the closest approach of an electron to the Mn ion is the distance of the next nearest neighbour. He uses this assumption so that he can take the electric field of the incident electron to be the same as the crystal field due to the next nearest neighbour which he finds from his optical

measurements. This assumption is not justified and by fixing the closest approach he has already defined the size of his cross-section since this implies that there exist physical forces which prevent a closer approach.

Using the parabolic-band approximation Allen [4.5] calculated that for direct excitation the Mn cross-section should be $\sim 10^{-18}$ cm^2 , 2 orders smaller than estimated from Auger experiments (this cross-section is for electrons a few tenths of an electron volt above threshold where the parabolic and partially-parabolic band cross-sections are very similar). Allen argues that the direct excitation process is too weak to give the large experimental cross-section. Though not explicitly stated in the earlier cross-sections, Bernard and Hagston have also assumed a direct interaction because they do not consider any change in the spin of the incident electron.

Mach & Müller [4.8] avoid the problem of the type of interaction by considering only the efficiency of the excitation process. From their experiments they derive a cross-section of 4×10^{-16} cm^2 in agreement with other values. This estimate assumes that all the conduction electron are of excitation energy rather than having an exponential energy distribution. For Mn then we find that the average experimental cross-section is $\sim 10^{-16}$ cm^2 in ZnS but there is no comparable theoretical cross-section.

For Er the cross-section has been measured by Luo et al [4.6] and Xu et al [4.7]. Both cross-sections are based on the proposition that in an electroluminescent device simultaneously doped with Er and Mn, the Er cross-section can be found from the relative intensities of the Er and Mn emissions. This assumes that the electron distributions are similar at both excitation thresholds. Xu et al do not consider how the band structure may affect the electron distribution or the cross-sections for either centre. In their optical work Xu et al consider that the $^4S_{3/2}$ emission can be efficiently excited via the higher $^2H_{11/2}$ state followed by a rapid, non-radiative relaxation to the $^4S_{3/2}$ state. For this to occur the transition rate from the $^2H_{11/2}$ state to the $^4S_{3/2}$ level must be greater than the transition rate directly to the $^4I_{15/2}$ state. This would show itself in photoluminescence by the $^4S_{3/2}$ emission being more intense and this they appear to find. We would also expect the same situation to occur in electroluminescence and this is found by Zhong & Bryant [4.22] but not by Krier & Bryant

[4.17]. Since the $^2H_{11/2}$ state is more easily excited in electroluminescence the experimental cross-section derived from the $^4S_{3/2}$ emission is more likely to refer to the $^2H_{11/2}$ excitation. Xu et al however take their experimental cross-section to refer to the $^4S_{3/2}$ state.

Xu et al measure the lifetime for the $^4S_{3/2}$ state to be 269 μsec which is quite different from the 50 μsec that they found in their optical experiments and the 6.9 μsec found by Krier & Bryant. Xu et al found the Mn and Er cross-sections to be nearly equal. They argue that this is because the Mn has a more spread out wave function, which increases the cross-section for a direct interaction, but the Er has a shorter lifetime (269 μsec is about 1/5 of the Mn lifetime) and these two factors cancel one another. However the measured cross-section is more likely to be for the $^2H_{11/2}$ transition (an opinion shared by Yu & Shen [4.15]) which has a lifetime ~1/500 of that of Mn and so one might expect the Er to have a cross-section 50 times greater than that of Mn. As this is not the case it would appear that the Mn cross-section is two orders of magnitude greater than expected for this simple theory. We need then to calculate the expected cross-section of the Er and hence the motivation behind this chapter.

Xu et al have assumed that the Er and Mn are both excited only by a direct impact excitation. However Rigby [4.24] has shown that Mn and Rare Earths in ZnS and ZnSe can be excited by energy transfer. Xu et al used low concentrations of Er and Mn in their devices to reduce possible energy transfer between the centres. However this will not prevent energy transfer from other centres into the Mn or Er. Unless it can definitely be shown that both the Mn and Er are excited only by impact excitation then it is invalid to compare the cross-sections for the two centres.

Yu & Shen [4.15, 4.23] used the parabolic-band approximation to calculate the cross-section for the $^2H_{11/2}$ and $^4S_{3/2}$ excited states. They took the excited state energy and lifetime from the work of Xu et al [4.7] and found that the cross-section for the $^2H_{11/2}$ state was the same as found experimentally by Xu et al. From this they conclude that in electroluminescence the $^4S_{3/2}$ state is mainly excited via the $^2H_{11/2}$ state as discussed earlier. However the cross-section used by Yu & Shen included an algebraic error increasing the cross-section by $(2\pi)^3$. When this factor is removed there is no longer any agreement with the experimental cross-section. The theoretical cross-section may be increased further by chosing a band structure

such that the X_3 valley (or other valleys in the second conduction band) is close to the $^2H_{11/2}$ excitation energy. As explained in Chapter 5 electrons in a high electric field may congregate at this valley which will further increase the averaged effective cross-section which is measured experimentally. Otherwise the only means of increasing the cross-section to agree with experimental values is to allow for an exchange component in the excitation as proposed by Allen for Mn in ZnS and ZnSe [4.5, 4.9].

4.8 Concluding Remarks

It is suggested in Chapter 5 that the non-parabolic dispersion found in ZnS can lead to a greater than expected hot-electron population. Furthermore in this chapter it is found that a non-parabolic dispersion alters the energy dependence of the impact cross-section. A previous calculation of the Er cross-section by Yu & Shen [4.15] contained several unrealistic assumptions. Screening of the Er electrons was taken as being minimal and the effective mass of the incident electron was not considered properly. Using a revised formula, correcting for these assumptions and an algebraic error, we re-calculated the cross-sections. For comparison we further calculated the same cross-sections using our own approximation based on a partially-parabolic conduction band.

Our conclusion is that a parabolic band underestimates the cross-section by as much as an order of magnitude. This is because the momentum change and electron velocity are over estimated. We found the following peak cross-sections for the Er excitations :

Table 4.4

	Parabolic-Band	Partially-Parabolic-band
$^4I_{15/2} — ^2H_{11/2}$	1.2×10^{-20} cm^2	2.5×10^{-19} cm^2 (c.f. 1.8×10^{-16} cm^2 [4.15])
$^4I_{15/2} — ^4S_{3/2}$	1.5×10^{-21} cm^2	2.5×10^{-20} cm^2 (c.f. 2.0×10^{-17} cm^2 [4.15])
$^4I_{15/2} — ^4H_{11/2}$	9×10^{-22} cm^2	9×10^{-21} cm^2 (no other value known)

We conclude therefore that the parabolic-band approximation is insufficient to accurately predict the cross-section for rare earth impurities in materials like ZnS where the conduction bands have slow, energetic electrons.

There is still however the unanswered question of why the experimental cross-sections are so much larger than the theoretical values. There is also some uncertainty about the

lifetimes that were used in the calculation of these cross-sections. The range of experimental values published for the lifetimes indicates that non-radiative processes can occur which reduce the lifetime. If a radiative lifetime is found this may still be inappropriate as the relaxation may not occur purely by the electric dipole transition.

The experimental cross-section published for Er by Xu et al can not yet be accepted until it has been definitely demonstrated that both the Er and Mn in the experiments were excited by a direct impact excitation process.

Chapter 4

4.8 References

[4.1] D.C.Krupka *J.Appl.Phys.* **43** (1972) 476

[4.2] J.W.Allen *J.Lumin.* **31&32** (1984) 665

[4.3] N.F.Mott & H.S.W.Massey *"Theory of Atomic Collisions"* *1st Edition,Oxford Uni. Press.* (1933) 96-98,159-177

[4.4] A.S.Baltenkov & E.D.Belorusets *Sov. Phys. Semicond.* **12** (1978) 1283

[4.5] J.W.Allen *J.Phys. C: Solid State Phys.* **19** (1986) 6287

[4.6] B.Luo, J.Yu & G.Zhong *J.Lumin.* **40/41** (1988) 786

[4.7] Xu-mou Xu, Jiaqi Yu, Gou-zhu Zhong *J.Lumin.* **36** (1986) 101

[4.8] R.Mach & G.O.Müller *Phys.Stat.Sol.(a)* **81** (1984) 609

[4.9] J.W.Allen *J.Lumin.* **23** (1981) 127

[4.10] N.E.Rigby & J.W.Allen *J.Phys. C: Solid State Phys.* **21** (1988) 3483

[4.11] N.E.Rigby, T.D.Thompson & J.W.Allen *J.Phys. C:Solid State Phys.* **21** (1988) 3295

[4.12] K.Brenan *J.Appl.Phys.* **64** (1988) 4024

[4.13] J.E.Bernard, M.F.Martens & F.Williams *J.Lumin.* **24&25** (1981) 893

[4.14] W.E.Hagston *Phys.Stat.Sol.(a)* **81** (1988) 6287

[4.15] J.Yu & Y.Shen *J.Lumin.* **40/41** (1986) 769

[4.16] Syed Razi *Optical Properties of Rare Earth Activated ZnS* *M.L. Report (Stanford University) no.* **1375** (1965) 76

[4.17] A.Krier & F.J.Bryant *Phys.Stat.Sol (a)* **83** (1894) 315

[4.18] M.Z.Huang & W.Y.Ching *J.Phys.Chem.Solids* **46** (1985) 977

[4.19] C.S.Wang & B.M.Klein *Phys. Rev.* **B 24** (1981) 3393

[4.20] J.P.Walter & M.L.Cohen *Phys. Rev.* **183** (1969) 763

[4.21] M.L.Cohen & T.K.Bergstresser *Phys Rev.* **141** (1966) 789

[4.22] Gu-mou Zhong & F.J.Bryant *J.Lumin.* **24/25** (1981) 909

[4.23] Yu Jiaqi & Shen Yongrong *J.Phys. C:Solid State Phys.* **21** (1988) 3381

[4.24] N.E.Rigby *PhD Thesis, University of St.Andrews* (1987) Chapter 4

Chapter 5

Hot Electron Distribution Functions

		Page
5.1	**Introduction**	**121**
5.2	**Background Theory and Calculation of Emission Intensities**	
5.2.1	Introduction	**122**
5.2.2	The Rate Equation	**123**
5.2.3	Approximation of the Electron Velocity $\upsilon(E)$	**125**
5.2.4	Approximation of the Impact Cross-section $\sigma(E)$	**125**
5.2.5	The Electron Distribution Functions $n(E)$	
a)	Introduction	**127**
b)	Theoretical Electron Distribution Functions	**128**
c)	Discussion and Experimental Evidence for Electron Distributions	**130**
5.3	**Evaluation of the Impact Excitation Rate**	
5.3.1	Introduction	**133**
5.3.2	Mathematical Evaluation	**133**
5.3.3	Experimental Evaluation of Impact Rate Equation : Thin Films	**137**
5.3.4	Experimental Evaluation of Impact Rate Equation : Schottky Diodes	**142**
5.4	**Critique of Other Work**	
5.4.1	Critique of Mathematical Evaluation of Rate Equation	**155**
5.4.2	Critique of Experiments on Thin Film Devices	**157**
5.4.3	Critique of Experiments on Schottky Diodes	**158**
5.5	**Conclusion**	**160**
5.6	**References**	**163**

Chapter 5

Hot Electron Distribution Functions

5.1 Introduction

Light emitting p-n junctions have been with us for many years and the physics of such devices is well understood. However the efficiency of these junctions decreases with increasing emission energy and not all semiconductors can be made both n-type and p-type as required. Another limitation with p-n junctions is that the cost of the materials becomes exorbitant for large area displays. To overcome these problems attention has shifted to a new type of device based on hot-electron impact excitation of luminescence centres [5.1]. These devices can be Schottky diodes, thin films or powder panels producing large area displays of a reasonable light output but low efficiency. Development of impact excitation devices has come a long way since the first thin film devices were produced by Inogochi et al [5.2] though most of this development has been directed towards the construction of thin films. The choice of the phosphor material for these devices is most often ZnS with Mn as the luminescence centre. Some work has been reported using CdF_2 with Mn or a rare-earth dopant. So far ZnS:Mn has dominated the research field because of its high efficiency. Progress in development of these devices is hampered by a lack of understanding of the physical processes occurring. If the high efficiency of the ZnS:Mn could be explained it would help the search for alternative phosphor materials.

The mechanism of impact excitation involves three stages [see reference 5.3 for a general discussion]

i) a source of conduction electrons

ii) a high field region in which the conduction electrons are accelerated to energies sufficient for impact excitation

iii) a region in the devices in which excited luminescence centres may radiatively emit their excitation energy.

Understanding of these three processes is developing but progress is slow because there are too many unknown factors. Our group has concentrated its research on Schottky diodes as

the electric fields and conduction processes are better understood in these devices compared with the situation in the thin film devices used in other groups. One of the main areas of uncertainty in either device type is the electron distribution function of the hot electrons. In this this chapter it is shown that for a simple model of the electron interaction, it is the electron distribution which mainly determines the intensity of the different luminescence emissions in a device. Without an accurate knowledge of this electron distribution it is impossible to test different theories explaining the impact excitation process.

A group at Hull University have produced a series of papers attempting to extract the electron distribution from various experiments. These experiments seem to indicate either a Maxwell-Boltzmann or Druyvesteyn type energy dependence for the electron population. In this chapter we review the theoretical background and then analyse the Hull work showing where any mistakes or misunderstandings are present.

We conclude with an assessment of the theoretical and experimental evidence for the electron distribution.

5.2 Background Theory and Calculation of Emission Intensities

5.2.1 Introduction

It has been proposed that the electron distribution may be found from an analysis of the different emissions produced by a centre in a luminescence device. In order to deconvolute the luminescence data we need to understand all the factors which determine the luminescence intensity. For this we need to know

i) the rate equation giving the energy dependence of the emission intensity. This equation will involve :-

ii) The impact excitation cross-section for each excited state

iii) The electron velocity

iv) The possible forms for the electron distribution.

We can guess at different types of electron distribution in order to evaluate the emission rates. By trying different models we can see which one produces the best fit. We now consider each of these steps.

5.2.2 The Rate Equation

A cross-section can be thought of as the perpendicular surface area offered by a target object to a stream of passing projectiles. If we have N such targets of impact cross-section σ and a single projectile of velocity υ we can define the collision rate as

$$N \sigma \upsilon. \qquad (5.1)$$

For a luminescence centre in a host lattice the collisions of interest are those inelastic collisions which result in the excitation of the centre. We can then define a cross-section using (5.1) which gives the rate of these impact excitations. The cross-section so defined by (5.1) will be dependent upon the energy of the colliding electron and will be zero below a minimum threshold energy equal to the energy of the excited state.

To find the excitation rate for a stream of electrons we need to know the energy distribution of the electrons. If such a distribution is n(E) then

$$n_c = \int_0^\infty n(E)\, dE \qquad (5.2)$$

where n_c is the density of the conduction electrons and all energies are measured relative to the bottom of the conduction band.

We can now define the excitation rate due to electrons of energy E as

$$dR_e = n(E)\, N\, \sigma(E)\, \upsilon(E)\, dE \qquad (5.3)$$

where R_e is the excitation rate and $\sigma(E)$ & $\upsilon(E)$ are the energy dependent forms of the impact cross-section and electron velocity respectively.

To find the total excitation rate we integrate (5.3) over the energy range of the conduction electrons

$$R_e = N \int_0^\infty n(E)\, \sigma(E)\, \upsilon(E)\, dE. \qquad (5.4)$$

In a steady state situation (which will be established within a few lifetimes of the excited state) we can equate this excitation rate to the relaxation rate of the luminescence centres.

$$\frac{dN^*}{dt} = 0 = R_e - \frac{N^*}{\tau} \tag{5.5}$$

where N^* is the number of excited luminescence centres and τ is the lifetime of the excited state. (We have assumed so far that $N^* \ll N$ otherwise N in the previous equations will need to be replaced by $(N - N^*)$ the number of unexcited centres).

If the relaxation of the excited centres is purely radiative then the photon emission rate I (i.e. the emission intensity) is

$$I = \frac{N^*}{\tau_r} \tag{5.6}$$

where τ_r is the radiative lifetime.

If there are competing non-radiative relaxation processes then (5.5) becomes

$$\frac{dN^*}{dt} = 0 = R_e - \frac{N^*}{\tau_r} - \frac{N^*}{\tau_{nr}}$$

$$= R_e - \frac{N^*}{\tau} \tag{5.7}$$

where τ_{nr} is the non-radiative decay time and τ is the measured lifetime such that

$$\frac{1}{\tau} = \frac{1}{\tau_r} + \frac{1}{\tau_{nr}} . \tag{5.8}$$

We can relate the excitation rate to the emission intensity by using the radiative efficiency η defined as

$$\eta = \frac{\tau}{\tau_r} \tag{5.9}$$

so that

$$I = \eta R_e. \tag{5.10}$$

A luminescence centre may have a number of excited states of different energies. If we assume that each state can only be directly excited by impact excitation (i.e. there is no energy transfer from higher excited states or other centres) we have a different impact excitation cross-

section for each state. To distinguish between each state we label the individual cross-sections and radiative efficiencies with a λ i.e.

$$I_\lambda = \eta_\lambda N \int_0^\infty n(E)\, \sigma_\lambda(E)\, \upsilon(E)\, dE \,. \qquad (5.11)$$

This equation (5.11) has been used by Krupka [5.4], Xu et al [5.5] and Ayling & Allen [5.6]. Papers by Bryant et al [5.7, 5.8, 5.9] erroneously include in their rate equation additional lifetimes of the excited state. They also do not properly include the radiative efficiency though its requirement is demonstrated in their emission data [5.7, 5.9].

To evaluate (5.11) we need to find approximate forms for n(E), σ(E) and υ(E) and these we consider next.

5.2.3 Approximation of the Electron Velocity υ(E)

In Chapter 3 it was noted that in a conduction band the electron velocity was a function of crystal momentum. Two electrons might have the same magnitude of momentum and yet have different energy and velocity. For a thorough description we would need to use

$$\underline{\upsilon}(\underline{k}) = \frac{1}{\hbar} \nabla_{\underline{k}}\, E(\underline{k}). \qquad (5.12)$$

Such a description is too cumbersome for our present requirements so we assume that it is sufficient to use the electron velocity as found for an isotropic parabolic conduction band. At first sight this would overestimate the excitation rate at higher energies as it gives a greater electron velocity than really exists. However the cross-section is underestimated if we also assume a parabolic conduction band and so the error is canceled. The electron velocity is

$$\upsilon(E) = \left(\frac{2E}{m^*}\right)^{1/2} \qquad (5.13)$$

where m* is the effective mass of the electron

5.2.4 Approximation of the Impact Cross-section σ_λ(E)

In section 5.2.3 we assumed that the conduction band was of a simple parabolic form. In keeping with this we use the cross-section derived in Chapter 3 for a parabolic conduction-band. We then have

$$\sigma_\lambda(E) = \left[\frac{\varepsilon_\infty^2\, n(n^2+2)^2}{9}\right]^{-1} \pi\, m^*\, e^2\, \hbar^2\, c^3\, \frac{1}{E_\lambda^3\, \tau_{r\lambda} E}\, \mathrm{Ln}\left\{\frac{\sqrt{E} + \sqrt{(E-E_\lambda)}}{\sqrt{E} - \sqrt{(E-E_\lambda)}}\right\} \quad (5.14)$$

where ε_∞ is the high frequency dielectric constant of the host lattice

n is the refractive index of the host lattice

m* is the effective mass of the conduction electron in the host lattice

E_λ is the energy of the excited state

$\tau_{r\lambda}$ is the radiative lifetime of the excited state

E is the energy of the conduction electron relative to the bottom of the conduction band.

(For a derivation of this cross-section see Chapter 3). In using this cross-section we are making three assumptions. First that each excited state is only directly excited in the device and so there is no relaxation from a higher state. Second that the lifetimes used are for the pure electric dipole relaxation of the excited state. Lastly we are assuming that each excited state is excited by impact excitation and not by energy transfer from other centres present in the device.

It is expected that the electron distribution will be a rapidly decreasing function of energy. We are therefore only concerned with the variation of σ_λ near to the threshold energy. We can approximate (5.14) near threshold by assuming that $E \approx E_\lambda$ so that

$$\mathrm{Ln}\left\{\frac{\sqrt{E} + \sqrt{(E-E_\lambda)}}{\sqrt{E} - \sqrt{(E-E_\lambda)}}\right\} = \mathrm{Ln}\left\{\frac{\sqrt{E} - \sqrt{(E-E_\lambda)}}{\sqrt{E} - \sqrt{(E-E_\lambda)}} + \frac{2\sqrt{(E-E_\lambda)}}{\sqrt{E} + \sqrt{(E-E_\lambda)}}\right\} \quad (5.15)$$

$$= \mathrm{Ln}\left\{1 + \frac{2\sqrt{(E-E_\lambda)}}{\sqrt{E} + \sqrt{(E-E_\lambda)}}\right\}. \quad (5.16)$$

If $E \approx E_\lambda$ then

$$\sqrt{E} + \sqrt{(E-E_\lambda)} \approx \sqrt{E} \quad (5.17)$$

and

$$\frac{2\sqrt{(E-E_\lambda)}}{\sqrt{E}} \ll 1 \quad (5.18)$$

so we may expand the log function as

$$\mathrm{Ln}\left\{\frac{\sqrt{E} + \sqrt{(E-E_\lambda)}}{\sqrt{E} - \sqrt{(E-E_\lambda)}}\right\} = \frac{2(E - E_\lambda)^{1/2}}{E^{1/2}}. \quad (5.19)$$

Substituting this into (5.14) we get

$$\sigma_\lambda(E) = \left[\frac{\varepsilon_\infty^2\, n(n^2+2)^2}{9}\right]^{-1} 2\pi\, m^*\, e^2\, \hbar^2\, c^3 \frac{(E - E_\lambda)^{1/2}}{E_\lambda^3\, \tau_{r\lambda} E^{3/2}} \quad (5.20)$$

$$= \frac{\alpha\,(E - E_\lambda)^{1/2}}{E_\lambda^{3}\,\tau_{r\lambda}E^{3/2}} \qquad (5.21)$$

where α is the same for any centre and any excited state in the host material. (5.21) is essentially the same as that given by Yu & Shen [5.10] (except that their cross-section has a different screening factor and contains an algebraic error) and is equivalent to equation (4) in the paper by Allen and Ayling [5.6].

In using this cross-section we are assuming that the impact excitation is a direct process and that the relaxation is by an electric-dipole transition. In Chapter 2 experiments on Auger quenching of Mn in ZnSe and ZnS gave a cross-section for the Mn excitation that is much larger than the cross-section expected for a direct excitation. This cross-section is therefore unsuitable for calculating the Mn electroluminescence in these materials. As yet a suitable exchange cross-section has not been calculated for Mn and so we continue to use the direct cross-section. It is not yet known if an exchange cross-section is also required for Er in these materials.

(For a discussion of the cross-section used by other groups see Chapter 3)

5.2.5 The Electron Distribution Function n(E)

5.2.5 a Introduction

The electron distribution function for no applied field can be written in four parts

$$n(E) = n_c\, B\, D(E)\, f(E) \qquad (5.22)$$

where n_c is the density of the conduction electrons, D(E) is the density of states of energy E, f(E) is a statistical distribution function and B is a normalising constant defined so that

$$\int_0^\infty B\, f(E)\, dE = 1 \; . \qquad (5.23)$$

For a non-degenerate semiconductor with no applied field f(E) can be approximated to the high energy tail of a Fermi-Dirac distribution

$$f(E) \propto \exp\left(-\frac{E}{k\,T}\right) \qquad (5.24)$$

where T is the temperature of the lattice.

In a parabolic conduction band the density of states D(E) is given by

$$D(E) = \frac{1}{2\pi^2}\left(\frac{2m}{\hbar^2}\right)^{3/2} E^{1/2} . \qquad (5.25)$$

We use the parabolic band approximation to be consistent with the earlier approximations for $\upsilon(E)$ and $\sigma_\lambda(E)$.

Together we now have

$$n(E) = n_c \cdot \frac{1}{2\pi^2}\left(\frac{2m}{\hbar^2}\right)^{3/2} E^{1/2} . B \exp\left(-\frac{E}{kT}\right)$$

$$= \beta E^{1/2} \exp\left(-\frac{E}{kT}\right) . \qquad (5.26)$$

We now consider what will be the effect of an applied electric field on the electron distribution .

5.2.5 b Theoretical Electron Distribution Functions

To find the effect of an electric field or thermal gradient on an electron distribution one can solve the Boltzmann transport equation

$$\left(\frac{dn(E)}{dt}\right) = \left(\frac{dn(E)}{dt}\right)_{field} + \left(\frac{dn(E)}{dt}\right)_{scattering}$$

$$+ \left(\frac{dn(E)}{dt}\right)_{excitation} + \left(\frac{dn(E)}{dt}\right)_{ionisation} . \qquad (5.27)$$

The left hand side of the equation is the rate at which the distribution is changing with time.This is to be zero for a steady state solution as in a d.c. device or for an instantaneous field in an a.c. device. The first term on the right hand side of the equation is the rate at which energy is supplied to an electron by the electric field. This may be written as

$$\left(\frac{dn(E)}{dt}\right)_{field} = \left(\frac{\partial \upsilon}{\partial t}\right)\left(\frac{\partial n(E)}{\partial \upsilon}\right) = -\frac{e\mathcal{E}}{m^*}\left(\frac{\partial n(E)}{\partial \upsilon}\right) . \qquad (5.28)$$

The next term is the rate at which scattering by acoustic and optical phonons removes energy from the electron and may be written as

$$\left(\frac{dn(E)}{dt}\right)_{scattering} = \frac{1}{\tau} n(E) \qquad (5.29)$$

where τ (the scattering time) may also be extended to include collisions between electrons.

The next term only affects electrons of energy greater than or equal to the excitation energies for a centre in the host. If the centres are concentrated then they may alter the electron distribution. Normally it is assumed that this term is negligible though it gives the rate of energy transfer to the luminescence centres i.e. equation (5.3).

The last term has an energy threshold and involves only those electrons of sufficient energy to ionise the luminescence centre or the deep donors. This term will include multiplication and avalanching mechanisms in the semiconductor if the electrons have sufficient energy to promote valence electrons across the band gap.

Assuming a parabolic conduction-band Fröhlich attempted to solve the Boltzmann equation in a high electric field [5.11, 5.12]. He assumed that the most common scattering event was an inelastic collision between conduction electrons which had the effect of sharing out the energy gained in the electric field. This resulted in the electron temperature in (5.26) no longer being equal to the lattice temperature.

The rate at which an electron gains energy is dependent on its velocity through the electric field, but the rate at which it losses energy through optical phonon scattering is constant. Fröhlich therefore proposed that the net rate of energy loss decreased as the electron gained energy. He suggested that there would exist an equilibrium energy at which energy lost through phonon scattering would equal energy gained in the electric field. Since only the energy gain is dependent on the electric field strength there exists for any field a certain energy above which an electron gains energy faster than it is lost. If this equilibrium energy is greater than the ionisation energy of the material then electrons are very unlikely to reach this constantly accelerating state (called runaway). At higher field strengths this equilibrium energy can be brought below the ionisation energy. Then significant numbers of electrons are accelerated up to ionisation energies. If the field is increased further a catastrophic breakdown occurs similar to that seen in gasses.

The size of the breakdown field will increase with increased scattering due to phonons, impurities or conduction electrons. Fröhlich & Paranjape [5.13] proposed that the conduction electron scattering would only be significant for electron densities of 10^{14} cm^{-3} or greater. In

thin film devices with no donors and in the depletion region of a Schottky diode the electron densities are very low. It is unlikely therefore that the conduction electron scattering will be important and so conduction models for insulators would be more appropriate [5.14, 5.15]. If the material is heavily doped it may be feasible to use models developed for impure ionic crystals [5.16] in which the impurity scattering further increases the breakdown field. Once breakdown is achieved the Boltzmann equation will of course have no steady state solution.

Barker [5.17] calculated the effect of a constant, uniform electric field on a Maxwell-Boltzmann (M-B) distribution. Provided that the field was below the breakdown threshold the result was a displaced M-B distribution. At higher fields the electron distribution becomes streaming but to some extent could be related to the initial distribution.

The most commonly quoted electron distributions are those calculated by Baraff [5.18, 5.19]. Using spherical harmonics he expanded the electron distribution and solved the Boltzmann equation for a parabolic band structure, which is in keeping with our requirements. Because ionisation is energy dependent he found two distributions. For low fields where the characteristic energy (E_o) was less than the ionisation energy he found a M-B distribution

$$f(E) \propto \exp\left(-\frac{E}{E_o}\right). \qquad (5.30)$$

For higher fields where the E_o was comparable with the ionisation energy he found a Druyvesteyn (D) type distribution

$$f(E) \propto \exp\left(-\frac{E^2}{E_o^2}\right). \qquad (5.31)$$

These are the two distributions that we have used.

5.2.5 c Discussion of Theory and Experimental Evidence for the Electron Distribution

In the previous section we considered how a number of authors had attempted to calculate the electron distribution function. Fröhlich noted that at sufficiently high field strengths the electron population constantly gained energy and ionisation released more conduction electrons until a catastrophic breakdown occurred. However in ZnS and ZnSe this breakdown does not occur until higher fields than predicted are present.

Stratton [5.20] further developed the theory of Fröhlich and Paranjape finding that at high electron densities inter-electron collisions determined both the momentum and energy distribution of the electrons. In his second paper [5.21] he calculated the runaway field for a known electron density. Rigby & Allen [5.22] applied this theory to ZnSe and found the runaway field to be 2.8×10^4 Vcm^{-1} which is close to the field Ludwig & Aven [5.23] found for the Gunn effect in ZnSe (3.8×10^4 Vcm^{-1}). For ZnS Rigby & Allen estimate that in the Γ_1 valley the runaway field might be 1.1×10^4 Vcm^{-1} . Since most devices have fields of $\geq 5 \times 10^5$ Vcm^{-1} one might expect the electrons to be transferred to the X_1 and X_3 valleys. In these valleys the high effective mass and low velocity increase the scattering and the electrons require a much larger field to gain more energy and start ionisation. Thompson & Allen [5.24] give the ionisation field as 2×10^6 while Rigby et al [5.25] give a value of $1.2 - 1.6 \times 10^6$ Vcm^{-1} depending on the preparation of the ZnS sample.

Another reason that devices do not break down as expected is that a non-uniform electric field may be present. In a Schottky diode the field is considered to decrease linearly in the depletion region. At the metal contact electric fields are greater than 10^6 Vcm^{-1} and avalanching can occur. However the field quickly decreases away from the contact and the avalanching ceases when the local field is too weak to sustain it. For catastrophic breakdown the avalanching region needs to be quite large to damage the device. If the material is ion implanted the bombardment introduces acceptors which reduce the conductivity of the material [5.26]. With fewer donors available the local electric field will be reduced decreasing the possibility of runaway. The lattice damage also reduces the electron mean free path by increasing the scattering which in turn raises the runaway field.

In thin film devices the polycrystalline structure has the effect that the electric field may be different in neighbouring domains. A large part of the applied voltage may therefore be dropped across a single domain but breakdown is prevented by the high resistance of the neighbouring domains.

Theoretical models are available which take into account the band structure, however only one has been applied to ZnS and ZnSe and it does not include the second conduction band [5.27].We might therefore try to find the electron distribution from experiments. Marrello et al

[5.28, 5.29] carried out a series of experiments in which thin film devices of the MISIM structure were constructed with only a thin layer of the ZnS phosphor containing Mn. Experiments showed that the Mn did not significantly affect the electron distribution so the authors are confident that their results represent a typical electron distribution. By producing a series of such devices with the Mn layer in different positions within the film they were able to measure the relative fraction of hot electrons in the phosphor. They found that the fraction of hot electrons decreased approximately exponentially from the cathode. Marrello expected the internal fields to be 2 to 3 x 10^6 Vcm^{-1} , about the ionisation threshold. One would expect that after impact excitation the "cooled" electrons would be accelerated again up to excitation energies. The luminescence should then have remained constant or increased away from the cathode. Instead we conclude that the field was in fact at a maximum close to the cathode and that runaway decreased away from the cathode.

Marrello et al gave no data for a changing applied voltage so it is not possible to say if the field distribution was voltage dependent. The thin Mn layer was 20, 35 or 50nm wide depending on the thickness of the phosphor layer. Luminescence was possible even when the Mn layer was adjacent to the cathode showing that energies of 2-3 eV could be attained in less than 20nm and so fields of greater than 10^6 Vcm^{-1} existed at the cathode. They did however find that in the first grown 200nm of the film the electroluminescence was appreciably reduced. This they attribute to poor crystal structure reducing the hot electron population.

Marrello's experiments show that the electron distribution is a function of the local field. When experiments are performed however we usually only know the average fields. Therefore when luminescence and ionisation experiments are performed it is usual to use a distribution that describes the average electron distribution. This distribution has the ability to reproduce the effect of the real distribution. This is because distributions like those of Baraff have been calculated for a uniform electric field. Most authors use a qualitative fit to their data [5.4, 5.25, 5.30, 5.31, 5.32, 5.33].

In Krupka's original experiment [5.4] he looked at the emission ratio from just two levels of Tb^{3+} in ZnS. By the faster increase of the higher energy emission with increased voltage Krupka reasoned that the electron distribution was shifting to higher energies. At Hull

a series of similar experiments were performed using eight of the Er^{3+} emissions in ZnS ranging in energy from 1.26 to 3.22 eV. From these experiments the authors derived evidence for a M-B distribution [5.7, 5.8, 5.9]. In section 5.4 we shall take a closer look at these results.

5.3 Evaluation of the Impact Excitation Rate

5.3.1 Introduction

In section 5.2 we derived a rate equation which predicted the various emission intensities of a luminescence centre (5.11). The equation was based on the assumption of a parabolic conduction band. If we now mathematically evaluate this rate equation we can use it to analyse experimental results from real devices and thus check the validity of the models.

5.3.2 Mathematical Evaluation

In section 5.2 the following general rate equation for any emission was found

$$I_\lambda = \eta_\lambda N \int_0^\infty n(E)\, \sigma_\lambda(E)\, \upsilon(E)\, dE. \qquad (5.11)$$

$\upsilon(E)$ and $\sigma(E)$ were found for a parabolic conduction band and approximate forms given in (5.13) and (5.21) respectively. For n(E) two forms were suggested for simple models. First we shall consider the Maxwell-Boltzmann (M-B) distribution. For this (5.26) is replaced by

$$n(E) = \beta\, E^{1/2} \exp(-E/E_o). \qquad (5.32)$$

Putting all these elements into (5.11) we have

$$I_\lambda = \frac{\tau_\lambda}{\tau_{r\lambda}} N \int_{E_\lambda}^\infty \beta\, E^{1/2} \exp\left(\frac{-E}{E_o}\right) \frac{\alpha(E-E_\lambda)^{1/2}}{E_\lambda{}^3\, \tau_{r\lambda}\, E^{3/2}} \left(\frac{2}{m^*}\right)^{1/2} E^{1/2}\, dE$$

$$= \Delta \frac{\tau_\lambda}{E_\lambda{}^3\, \tau_{r\lambda}{}^2} \int_{E_\lambda}^\infty \frac{(E-E_\lambda)^{1/2}}{E^{1/2}} \exp\left(\frac{-E}{E_o}\right) dE \qquad (5.33)$$

where Δ is a constant and has the same value for all emissions in the host lattice.

To evaluate this integral we first assume that if $E_\lambda \gg E_o$ then the exponential term is rapidly decreasing and the integral becomes negligible for values of $E > E_\lambda + E_o$. In this

situation $E^{1/2}$ may be considered to be approximately of constant value $E_\lambda^{1/2}$ and can be brought out of the integral with out significant loss of accuracy. We then have

$$I_\lambda = \Delta \frac{\tau_\lambda}{E_\lambda^{7/2}\,\tau_{r\lambda}^2} \int_{E_\lambda}^{\infty} (E-E_\lambda)^{1/2} \exp\left(\frac{-E}{E_o}\right) dE. \qquad (5.34)$$

We now make the substitution $E = E_\lambda + x$ and find

$$I_\lambda = \Delta \frac{\tau_\lambda}{E_\lambda^{7/2}\,\tau_{r\lambda}^2} \exp\left(\frac{-E_\lambda}{E_o}\right) \int_0^{\infty} x^{1/2} \exp\left(\frac{-x}{E_o}\right) dx$$

$$= \Delta \frac{\tau_\lambda}{\tau_{r\lambda}^2} \left(\frac{E_o^3}{E_\lambda^7}\right)^{1/2} \exp\left(\frac{-E_\lambda}{E_o}\right) \frac{\sqrt{\pi}}{2} . \qquad (5.35)$$

Rearranging this we can write

$$\exp\left(\frac{-E_\lambda}{E_o}\right) \propto I_\lambda \frac{\tau_{r\lambda}^2}{\tau_\lambda} \frac{E_\lambda^{7/2}}{E_o^{3/2}} . \qquad (5.36)$$

If we plot the logarithm of the right hand side of (5.36) against E_λ and find a straight line behaviour this would show that a M-B distribution is consistent with the experimental data.

An alternative electron distribution is the Druyvesteyn (D) distribution. If the electrons obey this distribution n(E) in (5.26) is replaced by

$$n(E) = \beta\, E^{1/2} \exp(-E^2/E_o^2) \qquad (5.37)$$

and our rate equation is now

$$I_\lambda = \frac{\tau_\lambda}{\tau_{r\lambda}} N \int_{E_\lambda}^{\infty} \beta\, E^{1/2} \exp\left(\frac{-E^2}{E_o^2}\right) \frac{\alpha(E-E_\lambda)^{1/2}}{E_\lambda^3\, \tau_{r\lambda}\, E^{3/2}} \left(\frac{2}{m^*}\right)^{1/2} E^{1/2}\, dE$$

$$= \Delta \frac{\tau_\lambda}{E_\lambda^3\, \tau_{r\lambda}^2} \int_{E_\lambda}^{\infty} \frac{(E-E_\lambda)^{1/2}}{E^{1/2}} \exp\left(\frac{-E^2}{E_o^2}\right) dE. \qquad (5.38)$$

For the D distribution E_o is normally greater than the mean energy for the M-B distribution. It is therefore more difficult to make simple approximations. Let us start by making $E = E_\lambda + x$, we then have

$y = \frac{E-E_\lambda}{E_o}$

$$I_\lambda = \Delta \frac{\tau_\lambda}{E_\lambda{}^3 \tau_{r\lambda}{}^2} \int_0^\infty \frac{x^{1/2}}{(x + E_\lambda)^{1/2}} \exp\left(- \frac{x^2}{E_o{}^2} - \frac{2xE_\lambda}{E_o{}^2} - \frac{E_\lambda{}^2}{E_o{}^2} \right) dx \qquad (5.39a)$$

$$I_\lambda = \Delta \frac{\tau_\lambda}{E_\lambda{}^3 \tau_{r\lambda}{}^2} \{INT\} \qquad (5.39b)$$

where {INT} is the result of the integral. To find {INT} we consider terms inside and outside the exponential separately. We find six approximations as summarised in table 5.1.

Table 5.1

Pre-exponential Term		Exponential Term: $E_o \ll E_\lambda$ $\frac{2xE_\lambda}{E_o}$	Exponential Term: $E_o \cong E_\lambda$ $\frac{x^2}{E_o{}^2}+\frac{2xE_\lambda}{E_o}$	Exponential Term: $E_o \gg E_\lambda$ $\frac{x^2}{E_o{}^2}$
$E_o \leq E_\lambda$	$\frac{x^{1/2}}{E_\lambda}$	(a)	(b)	(c)
$E_o \geq E_\lambda$	1	(d)	(e)	(f)

These integrals are

(a) $$\{INT\} = \frac{1}{E_\lambda{}^{1/2}} \exp\left(\frac{-E_\lambda{}^2}{E_o{}^2}\right) \int_0^\infty x^{1/2} \exp\left(\frac{-2xE_\lambda}{E_o{}^2}\right) dx$$

$$= \frac{E_o{}^3}{E_\lambda{}^2} \left(\frac{\pi}{32}\right)^{1/2} \exp\left(\frac{-E_\lambda{}^2}{E_o{}^2}\right).$$

(b) $$\{INT\} = \frac{1}{E_\lambda{}^{1/2}} \exp\left(\frac{-E_\lambda{}^2}{E_o{}^2}\right) \int_0^\infty x^{1/2} \exp\left(\frac{-x^2}{E_o{}^2} + \frac{-2xE_\lambda}{E_o{}^2}\right) dx$$

$$= \text{no algebraic solution known.}$$

(c) $$\{INT\} = \text{approximations are contradictory.}$$

(d) $$\{INT\} = \text{approximations are contradictory.}$$

(e) $$\{INT\} = \exp\left(\frac{-E_\lambda^2}{E_o^2}\right)\int_0^\infty \exp\left(\frac{-x^2}{E_o^2} + \frac{-2xE_\lambda}{E_o^2}\right)dx$$

$$= \frac{1}{2}E_o\sqrt{\pi}\exp\left(3\frac{E_\lambda^2}{E_o^2}\right)\left[1 - \Phi\left(2\frac{E_\lambda}{E_o}\right)\right]$$

where Φ is the normal distribution integral. This solution is inconvenient since E_o is required to evaluate Φ but E_o can only be found from the distribution.

(f) $$\{INT\} = \exp\left(\frac{-E_\lambda^2}{E_o^2}\right)\int_0^\infty \exp\left(\frac{-x^2}{E_o^2}\right)dx$$

$$= \frac{1}{2}E_o\sqrt{\pi}\exp\left(-\frac{E_\lambda^2}{E_o^2}\right).$$

We used the two extreme integrals (a) and (f) knowing that the true solution would lie between them. Therefore we have :

For $E_o < E_\lambda$ where $x < E_\lambda$ we use (a)

$$I_\lambda = \Delta\left(\frac{\pi}{32}\right)^{1/2}\frac{\tau_\lambda}{\tau_{r\lambda}^2}\frac{E_o^3}{E_\lambda^5}\exp\left(\frac{-E_\lambda^2}{E_o^2}\right) \qquad (5.40)$$

from which

$$\exp\left(\frac{-E_\lambda^2}{E_o^2}\right) \propto I_\lambda\frac{\tau_{r\lambda}^2}{\tau_\lambda}E_\lambda^5 . \qquad (5.41)$$

For $E_o \cong E_\lambda$ where $x \geq E_\lambda$ we use (f)

$$I_\lambda = \Delta\frac{\sqrt{\pi}}{2}\frac{\tau_\lambda}{\tau_{r\lambda}^2}\frac{E_o}{E_\lambda^3}\exp\left(\frac{-E_\lambda^2}{E_o^2}\right) \qquad (5.42)$$

from which

$$\exp\left(\frac{-E_\lambda^2}{E_o^2}\right) \propto I_\lambda\frac{\tau_{r\lambda}^2}{\tau_\lambda}E_\lambda^3 . \qquad (5.43)$$

We expect the emission intensities to give an electron distribution that lies between these limits.

An alternative solution to this integral has been suggested by Bryant et al [5.34] using the substitution $E^2 = (1 + x^2)E_\lambda^2$. With this substitution (5.38) becomes

$$I_\lambda = \Delta \frac{\tau_\lambda}{E_\lambda{}^3 \tau_{r\lambda}{}^2} \int_0^\infty \frac{(E_\lambda(1 + x^2)^{1/2} - E_\lambda)^{1/2}}{E^{3/2}\,(1 + x^2)^{3/2}} \exp\left(\frac{-E_\lambda{}^2}{E_o{}^2} - x^2 \frac{E_\lambda{}^2}{E_o{}^2}\right) x E_\lambda{}^2 \, dx$$

$$= \frac{\Delta}{\sqrt{2}} \frac{\tau_\lambda}{E_\lambda{}^3 \tau_{r\lambda}{}^2} \exp\left(\frac{-E_\lambda{}^2}{E_o{}^2}\right) \int_0^\infty \frac{x^2}{(1 + x^2)^{3/2}} \exp\left(- x^2 \frac{E_\lambda{}^2}{E_o{}^2}\right) dx \; . \qquad (5.44)$$

Assuming that $(1 + x^2)^{-3/2} \cong 1$ for significant values of the exponential we have

$$I_\lambda = \Delta \frac{\tau_\lambda}{E_\lambda{}^2 \tau_{r\lambda}{}^2} \exp\left(\frac{-E_\lambda{}^2}{E_o{}^2}\right) \frac{1}{2} \left(\frac{E_\lambda{}^2}{E_o{}^2}\right)^{-\frac{3}{2}} \Gamma\left(\frac{3}{2}\right)$$

$$\cong \frac{\Delta\sqrt{\pi}}{4\sqrt{2}} \frac{E_o{}^3}{E_\lambda{}^5} \frac{\tau_\lambda}{\tau_{r\lambda}{}^2} \exp\left(\frac{-E_\lambda{}^2}{E_o{}^2}\right) \qquad (5.45)$$

which is the lower limit that we have previously found.

5.3.3 Experimental Evaluation of the Impact Rate Equation: Thin Films

In the last section we integrated the rate equation using two quite different electron distribution functions. We now use these solutions to examine experimental data to see if they provide adequate agreement.

We had no experimental data of our own so we used data published by Zhong & Bryant [5.8] and by Krier & Bryant [5.9]. Both sets of data refer to the Erbium (Er) emissions in ZnS d.c. thin films. Zhong & Bryant's data was measured at 10K but the driving voltage for the device was not given. The data from Krier & Bryant appeared to be for room temperature measurements and had to be corrected for non-radiative processes that reduce the Er lifetime and emission intensity. This can be done by calculating the radiative efficiency using the radiative lifetimes at 10K given by Zhong & Bryant .(As explained in Chapter 3 it is not clear whether these measured lifetimes at low temperatures are for the purely radiative relaxation as they may include energy transfer to lower excited states which will still occur at low temperatures. Since we do not have this information we are forced to use these as the pure radiative lifetimes). This corrected data was normalised to the 3.22 eV emission and is summarised in table 5.2 .

Table 5.2

Wavelength (nm)	E_λ (eV)	$\tau_{r\lambda}$ (μsec)	Normalised Luminescence [5.8]	Corrected and Normalised Luminescence[5.9]
385	3.22	2.1	1.00	1.00
411	3.01	4.0	1.84	2.14
457	2.71	—	1.50	—
495	2.50	—	2.92	—
532	2.33	6.4	16.6	795
552	2.25	6.9	54.4	388
666	1.85	36	20.6	594
809	1.53	—	79.6	—
985	1.26	220	786	3206

We did not have all the lifetimes for the transitions so only part of the data was used.

To test the different electron distributions we first plotted both sets of data using (5.36) for the M-B distribution. For the data of Zhong & Bryant the agreement across the whole energy range was quite good as shown in figure (5.1). From figure (5.1) we estimated the characteristic energy to be 0.25 eV. The emissions at 2.33 eV and 1.85 eV appear to be a little weak (by a factor of 3 to 5 in intensity). This might be explained if the radiative decay has a significant magnetic component since the cross-sections are based on the assumption that the decay is a pure electric-dipole transition (see [5.35] for the example of Gd^{3+} in CdF_2).

For the data of Krier & Bryant we found the agreement was not so good. It could be conceived that the data is best described by two M-B distributions. At low energies the M-B distribution had a characteristic energy of 0.30 eV while at high energies the characteristic energy was 0.15 eV . The decrease in characteristic energy would be consistent with increased scattering occurring at high energies (e.g. [5.19]) as found in the X_3 valley.

Using the same data we then used (5.41) and (5.43) to plot the extreme behaviour of a D distribution. Zhong & Bryant's data is plotted in figure (5.2). The agreement was not very good but if we neglect the emissions at 2.33 and 1.85 eV the characteristic energy for (5.43) is 1.56 eV,

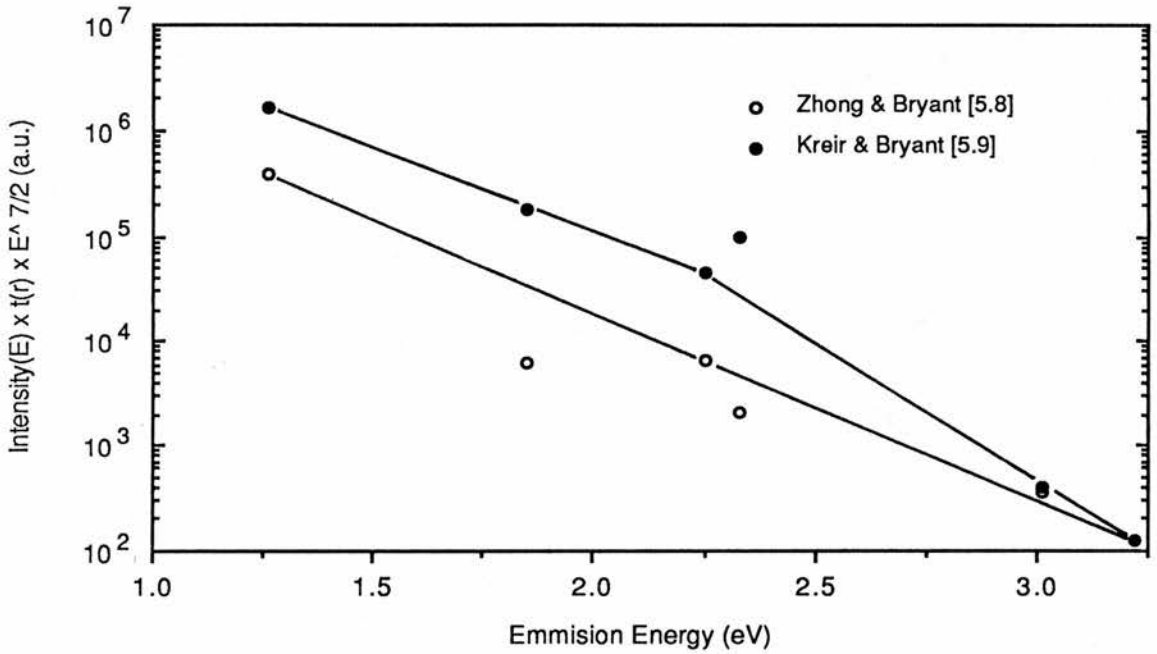

Figure 5.1 Emission data from Zhong & Bryant [5.8] and Kreir & Bryant [5.9] plotted according to equation (5.36) to demonstrate a Maxwell-Boltzmann electron distribution.

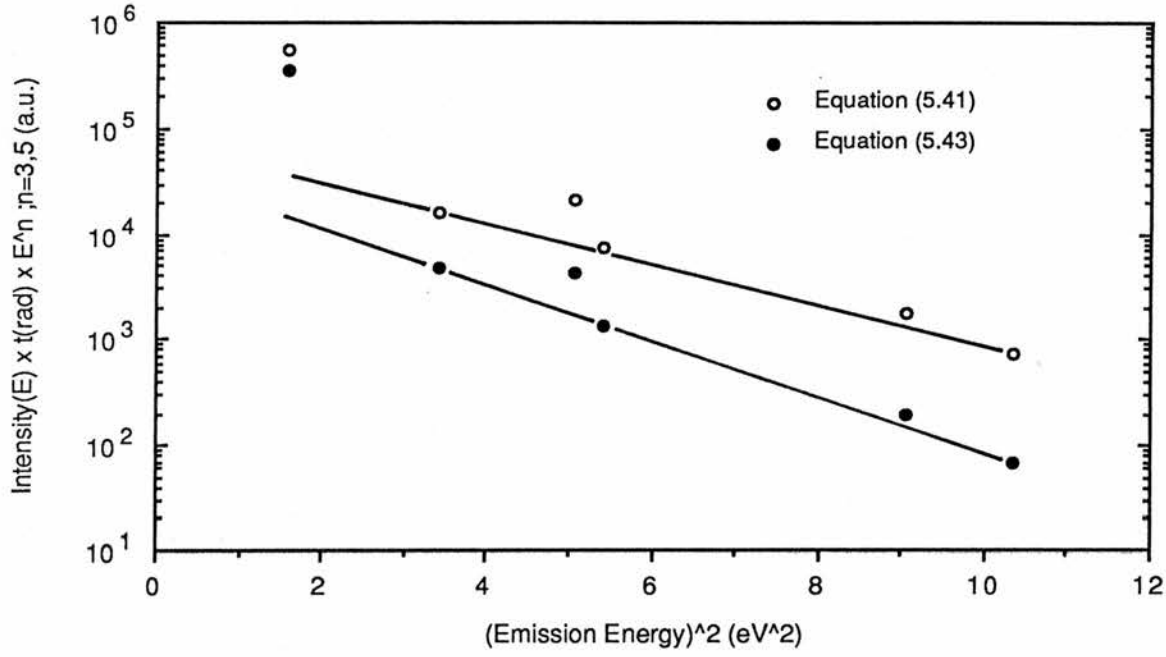

Figure 5.2 Emission data from Zhong & Bryant [5.8] plotted according to equations (5.41) and (5.43) to demonstrate a Druyvesteyn electron distribution.

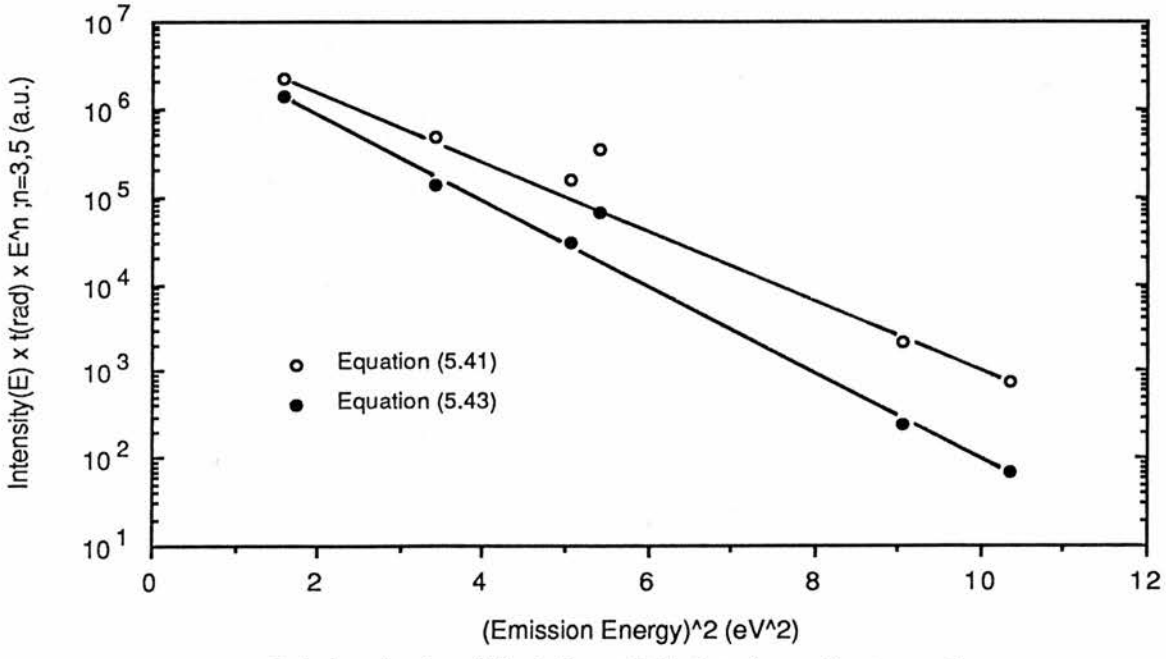

Figure 5.3 Emission data from Krier & Bryant [5.9] plotted according to equations (5.41) and (5.43) to demonstrate a Druyvesteyn electron distribution.

which showed that the assumption of $E_o \cong E_\lambda$ was consistent with the data. In figure (5.3) we plotted the data of Krier & Bryant for a D type distribution and found a better agreement than for the M-B distribution. If we use (5.41) we have a characteristic energy of 0.94 eV which is consistent with $E_o < E_\lambda$.

At first sight we appear to have two thin film devices which have a M-B or a D electron distribution but we need to ask if these are consistent with our expectations. Zhong & Bryant measured their data at 10K so a high voltage would have been required to give a sufficient emission intensity [5.9]. At lower temperatures scattering would be reduced and with the higher electric field one would expect a higher characteristic energy. Therefore we might expect the data of Zhong & Bryant to fit a D type distribution and that of Krier & Bryant to fit a M-B distribution. In fact the opposite was found.

There appears to be an additional complication of energy transfer occurring in these experiments. Zhong & Bryant showed that different emissions were quenched by different amounts. Both Zhong & Bryant and Krier & Bryant noted that the $^4S_{3/2}$ (2.25 eV) and $^2H_{11/2}$ (2.33) changed in relative intensity as the temperature was raised. Correcting for the non-radiative processes is not sufficient to correct this, which suggests that at low temperatures energy is being transferred from the 2.33 eV state to the 2.25 eV state. This makes both points unreliable though the general position in figures (5.1, 5.2 & 5.3) might be guessed by averaging their intensities. If this is done our previous conclusions remain the same. Energy exchange between these two levels is considered in more detail in Chapter 4.

So far we have plotted our luminescence data in a way that should demonstrate the exponential energy dependence of the electron distribution. An alternative test would be to start with an assumed electron distribution and from the emission intensities calculate the oscillator strength (equivalent to $\frac{E_\lambda}{\hbar}|x_{eg}|_\lambda^2$ in (3.22)) for each emission.

For a D distribution the oscillator strength is given by

$$P' = \sum_{k=2}^{6} T_k \frac{E_\lambda}{h} \left(\psi_k \| U^k \| \psi_k \right)^2 \propto I_\lambda \frac{\tau_{r\lambda}}{\tau_\lambda} \frac{E_\lambda^3}{E_o^3} \exp\left(\frac{E_\lambda^2}{E_o^2}\right) \qquad (5.46)$$

and for the M-B distribution we have

$$P' = \sum_{k=2}^{6} T_k \frac{E_\lambda}{h} \left(\psi_k \| U^k \| \psi_k \right)^2 \propto I_\lambda \frac{\tau_{r\lambda}}{\tau_\lambda} \frac{E_\lambda^{3/2}}{E_o^{3/2}} \exp\left(\frac{E_\lambda}{E_o}\right) \qquad (5.47)$$

where T_k are the Judd-Ofelt parameters which are equivalent to the Ω phenomenological lifetime parameters [5.8 and 5.36]. Zhong & Bryant and Buddhudu et al [5.8 and 5.36] have performed these calculations and we discuss their work in section 5.4.2 .

In conclusion then we found that the results from these experiments on thin film devices did not show which of the two different distributions was actually present.

5.3.4 Experimental Evaluation of Impact Rate Equation : Schottky Diode

In section 5.3.3 we considered results of emission intensities in thin film devices. As mentioned in section 5.2.5c the field in these devices is uncertain and indeed we were able to find evidence for a M-B electron distribution in one device and a D distribution in the other. Allen and co-workers have concentrated their work on Schottky diodes in which the field may be considered as decreasing linearly across a narrow depletion region adjacent to the cathode [5.22, 5.24, 5.25, 5.30, 5.31, 5.37, 5.38, 5.39, 5.40, 5.41, 5.42]. In this section we examine experimental work on ion implanted diodes which, it has been claimed [5.36, 5.43], can been shown to have a D. distribution. This proposal is based on the voltage dependence of the emission intensities rather than their relative intensities.

Bryant and co-workers first produced ZnS and ZnSe diodes in 1982 [5.26]. Crystals were grown by the Bridgman method and fired at 1000°c in liquid zinc (+ Al & Ga) to give resistances of 1-10 Ωcm for ZnSe and 10^3 Ωcm for ZnS. Ion implantation at 20 keV and ~10^6 ions cm^{-2} produced a doping of $\leq 10^{21}$ cm^{-3} at a mean depth of 8nm.(In this the diodes are different from those used by Allen et al which are doped during growth). Hall effect measurements on early samples of unimplanted ZnSe gave a donor concentration of ~$10^{17}cm^{-3}$ which for the applied voltages used would give a depletion region of 100 to 200nm width and a maximum field strength of ~10^6 Vcm^{-1} [5.44]. Zhong & Bryant [5.26] have shown that ion bombardment increases the diode resistance. This may be due to lattice damage increasing

scattering and the production of Zn vacancies which act as acceptors. A reduced electron concentration will increase the width of the depletion region and reduce the internal field.

The crystals were cleaved in a high vacuum, implanted with Er and Mn and metal contacts evaporated onto the surfaces. The diodes so produced emitted light from the Al contact and gave different I/V characteristics as shown in figures (5.4, 5.5, 5.6, 5.7). From the logarithmic plots (figures 5.5 & 5.7) we see no sign of current limiting by the bulk resistance of the diode so the whole of the applied voltage was across the depletion region. For a tunneling mechanism we expected the current to be described by

$$J = J_o(T) \exp\left(\frac{V}{V'}\right) \tag{5.48}$$

where $J_o(T)$ is a temperature dependent current factor and V' is temperature independent [5.39]. For the ZnSe diode Bryant suggests [5.43] a current dependence of

$$J(V) = \frac{J_o(T)}{V} \exp\left(\frac{1}{\sqrt{V}}\right) \tag{5.49}$$

but we know of no process that gives this type of dependence.

Bryant et al derived evidence for the types of electron distribution from the voltage dependence of the emission intensities. We now derive this relationship but any differences between our derivation and Bryant's will be discussed in section 5.4.3.

We start with an excitation rate equation in terms of energy (5.11) and find from this equation a new form related to the current and voltage of a Schottky diode. We have for the rate equation

$$I_\lambda = \eta_\lambda N \int_0^\infty n(E)\, \sigma_\lambda(E)\, \upsilon(E)\, dE. \tag{5.11}$$

The current density can be written as

$$J = e \int_0^\infty n(E)\, \upsilon(E)\, dE$$

$$= n_c\, e\, \overline{\upsilon} \tag{5.50}$$

where $\overline{\upsilon}$ is the mean electron velocity

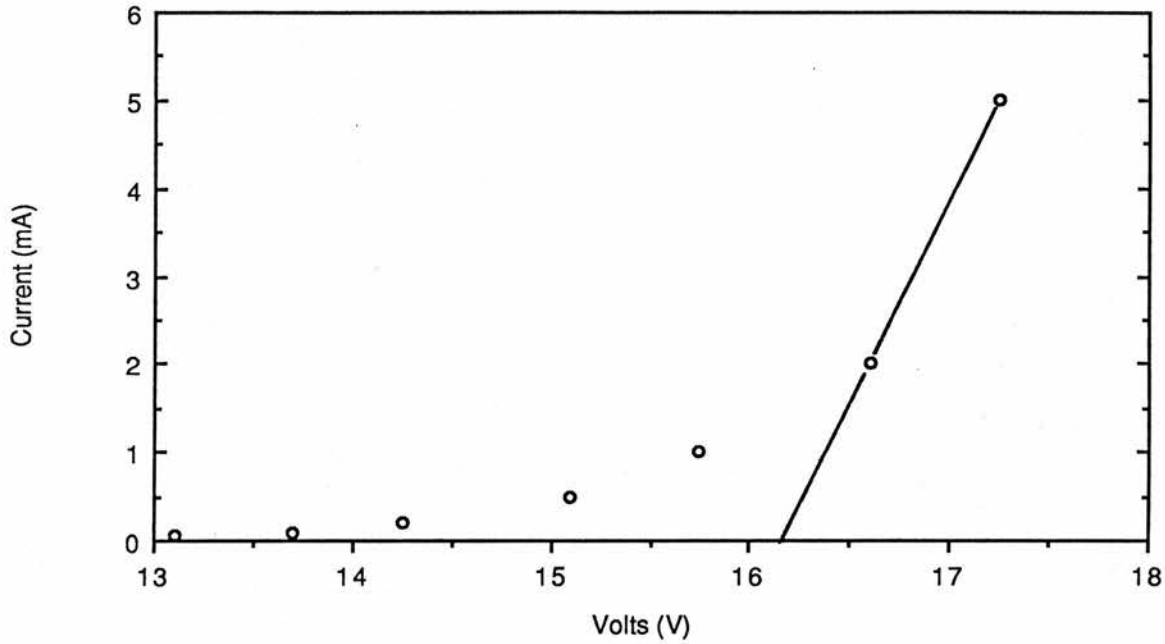

Figure 5.4 I/V characteristic of ZnS diode from Bryant et al J.Lumin. 40/41 (1988) 767

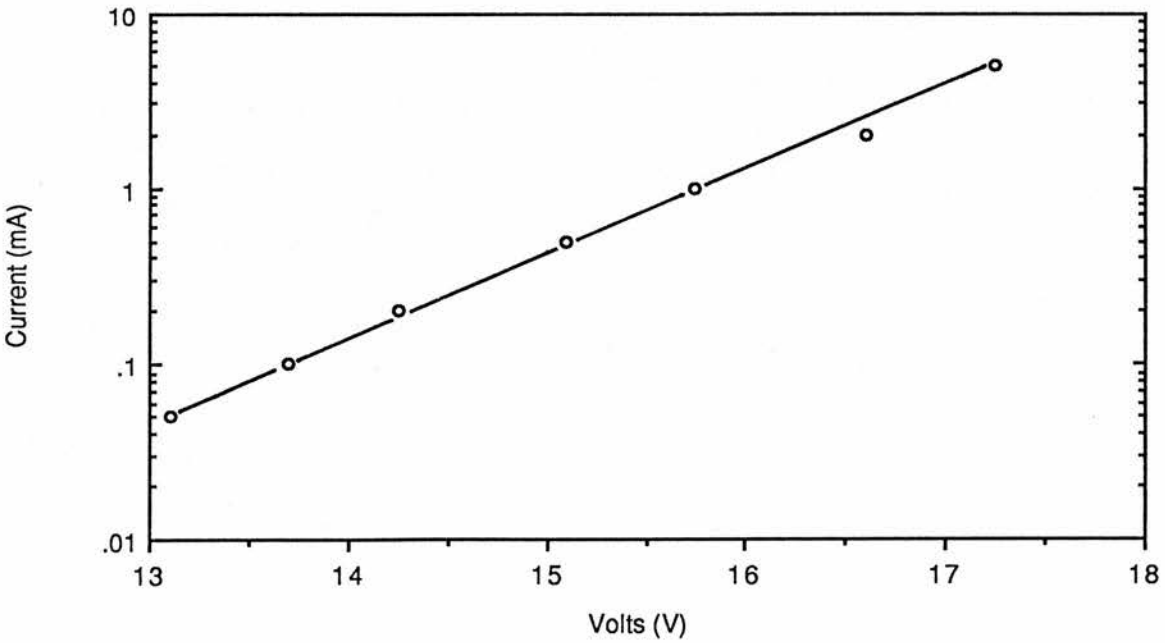

Figure 5.5 I/V characteristic of ZnS diode from Bryant et al J.Lumin. 40/41 (1988) 767

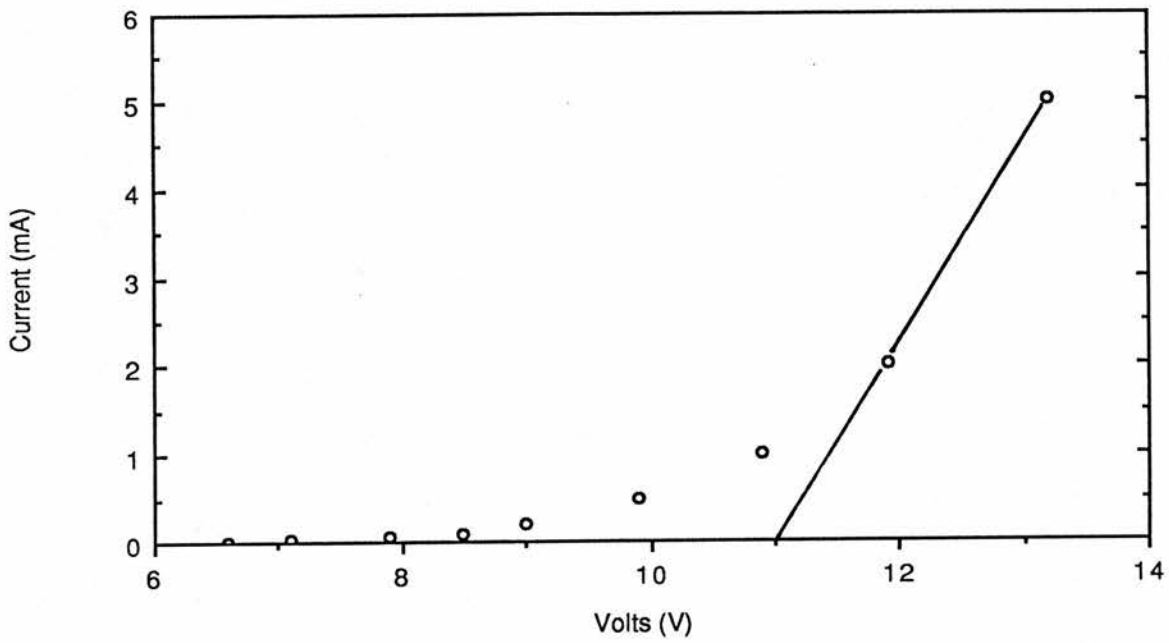

Figure 5.6 I/V characteristic of ZnSe diode from Bryant et al J.Lumin. 40/41 (1988) 767

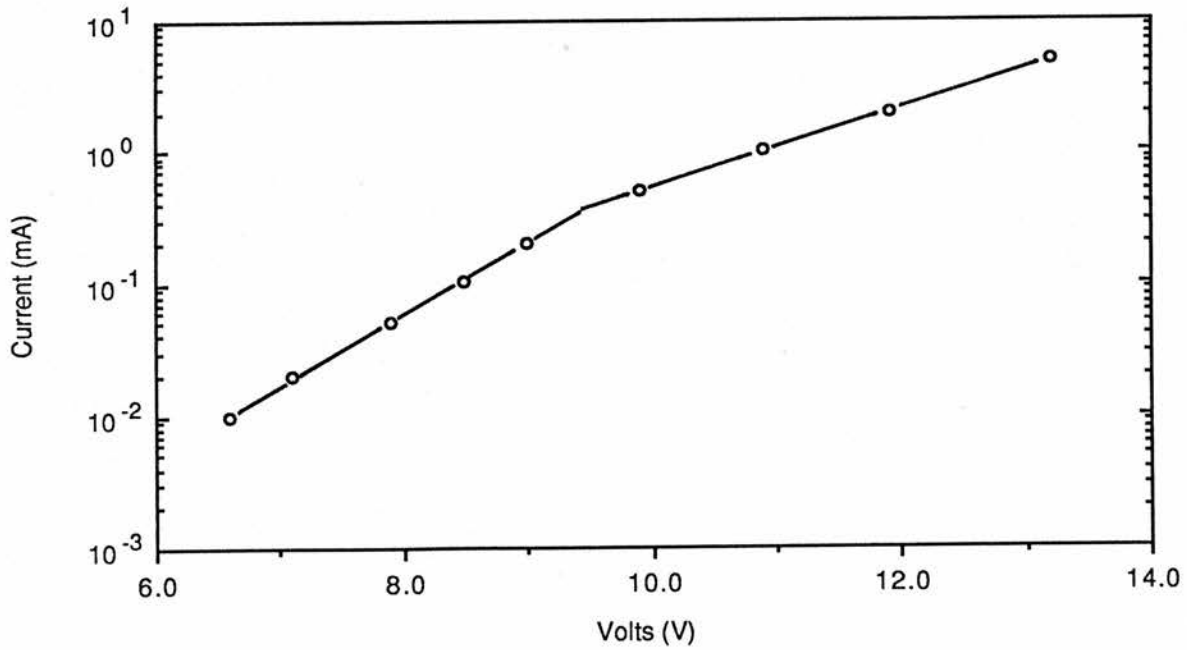

Figure 5.7 I/V characteristic of ZnSe diode from Bryant et al J.Lumin. 40/41 (1988) 767

$$\overline{\upsilon} = \int_0^\infty B\, D(E)\, f(E)\, \upsilon(E)\, dE. \qquad (5.51)$$

If the electron distribution is M-B or D. the majority of the electrons are in low energy states so $\overline{\upsilon}$ will not change exponentially with the applied voltage (e.g. in Ohm's law $\overline{\upsilon}$ is proportional to the applied voltage). To explain the exponential rise in current with voltage we need to understand that the electrons moving through the depletion region have tunneled through the barrier having come from the metal contact. The exponential rise in current is therefore due to the exponential increase in the tunneling probability. So in (5.50) what is changing the most with voltage is n_c the electron density as this is a measure of the number of tunneling electrons. So

$$J(V) \approx n_c(V)\, e\, \overline{\upsilon}\,. \qquad (5.52)$$

The emission intensities depend on the fraction of the tunneling electrons that have energies above the impact thresholds. We may rewrite (5.11) as

$$I_\lambda(V) = \eta_\lambda N\, n_c(V) \int_{E_\lambda}^\infty B\, D(E)\, f(E,V)\, \sigma_\lambda(E)\, \upsilon(E)\, dE. \qquad (5.53)$$

To remove the voltage dependence of n_c we divide by the current density,

$$\frac{I_\lambda(V)}{J(V)} = \frac{\eta_\lambda N}{e\,\overline{\upsilon}} \int_{E_\lambda}^\infty B\, D(E)\, f(E,V)\, \sigma_\lambda(E)\, \upsilon(E)\, dE. \qquad (5.54)$$

The integral can then be calculated for either a M-B or D electron distribution. For a M-B distribution we have

$$\frac{I_\lambda(V)}{J(V)} = \zeta \frac{\tau_\lambda}{{\tau_{r\lambda}}^2} \left(\frac{{E_o}^3}{{E_\lambda}^7}\right)^{\frac{1}{2}} \exp\left(-\frac{E_\lambda}{E_o}\right) \qquad (5.55)$$

and for a D distribution

$$\frac{I_\lambda(V)}{J(V)} = \frac{\zeta}{2\sqrt{2}} \frac{\tau_\lambda}{{\tau_{r\lambda}}^2} \frac{{E_o}^3}{{E_\lambda}^5} \exp\left(-\frac{{E_\lambda}^2}{{E_o}^2}\right) \qquad (5.56)$$

or

$$\frac{I_\lambda(V)}{J(V)} = \zeta \frac{\tau_\lambda}{{\tau_{r\lambda}}^2} \frac{E_o}{{E_\lambda}^3} \exp\left(-\frac{{E_\lambda}^2}{{E_o}^2}\right) \qquad (5.57)$$

where $$\zeta = \frac{\sqrt{\pi}}{2}\frac{N\alpha}{e\,\bar{\upsilon}}\frac{1}{2\pi^2}\left(\frac{2m}{h^2}\right)^{\frac{3}{2}}B \,. \qquad (5.58)$$

ζ is voltage dependent because of $\bar{\upsilon}$ but this is not expected to be greatly important over the voltage range considered. I/J is then proportional to the number of photons emitted per conduction electron. An increase in I/J will correspond to a shift in the electron population to higher energies and vice versa.

In tables 5.3 and 5.4 we give the current, voltage, luminescence and luminescence per mA from the data given of Bryant et al.

Table 5.3

ZnSe

Current(mA)	Volts(V)	I_{Er}	I_{Mn}	$\frac{I_{Er}}{J}$	$\frac{I_{Mn}}{J}$
0.05	7.9	0.7	1	14	20
0.1	8.5	1.9	2.5	19	25
0.2	9.0	4.2	5.0	21	25
0.5	9.9	13.3	13.8	26.7	27
1	10.9	31.2	26.5	31.2	26.5
2	11.9	63.7	48.2	31.9	24.1
5	13.2	176.2	119.2	35.2	23.8

Table 5.4

ZnS

Current(mA)	Volts(V)	I_{Er}	I_{Mn}	$\frac{I_{Er}}{J}$	$\frac{I_{Mn}}{J}$
0.1	13.7	3.3	4.7	33	47
0.2	14.25	4.0	6.3	20	31.5
0.5	15.1	8.4	7.9	16.8	15.8
1	15.75	16.1	15.0	16.1	15.0
2	16.6	57.6	46.6	28.8	23.3
5	17.25	532.0	258.8	106.4	51.8

This data is plotted in figures (5.8) and (5.9) respectively. For ZnSe (figure 5.8) the Er and Mn intensities both deviate from their linear relationship at 9.9V (0.5mA). It is interesting to note that at 9.9V the I/V characteristic in figure (5.7) also changes, with the current

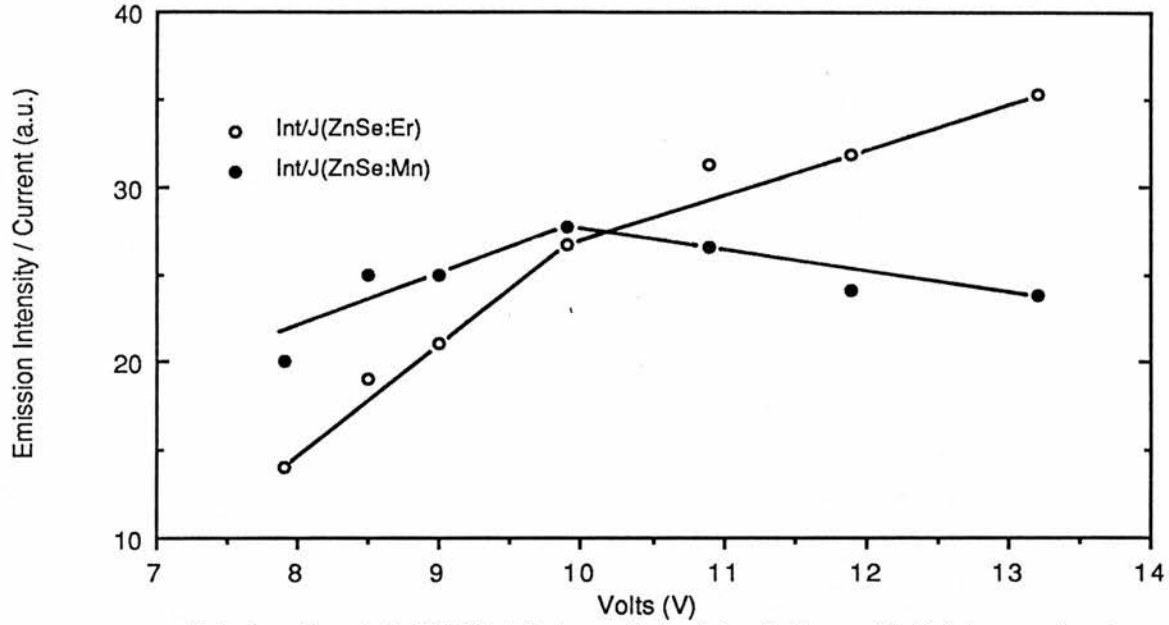

Figure 5.8 Data from Bryant et al [5.43] plotted as emission intensity / current (which is proportional to photons per conduction electron) against driving voltage for the ZnSe diode. This shows the fraction of conduction electrons of excitation energy.

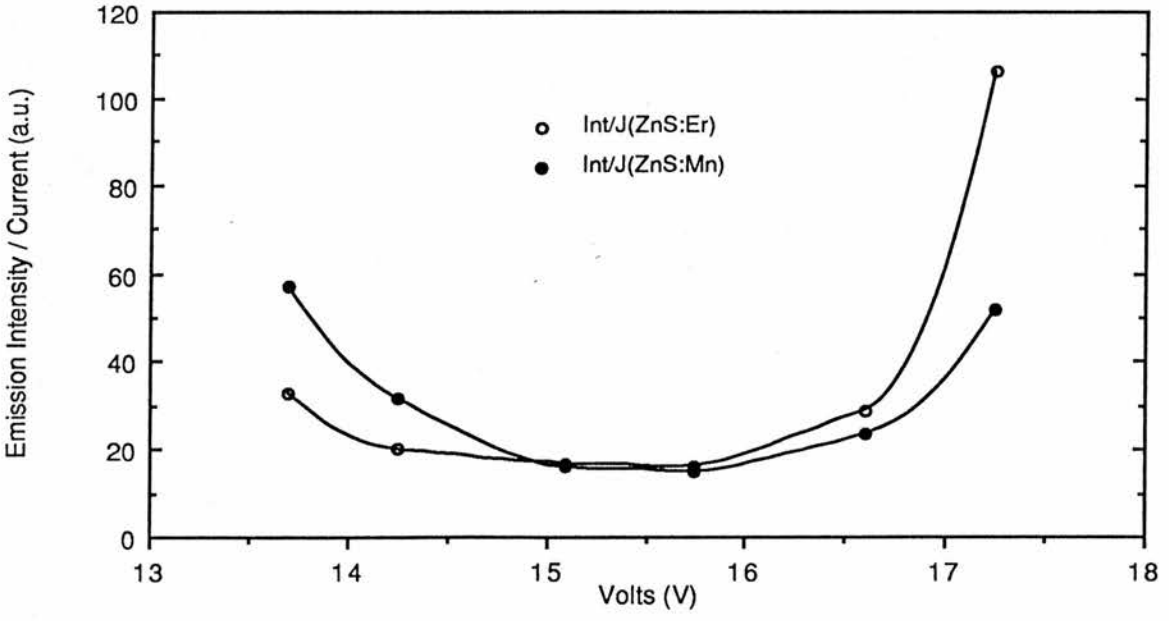

Figure 5.9 Data from Bryant et al [5.43] plotted as Emission Intensity / Current (which is proportional to the photons per conduction electron) against voltage for the ZnS diode. This shows the fraction of conduction electrons of excitation energy.

increasing less quickly with voltage. The change in current and emission intensity may well be linked.

In figure (5.9) we see that the Er and Mn emissions actually decrease for the initial rise in voltage. This would indicate a fall in the fraction of hot electron. Both emissions follow a similar behaviour and, as in ZnSe, the Er emission increases more than the Mn so that it is greater at 0.5mA. Current quenching can not be the cause of this behaviour since the quenching reduces with higher current and at 5mA the carrier density is only 10^{11} cm^{-3}, two orders below that for Auger quenching. There are other problems concerning the two Er emissions considered but this has been discussed in section 5.4.2 .

The two diodes are different essentially only in the material from which they are constructed. Both materials have similar band structures differing mainly in the size of the band gap. We can find the expected voltage dependence of the emission intensities. Baraff gives the characteristic energy for a M-B distribution as

$$E_o = \frac{2}{3} el\,\mathcal{E} + \frac{1}{3}\left[\frac{(el\mathcal{E})^2}{E_p}\right] \qquad (5.59)$$

where E_p is the optical phonon energy (E_p = 0.034 eV), l is the mean free path for phonon scattering and $\mathcal{E}$ is the electric field. For a Schottky diode the average electric field is

$$\overline{\mathcal{E}} = \frac{1}{2}\,\mathcal{E}_{max} = \left(\frac{e\,N_d\,V}{8\pi\varepsilon_o\varepsilon_r}\right)^{\frac{1}{2}} \qquad (5.60)$$

so

$$E_o = \frac{1}{3}\left(\frac{e^3\,N_d\,l^2}{2\pi\varepsilon_o\varepsilon_r}\right)^{\frac{1}{2}} V^{\frac{1}{2}} + \frac{1}{24E_p}\,\frac{e^3\,N_d\,l^2}{2\pi\varepsilon_o\varepsilon_r}\,V$$

$$= pV^{\frac{1}{2}} + qV \qquad (5.61)$$

where N_d is the donor density and ε_o,ε_r are the permitivities.

For a D distribution Bryant et al [5.43] and Buddhudu et al [5.36] state that for a parabolic conduction band where

$$E = \frac{1}{2}\,m\,\upsilon^2$$

then

$$E_o^2 = \frac{1}{3}\,m\,M\,a^2\,l^2 \qquad (5.62)$$

where m is the electron mass, M is the mass of the scattering centre, l is the mean free path of the electron and 'a' is the average acceleration of the electron i.e.

$$Ve = m\,a\,L \tag{5.63}$$

where L is the width of the depletion region. L is however dependent upon V so we write

$$L = \left(\frac{V\,2\varepsilon_o\varepsilon_s}{e\,N_d}\right)^{\frac{1}{2}}. \tag{5.64}$$

We now rewrite (5.62) eliminating 'a' to give

$$E_o^2 = \frac{1}{6}\frac{M\,l^2\,e^3}{m\,\varepsilon_o\varepsilon_r}N_d V$$

$$= \frac{V}{k}. \tag{5.65}$$

Let us return to our earlier expressions for the emission variation. We have for a M-B distribution (5.55) and (5.61) which gives

$$\frac{I_\lambda(V)}{J(V)} = \zeta\frac{\tau_\lambda}{\tau_{r\lambda}^2}\frac{(p\sqrt{V} + qV)^{3/2}}{E_\lambda^{7/2}}\exp\left(\frac{-E_\lambda}{p\sqrt{V} + qV}\right) \tag{5.66}$$

and for a D distribution (5.56, 5.46) and (5.65) give

$$\frac{I_\lambda(V)}{J(V)} = \frac{\zeta}{2\sqrt{2}}\frac{\tau_\lambda}{\tau_{r\lambda}^2}\frac{V^{3/2}}{E_\lambda^5\,k^{3/2}}\exp\left(\frac{-E_\lambda^2\,k}{V}\right) \tag{5.67}$$

or

$$\frac{I_\lambda(V)}{J(V)} = \zeta\frac{\tau_\lambda}{\tau_{r\lambda}^2}\frac{V^{1/2}}{E_\lambda^3\,k^{1/2}}\exp\left(\frac{-E_\lambda^2\,k}{V}\right) \tag{5.68}$$

None of the above curves predict the behaviour of the luminescence in figures (5.8) and (5.9).

Alternative data has been published by Buddhudu et al [5.36] for diodes made from single crystals of ZnSe (see Table 5.5 for data calculated from figure(1) of [5.36]) . If we compare emission intensities at different voltages we can remove the unknown constants in our equations by looking at relative intensities. For instance if we take emissions at V_1 and V_2 the ratio of the emission intensities for a M-B distribution (5.66) is

$$\frac{I_\lambda(V_1)}{I_\lambda(V_2)} = \frac{J(V_1)}{J(V_2)}\left(\frac{p\sqrt{V_1} + qV_1}{p\sqrt{V_2} + qV_2}\right)^{\frac{3}{2}}\exp\left(-E_\lambda\left[\frac{1}{p\sqrt{V_1} + qV_1} - \frac{1}{p\sqrt{V_2} + qV_2}\right]\right) \tag{5.69}$$

$$\text{so}\quad \mathrm{Ln}\left(\frac{I_\lambda(V_1)}{I_\lambda(V_2)}\right) = -E_\lambda\left[\frac{1}{p\sqrt{V_1} + qV_1} - \frac{1}{p\sqrt{V_2} + qV_2}\right] + \mathrm{Ln}\left[\frac{J(V_1)}{J(V_2)}\left(\frac{p\sqrt{V_1} + qV_1}{p\sqrt{V_2} + qV_2}\right)^{\frac{3}{2}}\right]. \tag{5.70}$$

If we plot the log of the ratio of the emission intensities (Table 5.5) against the emission energy (E_λ) we should get a straight line. This we have done in figure (5.10) and a reasonable agreement is found.

Table 5.5

Transition	E_λ(eV)	E_λ^2 (eV)^2	$\frac{I(V_1)}{I(V_2)}$
$^4I_{9/2}$	1.53	2.34	1.29
$^4F_{9/2}$	1.85	3.42	1.45
$^4S_{3/2}$	2.25	5.06	1.88
$^4H_{11/2}$	2.33	5.45	2.02
$(^4F_{5/2})^*$	2.81	7.9	2.02

* This emission has not been previously reported by Bryant and co-workers but is close to the 2.71 eV $^4F_{5/2} \rightarrow {}^4I_{15/2}$ transition.

We can perform a similar operation with the D distribution using equations (5.67) and (5.68) giving

$$\mathrm{Ln}\left(\frac{I_\lambda(V_1)}{I_\lambda(V_2)}\right) = \mathrm{Ln}\left[\frac{J(V_1)}{J(V_2)}\left(\frac{V_1}{V_2}\right)^i\right] - E_\lambda^2\, k\left[\frac{1}{V_1} - \frac{1}{V_2}\right] \qquad (5.71)$$

where i= 3/2 for $E_o < E_\lambda$ and i = 1/2 for $E_o \cong E_\lambda$. Since the first log term is constant we have one plot for both curves and this we have done in figure (5.11). The agreement appears to be as good as that in figure (5.10) and so the voltage dependence favours neither distribution. It may be that at higher voltages one distribution will give a better agreement however we do not have this data. The gradient of figure (5.11) is the constant $k\left[\frac{1}{V_1} - \frac{1}{V_2}\right]$. Since V_1 is fixed a plot of the different gradients against $1/V_2$ should give a straight line and this we show in figure (5.12). The values of $k\left[\frac{1}{V_1} - \frac{1}{V_2}\right]$ are derived from the data in figure(2) of [5.36] and are shown in Table 5.6 .

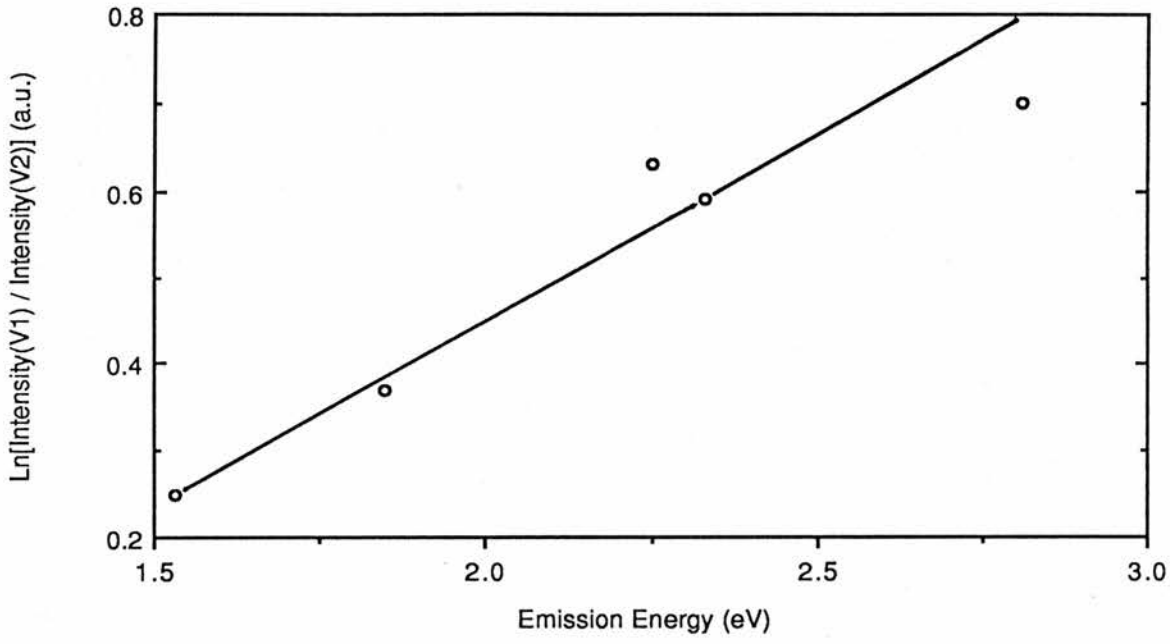

Figure 5.10 Data from figure(1) of Buddhudu et al [5.36] plotted for a Maxwell-Boltzmann electron distribution showing relative increase in emission intensity for each emission.

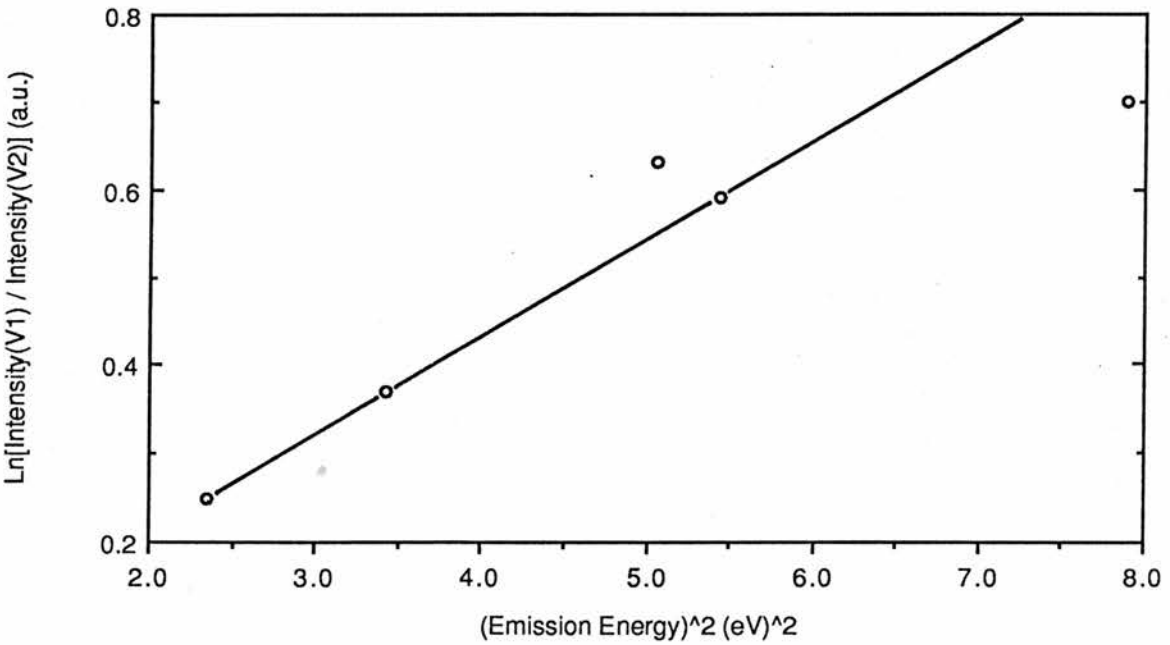

Figure 5.11 Data from figure(1) of Buddhudu et al [5.36] plotted for a Druyvesteyn electron distribution showing relative increase in emission intensity for each emission

Table 5.6

V_2 (Volts)	V_2^{-1} (x 10^{-2})	V_2^{-2} (x 10^{-5})	$k\left[\frac{1}{V_1} - \frac{1}{V_2}\right]$
24	4.17	174	-12.9
21	4.76	225	-19.3
19	5.26	275	-28.0
17	5.88	355	-39.4
15	6.67	443	-46.8

Figure 5.12 gives a reasonable agreement which would suggest that this diode shows emission intensities in keeping with a D electron distribution. However without access to the original emission data we can not show that a similar agreement does not exist for a M-B distribution as was found with figures (5.10) and (5.11).

Assuming that the electron distribution is D we can from k calculate the scattering length l in (5.65)

$$l^2 = \frac{6m\,\varepsilon_0\varepsilon_r\,4\pi}{MN_d\,e^3\,k}\,. \qquad (5.72)$$

From figure(5.12) we have $k = 10/e^2$, Buddhudu et al give $M/m \sim 10^6$ (this is based on the assumption that the scattering is via a large complex formed from over 10 atoms, this assumption has not been justified as discussed in section 5.4.3) and from [5.34] we use $N_d = 10^{17}$ cm^{-3} and $\varepsilon_r = 5.2$ from reference tables. Using these figure we find

$$l = 1.5\,\text{Å}$$

which is similar to the value given by Buddhudu. If this scattering results in the loss of energy equivalent to one optical phonon then

$$e\mathcal{E}l \geq E_p$$

$$\mathcal{E} \geq \frac{0.034}{1.5 \times 10^{-10}} = 2.3 \times 10^6\ \text{Vcm}^{-1} \qquad (5.73)$$

but this is the maximum expected value of the field at the cathode and so runaway can not occur through much of the depletion region, particularly as the fields should be lower than this due to the bombardment damage. It would seem then that this scattering length is unreasonable.

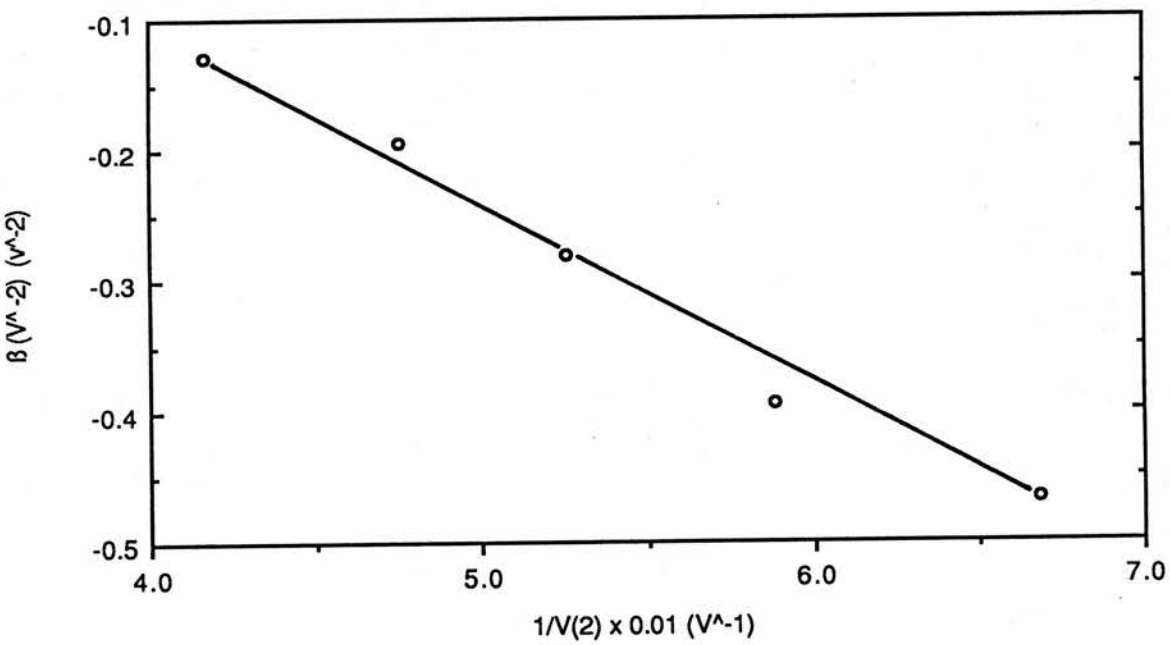

Figure 5.12 Plot of data from figure(2) in reference [5.36] with a correction included for the width of the depletion region. Electron distribution is assumed to be Druyvesteyn.

We have presented theoretical models and experimental results on thin films and diodes that attempt to distinguish between M-B and D distributions. The work presented in this and the previous section are partly our own and partly derived from others. In the next section we compare this work to that already published by others and where appropriate comment on the differences.

5.4.1 Critique on Mathematical Evaluation of Rate Equation.

As previously mentioned the rate equation (5.11) derived by us differs from that used by Bryant et al [5.7, 5.8, 5.9] by factors that they erroneously introduce.There is also a fundamental difference in the cross-section used. The probability of one electron exciting a centre may be written as

$$P_{up} = \sigma(E)\upsilon(E). \tag{5.74}$$

Bryant et al use the Einstein formula to directly relate P_{up} to the spontaneous emission rate stating that

$$\frac{1}{\tau_{r\lambda}} = P_{down} = P_{up}\left(\frac{8\pi h\nu^3}{c^3}\right). \tag{5.75}$$

However the Einstein formula is only valid for excitation by photons and the above formula is misquoted so that "P_{up}" in (5.75) is really the Einstein coefficient of absorption [5.45].

Another misunderstanding present is in the use of a delta function to evaluate the integral of the rate equation. It is argued that as the electron distribution is rapidly decreasing with energy then the integral is dominated by the values near the threshold. Bryant et al [5.7, 5.9] use the approximation

$$\sigma(E)\,\upsilon(E)\,n(E) \cong \sigma(E_\lambda)\,\upsilon(E_\lambda)\,n(E_\lambda)\,\delta(E - E_\lambda) \tag{5.76}$$

However $\delta(E - E_\lambda)$ has the dimensions of energy^{-1} so the rate equation is no longer dimensionaly balanced.

Krupka in his paper [5.4] used a step function for his cross-section

$$\sigma(E) = \begin{cases} 0 & E < E_\lambda \\ \sigma(E_\lambda) & E > E_\lambda \end{cases} \tag{5.77}$$

which is a good approximation provided that we know what value to use for $\sigma(E_\lambda)$. If we average $\sigma(E)$ over the electron distribution we have

$$\sigma(E_\lambda, E_o) = \int_0^\infty \sigma(E)\, n(E, E_o)\, dE \qquad (5.78)$$

where E_o is the characteristic energy of the electron distribution. If we now express E_o in terms of the electric field we have a field dependent cross-section. This is derived by Baraff [5.18] and used by others [5.24, 5.25, 5.30, 5.31, 5.37, 5.39]. This is not the the real cross-section but is a function for describing the combined effect of the cross-section and the electron distribution. We have not had to use this approximation.

Bryant et al [5.7, 5.8, 5.9] assume for simplicity that the electron velocity and density of states remain constant in the conduction band which is invalid for a parabolic band.(In their latter papers [5.36, 5.43] they assume that the electron velocity is exponentially increasing with the field. This is assumed to explain the exponential rise in current with field which is really due to the exponential rise in the electron density.) Because the velocity and density of states are assumed to be constant their integral of the rate equation (equivalent to (5.36)) differs from ours by a E_λ/E_o . When Allen and Ayling [5.6] published a correction of this work they used a compromise power of E_λ^4 to make some allowance for these over simplifications. The close agreement of the characteristic energies in both papers [5.6, 5.9] is due to the exponential function being the dominant term.

Zhong & Bryant [5.7] relate the characteristic electron energy to the field as we have done in (5.59). However they use the approximation that $E_o = el\mathcal{E}$ which is only valid in weak fields or where l is small . The values that they quote are not consistent with Baraff's distribution. To have E_o = 0.16 eV we require $el\mathcal{E} \cong$ 0.1 eV which for fields of 10^6 Vcm^{-1} implies a scattering length of 1nm.

Should we expect the electron distribution to be M-B in form? Fröhlich [5.11] estimates that an electron concentration of 10^{18} cm^{-3} is required for adequate thermalisation amongst the electrons. In the thin films used the electron concentration is about 5×10^{12} cm^{-3} [5.9]. It would therefore be surprising if Baraff's distribution was valid unless the electrons were produced in a M-B distribution and retained that distribution while they were accelerated as suggested by Barker [5.17].

When the rate equation was integrated we noted that different results could be produced by using different approximations and substitutions. We noted that the solutions found by

Bryant et al [5.34] differed from ours even when we started with the same equations. Finally there is a difference because we have continually allowed for non-radiative processes in our theory which are not included by Bryant et al.

5.4.2 Critique of Experiments on Thin Film Devices.

Thin film devices grown by evaporation are very resistive, having low electron concentrations. The evaporated contacts do not therefore form Schottky contacts since the depletion region would normally exceed the dimensions of the thin film by many times. Bryant and co-workers have however assumed that a Schottky contact exists to provide the high fields needed for their theories [e.g. 5.7].

As mentioned at the end of section 5.3.3 Bryant et al [5.8] and Buddhudu et al [5.36] have used these thin films to calculate the Judd-Ofelt parameters for Er^{3+} in ZnS. Both papers give incorrect oscillator strengths for the M-B and D distributions (see (5.46) and (5.47) for the correct forms). However by following through their calculations they find the following values:

Table 5.7

	T_2	T_4	T_6
Buddhudu et al [5.36]	3.9×10^{-9}	0.44×10^{-9}	1.52×10^{-9}
Zhong & Bryant [5.8]	3.9 ± 1.4	$0.94 \pm .32$	1.52 ± 0.69
Equivalent Ω's	3.90	0.94	1.52

In this table values for Buddhudu et al are calculated for a D distribution and those of Zhong & Bryant for a M-B distribution. The values of Ω have been taken from [5.8] and are reduced to give Ω_2 as 3.90 to make comparison easier with the T values. As can be seen it is possible to produce the expected values from incorrect equations and two different electron distributions. This must lead to doubt as to the validity of these experiments. It may be possible that the different devices had different electron distributions as was suggested by the results of Krier et al [5.9] and Zhong et al [5.8] in section 5.3.3 .

In section 5.2.5c we discussed the experiments of Marrello which demonstrated that the electron distribution in a thin film varied across the film. This means that interpretation of the emission data in terms of an electron distribution is in fact rather difficult. It also shows that one must be careful about applying the theory and results gathered for different types of device

especially as the same devices can show different distributions as seen if figure (5.1). Marrello also showed [5.29] that Tb in ZnS behaves differently from Mn in the same type of device. We must be careful when comparing the electron distributions found in differently doped thin films e.g. ZnS:Cu:Nd:Cl [5.7] and ZnS:Cu:Cl:Er [5.9] and in Schottky diodes (see next section).

5.4.3 Critique of Experiments on Schottky Diodes.

Experimental measurements of the cross-section for impact excitation of single ions of Mn and Er give values of ~ 10^{16} cm^2 [5.46, 5.47, 5.48]. Assuming an implantation density of about 10^{20} ions cm^{-3} [5.43] the mean free path for excitation is

$$l = \frac{1}{N\sigma} = \frac{1}{10^{20}.10^{-16}} = 1000\ \text{nm}. \qquad (5.79)$$

If the ions are implanted to a mean depth of 8nm the probability of excitation is

$$P = 1 - \exp\left(-\frac{x}{l}\right) = 1 - \exp\left(-\frac{8}{1000}\right) = 0.008\,. \qquad (5.80)$$

Without absolute emission intensities we can not test to see if it is reasonable for only 0.8% of the hot electrons to be involved in the impact excitation. Furthermore in a field of 10^6 Vcm^{-1} the electrons would need to cross at least 20nm to gain the 2 eV needed for impact excitation and 20nm is the maximum depth for a 20 keV implantation. Ion bombardment however increases the resistance of a material. Bryant et al [5.44] carried out Hall effect measurements on un-implanted material which then gives an upper limit to the donor concentration in the implantation region. The field in the implantation region will then be less than 10^6 Vcm^{-1} and it may not be possible for any electrons to reach excitation energies within the implantation region.

To overcome this rather low efficiency for the excitation process Bryant et al have suggested that the implanted ions form large complexes which transfer energy into the ions. These complexes are postulated to have cross-sections of $\geq 10^{-14}$ cm^2 giving a mean free path of ≤ 10 nm. A similar proposal has been made by Hagston [5.49]. To reduce the acceleration length of 20nm it is also proposed that the field is enhanced at the cathode to give an acceleration length of ≤ 10 nm. There is however no evidence for these large complexes. Spectral emissions from Mn and Er have been successfully interpreted in terms of single ions or small complexes in

various lattice sites [5.50, 5.51, 5.52, 5.53, 5.54]. Some sites only appear in electroluminescence and others in photoluminescence but no large complexes have been found. These large complexes might also be expected to have a greater probability of non-radiative decay as occurs with excessive Mn concentrations [5.55, 5.56, 5.57]. Some evidence of non-radiative decay is seen but large complexes have not been proposed as the cause. Lastly the field enhancement proposed is contrary to the evidence of the increased diode resistance.

ZnSe and ZnS diodes in reverse bias normally show a blue luminescence due to intraband transitions of hot electrons. This seemed to be greatly reduced in these diodes and this suggests that the fraction of hot electrons is smaller than expected. If this is true then combined with the low expected efficiency it is questionable whether the excitation mechanism is in fact impact excitation.

It is unfortunate that Buddhudu et al had to use measurements for the Er emissions from the $^2H_{11/2}$ (2.35 eV) and $^4S_{3/2}$ (2.25 eV) levels [5.43] since these emissions appear to transfer energy from the higher to the lower energy level. These emissions were chosen since they are close to the Mn emission at 2.12 eV. In Chapter 4 the energy transfer between these levels is considered in greater detail. Marrello et al and Theis [5.28, 5.29, 5.58] have shown that different centres can behave differently in the same electron distribution (e.g. Tb and Mn). This may explain the different voltage/brightness relationships for the Mn and Er as seen in figures (5.8) and (5.9) .

In section 3.4.3 we derived the voltage dependence for the emissions in a Schottky diode. Our formulae differ from those of Buddhudu et al [5.36] because they have all their energies in electron volts. Also we have allowed for the voltage dependence of the depletion region and the carrier density . The carrier density cancels when the ratio of the emission intensities is taken (5.71) but the depletion region gives this ratio a voltage dependence of V^{-1} while Buddhudu have V^{-2} . The two voltage predictions give equally good agreement with experimental data because the scatter in the data is larger that the differences in the theories.

5.5.5 Conclusions.

In this chapter a great deal of conflicting experimental and theoretical work has been considered thus giving a confusing picture. Measurements of different emissions seem to show that the intensities decrease exponentially with the increasing emission energy. From this we conclude that the electron distribution is an exponentially decreasing function of energy. The question remains though of whether it is possible to determine if this function is Maxwell-Boltzmann or Druyvesteyn in form or of some other type. There is also the question of how the device voltage and temperature affect this distribution.

If we try to fit experimental data to our theoretical expressions we seem to find the agreement to be equally good for both distributions. To explain this we tried to find the difference in behaviour between a linear and parabolic function of energy. In figure (5.13) we have plotted two functions of energy over the energy range of the Er emissions. One function is simply the square of the energy and the other is a least square fit (of a linear function of energy) to the first function. The fractional error of the least squares fit is 9% which means that the approximations in the theories must introduce a total error of less than this if we are to distinguish between them.

How accurate do we expect these theories to be ? The differences in the integral approximations is one source of error but do not change the energy dependence of the graphs produced. The assumption of a parabolic conduction band does affect the electron velocity but this affect is negated by the same electron velocity appearing in the approximation for the cross-section. The cross-section should be fairly good close to the threshold where the approximations used are valid provided that the pure radiative lifetime was used in the derivation. We also need to be sure of the nature of the excitation process for each excited state. Some states may be populated by relaxation from a higher excited state rather than by direct excitation. Some states may be excited by a direct transition while others by the exchange component. There is also the possibility of energy transfer from other centres in the device. Unless the excitation processes can be identified for each state direct comparison of each state is not really valid. If we can assume that excitation is always by impact excitation and the number of electrons is rapidly decreasing at high energies these approximations should be valid. One source of error is the

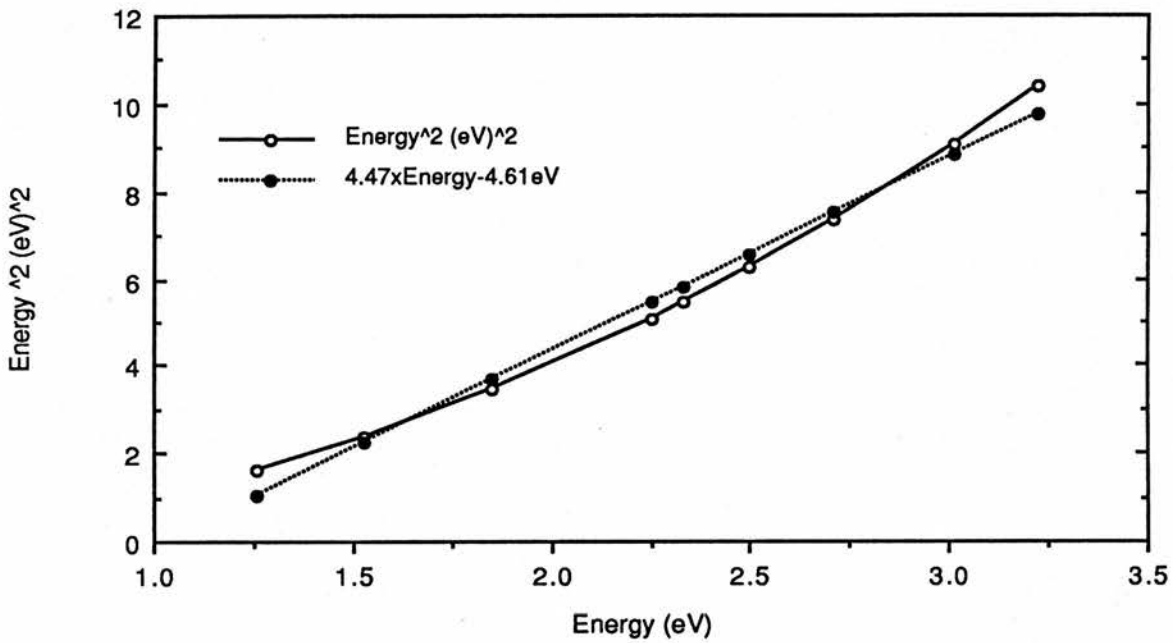

Figure 5.13 Comparison of linear and parabolic energy dependence over the energy range of the Er emissions measured in the Hull papers.

density of states. This is quite different in a non-parabolic band as explained in Chapter 3 . This factor will be most different in the X_1 and X_3 valleys of the conduction band which have energies comparable with the 2.25 eV and 2.33 eV Er emissions and the 2.12 eV Mn emission. It has been proposed that the high density of states in these valleys contributes to the high electroluminescence efficiency of the Mn. It has also been proposed that the low electron velocity in the X_3 valley favours the exchange interaction over the direct interaction. Such a change would greatly alter the character of the cross-section. It should be noted also that it is these two Er emissions which often account for the largest error in the different models.

In this chapter we have improved the work of others, correcting some assumptions and pointing out unphysical interpretations and proposals. We have also demonstrated a fundamental problem in distinguishing between different models. We propose five steps forward:

i) An improvement in the theoretical models to allow for the effect of a non-parabolic conduction band on the electron distribution.

ii) An improvement in the cross-section to allow for the exchange component in the excitation process.

iii) Increase the energy range over which emissions are recorded.

iv) Further experiments to identify the true nature of the excitation process for each excited state.

v) Further experiments to establish the electric dipole component of each radiative lifetime.

These five steps should help to distinguish between the M-B and Druyvesteyn distributions or demonstrate the existence of a different distribution.

5.6 References

[5.1] P.J.Dean *J.Lumin.* **23** (1981) 17

[5.2] T.Inoguchi, M.Takeda, Y.Kakihara, Y.Nakala & M.Yoshida
1974 SID Int.Sump.Digest, Los Angeles, p84

[5.3] F.Williams *J.Lumin.* **23** (1981) 1

[5.4] D.C.Krupka *J.Appl.Phys.* **43** (1972) 476

[5.5] Xu-mou Xu, Jiaqi Yu & Guo-zhu Zhong *J.Lumin.* **36** (1986) 101

[5.6] J.W.Allen & S.G.Ayling *J.Phys.C:Solid State Phys.* **19** (1986) L369

[5.7] G.Z.Zhong & F.J.Bryant *J.Phys.C:Solid State Phys.* **14** (1981) 2175

[5.8] G.Z.Zhong & F.J.Bryant *J.Lumin.* **24/25** (1981) 909

[5.9] A.Krier & F.J.Bryant *Phys.Stat.Sol.(a)* **83** (1984) 315

[5.10] Jiaqi Yu & Yongrong Shen *J.Phys.C:Solid State Phys.* **21** (1988) 3381

[5.11] H.Fröhlich *Proc.Roy.Soc.* **A188** (1947) 521

[5.12] H.Fröhlich *Proc.Roy.Soc.* **A188** (1947) 532

[5.13] H.Fröhlich & B.V.Paranjape *Proc.Roy.Soc.* **B69** (1956) 21

[5.14] H.Fröhlich *Proc.Roy.Soc.* **A160** (1937) 230

[5.15] H.Fröhlich *Proc.Roy.Soc.* **A172** (1939) 94

[5.16] H.Fröhlich *Proc.Roy.Soc.* **A178** (1941) 493

[5.17] J.R.Barker *J.Lumin.* **23** (1981) 101

[5.18] G.A.Baraff *Phys.Rev.* **128** (1962) 2507

[5.19] G.A.Baraff *Phys.Rev.* **133** (1964) A26

[5.20] R.Stratton *Proc.Roy.Soc.* **242** (1957) 355

[5.21] R.Stratton *Proc.Roy.Soc.* **A246** (1958) 406

[5.22] N.E.Rigby & J.W.Allen *J.Phys.C:Solid State Phys.* **21** (1988) 3483

[5.23] G.W.Ludwig & M.V.Aven *J.Appl.Phys.* **38** (1967) 5326

[5.24] T.D.Thompson & J.W.Allen *J.Phys.C:Solid State Phys.* **20** (1987) L499

[5.25] N.E.Rigby, T.D.Thompson & J.W.Allen
J.Phys.C:Solid State Phys. **21** (1988) 3295

[5.26] G.Z.Zhong & F.J.Bryant *J.Phys.D:Appl.Phys.* **15** (1982) 705

[5.27] K.Brenan *J.Appl.Phys.* **64** (1988) 4024

[5.28] V.Marrello & A.Onton *Appl.Phys.Lett.* **34** (1979) 525

[5.29] V.Marrello, L.Samuelson, A.Onton & W.Reuter *J.Appl.Phys.* **52** (1981) 3590

[5.30] A.W.Livingstone & J.W.Allen *J.Phys.C:Solid State Phys.* **6** (1973) 3491

[5.31] N.T.Gordon, M.D.Ryall & J.W.Allen *Appl.Phys.Lett.* **35** (1979) 691

[5.32] P.A.Wolff *J.Phys.Chem.Solids.* **16** (1960) 184

[5.33] I.Szczurek, H.J.Łozykowski & T.Szczurek *J.Lumin.* **23** (1981) 315

[5.34] F.J.Bryant, W.E.Hagston & A.Krier
J.Phys.C:Solid State Phys. **19** (1986) L375

[5.35] J.M.Langer & Lee Van Hong *J.Phys.C:Solid State Phys.* **17** (1984) L923

[5.36] S.Buddhudu, W.E.Hagston, M.J.R.Swift & A.J.Waring
J.Phys.C:Solid State Phys. **21** (1988) L725

[5.37] J.W.Allen, A.W.Livingstone & K.Turvey *Solid State Elec.* **15** (1972) 1363

[5.38] A.W.Livingstone, K.Turvey & J.W.Allen *Solid State Elec.* **16** (1973) 351

[5.39] J.W.Allen *J.Lumin.* **7** (1973) 228

[5.40] K.Turvey & J.W.Allen *J.Phys.C:Solid State Phys.* **6** (1973) 2887

[5.41] N.T.Gordon *I.E.E.E. Trans. E.D.* **28** (1981) 434

[5.42] D.Hommel, N.E.Rigby & J.W.Allen *Semicond.Sci.Technol.* **2** (1987) 112

[5.43] F.J.Bryant, W.E.Hagston & M.J.R.Swift *J.Lumin.* **40/41** (1988) 767

[5.44] F.J.Bryant, W.E.Hagston & A Krier *Phys.Stat.Sol.(a)* **94** (1986) 701

[5.45] R.M.Eisberg "Fundamentals of Modern Physics"
(Wiley, 1961) Chapter 13.Sec 12

[5.46] R.Mach & G.O.Müller *Phys.Stat.Sol.(a)* **81** (1984) 609

[5.47] Baozhu Luo, Jiaqi Yu & Guo-zhu Zhong *J.Lumin.* **40/41** (1988) 786

[5.48] J.W.Allen *J.Phys.C.Solid State Phys.* **19** (1986) 6287

[5.49] W.E.Hagston *Phys.Stat.Sol.(a)* **81** (1984) 687

[5.50] M.R.Brown, A.F.J.Cox, W.A.Shand & J.M.Williams
J.Phys.C.Solid State Phys. **4** (1971) 1049

[5.51] W.Busse, H.-E.Gumlich, B.Meissner & D.Theis

J.Lumin. **12/13** (1976) 693

[5.52] W.Busse, H.-E.Gumlich, A.Geoffroy & R.Parrot

Phys.Stat.Sol.(b) **93** (1979) 591

[5.53] C.C.Yu & F.J.Bryant *Phil.Mag.* **40B** (1979) 209

[5.54] C.C.Yu & F.J.Bryant *J.Lumin.* **18/19** (1979) 841

[5.55] R.Törnqvist *J.Appl.Phys.* **54** (1983) 4110

[5.56] O.Goede & D.D.Thong *Phys.Stat.Sol.(b)* **124** (1984) 343

[5.57] D.D.Thong, W.Heimbrodt, D.Hommel & O.Goede

Phys.Stat.Sol.(a) **81** (1984) 695

[5.58] D.Theis *Phys.Stat.Sol.(a)* **81** (1984) 647

Chapter 6

Conclusions

6.1 This Thesis

Auger quenching has been measured in ZnS:Mn by Gordon & Allen [6.1] and an Auger coefficient was found of about 10^{-10} cm^3 s^{-1} . If the Auger quenching occurs via a direct electron interaction the Auger coefficient in ZnSe should be about $10^{-9}cm^3$ s^{-1} because of the shorter Mn lifetime in ZnSe. We measured for the first time the Auger coefficient for Mn in ZnSe exciting the Mn emission via two higher excited states. The Auger coefficient was then determined from the temperature and electron concentration dependence of the emission intensity and lifetime. By using two different excitations and two different measures of the quenching we were able to show that one process was responsible for all the quenching behaviour. By relating this quenching directly to electrical measurements of the free electron concentration we were able to show that this was indeed an Auger process. The Auger coefficients from different samples and experiments covered a range of values so a precise value can not be given because of nature of the quenching, but all the values were found in the range 1-11 $x10^{-10}$ cm^3 s^{-1} . This is of the same magnitude as the value of 5 $x10^{-10}$ cm^3 s^{-1} that we found for ZnS:Mn.

The value for ZnS:Mn was determined from one sample using intensity measurements only but was shown to be dependent on the electron concentration. This value for ZnS:Mn is in the range previously given by Gordon & Allen. The coefficients for ZnS:Mn and ZnSe:Mn are about three orders of magnitude greater than the expected value for a direct interaction process. From the Auger coefficients we estimated the impact cross-sections to be about 10^{-16} cm^2 . This value for the impact cross-section is the same order as the lower limit for the cross-section as found by Mach & Müller [6.2].

Using the Born approximation we derived a theoretical cross-section assuming a direct coulomb interaction for the impact excitation. We originally derived a cross-section which required no parabolic energy dependence in the conduction bands. We then approximated this cross-section to allow the lower part and then the whole of the conduction band to be parabolic. It was found that for most reasonable situations it was satisfactory to allow the bottom of the conduction band

to be parabolic. It was found however that if the whole of the conduction band was assumed to have a parabolic energy dependence then the electron velocity was over estimated by as much as an order of magnitude at high energies. This had the effect of producing an order of magnitude reduction in the high energy cross-section. Yu & Shen [6.3] have published cross-sections for Er in ZnS where they have assumed a completely parabolic conduction band. Their cross-section also contained an algebraic error of $(2\pi)^3$.

When the partially-parabolic-band cross-section was applied to Er in ZnS it was found that the theoretical cross-section was three orders of magnitude below the experimental value of Luo et al [6.4]. If Luo's cross-section is for impact excitation (and this is uncertain) then these calculations show that the impact process is not a purely direct interaction process. Further work is needed to include the exchange component of the impact excitation as this may be greatly enhanced by the low electron velocity at high electron energies. However the large Er cross-section may be due to other effects. Xu et al [6.5] show that the two excited states interact strongly, with the higher excited state quickly relaxing to the lower. Therefore in experiments the lower excited state cross-section includes a significant contribution from the higher state. There was also the problem that in order to calculate the cross-section we need to know the electric dipole radiative lifetime which is not necessarily the experimental lifetime that was measured. Rare earth elements in ZnS are also prone to excitation by energy exchange from other centres [6.6] which would give a larger experimental cross-section though this cross-section has nothing to do with impact excitation.

We considered the electron distribution in ZnS thin films and Schottky diodes. We first derived the excitation rate equation to get the expected emission intensities for each excited state of the luminescence centre. Our rate equation was different from those of Bryant et al because of their incorrect use of the lifetime [6.7]. The rate equation was based on the assumption that the excitation cross-section for each excited state was the direct form of the impact excitation cross-section. From the rate equation we hoped to deconvolute the emission intensities to find the electron energy distribution.

The experimental results sometimes favoured a Maxwell-Boltzmann distribution, sometimes a Druyvesteyn distribution and sometimes neither. It would be surprising if the

electron distribution was of either of these two forms because the electron concentration in the devices is normally considered to be too low for these distribution to be established. There was some doubt, from Chapter 4, that the Er excitation was a direct interaction or that the true radiative lifetimes for the different excited states were known. In the Schottky diodes it was noted that for the expected electric fields the conduction electrons would not be accelerated to optical energies within the implantation region. Therefore the whole of this deconvolution becomes questionable since a direct impact excitation cross-section was assumed in the analysis of the emission intensities. If the excitation involves an exchange term or energy transfer then the analysis in Chapter 5 will be wrong. Before this work can progress any further the nature of the Er excitation must be clarified. So far all that can be said is that if the Er is excited by a impact excitation then the electron distribution is an exponentially decreasing function of energy.

6.2 Future Work

From our work in electroluminescence efficiency a number of areas of weakness in our current understanding and knowledge have been highlighted.

1) A better band structure is needed for the conduction bands in ZnS and ZnSe. Better experiments are needed to find the energy of the X_1 and X_3 critical points and the other minima of the conduction bands.

2) We need to grow better samples of ZnSe:Mn without the S.A. centre to improve the measurement of the Auger coefficient. The experimental set up used in our experiments needs to be improved to overcome the problem of the contracting sample arm at low temperatures.

3) The conductivity treatment for ZnS:Mn needs to be improved to increase the homogeneity of the conductivity.

4) A better understanding of the Er excitation is needed to identify which processes are involved. If the excitation is a direct interaction we need to find the electric dipole component of the lifetime. We need to understand how energy is transferred between the excited states and to or from external centres. If we can find out what is boosting the Er excitation this might be usefully enhanced to further improve efficiency.

5) To find the electron distribution we need to be more aware of the physics involved to ensure that we have taken into account all the relevant factors. We need to extend theoretical work like that of Brenan [6.8] on the electron distribution to the second conduction band.

6) If we want to use experiments like those of Bryant et al to deconvolute to electron distribution from the different emission intensities then we need to have a better understanding of how each emission is excited. We need to extend the energy range over which the emissions are considered to test more realistic models that take into account the changing band structure. Finally we need to be prepared to find that the electron distribution does not fit any exact formula.

6.3 References

[6.1] N.T.Gordon & J.W.Allen *Solid State Comm.* **37** (1981) 441

[6.2] R.Mach & G.O.Müller *Phys. Stat. Sol. (a).* **61** (1984) 609

[6.3] Jiaqi Yu & Yongrong Shen *J.Phys. C:Solid State Phys.* **21** (1988) 3381

[6.4] Baozhu Luo, Jiaqi Yu & Gou-zhu Zhong *J.Lumin.* **40/41** (1988) 786

[6.5] Xu-mou Xu, Jiaqi Yu & Gou-zhu Zhong *J. Lumin.* **36** (1986) 101

[6.6] N.E.Rigby *Ph.D. Thesis University of St.Andrews* (1987) Chapter 4

[6.7] G.Z.Zhong & F.J.Bryant *J.Lumin.* **24/25** (1981) 909

A.Krier & F.J.Bryant *Phys. Stat. Sol. (a).* **83** (1984) 315

S.Buddhudu, W.E.Hagston, M.J.R.Swift & A.J.Waring

J.Phys. C: Solid State Phys. **21** (1988) L725

[6.8] K.Brenan *J. Appl. Phys.* **64** (1988) 4024